Prepreg forming numerical analysis and experimental characterisation for a novel high-volume forming process

by

Corentin E Pasco

Innovation Report

Submitted to the University of
Warwick in partial fulfilment of the
degree of

Doctor of Engineering

September 30, 2018

Declaration

This Innovation Report is submitted to the University of Warwick in support of my application for the degree of Doctor of Engineering. It has been composed by myself and has not been submitted in any previous application for any degree. The work presented (including data generated and data analysis) was carried out by the author.

Academic Mentors: Professor Kenneth Kendall, Professor Steven Maggs, Dr Muhammad Khan

Industrial Mentor: Pete Jolley, Ben Desai, Frederick Walker

Funding Body: EPSRC and Aston Martin Lagonda Ltd

Acknowledgements

First of all, I would like to thank the University Of Warwick, EPSRC and Aston Martin Lagonda Ltd for supporting this project.

A particular thanks goes to Professor Ken Kendall for giving me the opportunity to carry out this Engineering Doctorate at the Automotive Composites Research centre in WMG, the University of Warwick. I am also grateful for the trust and support shown along the way. Finally, a particular thanks for giving me the opportunity to carry out my international placement at Ford, Dearborn, MI, USA.

I would also like to thank all the technical staff in WMG for helping me throughout my entire project. Martyn Wilkins, Darren Stewardson and Lukasz Glinka, your help and advice have always been much appreciated.

Thanks, to all my colleagues at Aston Martin, Pete Jolley, Ben Desai and Roland Snell. A special thanks to Fred Walker for his involvement in reviewing the progress of the work and appraising its relevance and applicability to Aston Martin Lagonda Ltd. R&D activities.

I would like to express my deepest gratitude to Muhammad Khan. Thanks for your great support throughout this whole project. All the interesting and challenging discussions we had were very useful and contributed to the successful completion of this work.

I would like to thank all my friends, my parents and my brother for their support and finally Chloe for her unconditional love, patience and support throughout this whole journey.

Abstract

With stringent emission standards being introduced, the demand for lightweight materials in the automotive industry has significantly increased. The use of carbon fibre reinforced plastics (CFRP) in automotive structures could deliver significant weight saving over more traditional materials, without having to compromise on other mechanical properties. However, high costs and long production time have precluded their use for volume application. Aston Martin have identified a novel manufacturing process which could produce CFRP parts economically by utilising rapid-cure prepregs. The integrated process consists in the combined application of double diaphragm forming with compression moulding techniques to produce a single-step manufacturing process.

A challenging step identified in the manufacture of CFRP components is the forming of initially flat laminate into a three-dimensional shape. Due to the flexible and inhomogeneous nature of the reinforcement, the composite blank can undergo severe deformation such as wrinkling which compromises the mechanical performances of the final component. To predict these defects, forming simulation tools can be used in the product design phases. Within this project, a commercial forming simulation software is used to support the development of this novel manufacturing process.

During forming, the fibrous reinforcement is subjected to several deformation modes, including intraply shear, interply shear and out-of-plane deformation. Within the software, these mechanisms are represented using material models, which are defined by input data. These are obtained through extensive characterisation of the uncured materials. In this work, the mechanical properties of a 2x2 twill woven and a unidirectional (UD) epoxy prepregs are investigated, under conditions representative to those expected during the manufacturing process, including, high deformation rate, elevated temperature and high normal pressures. To that aim, novel characterisation test methods were developed to evaluate the material behaviour under these specific conditions.

Experimental forming experiments were carried out for each material, with three different lay-ups using a double-dome benchmark tool and a representative numerical model was setup. Comparisons between experimental and numerical results (in terms of material draw-in, defects position, shear angle and relative ply slippage) demonstrate the ability of the software to predict the deformation of the woven prepreg. For the UD prepreg, two modelling approaches are used: (1) a single ply approach where each ply is modelled using

a UD material model, and (2) a cross-ply approach which relies on a woven fabric material model. Simulation results demonstrate that for the prediction of defects, the single ply approach provides better results. In addition, unlike the cross-ply approach, the model is able to identify areas of high stress perpendicular to the UD fibres, which may indicate ply splitting. For both approaches, the prediction of material draw-in is however challenging since it is influenced by fibre splitting, which cannot be modelled in the simulation.

Table of Contents

List of Figures

List of Tables

Nomenclature

3DF- Double-diaphragm Die Forming

CFRP- Continuous Fibre Reinforced Plastics

CCD- Charge-Coupled Device

DDF- Double-diaphragm forming

DIC- Digital Image Correlation

DMA- Dynamic Mechanical Analysis

DSC- Differential Scanning Calorimetry

ETFE- Ethylene Tetrafluoroethylene

FE- Finite Element

KES- Kawabata Evaluation System

NCF- Non-Crimp Fabric

Pre-Preg - "Pre-impregnated" composite fibres where a matrix material is already present

PCM- Prepreg Compression Moulding

PEEK- Polyether ether ketone

PJN- Pin-jointed Net

PP- Polypropylene

RSD- Relative Standard Deviation

RTM- Resin Transfer Moulding

TP- Thermoplastic

TS-Thermoset

UD-Unidirectional

1 Introduction

Anticipated CO_2 emission regulations and the increased demand for more efficient vehicles are forcing car manufacturers to seek new technologies that address these challenges. In 2017, the average CO_2 emissions level of new car sold was 118.5 grams per kilometre, still significantly below the 2020 target set by the European Commission of 95 grams per kilometre [1]. To reach this target, OEMs may adopt different strategies, from electrification of the powertrain to improvement of the engine efficiency. However, these solutions often come at the cost of increased weight, in turn decreasing the performances of the vehicle. As a consequence, the automotive industry is currently witnessing the increasing use of lightweight materials. Recent progress has been achieved through the use of aluminium intensive automotive body structures [2], achieving weight savings of about 40% in comparison to steel. The use of carbon fibre-reinforced plastics (CFRP) seems inevitable in order to attain further weight reduction.

CFRP materials offer excellent strength-to-weight properties, achieved by combining a stiff and strong fibrous reinforcement with a polymeric resin (also called matrix), both of which have low density. The reinforcement carries the load while the matrix holds the fibres together and transfers the load between them. The resin also provides protection from environmental attack on the fibres. The mass reduction, which results from the implementation of CFRP in automotive construction enables lower vehicle emissions as well as many other benefits, including improved driving dynamics, vehicle agility and part-count reduction. However, despite all these benefits, the uptake of CFRP has been limited in the automotive industry due to high costs and long production time. Although lighter than conventional materials, CFRP components are significantly more expensive (Figure 1).

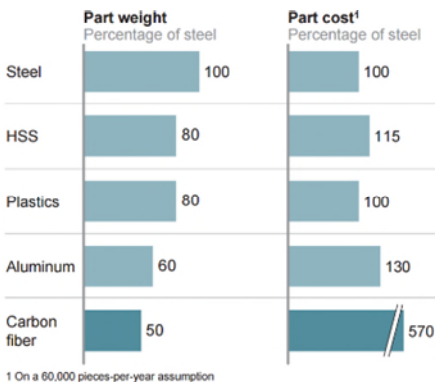

Figure 1: Weight saving potential and part cost of different materials - adapted from [3]

To reduce CFRP part cost, BMW has adopted a vertically integrated approach, establishing a joint venture with carbon fibres manufacture SGL. This strategy, combined with the use of automated processes has allowed manufacturing cost for CFRP body components to be reduced by approximately 50% [4]. In 2013, the automaker unveiled the BMW i3, the largest-volume production car to extensively use CFRP, which accounts for the major part of the body (Figure 2). In total, 34 CFRP parts are used, manufactured using different processes including resin transfer moulding (RTM) and compression moulding. However the I3 is priced above average in its segment, partly due to the extensive use of CFRP.

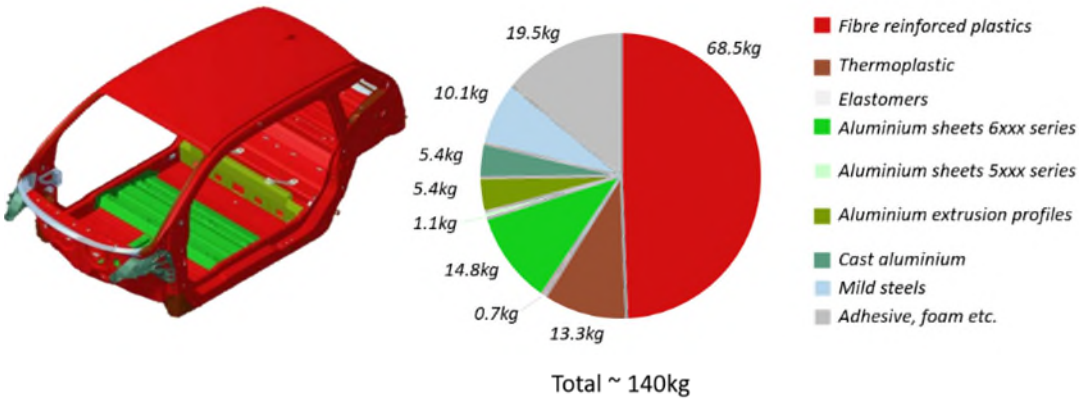

Figure 2: BMW I3 body structure - Reproduced from [5]

It seems inevitable that current production techniques, as well as design practices need to reach a higher level of maturity for CFRP to become widely accepted by other automakers. Recently, the developments in fast-curing epoxy prepreg created new opportunities for cycle time reduction, enabling cure time as low as 2 minutes [6]. While the advancement in material technologies is a promising step towards the high-volume manufacture of CFRP, there is a need for processing method to develop further for the technology to be implemented to its full potential and fulfil market demands.

1.1 Industrial context and project specifications

Aston Martin Lagonda Ltd is one of the world's leading luxury automotive manufacturer brands. Dr Andy Palmer, CEO of Aston Martin Lagonda Ltd recently announced the "Second Century" transformation plan, a comprehensive strategy for the ongoing growth and development of the OEM, focused on new products introduction and increase overall production volume.

Fundamental to this strategy, is the ambition of Aston Martin to increase its R&D activities and explore new technologies in order to increase competitiveness. One particular research area identified focuses on the development of CFRP technologies. New processes need to be developed to fit the cost model of low volume manufacturers. This is particularly true for Aston Martin, being the only global luxury carmaker that is not owned by a larger OEM. A suitable process should involve the correct level of tooling and capital investment balanced with a level of automation for repeatability and compensate the high raw material cost. The following high-level project specifications were gathered from Aston Martin:

- Cycle time under 5 minutes
- Part cost below £25/kg
- Fibre volume fraction of approximately 55%
- Automated moulding
- Automated preforming

In order to meet these requirements, the process route identified by Aston Martin is pre-impregnated (prepreg) compression moulding (also known as PCM) of continuous carbon fibre/fast-curing epoxy prepregs. Combining the advantages of prepreg materials to those of compression moulding processes allows the production of structural parts with a cycle time under 5 min, providing that a suitable level of automation is used. The PCM process typically requires a preforming stage prior to the compression phase, whereby the initially flat laminate is shaped into its final form. Preforming has often been identified as a bottleneck step in the manufacturing process of continuous CFRP, hindering large volume production [7]. The flexible nature of the fibrous reinforcement makes its handling, cutting and positioning challenging, limiting the potential for automation. Preforming is often performed in a dedicated tool prior to moulding, adding additional manufacturing costs.

To overcome these issues, a novel method is investigated, consisting in the application of double diaphragm forming (DDF) techniques with PCM. DDF initially gained popularity as a thermoforming process for thermoplastic materials and is based on vacuum forming principles [8]. The laminate is held between two diaphragms, where a vacuum is drawn thereby applying tension on the reinforcement and preventing wrinkling. Combined with PCM, the diaphragms serve as a carrier and facilitate the forming of the prepreg blank over the tool. Essentially, the resulting process is a single-step operation, whereby the forming operation is directly integrated into the moulding stage. By combining DDF and PCM, the

novel process offers excellent potential for a short manufacturing cycle, a high level of automation and controlled reproducibility, which are critical for high-volume production of structural CFRP automotive components. This process identified by Aston Martin, was developed at WMG as part of an Innovate UK funded project. A schematic of the process is shown in Figure 3.

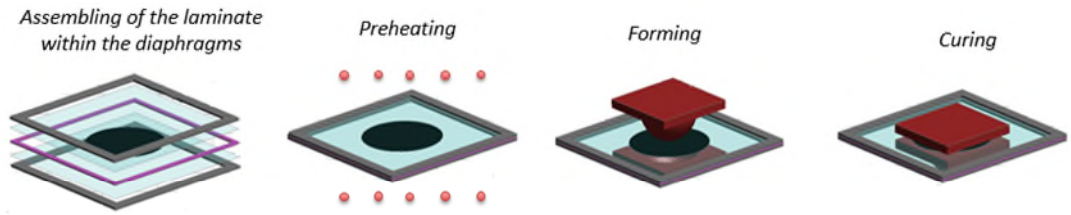

Figure 3: Schematic of the identified process

From a material forming standpoint, deformation of the laminate occurs under the action of the pressure exerted by the diaphragms, and the stroke of the die. From this point forward, the novel process will be referred to as double-diaphragm-die forming (3DF).

1.2 Motivation and objectives

Forming of composite materials over doubly-curved surfaces is a complex process during which, the laminate deforms in- and out-of-plane by a combination of intraply shear, interply slippage and bending. If not properly controlled the forming process can lead to unforeseen issues such as material wrinkling, distortion, and/or tearing which can compromise the mechanical performances of a part. An example of process-induced defects is shown in Figure 4.

Figure 4: Wrinkling on a woven double dome preform

These defects can be predicted using two different methods: a trial-and-error approach or, using specific simulation software. The former approach can lead to expensive tool modifications and is often time-consuming. To minimise development costs and identify manufacturing issues upfront, forming simulation software based on Finite Element (FE)

methods can be used [9, 10]. Because these methods take into account the mechanical behaviour of the fibrous reinforcement as well as process boundary conditions (e.g. temperature, tool speed), complete mechanical analysis can be performed. This however requires a thorough material characterisation. As a result, preforming simulation based on FE method is particularly useful in order to provide design guidelines, and help define optimal process parameters. The main goal of this project is to support the development of a novel manufacturing process through the use of forming simulation. To that aim, the following objectives were identified:

- Obtain a thorough understanding of the deformation mechanisms involved during the forming of UD and woven carbon fibre thermoset prepreg materials when subjected to elevated temperature and high deformation rate, specifically those that occur during the 3DF process.
- Perform extensive material characterisation of UD and woven carbon fibre thermoset prepregs under representative conditions, and if required, develop new test methods.
- Develop a macroscale numerical model representative of the 3DF process using a commercial preforming simulation software.
- Assess the capabilities of the simulation software to predict the forming behaviour of UD and woven carbon fibre thermoset prepregs and understand the limitations of the selected forming simulation software.
- Perform a comprehensive sensitivity analysis in order to understand the effect of different inputs and parameters (e.g. material parameters) on the simulation results.
- Perform a detailed experimental forming analysis using the 3DF process with the double-dome benchmark geometry and understand the influence of process parameters (e.g. lay-up design) on the forming behaviour of UD and woven prepregs.
- Develop and exploit optical strain measurement techniques to quantify the deformation behaviour of material in 2D and 3D forming cases.
- Correlate the simulation results with forming experiments.

1.3 Contributions and Innovation

The findings from this research project are fundamental to Aston Martin Lagonda Ltd. The deliverables from this work have helped accelerate the development of a novel composite manufacturing process, and have increased the knowledge base in the field of composite forming. The main contributions from this work are:

- A comprehensive and critical analysis of the literature on composite forming technologies. This can be used as a source of information on forming processes, material characterisation and process modelling. In addition it highlights further research opportunities.
- The development of material characterisation methods and test rigs, including the design and development of a bespoke friction test rig as well as the development of a novel method for the longitudinal in-plane shear characterisation of UD prepreg. These methods enable the characterisation of the materials under a range of conditions, representative to the novel forming process.
- The development of an innovative shear angle measurement method for in-plane shear properties of thermoset prepreg using a point-tracking algorithm.
- The development of an innovative methodology for the simulation of the forming behaviour of UD prepreg.
- The development of a complete simulation model of a novel composite manufacturing process, referred as 3DF.

1.4 Portfolio layout and outline of the Innovation Report

This section describes the outline of the work presented in this Innovation report. Table 1 presents a list of submissions that were submitted within this EngD portfolio and from which the chapters of this Innovation Report are developed.

The research methodology employed throughout this EngD project is linear waterfall approach, which seemed best suited for this type of work. First of all, a comprehensive and critical review of the literature in composite forming was conducted, with a particular focus on the forming behaviour of UD and woven reinforcements as well as forming simulation methods. This enabled to identify potential research opportunities and helped define the

structure of this project. The findings from the literature review are presented in **chapter 2** and **chapter 3**. Building on these findings, test methods for the characterisation of the mechanical properties of both UD and woven carbon fibre thermoset prepregs were identified. In addition, bespoke test methods and measurement methods were developed. Extensive material characterisation was carried out, under conditions similar to those occurring during forming. A diaphragm material was also identified and characterised. Results are presented in **chapter 4** to **chapter 8**. The experimental data were then exploited in **chapter 9** in order to develop material cards for each material. The research findings culminate in the **chapter 10** of this Innovation report, focusing on the numerical simulation of the novel forming process.

	Submission title	***Chapter discussed***
1	*State of the art review: Prepreg forming numerical analysis and experimental characterisation for a novel high volume forming process*	2, 3, 4
2	*International Placement at Ford, MI, USA: Characterisation of biaxial and triaxial reinforcements and numerical simulation of matched die forming*	2
3	*Shear characterisation of woven thermoset prepreg materials*	5
4	*Shear characterisation of unidirectional thermoset prepreg materials*	5
5	*Experimental investigations on the bending properties of thermoset prepreg systems*	8
6	*Experimental investigation on interply friction properties of thermoset prepreg systems (Published in Journal of Composite Materials)*	6
7	*A novel discrete-method of shear angle measurement for in-plane shear properties of thermoset prepreg using a point tracking algorithm (Published in Journal of Composite Materials)*	5
8	*Characterisation of the thermoset prepreg compression moulding process (Conference paper presented at SPE ACCE 2016)*	2, 3

Table 1: Details of the portfolio submissions and their relation with the innovation report chapters

The methodology highlighting the list of activities carried out during this project is shown in Figure 5.

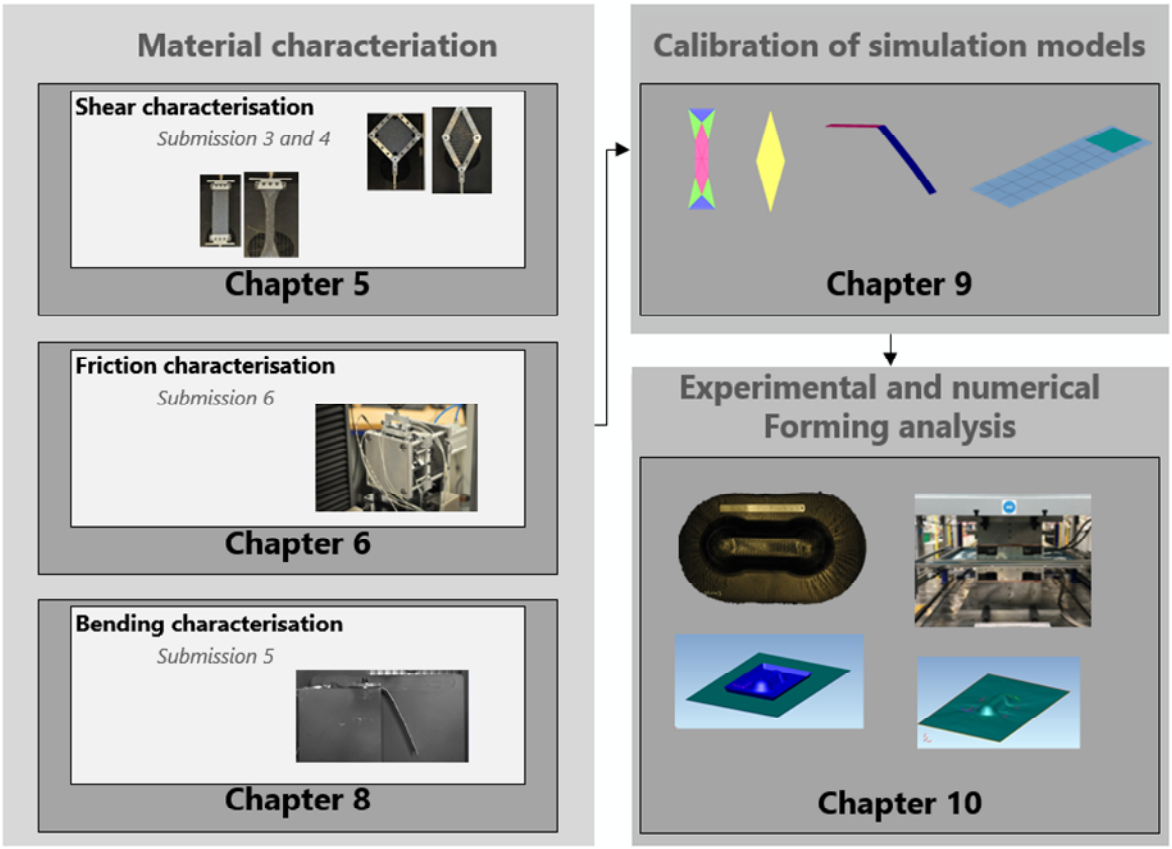

Figure 5: Scope and chapter outline

2 Literature review: Composite forming technologies

This chapter first discusses the different textile reinforcement geometries. Then forming processes of continuous fibre reinforcements suitable for automated, high-volume applications are introduced. Finally a comprehensive description of the deformation mechanisms that can occur during forming of continuous fibre reinforcements is given.

2.1 Composite materials

Carbon fibre-reinforced plastics (CFRP) are composite materials consisting of fibres within a polymeric resin. The fibres provide strength and stiffness to the material while the resin transfers load between the fibres. Both constituents typically possess a low density, which gives the composite material very good specific mechanical properties (i.e. stiffness and strength per unit density). These materials are particularly attractive due to their exotic properties. Depending on the resin formulation, the reinforcement forms, the fibre types and their orientation, a very broad range of mechanical performances can be obtained. The most common fibre materials are glass, carbon and aramid fibres.

2.1.1 Fibre reinforcement forms.

The main role of fibre reinforcements in composite materials is to provide the structural performance of the final part. There are many types of reinforcements available for composite materials. The formability and the structural performances of reinforcements are directly related to the fibre's material and orientation. Whether it is made out of glass, aramid or carbon fibre or even a combination of them in a chopped strand mat, textile or non-crimped fabric, a wide range of properties are available for design engineers. The main type of reinforcements available is shown in Figure 6. This project focuses on unidirectional (UD) and woven reinforcements. UD reinforcements, as their name suggest are reinforcements in which the fibres run in only one direction. Woven reinforcements consist of two sets of tows (i.e. warp and weft) interlaced with each other at a 90° angle. The point where a tow passes beneath or above a perpendicular tow is referred to as a crossover point. Woven reinforcements are the most widely used form of reinforcement for structural applications due to their excellent formability and ease of handling [11], which makes them suitable for complex three-dimensional shapes.

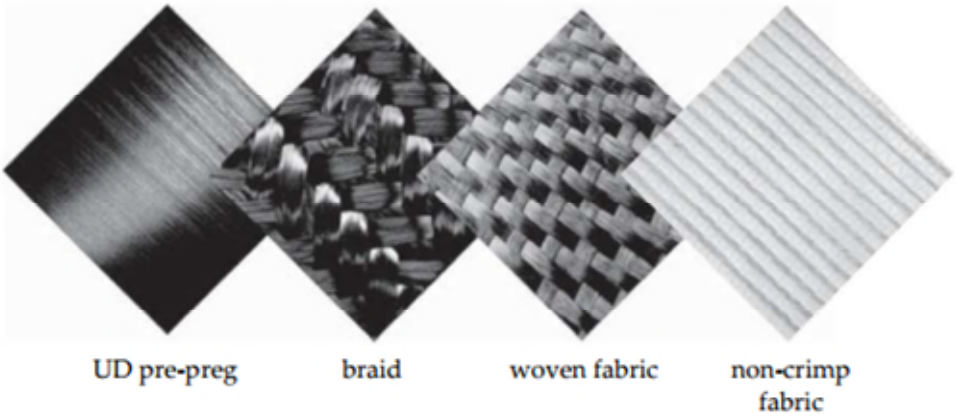

Figure 6: Different reinforcement forms [12]

2.2 Composite forming processes

Irrespective of the manufacturing process used, forming of initially flat material is a common and critical step when processing continuous CFRP. The process of forming thermoset prepreg is not as widely known as the corresponding one for dry reinforcement (preforming) or for thermoplastic laminate (thermoforming) for which most of the material characterisation techniques have been developed. Preforming is typically conducted before compression (in the case of PCM) or injection (in the case of RTM) in a separate and dedicated tool and helps give the final part a correct fibre orientation while reducing part to part variability. Preforming has been seen as a key bottleneck step in the manufacturing process of continuous CFRP. The next section gives a review of different preforming methods and describe their advantages and disadvantages. Although processes such as hand-lay-up [13], and automated tape lay-up [14], are also commonly used to form thermoset materials, they will not be treated here since they are generally used for low-volume applications (e.g. Formula 1 and aerospace industry).

2.2.1 Matched die forming

In order to increase automation and repeatability of the forming process, the aerospace industry reorganised the layup process in two stages, similar to forming processes used in metal forming: first, a flat stack of plies is created using either manual or automated process. Then, the stack is transferred into a matching metallic mould tool where it is shaped. The process is commonly referred to as matched-die forming, sheet forming or stamping, a schematic is shown Figure 7. A variation of this process employs rubber tool on

one or both mould halves in order to keep an even consolidation pressure across the part and therefore reduce the risk or wrinkles [15]. Many of the initial developments on sheet forming were done on thermoplastic materials, but similar techniques can be employed to form thermoset [16]. This process can be used for both prepreg and dry fabric. For dry fabric, thermoplastic binders are typically added to the fabric. The reinforcement is preheated to soften the binder, before being transferred into the tool. In contact with the cold tool the binder will stiffen and hold the shape. For prepreg materials, a preheating phase is required in order to soften the matrix and therefore facilitate the deformation of the material. When using thermoset resin, a rigorous control of the preheating temperature and time is required. While a higher temperature is desirable in order to reduce the viscosity of the resin and facilitate deformation (i.e. in-plane shear and interply shear), it can also lead to the initiation of the curing reaction. Once the preheating temperature has been reached, the flat blank is then stamped against the tool surface and maintain at a set consolidation pressure until the part is cooled and sufficiently stiff to be handled. The preformed part can then be removed and cured using RTM for dry reinforcement, or PCM for prepreg materials. Forming is usually done in a separate process stage, using a dedicated forming tool prior to curing for several reasons: First, the preforming process has always been considered as a bottleneck in any composite manufacturing processes [17]. Therefore, preforming in a dedicated tool does not tie up the expensive tooling/equipment required for compaction and curing of the part. Secondly, preforming does not require high compaction force, unlike the moulding process, therefore less expensive tool and equipment (e.g. preforming press) can be used for the preforming.

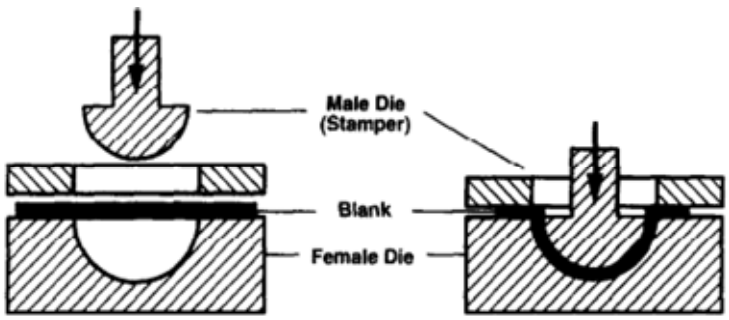

Figure 7: Matched-die forming of composite material [18]

Blank holders are typically used in order to hold the reinforcement and reduce compression forces within the laminate during preforming. While this prevents the material from wrinkling and buckling, it also limits movement of the laminate in the fibre direction, which can result in local thickness variation. Unlike metallic materials where deformations occur

in an isotropic manner, continuous fibre-reinforced laminates exhibit a significant anisotropic behaviour due to the inextensibility in the fibre direction. Consequently, deformations and conformity to the tool can be achieved through process such as transverse flow, while axial flow is prohibited. This uneven behaviour causes local tension in curved area and pressure gradient within the material which can result in important thickness variation [18, 19]. In addition, matched-die forming forces the material thickness to remain constant, which can cause resin percolation. This can ultimately lead to changes in fibre volume fraction and thermo-mechanical properties of the moulded parts.

2.2.2 Diaphragm forming

Two variants of diaphragm forming technique exist, using either a single diaphragm or two diaphragms. The latter technique is also referred to as double diaphragm forming (DDF). DDF is a sheet forming method which consists of forming a flat blank of material sandwiched and vacuumed between two diaphragms. The process initially gained popularity with thermoplastic material [8, 18, 20], but found increasing use with thermosets [21, 22], as well as dry reinforcements [23, 24]. Diaphragm forming of thermoset materials is similar to that of thermoplastic prepreg. However, unlike thermoplastic, the thermoset prepreg is not melted prior to curing, but preheated to reduce the resin viscosity. In addition, the thermoset preform requires a curing process, which can be done on the same tool in an autoclave, or in a subsequent moulding step. A schematic of the DDF process is shown Figure 8. A flat blank is initially laid up manually or automatically using ATL or automated cutting in conjunction with a pick and place machine. The blank is then placed between two polymeric diaphragms, most commonly a polyamide or polyimide films designed to possess high elongation properties that allow high drawing ratio. Thermoset rubber and superplastic aluminium have also been used as diaphragm materials [8]. A clamp ring, or frame is used to hold the assembly during preforming. Only the diaphragms edges are clamped in order to limit the introduction of high tensile strain into the inextensible fibres. The diaphragm materials and the workpiece are then preheated and deformed over a female tool using positive pressure. Throughout the whole preforming step, a vacuum is drawn between the two polymeric films.

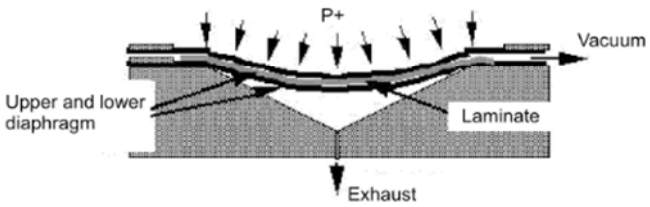

Figure 8: Schematic of the double diaphragm forming [25]

Careful attention should be given when selecting a diaphragm material. Bersee *et al.* [21], while studying diaphragm forming of thermoset composites, found that in order to prevent diaphragm rupture, thicker and stiffer diaphragms were required when forming thick laminate. In addition, less wrinkles were observed when stiffer diaphragm were used. Diaphragm stiffness also influences the degree of squeeze flow, or transverse movement of fibres [26]. Indeed, it was shown that forming with stiffer diaphragms require higher positive pressure, consequently resulting in a greater degree of squeeze flow. Excessive squeeze flow can lead to thickness variations within the part if not properly controlled. Diaphragm forming offers several advantages over other conventional forming techniques. It allows the forming of parts with a degree of complexity generally higher than that achieved with matched-die forming. In addition, due to the use of hydrostatic pressure throughout the whole preforming step, diaphragm forming tend to produce uniform thickness distribution, unlike matched-die forming where pressure within the laminate can be significantly different during forming, potentially causing high localised stresses. DDF produces parts with few out-of-plane defects. Krebs *et al*. [18], in an effort to compare preforming method, manufactured a thermoplastic part using both double diaphragm and matched die forming method. They found that the part formed with matched-die forming exhibits severe out-of-plane wrinkling due more restriction of the movement of the material. Indeed, due to the inextensibility of the fibres, stretching of the material along the fibres direction is not possible, precluding clamping of the laminate edges. In DDF, because the laminate is not clamped, deformation can be accommodated by trellising or shearing of the fibres, which is required to achieve full die conformity. In addition, because forming is done under vacuum, compression forces are normal to the surface of the laminate allowing a better control of fibre motions while limiting out-of-plane buckling and providing *in situ* consolidation. Also, the tensile stresses present in the diaphragm materials due to stretching reduce the compressive stresses within the laminate through interfacial friction. This eventually maintains a biaxial tension state within the laminate and prevent wrinkling. However, DDF process has some disadvantages. Due to the use of positive

pressure, DDF is typically carried out in a chamber, which results in long cycle time. This limits the use of double diaphragm to small volume production, and makes the process relatively costly. An alternative solution was investigated by Chen *et al.* [23], whereby instead of using positive pressure, a vacuum was drawn between the lower diaphragm and the tool in order to complete the forming. This method significantly reduces capital cost since it removes the need for a pressure vessel, however compaction pressure is limited to 1 bar.

2.3 Deformation modes and mechanisms

The main deformation mechanisms occurring during forming of continuous reinforcements are represented in Figure 9, and include resin percolation (i.e. in the case of prepreg material, the flow of resin travelling along or across the fibrous reinforcement, creating matrix rich regions), intraply shearing, interply slip (also referred to as interply shear), axial and transverse loading and ply bending. These different mechanisms are explained in details in the next sections.

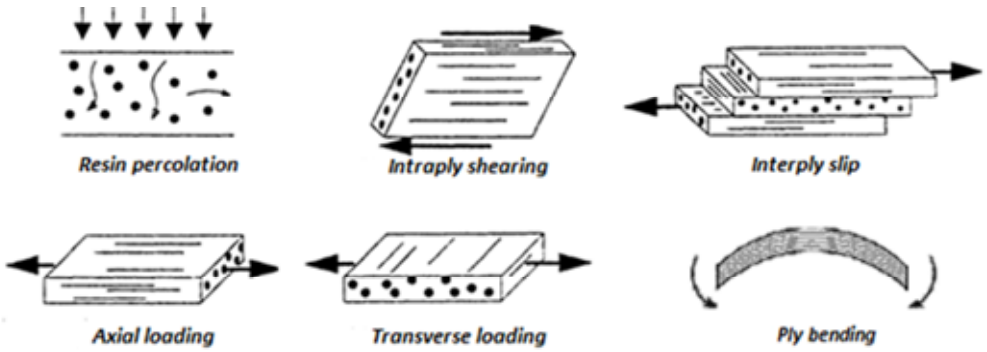

Figure 9: Forming mechanisms for continuous fibre reinforced materials – Adapted from [11]

2.3.1 Intraply shearing

Intraply shearing is one of the main deformation modes for aligned reinforcements and occurs when the material is subjected to in-plane shear [27, 28]. This shear can be induced while handling the material, or by the interaction of the material with the dies or forming diaphragms during the preforming stage. For woven reinforcements [27, 29], intraply shear is characterised by trellising or rotation of warp and weft tows at their crossovers, resulting in a change of angle between the tows, known as shear angle. This deformation mode is often conceptualised using the analytical approach known as the pin-jointed net (PJN). The

PJN model was first introduced by Mack and Taylor, [30], and assumes that: (1) the tows are inextensible with no thickness and no width, (2), warp and weft tows are free to rotate at their crossover points (i.e. as if they are pinned) without relative slippage and (3) the tows remain straight between the crossover points during deformation. Figure 10 shows a schematic representation of the PJN model.

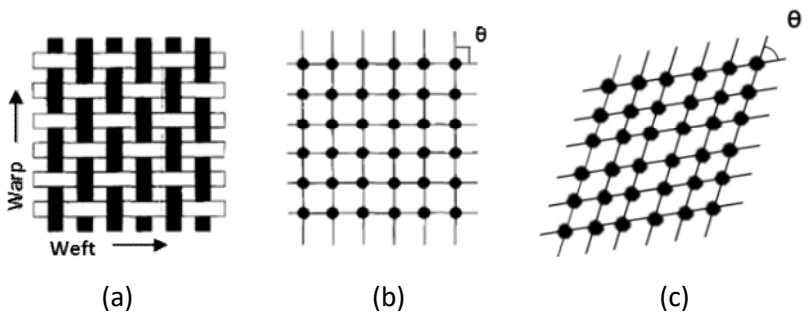

Figure 10: Schematic representation of the pin-jointed net (PJN) model. (a) Woven fabric structure, (b) Ideal equivalent representation in the initial state and (c) ideal equivalent representation after deformation

This model has been extensively used to study the drapability of woven fabrics. However, it does not take into account the relative sliding of parallel tows within a fabric layer or tow slippage that may occur during the preforming process. Shearing is typically followed by compressive forces that built-up up to a critical amount. The material will eventually deforms by buckling or out-of-plane deformation, leading to the formation of wrinkles (Figure 11), subsequent changes in the local fibre volume fraction and fibre reorientation [31, 32]. The initiation point of this phenomenon is characterised by the locking angle, which corresponds to the angle achieved between the warp and weft tows just before the onset of buckling and is accompanied by an increase in shear stiffness.

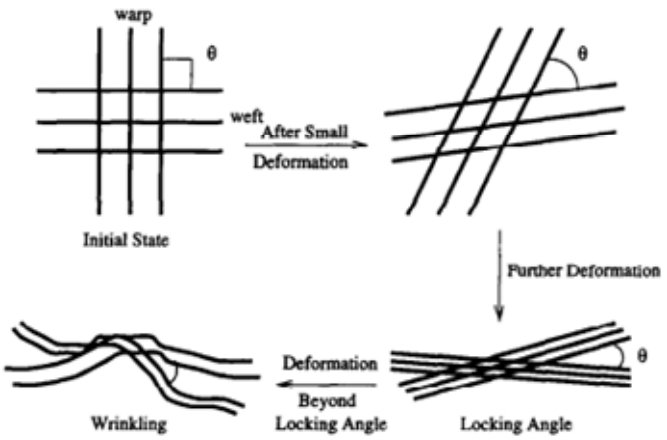

Figure 11: In-plane shear deformation of biaxial reinforcements [29]

This angle is of particular interest for forming simulation and characterisation of fabrics as it directly represents the ability of a fabric to conform to a 3D shape. Promodrou and Chen [29] demonstrated that higher friction coefficient, interply shear interaction and local reduction in global stiffness accelerate the onset of out-of-plane buckling and the formation of wrinkles. Bloom *et al*. [33] have demonstrated that in the most severe cases, wrinkles present in composite components could cause a decrease in strength of up to 40% when compared with unwrinkled components.

For UD reinforcements, the in-plane deformation mechanisms are different to those of woven materials due to their highly anisotropic behaviour. The principal characteristic of UD reinforcements is their extremely high resistance to deformation in the fibre direction. Given their high strength and high modulus, carbon fibres are generally considered inextensible. In contrast, they offer very little resistance in the transverse direction, which may lead to ply splitting during forming. To avoid this, it is essential to ensure that intraply shear becomes the dominant deformation mechanism during forming of UD materials. Intraply shear of UD is typically characterised by the relative sliding of adjacent tows. In a UD prepreg ply, these tows are separated by viscous resin, which will be sheared to accommodate the displacement of the tows. Two types of intraply shearing mechanism exist [34], namely longitudinal shearing (i.e. along the fibres) and transverse shearing. Figure 12 schematically displays the different shearing mechanisms for a UD ply. Transverse shearing is generally of less importance. Longitudinal shearing will occur when forming doubly curved parts, along with other deformation mechanisms such as bending. Typical forming defects such as wrinkles can be avoided by ensuring that longitudinal shear deformations are more important than out-of-plane ones. Therefore, a detailed understanding of each mechanism is essential.

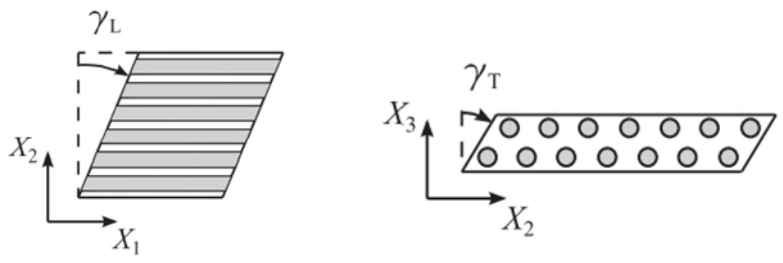

(a) (b)

Figure 12: : Intraply shear mechanism for a UD ply, (a) along the fibre direction and (b), transverse to the fibre direction – adapted from [35]

Unlike woven materials, there is no limit as to how much intraply shear can be accommodated in a UD material [36]. A similar observation was made for cross-plied UD [37, 38]. Because there are no physical connections between the orthogonal fibres, the material does not experience locking upon shearing. As a consequence, any sign of buckling in cross-plied UD prepreg is caused by compressive loads.

2.3.2 Interply slip

When preforming multi-layered prepregs, relative sliding of the plies might occur due to the presence of curved geometries. The interply friction is of great importance for multi-layered laminate, as it helps improving the forming behaviour by providing a connection between the layers but can be detrimental and introduce defects such as shape distortions and residual stresses if not properly controlled [39, 40]. In some cases, interply slip can contribute more to the formation of wrinkles than intraply shear [41]. It is generally accepted, that slip between the plies need to be encouraged in order to avoid out-of-plane wrinkling [42]. If no fluid separates the interface between two surfaces, the friction coefficient is usually represented by Coulomb friction:

$$F_f \leq \mu N \tag{2.1}$$

Where F_f is the friction force, or tangential force exerted by each surface on the other, μ is the coefficient of friction and N is the normal force. This equation is true for dry surfaces but becomes limited when fluids are present between the surfaces. In that case, a thin fluid film separates the surfaces, and the friction behaviour can be estimated by a hydrodynamic model, where the friction is characterised by the traction force acting on the film [43].

$$\tau = \frac{\eta}{d} v \tag{2.2}$$

Where τ is the shear stress, η is the viscosity of the fluid separating the two surfaces, d is the film thickness and v is the relative speed between the surfaces. However, for prepreg, this equation is not fully accurate due to the coexistence of two lubrication modes. There exist some areas with asperity contacts where surfaces are separated by a thin film of molecular thickness permitting momentary dry contacts, known as boundary lubrication, and other areas with lubricating film contact, known as hydrodynamic lubrication. In addition, this model does not account for influential factors such as temperature, normal pressure fibre orientations and fibres intermingling. Several studies [40, 44] have modelled

this phenomenon through the Stribeck theory. The Stribeck theory was initially developed to describe the friction properties between two surfaces in relation to the sliding rate, lubricant viscosity and bearing pressure. Figure 13 shows a typical Stribeck curves, which plots the coefficient of frictions against the Hersey number given as:

$$H = \frac{\eta v}{p} \tag{2.3}$$

Where η is the dynamic viscosity of the film, v is the velocity at the contact surface and p is the pressure. This theory categorises the lubrication mode in three areas, the first one is governed by dry boundary condition, the second is a mixed mode friction and the third is hydrodynamic region.

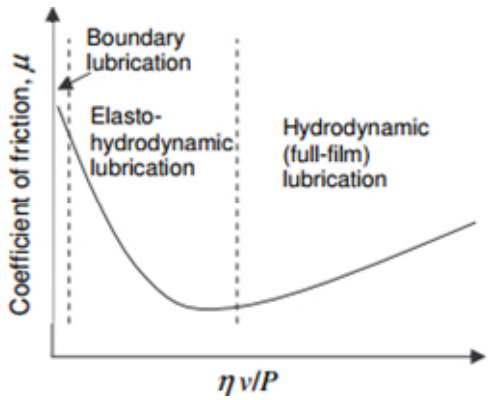

Figure 13: Typical Stribeck curve showing the different lubrication regimes

2.3.3 Out-of-plane bending

Out-of-plane bending is an important parameter in composite forming and cannot be obtained from the in-plane properties as is the case for continuous materials [45]. Bending rigidity has often been neglected in finite element simulation due to values significantly lower than the in-plane properties of fabric reinforcement. For these reasons most FE models are based on membrane approaches [46-48] where the bending stiffness is not taken into account. However, recent studies have demonstrated the importance of bending properties during forming and especially their influence on the out-of-plane deformations [39, 49]. When subjected to small compressive loads, a fabric reinforcement will tend to buckle and start wrinkling as the bending strain energy becomes lower than the decrease of compression strain energy. An increase in the reinforcement bending stiffness will lead to less but bigger wrinkles while a lower bending stiffness will lead to more but smaller

wrinkles (Figure 14), which is generally preferable when surfaces with high curvatures are involved [50]. One solution to overcome compressive loads is the use of blank holders, which impose a tension on the preform and consequently reduce the formation of wrinkles [51].

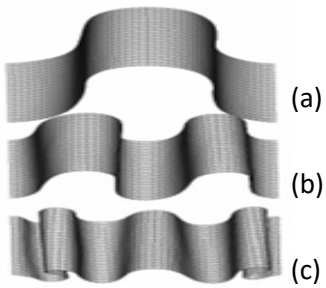

Figure 14: Wrinkles due to compressive force, and the influence of bending rigidity: (a) High rigidity, (b) medium rigidity and (c) low rigidity [39]

Typical compression force versus displacement curves show an initial peak load corresponding to the initiation of buckling followed by a small decrease and then a plateau in the force. Unlike woven prepreg, unidirectional prepregs do not exhibit a plateau but show a non-linear decrease of the force as the displacement increases, suggesting that the fibre architecture affects the bending stiffness. For dry textiles, no rate dependency on bending stiffness has been observed.

2.3.4 Transverse loading

Transverse loading can also be referred to as transverse flow, where the matrix and fibres move together. Resistance is relatively small compared to axial loading. It is specific to unidirectional reinforcements and occurs when the load is applied perpendicularly to the fibre direction. Deformations are possible until fibre splitting. On a single ply, very low loads are required to reach the onset of transverse splitting. However, the situation is different in reality as most lay-ups have more than one fibre direction. Therefore, off-axis plies limit the extent of transverse deformation of neighbouring plies due to their inextensibility.

2.4 Parameters influencing the formability of prepreg reinforcements

Depending on the forming process used, whether it is manual or automatic, many parameters are involved and affect each of the aforementioned deformation mechanisms. Irrespective of the material used, its form, the fibre architecture and properties, it is necessary to understand and control the effect of these parameters on the formability of a reinforcement in order to optimise the forming process. The next section will provide a detailed description of the different parameters and how they influence the formability of reinforcements.

2.4.1 Material properties

Both the fibre types and the architecture affect the formability of reinforcements, irrespective of their form. The forming behaviour of prepreg materials is generally more complex than that of woven fabrics due to the presence of resin. The formability of prepreg is highly influenced by the uncured properties, which are mainly dependent on the fibres type, the thickness of the ply, the resin compound, the fibre volume fraction, the degree of impregnation, the level of consolidation and the viscosity of the matrix [52-54]. Previous work [55] has shown that the matrix viscosity affects the bending stiffness, highlighting the important role of the matrix in the bending behaviour of prepregs.

2.4.2 Temperature

Temperature is a paramount parameter when forming prepreg materials. It has been shown [56], that increasing the temperature is one of the most effective approaches to reduce wrinkling and facilitate forming of a stack of prepreg plies. Forming at higher temperature significantly helps reduce the characteristic springback phenomenon that occurs at room temperature due to the presence of viscoelastic resin. In addition, when increasing temperature, the friction coefficient between two plies decreases until it reaches a minimum [57]. However, upon further heating it increases again as a result of viscosity changes. As the temperature increases, the resin viscosity becomes too low to

build up a sufficiently thick film and maintain the surfaces apart, which results in higher friction coefficients.

2.4.3 Forming rate

Wang *et al*. [55] demonstrated that for woven carbon/epoxy prepreg, the bending stiffness is rate dependent, with higher stiffness obtained when forming at higher speed suggesting that this deformation mode is dominated by flow of the polymer between the layers. In addition, Larberg *et al*. [58] have stated that the formability of prepreg materials depends on the strain rate due to their viscoelastic nature. As the forming speed increases, higher forces are necessary to shear the resin, which results in higher frictional resistance. Generally a decrease in forming speed reduced the formation of wrinkling [56]. For dry fabric material however, no strain rate effect on the forming behaviour has been observed [59].

2.4.4 Lay-up sequence

The lay-up sequence has an effect on both the in-plane and out-of-plane properties of unidirectional prepreg reinforcements. Larberg *et al*. [54] have demonstrated through bias extension test using different lay-ups i.e. $[45/-45/90]_n$ and $[45/90/-45]_n$ that even though having the same global ply orientations, two different stacking sequences can have a significantly different shear behaviour. The former lay-up allows to reduce the required shear resistance to forming through the ±45° interface which enables higher degree of intraply shear and therefore reduced the deformation resistance. The latter lay-up showed a much higher shear load-deformation response as a result of the separation of the ±45° plies. Adding a 90° ply in between the ±45° prevents the fibres rotation and subsequently results in higher shear load, thereby increasing the resistance to forming. This is in accordance with Åkermo *et al*. [60] who have shown that ±45° interface offers the lowest resistance to deformation compared to other fibre lay-up angle. Reducing the fibre angle lay-up (e.g. ±30°) and/or adding one ply in the transverse direction results in higher degree of slippage and higher resistance.

In addition, optimisation of the lay-up sequence can reduce out-of-plane defects. Hallander *et al*. [61], stated that [0/90] and [-45/45] UD prepreg lay-ups are less sensitive to out-of-

plane defects compared to a quasi-isotropic lay-up and any attempt to promote material shear will result in lower deformation resistance.

Recent studies on the interply friction [57], showed that the relative fibres angle at the interface between two plies affect the interlaminar slippage behaviour. [0/90] and [0/0] interfaces show friction coefficient generally 25% lower when compared to [0/45] and [0/30] interfaces.

2.4.5 Normal pressure

Previous studies on both fibrous [62] and prepreg materials [53, 57], have demonstrated that normal pressure affects the friction behaviour, with increasing pressure leading to compression and reduction of the roughness of the plies, resulting in lower friction coefficient. However, upon further increasing the pressure, no further compaction is possible and the friction coefficient reaches a plateau, in agreement with the definition of boundary conditions.

2.4.6 Aging of material

Aging of the prepreg, or in other words the time that the material is thawed and kept out of freezer at room temperature strongly influenced the prepreg forming behaviour. Larberg *et al*. [58], have reported a twofold increase in the load when comparing bias extension results after four days at room temperature with tests done day two. While Wang [63], reported a 300% shear resistance increase when comparing 6-day aged with 2-hour aged material. This stresses the importance of rigorous control on the aging history of prepreg materials. Aging noticeably changes the material properties, among which the resin viscosity, which tends to increase with the life of the prepreg [56].

3 Modelling of composite forming processes

Forming simulations are used to assist in the product development process. These methods allow to predict defects that may occur during forming (e.g. wrinkling, ply splitting) limiting the need for expensive practical tests, while reducing the development process time. In addition, it is possible to predict the orientation of the fibres of the final part, which can then be used for subsequent stress analysis. It is also possible to investigate the effect of process parameters (i.e. temperature, forming speed, boundary conditions…) on the formability of the composite materials.

To date there exist two different simulation approaches for composite forming, namely the kinematic mapping approach and the mechanical approach [10]. The former method is based on geometric approach and provides a quick and relatively efficient method in many draping cases, but does not take into account mechanical properties or boundary conditions. The mechanical approach however, requires a thorough mechanical characterisation of the material and can replicate the boundary conditions prescribed by the forming process. This approach is computationally intensive but provides accurate prediction of the deformations occurring during the forming process. Both method have been benchmarked previously [64, 65]; and are explained in the next sections.

3.1 Kinematic mapping approach

Kinematic approach based on geometry was developed decades ago in order to understand the draping of woven fabrics over curved surfaces and has been widely used in the composite industry since. These methods of draping essentially consist of fitting a flat layer of fabric, represented by a square mesh onto a surface using mapping techniques. Assuming the PJN assumptions (section 2.3.1), Mack and Taylor [30], in 1956 , developed an analytical model based on differential equations to determine the fibre redistribution of a fabric draped onto simple surfaces of revolution. Figure 15 shows an illustration of the kinematic mapping approach. The position of the node 3 can be determined from the position of its neighbours 1 and 2. Assuming that the lengths a and b are fixed, the solution to the draping of point 3 is equivalent to solving the equation that describes the intersection between two spheres (i.e. one sphere of centre *1* and radius *a* and another of centre *2* and radius *b*) and the surface. The two spheres correspond to all possible positions of the ends of a warp and weft pivot.

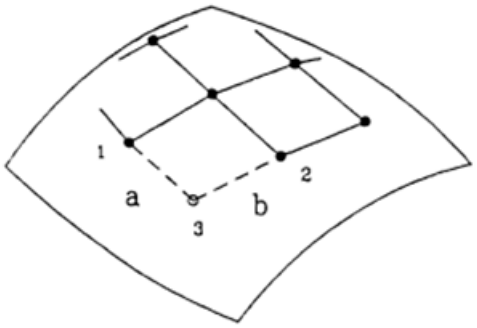

Figure 15: Illustration of the kinematic mapping approach [11]

Let x_i, y_i and z_i be the coordinates of the points, and *F* the surface equation. The draping of point 3 onto the surface *F* can then be determined by solving the following equations:

$$\left(x_3 - x_1\right)^2 + \left(y_3 - y_1\right)^2 + \left(z_3 - z_1\right)^2 = a^2 \tag{3.1}$$

$$\left(x_3 - x_2\right)^2 + \left(y_3 - y_2\right)^2 + \left(z_3 - z_2\right)^2 = b^2 \tag{3.2}$$

$$F\left(x_3, y_3, z_3\right) = 0 \tag{3.3}$$

3.2 Mechanical approach

Modelling of the forming process based on mechanical approach is relatively recent and was introduced to model the effects neglected in the kinematic mapping approach, i.e. material behaviour and process boundary conditions. Given that, much effort has been devoted to the development of new constitutive equations and material models in the past decades. The mechanical approach is based on finite element (FE), which requires the discretisation of the domain into finite elements that are connected by nodes. FE requires modelling the tools, the laminate, the contacts and friction between the different objects and the mechanical behaviour. The mechanical behaviour of composite reinforcement is often referred to as multiscale problem, i.e. the behaviour of the fabric (macro-scale) is highly dependent on the structure of the tows (meso-scale) which are themselves composed of fibres (micro-scale). Therefore when modelling a fabric material, different approaches can be used depending on the scale at which the analysis is done: The continuous approach consider the fibrous reinforcement as a continuum and

homogeneous material while the discrete approach represents each different tow. Although some microscopic analysis have been performed [66], the extremely large number of fibres within a tow make it impractical to model a complete part. Microscopic approaches are limited to the analysis of complex technical fabrics such as knitted fabrics and are not treated in this project. An alternative method to the continuous and the discrete approach is the combination of both and is referred to as semi-discrete approach. These different approaches will be detailed in the next section.

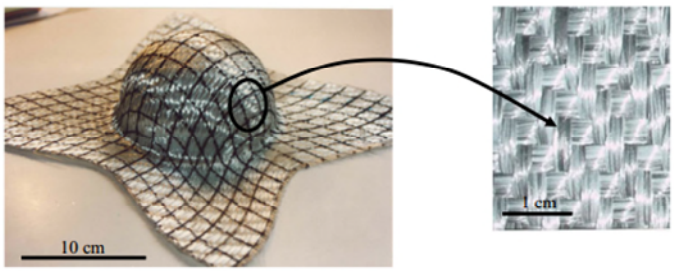

Figure 16: Macroscopic (left) and mesoscopic (right) scale of composite reinforcement [67]

3.2.1 Continuous approach

At a macro-scale level, fabrics can be seen as a continuous medium having high anisotropy and the ability to experience very large shearing and bending deformations. Assuming a continuous material means neglecting all interactions at a meso and micro-scale level, i.e. relative sliding and friction between tows and fibres. While these mechanisms occur, they are generally negligible at a macro-scale level and can be averaged out. Although fabrics are discontinuous medium at lower scale, the continuous approach has proven to be successful in many cases, most likely because it can easily be implemented in standard commercial FE codes – using continuum mechanics theory - via subroutines (as e.g. ABAQUS, LS-DYNA, PAM-FORM, ANIFORM). These sub-routine update the stress-strain state in an objective material frame, i.e. invariant with respect to a change of observer. In continuum mechanic, a fundamental quantity is the deformation gradient, i.e. the quantity that maps the initial undeformed configuration onto the current deformed configuration. The polar decomposition of the deformation gradient tensor can be expressed as:

$$F = R.U \tag{3.4}$$

With F the deformation gradient, R the rotation tensor and U the right stretch tensor. A schematic representation of the polar decomposition is shown Figure 17. The initial

undeformed material is stretched and then rotated, or vice versa. Note that U and V express similar quantities but are symmetric tensors. V is referred to as the left stretch tensor.

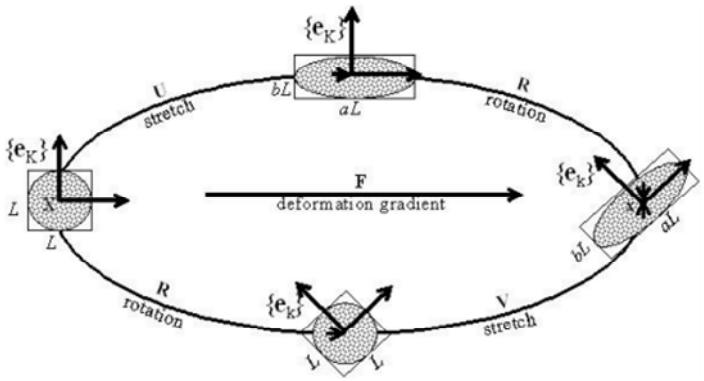

Figure 17: Schematic representation of the polar decomposition of the deformation gradient [68]

For non-linear, large strain analysis where significant rigid body rotation occurs, a co-rotational frame is typically employed and consists of a single-element frame that continuously rotates with the different elements [69]. One common approach is to use the Green-Naghdi formulation that uses the rotation tensor R from the polar decomposition above. Also known as Green-Nagdhdi objective derivative, this method is routinely used for the analyses of metal at finite strains [70]. It is a built-in user sub-routine within ABAQUS, to define material behaviour. Using the polar rotation is not well suited for fibrous materials under large strain, particularly because the tensor R is orthogonal and cannot be used to update the material orientation. During forming, the fabric can undergo large in-plane shearing, resulting in non-orthogonal orientation of the fibres. Much work has been done on the development of constitutive models that can represent the specific mechanical behaviour of fibrous reinforcements, which mostly depends on the fibre orientation, see for e.g. [71-73]. An accurate constitutive model should be able to track precisely the individual fibre directions, as they change during forming. To date, there is no widely accepted model that can describe all the important mechanical aspects of fabrics. Typical constitutive models can be classified into two categories: elastic (e.g. hypoelastic [74] and hyperelastic) and viscous-based material models (e.g. visco-elastic [75]). Constitutive models are then typically implemented within an explicit or implicit FE codes.

3.2.2 Discrete and semi-discrete approaches

An alternative to the continuous approach consists in modelling the components of the fibrous reinforcement at a lower scale, e.g. at the mesoscale. This method is also referred to as meso-model or meso-mechanical modelling, where each fibre, yarn, and also stitch can be individually modelled. Ben Boubaker *et al*. [76], proposed a discrete model of a woven structure where the fabric is represented as an orthotropic structure whose principal directions coincide with the warp and weft direction. The unit cell is being modelled by four extensible bars, represented by springs with rigidity C_{ex} which are connected at frictionless hinges. Each node possesses a mass *m* and a rotational rigidity C_b allowing rotation around the *x* and *y* axis. A set of other springs is used to describe stretching, shear and bending. The mechanical parameters of the trusses are the rigidity modulus in the warp and weft direction (i.e. E_1 and E_2), the shear rigidity G and the contraction coefficient in the warp and weft direction (i.e. ν_1 and ν_2). A representation of the model is shown Figure 18.

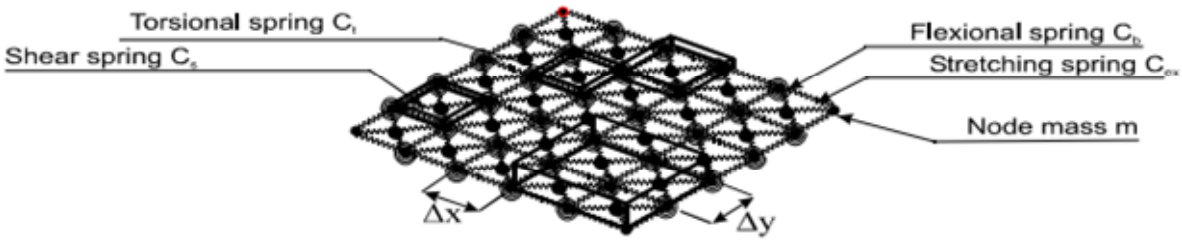

Figure 18: Discrete model of a textile reinforcement [76]

The equilibrium shape of the fabric is obtained by minimising the total potential energy of the structure, taking into account the kinematic constraints. Draping simulation over a square table and a portion of a sphere was performed. The model showed a good accuracy and a promising way of modelling deformation mechanisms at the mesoscopic scale. However, because of the extremely large numbers of fibres within a composite structure, the discrete approach is generally limited to small domains (i.e. a representative unit cell or a knitted loop). Larger domains would need oversimplifications of the model, at the expense of accuracy. For these reasons only small elements have been successfully modelled to date [77].

An alternative approach is the semi-discrete method and is a compromise between the continuous and the discrete approach. Hamila and Boisse [48], proposed a new semi-

discrete model for the simulation of composite reinforcement draping. Unlike the discrete approach where the strain energies of each component (i.e. yarns, fibres, unit cells) are calculated, the semi-discrete approach use finite elements. The kinematic and strains of those components at a micro and mesoscale is prescribed by the nodal displacement of the finite elements. Therefore, a degree of continuity is assumed within the elements, i.e. there is no relative translation sliding between warp and weft and two adjacent warp and weft stay superimposed throughout the whole draping. This was experimentally demonstrated in [78]. In the proposed approach, only the most dominant mechanical properties are taken into account (i.e. in-plane shear rigidities and fibre tensions), and are obtained based on classical experimental textile testing (tensile and bias extension). This approach is a compromise between the continuous and the discrete approach: it avoids the need for the determination of an equivalent continuous mechanical behaviour while reducing the computational time. Interactions between warp and weft and phenomenon such as uncrimping due to tensions are not taken into account. This is however well adapted for NCFs materials. Hamila *et al*. [79], later extended their approach to take into account the bending stiffness using shell elements in combination with the previously developed membrane approach. Hemispherical forming of an unbalanced 2x2 twill was performed and compared with a numerical model implemented in an explicit scheme (Figure 19). It can be seen that the simulation captures the deformation and that the formation of wrinkles is well predicted.

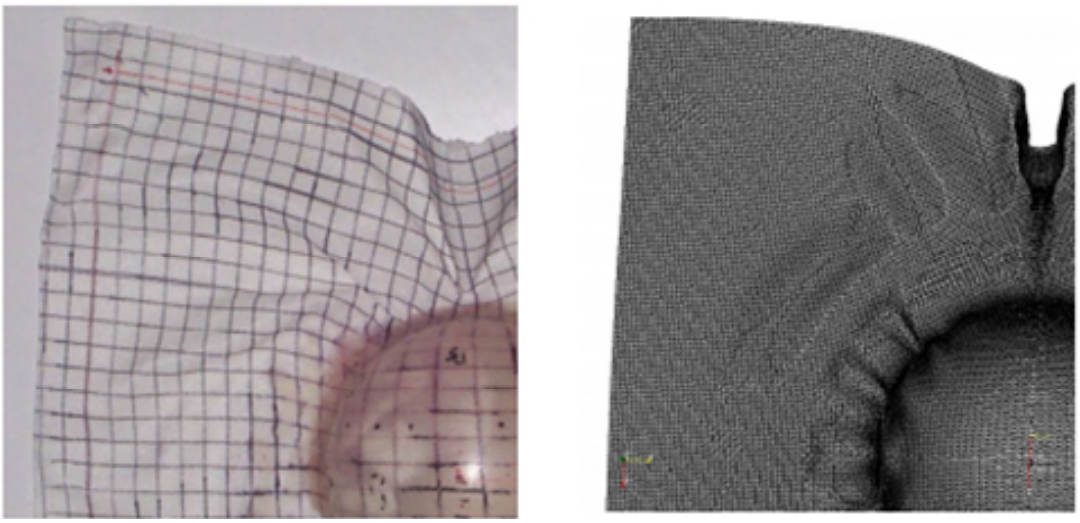

Figure 19: Hemispherical forming of an unbalanced fabric (left) experimental (right) simulation [80]

3.3 Identification of research opportunities

Within this project, the simulation approach should be able to model a complex forming process, within a reasonable computational time. Although discrete and semi-discrete approaches offer a promising way of modelling the forming process of composite materials, they are not mature enough to suit current automotive requirements. Multi-purpose FE packages (e.g. ABAQUS, LS-DYNA) for the simulation of composite forming offer great versatility and are supported by an extensive literature, however, the development of user-defined modelling approaches make their use relatively cumbersome. Therefore, the use of a dedicated commercial software for composite forming simulation seems a more viable solution. The software selected during this project is PAM-FORM, developed by ESI GROUP. The software is described in details in section (9.1). The use of a commercially available software was preferred over a multi-purpose FEA package principally due to: (1) a dedicated customer support, (2) the pre- and post-processing tools in a user-friendly graphical interface, (3) the presence of built-in material models for both UD and woven materials.

4 Materials and test parameters

This chapter gives a description of the materials, which have been used throughout this project and form the basis of the work presented thereafter in chapter 5 through to chapter 10.

4.1 Materials investigated

The material investigated during this project includes a woven and a unidirectional thermoset prepregs, as well as a polymeric diaphragm. Material properties are given in the following sections.

4.1.1 Carbon fibre thermoset prepregs

The woven prepreg used during this project is a commercially available 2x2 twill weave carbon/epoxy prepreg, with a fibre areal weight of 400 g.m-2, a 12k tow-size and a resin content of 40% by weight. The properties of the woven prepreg are listed in Table 2. The material is specifically designed for compression moulding and high-volume, automotive applications. Typical curing time is 5 minutes at 140°C but can be adjusted depending on the moulding temperature.

Reinforcement	Carbon fibres 2*2 twill
Tow size	12k
Thickness (mm)	0.44
Matrix	Epoxy
Resin content (wt%)	40
Fibre areal weight (g.m^{-2})	400
Prepreg areal weight (g.m^{-2})	667

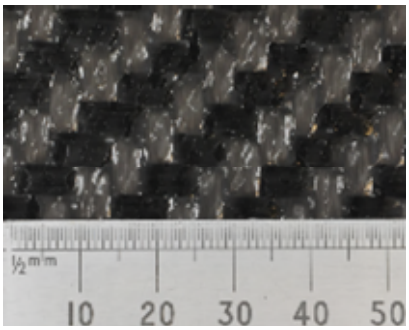

Table 2: Properties of the woven carbon fibre thermoset prepreg investigated

The UD prepreg investigated is a carbon fibre prepreg, with a fibre areal weight of 250 g.m-2, a 15k tow-size and a resin content of 30% by weight. The properties of the material are listed in Table 3. Both prepregs are based on the same epoxy rapid cure thermoset resin

system and are particularly attractive for Aston Martin due to a relatively short cycle time combined with the high specific mechanical properties of continuous carbon fibres.

Reinforcement	Carbon fibres UD
Tow size	15k
Thickness (mm)	0.226
Matrix	Epoxy
Resin content (wt%)	30
Fibre areal weight (g.m^{-2})	250
Prepreg areal weight (g.m^{-2})	357

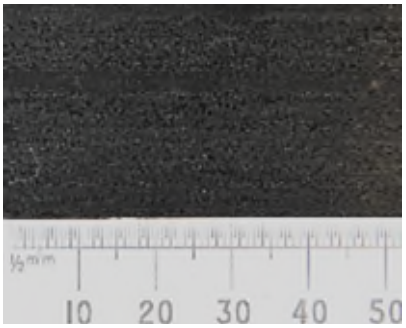

Table 3: Properties of the UD carbon fibre thermoset prepreg investigated

UD prepregs have unique advantages over woven prepregs. They offer highly tailorable properties, characterised by the possibility to adjust the orientation of each ply within the laminate, therefore providing strength in directions where it is most needed and ultimately reducing part weight. In addition, UD reinforcements are less expensive than other reinforcement types, since no stitching or weaving process is required in their manufacturing process. This can however be offset by a high material waste (i.e. resulting from a reduced material utilisation) when orientating plies at non-standard angle. In addition, it is generally accepted that the formability of UD reinforcement is far inferior to that of woven fabrics due to high anisotropy and poor mechanical properties of the material in the transverse direction.

Woven reinforcements however, possess excellent drapability, resulting from their ability to deform through shear by the relative movement of weft and warp at their crossovers. As such, woven materials are always seen as the standard against which formability of other reinforcements is assessed [42]. From a formability standpoint, the woven material will be used as a benchmark in the current study.

4.1.2 Initial thermoset resin characterisation

Awareness of the cure kinetics of the epoxy resin is important in order to define the operating temperature of the preforming process. This is particularly true for rapid-curing thermoset resins, which present unique challenges due to their fast-curing rate. During the preforming process, it is essential that the interaction between time and temperature on the curing kinetic be accurately controlled. Higher preforming temperatures are desirable

in order to reduce the resin viscosity and therefore facilitate the deformation of the laminate (Figure 20).

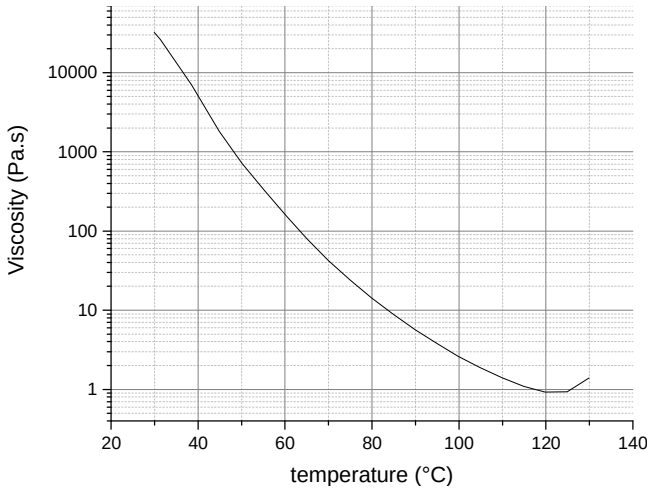

Figure 20: Variation of the epoxy resin viscosity as a function of temperature

However, temperatures above resin cure onset initiate resin-hardener cross-linking, leading to an increase in the molar mass and the resin viscosity and consequently, limiting the formability of the material. As a result, preforming time and temperature is critical. Although short cycle times are required to increase throughput, excessive deformation rates may result in extreme forces required to shape the material and therefore, increase the occurrence of defects such as wrinkles.

An initial analysis of the resin was carried out in order to investigate the time-temperature dependence of the epoxy resin and define the limits of the preforming process conditions. Differential scanning calorimetry (DSC) of the material was performed. A temperature ramp from 25°C to 250°C using a heating rate of 10°C.min^{-1} was performed in order to derive the exothermal energy released per unit mass of resin mixture during the cure process. The results are displayed in Figure 21 and show the heat flow against temperature. The maximum enthalpy in J.g^{-1} (i.e. normalised to the specimen weight) is calculated by integrating the heat flow with respect to time and corresponds to the area under the peak. A value of 94.15 J.g^{-1} is obtained and represents the total energy released by the resin to achieve complete cure. This value can then be compared against the residual enthalpy of samples that have previously undergone a heating cycle. The ratio of the residual enthalpy to the total reaction enthalpy yields the degree of cure. The degree of cure of different specimens was calculated as per BS EN ISO 11357-5:2014 [81], after various isothermal cycles (i.e. 80°C and 110°C for 2, 3 and 4 minutes) used to simulate the preforming process.

The residual enthalpy of each specimen was measured using a temperature ramp and compared to the total reaction enthalpy.

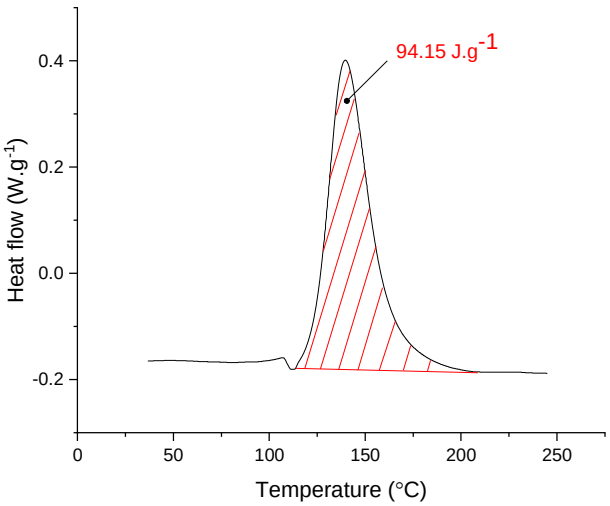

Figure 21: DSC scan of the uncured epoxy resin

The degrees of cure obtained (in percent) are reported in Figure 22, and shows that as expected, higher temperatures accelerate the curing process. At 110°C, the cross-linking reaction starts under two minutes, while at 80°C, the reaction starts under four minutes.

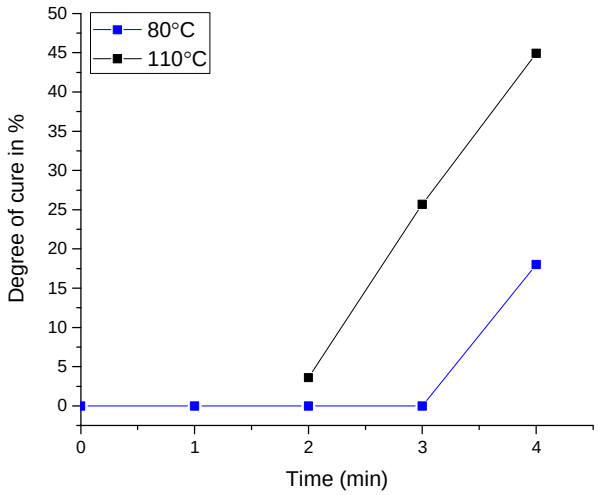

Figure 22: Degree of cure after different isothermal cycles

During forming, it is often preferable to delay the onset of cure as much as possible since curing of the resin increases the shear and the bending rigidity, thereby reducing the formability of the material. As a consequence, the preheating temperature was set to 80°C in the present study. To replicate these conditions, characterisation tests were also performed at 80°C. Although the forming process is non-isothermal (i.e. the blank is preheated to a temperature of 80°C before being transferred between matched tools at

150°C), it was demonstrated that forming of the blank occurs at a temperature of 80°C (section 10.1).

4.1.3 Diaphragm material

The material considered is a 50 µm thick, high-elongation, high temperature resistant ETFE (Ethylene tetrafluoroethylene) release film. The material is manufactured by Tygavac Advanced Materials Ltd. and is commercialised under the name Wrightlon® 5200. The properties of the material are listed in Table 4.

Material	ETFE (Ethylene tetrafluoroethylene)	
Thickness (µm)	50	
Elongation at break	350 %	
Max operating temperature (°C)	260	

Table 4: Properties of the diaphragm material

The mechanical properties of the diaphragm were investigated through tensile tests and were performed using grips specifically designed for thin materials. One grip was connected to a 500 N load cell, mounted onto the crosshead of the tensile testing machine, while the other grip was fixed. A 25 mm wide specimen was used, with an effective length between the grips of 50 mm as per BS EN ISO 527-3:1996 [82], for high elongation materials. Strain was recorded using a biaxial video-extensometer. The longitudinal and transverse gauge lengths were 25 an 12.5 mm, respectively. Tensile tests were performed at 80°C using different crosshead speeds (i.e. 1 and 8.33 $mm.s^{-1}$), along both the longitudinal and transverse orientations of the material. Results are reported in Figure 23. Although a slight difference was observed in the load obtained in the longitudinal and transverse direction (approximately 16%), an isotropic behaviour was considered. Similarly, the effect of speed has little effect on the tensile behaviour (Figure 23,b) of the diaphragm material, revealing a shear-rate independent behaviour.

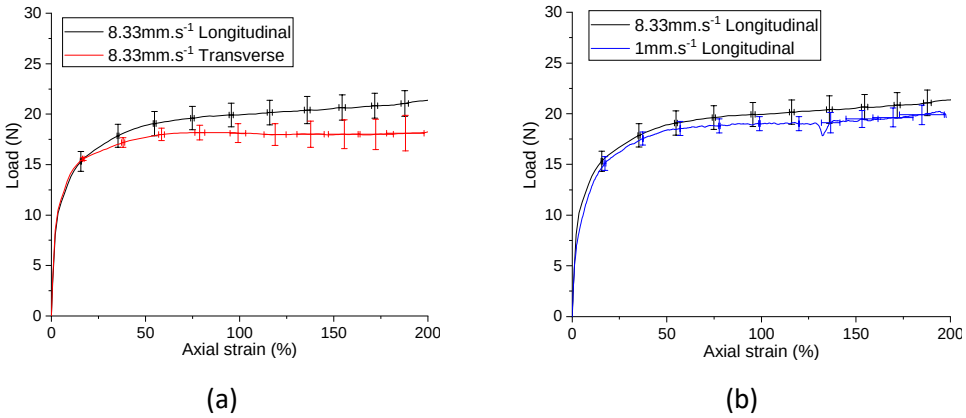

Figure 23: Load-strain curves from tensile test of diaphragm material showing the effect of specimen orientation (a) and speed (b).

4.2 Test parameters investigated

The influence of process conditions plays an important role one the forming behaviour of thermoset prepreg materials. When characterising materials for numerical simulation purpose, it is important to replicate these conditions so that consistency is maintained between the forming process and the simulation. This section will describe the parameters that were selected for each test variable.

4.2.1 Deformation rate

During forming, the deformation rate is directly related to the tool closing speed and plays an important role in the formability of thermoset prepreg. Most recent studies on the forming behaviour of thermoset prepreg materials report test results performed with a crosshead speed typically ranging from 1 to 100 $mm.min^{-1}$ [37, 53, 83], which are not applicable to high-volume processes. In this work, tests were performed with a maximum crosshead speed of 500 $mm.min^{-1}$ (i.e. 8.33 $mm.s^{-1}$, corresponding to the maximum speed of the Instron 5900) in order to simulate conditions representative of high-volume manufacturing processes.

4.2.2 Pre-compaction

Forming of prepreg thermosets typically requires a preheating stage prior to shaping the laminate into its final 3D shape. This stage is essential in order to help soften the matrix and reduce the amount of force required to deform the material. Preheating of the

laminate is carried out at a temperature high enough to lower the resin viscosity but low enough to delay the curing reaction which would reduce the formability of the prepreg. In this present work, a preheating temperature of 80°C is used. In addition, a vacuum is drawn between the two diaphragms, where the laminate is placed. Consequently, the preheating stage can essentially be likened to a debulking process, during which the material structure (i.e. the material compaction and the impregnation level), as well as its mechanical behaviour is likely to change from its initial condition. This is particularly true for fast cure out-of-autoclave woven prepregs, which are typically characterised by their partial impregnation, in that resin is only applied onto both outer surfaces of the prepreg, leaving the centre relatively dry and porous [84]. In order to understand the effects of the preheating stage on the material structure, scanning electron microscopy (SEM) micrographs of the cross-section of the uncured woven and UD prepreg in their as-received state and following vacuum bagging were analysed. The materials were vacuum bagged under 1 bar pressure at 80°C for 2 minutes in order to replicate the conditions obtained during the preheating stage of the forming process. SEM specimens were imaged using a Sigma Zeiss FEG SEM under InLens imaging mode with a 20 kV accelerating voltage. Samples were placed on an aluminium stub coated with adhesive carbon tape and held vertically using mounting clips to image the cross section of the specimen. Samples were sputter coated with Pd/Au prior to imaging.

Figure 24 shows the cross-section micrographs of a woven ply in its as-received state (Figure 24, a) and following vacuum bagging (Figure 24, b). In its as-received state, the woven prepreg shows a thick layer of resin on either side of the ply (locations 1 and 2 in Figure 24, a). In addition, the lack of consolidation between the warp and weft fibres (locations 3 and 4, respectively, in Figure 24, a) reveals dry fibres underneath the cross-sectional surface (location 5 in Figure 24, a), sign of a poor resin impregnation through-the-thickness. In contrast, once vacuum bagged, the woven prepreg exhibits a more uniform structure with a more uniform resin distribution and impregnation through-the-thickness (Figure 24, b). Compaction is greatly improved between warp and weft tows, with a clear limit between them characterised by a resin-rich interface (location 6, in Figure 24, b). In addition no significant voids can be observed.

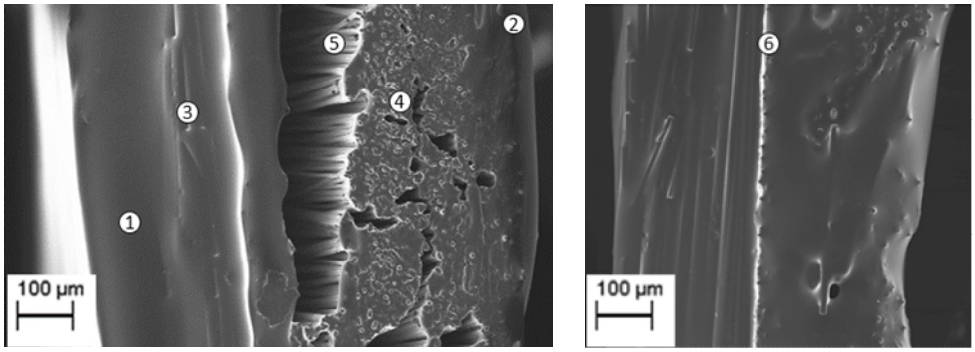

(a) (b)

Figure 24: SEM micrographs of the cross-section of the woven prepreg (x150): (a) in its as-received state, and (b) after vacuum bagging under 1 bar pressure at 80°C

Figure 25 shows the cross-section micrographs of the UD prepreg before (Figure 25, a) and after compaction (Figure 25, b). Unlike the woven prepreg, the UD material shows a more uniform resin impregnation in its as-received state. Although a slightly greater resin content in either side of the specimen (locations 1 and 2 in Figure 25, a), and a lack of compaction (location 3 in Figure 25, a) can be observed, no dry fibres are visible, indicating complete impregnation. A similar structure is observed after vacuum bagging (Figure 25, b).

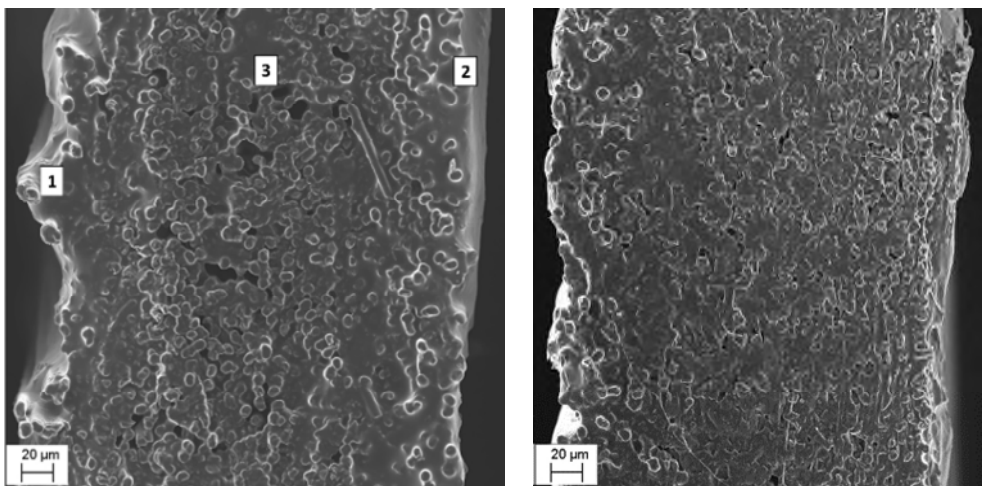

(a) (b)

Figure 25: SEM micrographs of the cross-section of the UD prepreg (x250): (a) in its as-received state, and (b) after vacuum bagging under 1 bar pressure at 80°C

4.2.3 Normal pressure

Normal pressure plays an important role on the frictional behaviour of prepreg materials. The dynamic of the preforming stage and the global lack of cohesion between plies makes it challenging to measure the pressure within the blank during preforming. In addition, the normal pressure during preforming is highly non-uniform on the surface and within the

blank and will vary significantly depending on the tool design features (i.e. sharp radii). During the 13th edition of ESAFORM conference (European Scientific Association for Material Forming), a benchmark study between five different research groups on friction testing of composite reinforcements was proposed [85]. The benchmark study is based on the ASTM standard D1894 [86], and accounts for several parameters among which the normal pressure. Normal pressure of 10, 40 and 100 kPa were prescribed. For the present study, in order to replicate both current practices and the conditions expected during 3DF, normal pressure of between 25 kPa and 200 kPa were investigated.

5 Intraply shear characterisation of thermoset prepreg

This section presents the results from characterisation of the intraply shear properties of prepreg materials. First, the development of a novel shear angle measurement method is introduced. Then intraply shear characterisation of both woven and UD prepregs carried out under forming conditions is presented. This is supported by shear angle measurement using the novel method. Because they exhibit different shear deformation mechanisms, both woven and UD materials will be treated in different sections.

5.1 Development of a novel shear angle measurement method [i]

Determining accurate in-plane shear properties of fabrics and prepregs is largely dependent upon the correct measurement of actual shear strain. It was demonstrated in [87] that upon deformation, dry and prepreg biaxial reinforcements behave almost entirely like a PJN (section 2.3.1), provided that the blank size is considerably greater than the warp and weft tow size. As a consequence, it is common practice to determine the shear angle (i.e. the angle variation between the warp and weft tows) using equations based on geometrical considerations [88]. However, for large deformations, the PJN assumptions are no longer valid since the actual material shear angle deviates from the theoretical one [89]. This phenomenon is caused by inter-tow slippage at higher shear angle. As a consequence, an accurate measurement method must be employed when characterising the in-plane shear behaviour of reinforcements.

Although there exist different method such as image analysis [88, 90], specific bespoke algorithms [91, 92] or digital image correlation (DIC) [93, 94], none of them are well suited for the determination of shear angle of thermoset prepreg materials when tested at high rate and elevated temperature. An example of image analysis and the use of a bespoke algorithm is shown in Figure 26. While image analysis methods are subject to human error and only provide a local shear angle, the use of bespoke algorithms is generally restricted

[i] **This section is partly reproduced from: C. Pasco, K, Muhammad, K, Kendall. A novel discrete-method of shear angle measurement for in-plane shear properties of thermoset prepreg using a point tacking algorithm. Journal of Composite Materials, 2019, 53(14), 2001–2013.*

to their developers. DIC has been successfully applied for the measurement of shear angle during bias extension test of dry reinforcements [93, 94], and more recently with prepreg materials [37], however with partial success. Personal attempts have also been unsuccessful, due to reflection of external light against the window of the thermal chamber and the glossy resin of the specimen. In addition, a significant loss of data points was observed at large shear angle due to excessive compaction of the adjacent tows, resulting in excessive disruption of the speckle pattern required for DIC analysis. This addresses the need for an alternative method for shear angle measurement during in-plane shear test of thermoset prepreg.

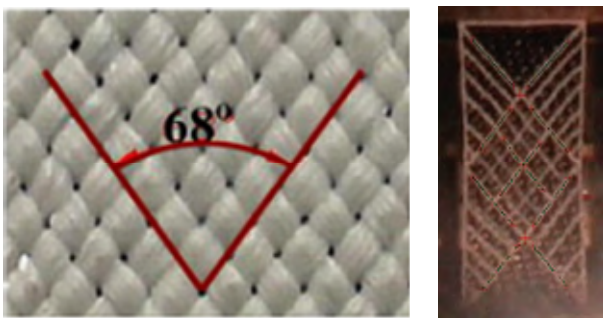

(a) (b)

Figure 26: Determination of the shear angle using (a) image analysis [88], and (b) bespoke algorithm [91]

The novel method referred to as discrete method, is able to measure the displacements of dots drawn on a specimen by means of a point tracking algorithm. The method relies on an open source Fiji (https://fiji.sc/) plugin named Trackmate [95]. This technique, mostly used in biology (for e.g. cell-tracking [96, 97]) consists in a wizard-like GUI providing the tools to perform single particle tracking (SPT). The plugin enables the identification and tracking of bright particles and/or spot-like structures over a dark background, within consecutive frames (i.e. images). Each particle is assigned an identity and its trajectory (referred to as "track") is reconstructed, yielding information such as its coordinates, total displacement, velocity and so forth. The Trackmate plugin is practically automated and guides the user through several steps, consisting of a spot detection step, a spot analysis step and a spot tracking step.

Prior to launching the plugin, a sequence of temporally related frames of equal size and bit depth must be imported into Fiji and combined into a single stack. Spatial calibration is then performed to translate pixel units into physical units (i.e. mm). If required, frames can be pre-processed in order to enhance contrast and reduce noise. It was generally found

that this technique is significantly more forgiving than 2D-DIC as far as samples preparation, lighting conditions and image analysis are concerned.

First, an initial spot detection stage is carried out using a Laplacian of Gaussian (LoG) filter. LoG filter is a two-step operation consisting in smoothing and filtering images in order to find local maxima, corresponding to spot locations. Each spot is assigned a quality value by taking the local maxima. Spots of quality lower than that set in the LoG filter will be automatically discarded. Spots are then analysed using a number of filters. The user can discard or keep spots based on, for instance, their intensity index and/or their estimated diameter. Finally, the movement of the filtered spots is tracked in consecutive frames using a simple Linear Assignment Problem (LAP) algorithm. LAP is a mathematical framework consisting of assigning a set of objects (in this case spots) identified in a next frame, to existing tracks (i.e. trajectories) at a minimum cost. Here, the cost refers to possible physical assignment between tracks and detected spots (e.g. potential links between two spots). The LAP algorithm returns the assignment list that minimises the sum of their costs. Spot-linking processes can be visualised immediately and at any stages and the user can easily navigate back and forth through the different steps to modify the settings if required. Tracking results consisting of each track along with the spots coordinates can then be exported into an xml file and retrieved using a Matlab routine provided by [95]. Finally, a custom algorithm was developed and used to convert the displacement of each dot into local shear angle variation, using the law of cosines.

In order to provide a spot-like structure, a discrete-method, evenly spaced array of 3 mm diameter dots was drawn on the surface of the sample using white acrylic paint. A stencil was designed so that the dots were placed at every other tow crossovers in both the warp and weft directions (Figure 27). A CCD (charge-coupled device) camera was used to capture images of the sample at regular time intervals (i.e. 0.25 s in this case). It is also worth mentioning that later trials in a different study were successfully performed using a standard 1080p HD webcam, highlighting the simple and inexpensive nature of the proposed discrete-method.

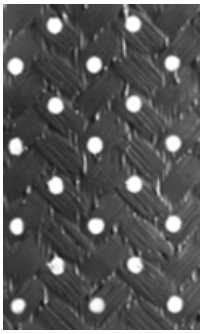

Figure 27: Dots array on the surface of a woven prepreg specimen

The accuracy and effectiveness of this method is demonstrated in the next sections, where it is applied to two commonly used in-plane shear tests for fibrous reinforcements, on both the woven and the cross-plied UD prepregs.

5.2 Intraply shear characterisation of woven thermoset prepreg

5.2.1 Literature review

In-plane shear of woven reinforcements is typically characterised by the relative rotation between warp and weft tows. Upon deformation, the initially orthogonal tows will rotate relative to each other around their crossover points, resulting in a change of shear angle. This particular shearing mechanism gives woven reinforcements the ability to be shaped over doubly-curved surfaces without forming folds or wrinkles and is often conceptualised using the analytical approach known as the pin-jointed net (PJN). The in-plane shear characterisation of woven reinforcements is particularly challenging due to the lack of standard test methods, despite previous benchmarking efforts [88]. However, two test methods are widely accepted as *de facto* standards for intraply shear characterisation. These include the picture frame (PF) and the bias extension (BE) test. Both tests were used and compared, with the aim of determining their suitability for testing the in-plane shear properties of woven prepreg material under conditions similar to those used for the forming process (i.e. elevated temperature and high deformation rates). Firstly, both test methods are explained and raw experimental data are presented. Finally, normalised test data are compared and the relative merits of both test methods are discussed. The effect of speed rate and compaction level was investigated. The test matrix showing the different test conditions is shown in Table 5.

Test method	*Parameters*	*Values*
Picture frame	Temperature [°C]	80
	Crosshead speed [mm.s^{-1}]	1/5/8.33
	Compaction level [-]	Non-compacted/Pre-compacted*
Bias extension	Temperature [°C]	80
	Crosshead speed [mm.s^{-1}]	1/5/8.33

**vacuum bagged under 1bar pressure at 80°C for 2 minutes*

Table 5: Test parameters investigated for the intraply shear characterisation of the woven prepreg

5.2.2 Picture frame tests

5.2.2.1 Experimental setup

During a test, the woven specimen is clamped in a square-shaped frame, hinged at each corner. The fibres of the specimen are carefully aligned with the edges of the frame. A tensile load is applied across two diagonally opposite corners of the frame, imposing pure shear deformation onto the specimen. One corner of the frame is fixed while the opposite one is connected to a 500 N load cell that measures the force exerted on the sample. The load cell is connected to the crosshead of an Instron 5900. The crosshead displacement and the force measured by the load cell are recorded during a test. Figure 28 shows the picture frame test setup used in this research.

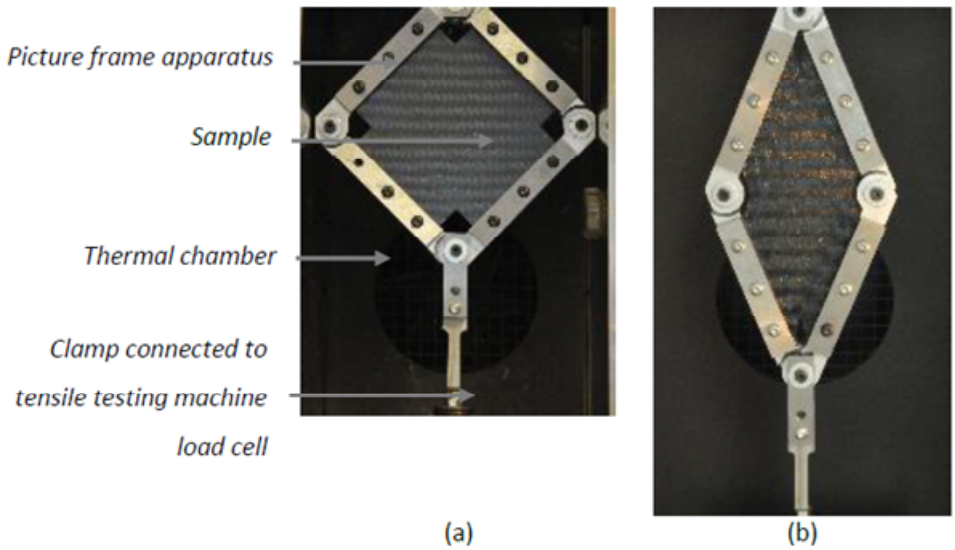

Figure 28: Picture frame of the woven prepreg: (a) before deformation and (b) after deformation

The corners of the specimen are typically cut out to prevent the specimen from interfering with the frame and limit excessive wrinkling of the material [98]. This essentially leads to a

cross shaped specimen consisting of a central, square shaped area with four flanges (i.e. edges of the specimen). The specimen dimensions are shown in Figure 29. Specimen were cut using a CNC cutting machine.

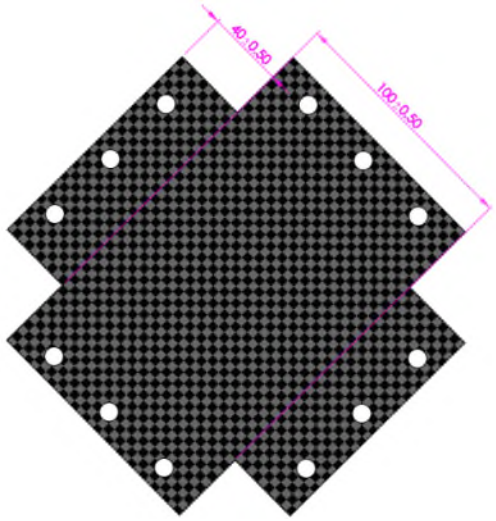

Figure 29: Dimensions of a picture frame test specimen

Before each experiment, a dry run (i.e. a picture frame test without a specimen) was carried out in order to assess the frictional force that develops in the fixture during a test. This force was then substracted from the total force (raw data) obtained during shear test of the prepreg material to yield the net load (i.e. the load required to shear the material only). Typical load-extension results from picture frame test show a larger scatter due to the random occurrence of spurious tension in the fibres. These tensile loads are typically caused by: (1) misalignment of the specimen with respect to the edges of the frame, and/or (2), the inherent variability of the prepreg manufacturing process, which may result in fibre misalignment. In order to filter inaccurate results and mitigate variability, a pragmatic approach was used whereby only the lowest load-displacement curves were considered for a given experimental setting (temperature and strain rate). On average, eight specimens were required in order to obtain three near identical results consisting of the lowest load-displacement values. Figure 30 shows the typical scatter among the raw load-displacement data for the same picture frame experiment (note that the load contribution from the picture frame fixture has not been substracted). In this particular example, a maximum relative difference of approximately 45% was obtained between the maximum and the minimum load values for a given extension. The curves with the plain symbols (i.e. specimens 1, 2 and 3) were discarded while the other three (i.e. specimens 4,

5 and 6) were kept to produce the averaged load-displacement curve. This technique was used to produce the picture frame data shown thereafter.

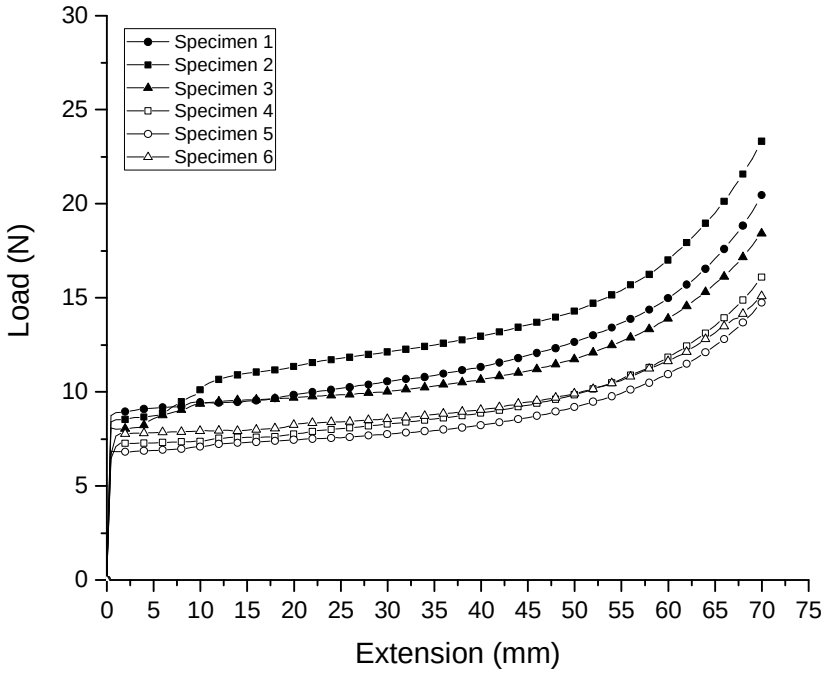

Figure 30: Typical raw load-extension curves from a picture frame experiments showing scatter between specimens

5.2.2.2 Determination of the shear angle

The picture frame test provides near-homogeneous shear deformations across the whole specimen. Due to the boundary conditions imposed by the frame, tow slippage is not possible and deformations are mostly dominated by pure shear. Considering the kinematic of the frame, the shear angle in the material can be directly related to the frame displacement (equivalent to crosshead displacement) using [88]:

$$\gamma = \frac{\pi}{2} - 2\cos^{-1}\left[\frac{1}{\sqrt{2}} + \frac{d}{2L_{pf}}\right] \tag{5.1}$$

With γ the shear angle, *d* the crosshead displacement and L_{pf} the side length of the frame between hinges. Lomov *et al*. [99], demonstrated using full-field strain measurement method during a picture frame test of a glass/polypropylene woven fabric, that the average angle between warp and weft tows within the material is similar to the angle of the frame (i.e. within 2°). This was also confirmed for the woven prepreg considered for this research, using the discrete measurement method introduced in section 5.1. In this case, the maximum difference observed between the average measured shear angle across the

whole specimen and the theoretical shear angle is 0.5° (Figure 31). In addition, it was seen that the shear angle distribution within the edges of the specimen is similar to that of the central region, suggesting that the load contribution is uniform across the whole specimen. This particular exercise demonstrates that the evolution of the shear angle can be directly determined from the frame displacement and can also be considered as a first step on validation of the novel discrete measurement method.

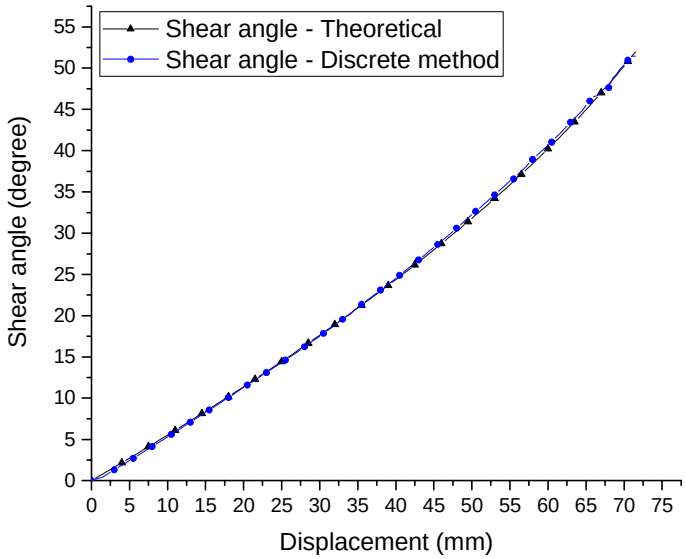

Figure 31: Theoretical and measured shear angle vs displacement curves during picture frame test of the woven prepreg

5.2.2.3 Influence of speed on the intraply shear behaviour of woven prepreg

Figure 32, a shows the influence of the crosshead speed on the picture frame test results. The error bars represent one standard deviation on either side of the mean. It can be observed that the load required to shear the specimen increases with increasing crosshead speed owing to the Newtonian behaviour of the epoxy resin. The load-extension curves in Figure 32,a can be divided into three distinct regions, corresponding to: (1) initial friction between adjacent tows, (2) pure shear and (3) shear accompanied with tow compaction past the shear locking angle value characterised by a sudden load increase. This phenomenon is characteristic of the in-plane shear behaviour of woven fabrics and typically occurs beyond the shear locking angle (i.e. the angle at which the rotating tows jam, preventing further rotation and resulting in a rapid increase in shearing force, after which pure shear becomes limited and deformations are dominated by out-of-plane movement. As seen previously, the crosshead displacement can be accurately used to determine the shear angle within the material using equation (5.1). The corresponding load-shear angle curves are shown in Figure 32, b.

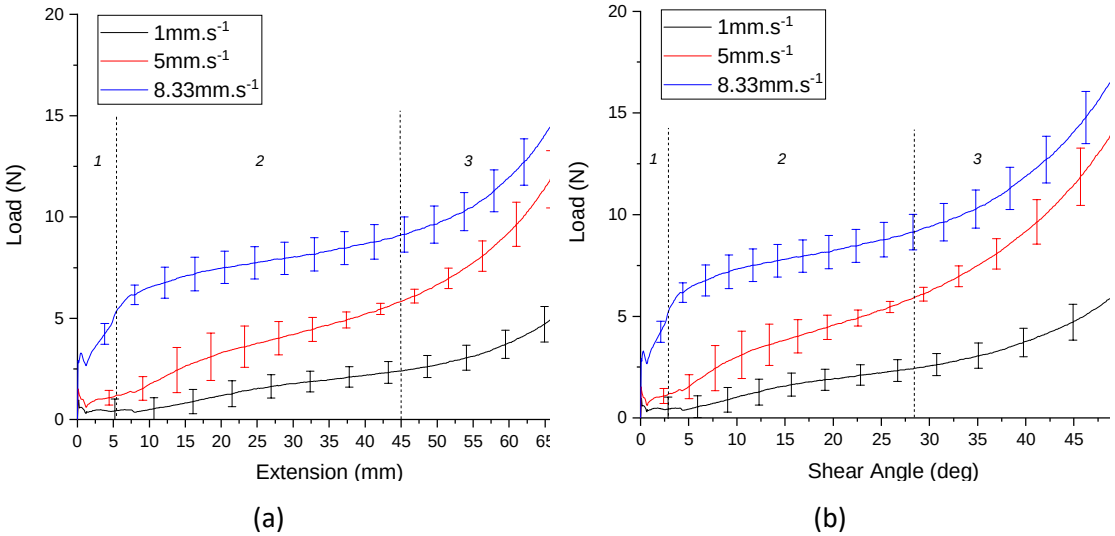

Figure 32: Picture frame test results under different crosshead speeds, showing: (a) net load-extension curve and (b) corresponding net load-shear angle curve.

5.2.2.4 Influence of pre-compaction on the intraply shear behaviour of woven prepreg

In order to understand the effect of normal pressure imposed by the diaphragm materials on the intraply shear properties of woven prepreg, picture frame test of pre-compacted specimens were performed. Load-displacement curves at different crosshead-speeds are shown in Figure 33 and are compared against non-compacted specimens (i.e. in their as-received state). It can be observed that, for a given crosshead speed, the force required to shear the specimens are significantly lower for pre-compacted specimens (solid lines and plain symbols). At a crosshead speed of 5, and 8.33 $mm.s^{-1}$, pre-compacting the specimen results in a 40% decrease in the load towards the end of the test. One possible explanation is that the higher level of impregnation resulting from pre-compaction facilitates shearing by providing lubrication between the warp and weft tows. In addition, the higher level of compaction provides a less chaotic structure, thereby reducing the global friction. Finally, it can be observed that the crosshead speed has a bigger influence on non-compacted specimens, i.e. an increase in crosshead speed results in a greater relative increase in the load for the non-compacted specimens. This suggests that, for non-compacted specimens, deformations are mostly dominated by resin shearing.

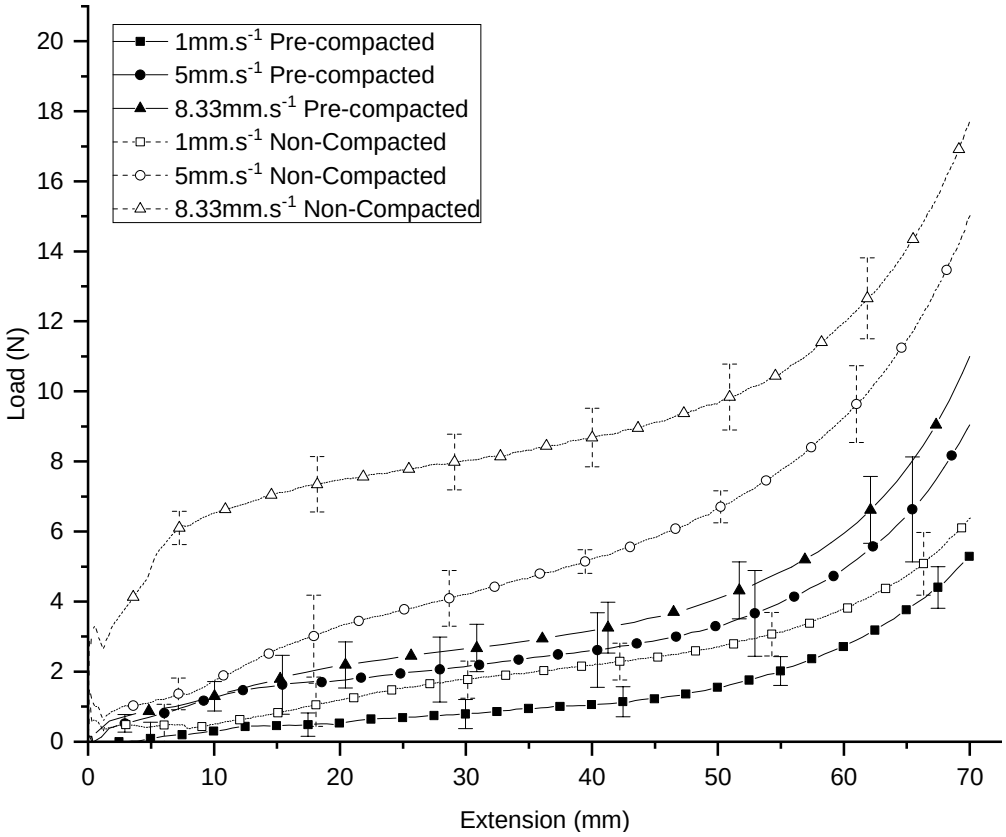

Figure 33: Net load-extension curves from picture frame experiments under different crosshead speeds using compacted and non-compacted specimens

5.2.3 Bias extension tests

5.2.3.1 Experimental setup

The bias extension test, similar to the picture frame test, is a *de facto* standard for measuring the in-plane shear behaviour of aligned fibrous materials. The test consists in a tensile test of a rectangular woven material with warp and weft tows initially oriented at ±45° to the direction of the applied load. The specimen is clamped at both ends and is placed within a thermal chamber. One clamp is fixed whilst the other one is connected to a 500 N load cell that measures the force exerted on the sample. The load cell is connected to the crosshead of an Instron 5900. Figure 34 shows the bias extension test setup used in this study. Sample temperature was monitored with a temperature probe placed on the surface of the specimen, which was removed before starting the test. The specimen dimensions between the grips are 222 mm by 74 mm. Specimen were cut using a CNC cutting machine.

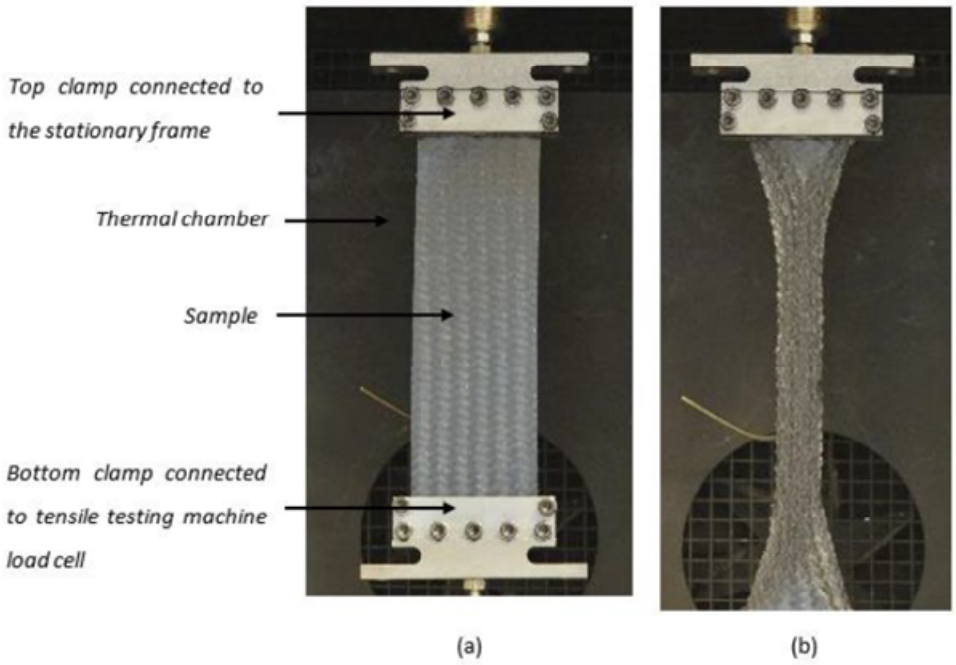

Figure 34: Bias extension of the woven prepreg: (a) before deformation and (b) after deformation

5.2.3.2 Determination of the shear angle

The specimen length must be at least twice the width in order to obtain pure shear deformation in the centre of the specimen. Under those conditions and assuming the PJN assumptions (section 2.3.1), it was shown [38] that three distinct zones will develop within the fabric as the specimen is pulled (Figure 35). If the tows are inextensible and no slippage occurs, it can be shown that the shear angle in region C is always twice that in region B, while region A remain underfomed. It is then possible to determine the theoretical fibre rotation as a function of the crosshead displacement and sample geometry using geometrical considerations [100]. The shear angle in the pure shear zone C can then be expressed as:

$$\gamma = \frac{\pi}{2} - 2\cos^{-1}\left(\frac{L_0 + d}{\sqrt{2} \times L_0}\right) \tag{5.2}$$

Where L_o is the difference between the length and the width of the sample and d is the crosshead displacement.

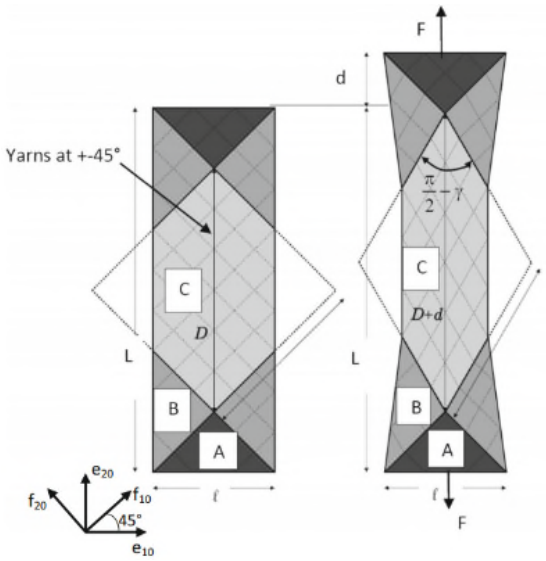

Figure 35: Illustration of an idealised bias extension and the different shear zones - [101]

A number of researchers have demonstrated that for large shear angles, equation (5.2) is no longer valid [91, 94, 102]. Due to inter-tow sliding, the PJN assumptions (section 2.3.1) cannot be maintained, stressing the importance of accurately monitoring the shear deformation during bias extension tests of reinforcements. In this work, the shear angle during bias extension test was measured using the novel shear angle measurement method introduced in section 5.1. Typical outputs from the method, applied to a bias extension test of the woven prepreg carried out with a crosshead speed of 8.33 $mm.s^{-1}$ are presented in Figure 36.

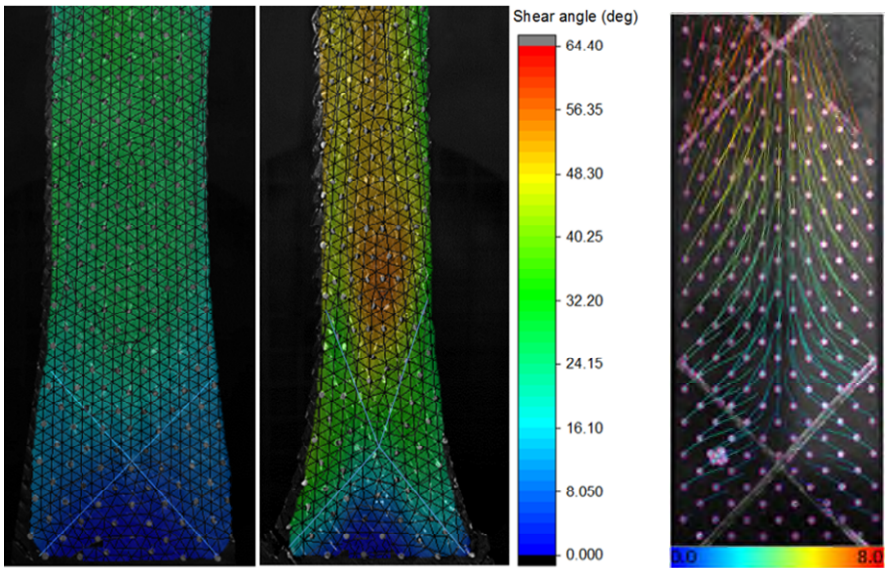

(a) (b) (c)

Figure 36: Outputs of the novel shear angle measurement method for a bias extension test performed at 1 $mm.s^{-1}$ showing shear angle contours for a crosshead displacement of 30 mm (a), and 65 mm (b). The resulting trajectories of each dot is shown in (c)

These include shear angle contour plots superimposed over pictures of the specimen at different stages (a and b, Figure 36), as well as the trajectory and speed of each dot (c, Figure 36). Lines were drawn on the surface of the specimen along the borders separating the different theoretical shear zones. The contour plots show the presence of three different shear zones, with a central area where peak values are twice that of the adjacent intermediate zones, and an area adjacent to the clamp with negligible shear. The trajectories (Figure 36, c) show the relative motion of each point throughout the entire test and reveal the existence of a bilateral symmetric deformation pattern. The speed can be visualised by means of the different colours and the corresponding legend, expressed in $mm.s^{-1}$.

In order to demonstrate the accuracy of the novel measurement method, shear angle values in the pure shear zone were averaged and compared to DIC data. Figure 37 shows the different results plotted against the crosshead displacement. Theoretical values, i.e. calculated using equation (5.2), are also reported for comparison. It can be seen that up to a displacement of approximately 38 mm, each approach provides similar shear angle values with a maximum deviation of 4°. Upon further displacement, the DIC method becomes ineffective due to significant loss of data points. In addition, the theoretical values deviate significantly from those obtained with the tracking method (i.e. referred to as discrete method). These observations serve to: (1) demonstrate that the shear angle can be accurately predicted using the theoretical equation (5.2) without requiring measurement method, up to approximately 35°; and (2) validate the new discrete measurement method as a way to determine the shear angle continuously throughout a bias extension test.

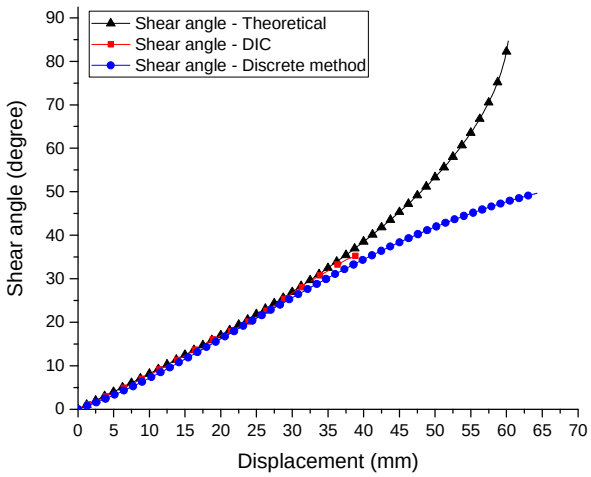

Figure 37: Comparison of the shear angle measured using the novel measurement method and the DIC system with the predicted shear angle calculated using the theoretical equation (5.2) during a bias extension test.

5.2.3.3 Influence of speed on the intraply shear behaviour of woven prepreg

Figure 38 shows the raw experimental data consisting of the tensile load and the crosshead displacement. For each test condition, the experimental results were averaged over three specimens. The error bars represent one standard deviation on either side of the mean. It can be seen that a higher crosshead speed and therefore higher shear rate, results in higher load. Similar to the picture frame test results, the load-extension curves can be divided in three regions: (1) As the test starts, a rapid increase in load can be observed corresponding to initial friction between warp and weft tows as they rotate relative to each other; (2) From an extension of approximately 5 mm onwards, the load increases marginally, corresponding to pure shear deformation; (3) From 40 mm onwards, a sharp rise in the load can be observed until the end of the test.

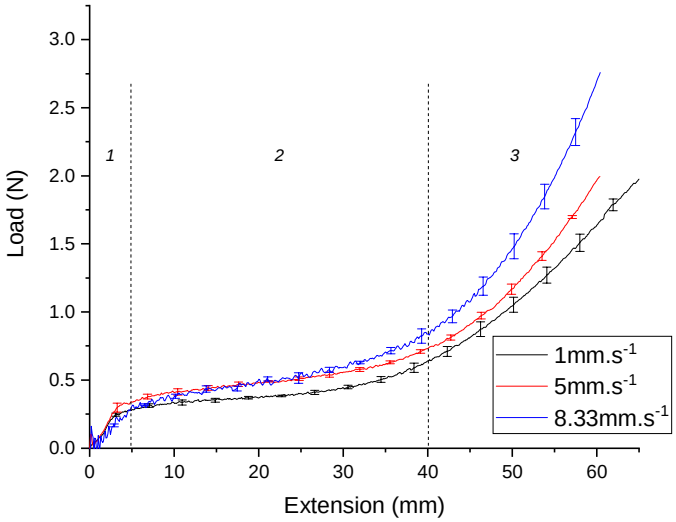

Figure 38: Load Vs displacement curves from bias extension tests under different crosshead speeds

Similar to picture frame data, the results can be expressed as a function of the shear angle. An example is given in Figure 39 and shows the load-shear angle curve for bias extension test performed at 8.33 $mm.s^{-1}$. For comparison purpose, the data using equation (5.2) are also plotted. Clearly, it is evident that the theoretical equation cannot be used to predict the shear angle values at large deformation. The difference between measured and theoretical shear angle is particularly noticeable beyond the shear angle (i.e. approximately 35°). In addition, the predicted shear angle reaches a maximum value of 90°, which suggests that the fibres are perfectly aligned with the direction of the applied load. This is highly unlikely as beyond the shear locking angle, the relative rotation of the warp and weft tows becomes hindered. In practice, shear angle values will tend to reach a limit. This shows that, in order to perform accurate preforming simulation, shear angle values based

on crosshead displacement should not be considered as input parameters when bias extension data are used. Failing that the numerical model may underestimate shear stresses.

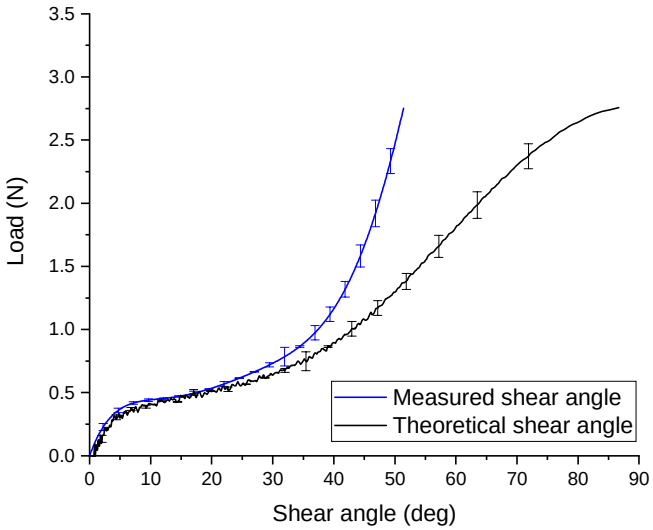

Figure 39: Comparison between measured and predicted shear angle for a bias extension test performed with a crosshead speed of 8.33 mm.s^{-1}

5.2.4 Normalisation and comparison of bias extension and picture frame data.

Since the picture frame and bias extension tests can both be used for measurement of in-plane shear behaviour of textile reinforcements, the data generated from these tests should be comparable. In order to compare bias extension and picture frame data for the same material, results must be normalised. Fundamental differences exist between the picture frame and the bias extension test due to the different kinematics and the sample geometry used during tests. Shear forces must be expressed in quantities that are independent of the sample geometry and the measurement device. Such a quantity is the shear force per unit length known as 'normalised shear force'. During a bias extension test, the energy required to deform the specimen is dissipated in two zones: zone B and zone C (Figure 35). The shear force required to produce ideal pure shear conditions in zone C can be written as:

$$F_{sh}(\gamma) = \frac{1}{(2L-3W)\cos\gamma}\left[\left(\frac{L}{W}-1\right)F_{be}\left(\cos\frac{\gamma}{2}-\sin\frac{\gamma}{2}\right)-W.F_{sh}\left(\frac{\gamma}{2}\right)\cos\frac{\gamma}{2}\right] \quad (5.3)$$

Where *L* and *W* are the length and width of the sample, respectively. γ is the shear angle and F_{be} is the load recorded by the load cell during the bias extension test. F_{sh} represents the shear force per unit length. The derivation of the equation can be found in [88].

For picture frame, a similar approach can be used. In the particular case where the length of the specimen is not equal to the length of the frame, it was shown in [103] and [88], that the normalised shear force per unit length F_{sh} can be written as:

$$F_{sh}(\gamma) = \frac{F_{norm}}{2\cos(\frac{\pi}{4} - \frac{\gamma}{2})} \tag{5.4}$$

Equation (5.4) yields the same property as (5.3) from the bias extension test. γ is the shear angle and F_{norm} is the normalised load exerted by the picture frame such that:

$$F_{norm} = \frac{F_c L_{frame}}{L_{fabric}^2} \tag{5.5}$$

Where F_c the load applied on the picture frame, L_{frame} and L_{fabric} the side length of the picture frame and of the sample, respectively.

The resulting normalised shear force vs shear angle curves from picture frame and bias extension tests performed using a similar shear rate are shown in Figure 40. All curves have been smoothed using fast Fourier transformation to reduce noise before normalisation. For the bias extension data, the shear force was calculated based on both the theoretical shear angles (dashed, black line) and the measured shear angles (solid, black line). It can be seen that both ways provide different data, in that the curves start deviating from a shear angle of 35 degrees onwards (i.e. when the pin-jointed assumptions are no longer valid). Beyond this value, inter-tow slippage occurs during bias extension test and influences the evolution of the shear angle. Measuring the actual shear angle that corresponds to the force required to deform the material enables to account for all the different mechanisms arising during bias extension test. Interestingly, bias extension results based on measured shear angle are much closer to the normalised picture frame data. In addition, the shear locking angle is relatively similar, i.e. 35 degrees. This is an important parameter as it typically reflects the onset of wrinkling. While the bias extension results based on the measured shear angle show a plateau from approximately 10 to 30 degrees, the picture frame data show a slight gradual increase between 15 to 45 degree. This relative difference is attributed to tension

in the fibres. Generally, the normalised results, based on the measurement of shear angle from discrete method, show that picture frame and bias extension provide similar data, suggesting that both test methods can be used for the measurement of reliable intraply shear properties of woven prepreg.

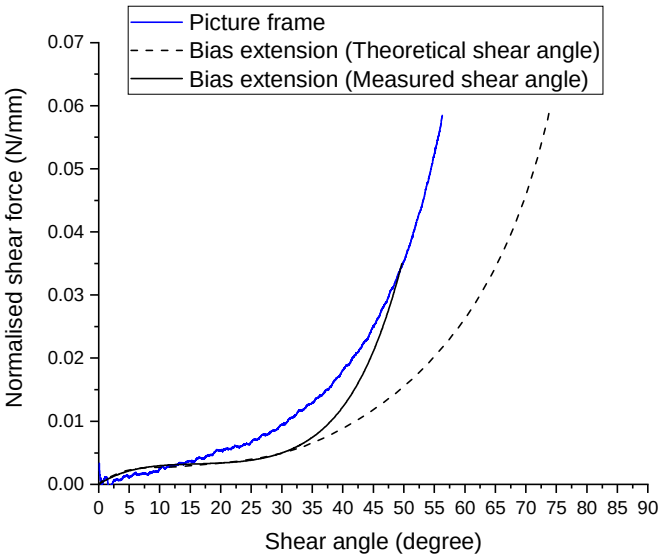

Figure 40: Normalised shear force vs shear angle curves from picture frame and bias extension tests of the woven prepreg performed at 80°C at an equivalent shear rate.

Generally, it was found that both methods have their pros and cons: While the bias extension method can be used as a simple and generally repeatable means to measure the shear properties of biaxial reinforcements, it suffers from the presence of parasitic deformation mode at high shear angle (in the form of tow slippage). These combined modes complicate the deformation field and make the processing of data laborious. As a consequence, measurement methods are required in order to determine the shear angle. In contrast, during a picture frame test, the entire sample undergoes pure shear, making the processing of experimental data significantly easier. In addition, it was proven that no measurement methods during test are required as the shear angle within the material can be accurately determined from the crosshead displacement. However, due to clamping of the specimen, small parasitic load can arise from tension in the fibres, making the test slightly less repeatable than bias extension.

5.3 Intraply shear characterisation of UD thermoset prepreg

5.3.1 Literature review

Similar to woven fabrics, there does not exist any test standard for the determination of the intraply shear properties of UD reinforcements. Although a few test methods have been proposed by research institutions, none has been accepted as a *de facto* test standard. In addition, most published research on longitudinal shear characterisation of UD reinforcement are focused on thermoplastic materials [35, 36, 104, 105]. A list of existing test methods is given in Table 6 along with a schematic of each method in Figure 41.

Using a commercial rheometer, Groves [104], proposed a test method featuring two parallel disc platens between which the laminate is placed and sheared under the rotating action of the upper disc. Both cross-ply and UD (i.e. parallel plies) laminates were investigated under dynamic and steady shear deformation and provided similar results. The behaviour of the material was consequently referred to as isotropic.

Ref.	***Figure 41***	***Variables***	***Device***	***Fixture movement***	***Material***
Groves, [104]	(a)	Rotational speed	Parallel plate in a rheometer	Rotation	Thermoplastic UD
McGuinness *et al.* [36]	(b)	Temperature, test speed	Picture frame test	Shearing	Carbon UD/PEEK
Potter, [38]	(c)	Temperature, test speed	Bias extension grips	Extension	Carbon UD/Epoxy
Stanley *et al*. [105]	(d)	Shear rate	Parallel shear plate tester	Shearing	Carbon UD/PEEK
Haanappel *et al*. [35]	(e)	Temperature, rotational speed	Torsion bar using standard rheometer	Rotation	Carbon UD/PEEK

Table 6: Existing shear characterisation tests for UD reinforcements

Later, McGuinness *et al*. [36], studied the in-plane shearing behaviour of both cross-plied UD (e.g. $[0°/90°]_s$) and unidirectional (e.g. [0°]) laminates over a range of processing temperatures using the picture-frame experiment. In order to avoid spurious tensioning

and allow rotation of the fibres at their ends, unidirectional laminates were held under vacuum between two diaphragms. The diaphragms were clamped to the picture-frame fixture, while the laminate, though pressed against the fixture, was not clamped. This approach is relatively cumbersome as it requires to determine the contribution of the diaphragm material to the overall load recorded during a test. Cross-plied laminates were successfully tested without diaphragms and were sheared by attaching an over-sized specimen to the faces of the fixture with pins. Results were compared to those obtained from torsional rheometry methods such as that proposed by Groves [104], and were found to differ by several orders of magnitude. Several explanations were given to justify this discrepancy, including: (1) the different boundary conditions between both test methods, (2) the difference in amplitude shear, and (3) the different sample geometry used. Ultimately, McGuinness *et al*. suggested that the picture frame experiment is a more appropriate shear characterisation technique. In a more recent paper, Harrison *et al*. [106], used the picture frame to characterise the shearing properties of cross-plied UD glass/polypropylene composite. Significant scatter was found within the data due to unavoidable misalignment of the sample, resulting in spurious tensile stresses in the fibres. As a result, out of 35 specimens tested, only 7 were deemed appropriate for analysis.

Potter [38], used the bias extension test to study the deformation of cross-plied UD thermoset prepreg. Although bias extension test is typically used for the in-plane shear characterisation of woven textiles, Potter reported that cross-plied UD laminates, when subjected to bias extension deformation, could be accurately modelled as a pin-jointed-net (section 2.3.1). Despite the fact that this test method does not allow to obtain the intraply shear properties of a single UD ply, the observations reported by Potter imply that a cross-ply UD laminate (i.e. [0°/90°]) can be modelled as a single woven ply. When using simulation tools based on the PJN behaviour, this assumption will greatly simplify the numerical model, and consequently improve computational time by reducing contacts and elements number.

Stanley *et al*. [105], proposed a different test method where specimens are positioned on either side of a central moving plate and pressed between two outer fixed plates. Pulling-out the centre plate at a constant velocity, a steady-shear deformation is introduced. Using different pulling-out speeds, longitudinal and transverse shear viscosities were determined for different shear rates. The values obtained were found to be significantly higher than those obtained using torsional rheometry techniques, but agree with picture frame data. A

power-law viscous model was used to model the material behaviour, similar to that used by McGuinness *et al*. [36].

Most recently, Haanappel *et al*. [35] developed an alternative test method for the analysis of the shear properties of UD using a commercial rheometer together with a standard torsion fixture. Specimens consist of a stack of 80 UD plies in the form of a prismatic bar with a rectangular cross-section. One end of the specimen is fixed while the other one is clamped to a moving fixture subjected to an angular displacement. The torsional load applied to the specimen introduces longitudinal shear. Dynamic moduli from linear visco-elasticity theory were determined and an elastic behaviour was found for small strains. This test method showed promising results for the determination of in-plane shear properties of UD materials. However, it is limited to small shear strains and requires further validation through round-robin benchmarking.

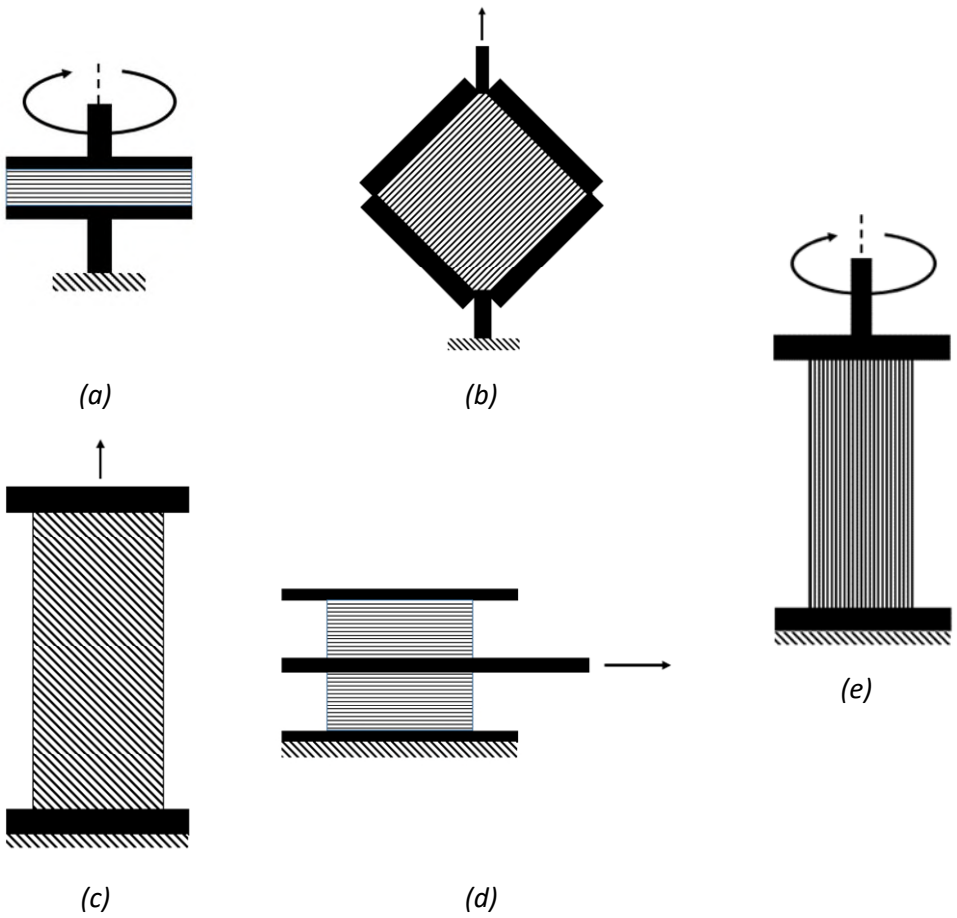

Figure 41: Schematics of previously developed shear characterisation tests for UD reinforcements – The letters refer to Table 6

This review shows that to date, there exists no designated test standard for the in-plane characterisation of UD materials. Most recent test methods require custom-built fixture,

which limits the test's implementation, as few information with respect to the fixture specifications is available in the literature. In addition, there have been few attempts to characterise the longitudinal shear behaviour of UD thermoset prepreg.

For the present work, a novel method for intraply shear properties of UD prepreg based on rail shear test was investigated. The method was suggested by David Prono [107], product manager at ESI Group, in collaboration with the mechanical test centre Mecanium (Lyon, France). The motivation for choosing the outlined test was based on the assumption that the longitudinal intraply shear of UD prepreg is mainly dominated by the shear stiffness of the matrix material, which is characterised by inter-tow shearing.

5.3.2 Experimental procedure

The rail shear test method consists of clamping both sides of a specimen to steel rails. When loaded in tension, the rails introduce shear forces into the specimen through the clamped specimen sides. One rail is connected to a 500 N load cell mounted on the moving crosshead of an Instron 5900 tensile testing machine, while the other rail is fixed. The horizontal distance between the rails stays constant throughout the test, providing conditions of simple shear. The specimen fibres are parallel to the applied shear loading direction. Other specimen orientation would give rise to tensile stresses in the fibres. The test can be performed at room temperature or at processing temperature by placing the specimen within a thermal chamber. A picture of the test set-up is shown in Figure 42. In the present work, all tests were performed at 80°C (i.e. actual preheating temperature). The development of the test method was done using a crosshead speed of 1 $mm.s^{-1}$ and 5 $mm.s^{-1}$.

Initial tests were carried out using rectangular specimens, as per ESI Group recommendations [107]. The test set up is shown in Figure 42. Specimens were made up of four UD plies, which were stacked and vacuum bagged under 1 bar pressure at 80°C for 2 minutes for consolidation prior to the test. Multiple plies were used in order to increase both the force required to shear the material and the bending rigidity, thereby limiting the possible occurrence of out-of-plane deformations. The specimen dimensions between the clamps are 50x25 mm, with a thickness of 0.904 mm.

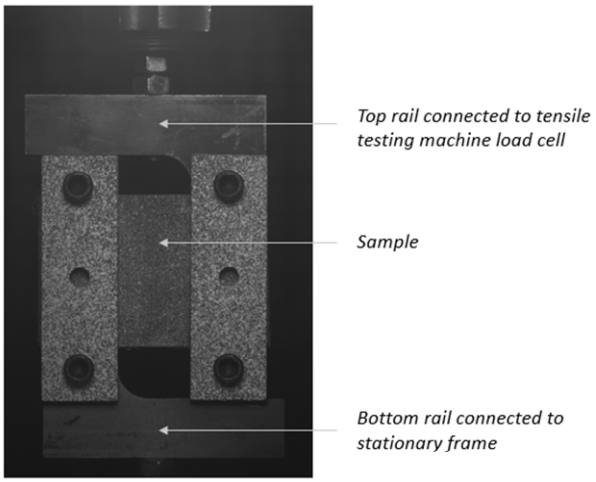

Figure 42: Rail shear test set up.

In order to evaluate the full-field strain distribution on the specimen surface during the test, digital image correlation (DIC) technique was used. For a detailed explanation on DIC principles, as well as a description of the basics of strain calculation, the reader is referred to the appendix A and b.

DIC results are shown in Figure 43 in the forms of major strain and shear angle distributions at a mean shear strain of 3%. The major strain distribution (Figure 43,a) reveals that the specimen is largely affected by edge effects at diagonally opposite corners. As the rail moves vertically, the sample rotates around its centroid, resulting in out-of-plane displacements. The shear angle distribution (Figure 43,b) shows significant shear banding in the centre of the specimen, corresponding to inter-tow sliding, which is characteristic of longitudinal shear deformation of UD material. Unless the test is carried out at very small strains, it is impossible to obtain homogeneous inter-tow sliding across the whole sample. Consequently, this phenomenon will always be localised, such as in (Figure 43,b). These DIC images indicate that the use of rectangular specimens fails to provide the desired boundary conditions, resulting in a non-uniform, localised shear stress combined with parasitic out-of-plane displacements due to rotation of the sample.

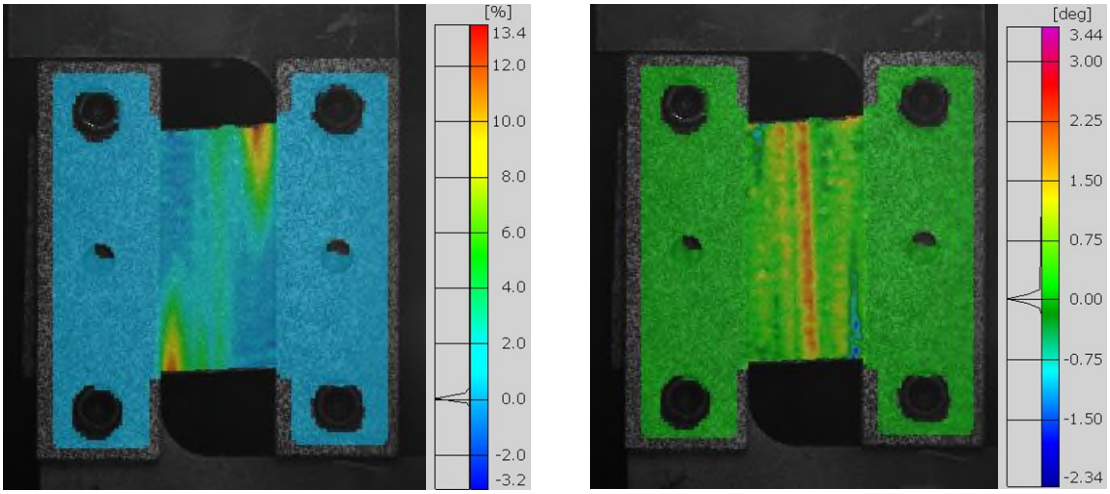

(a) (b)

Figure 43: DIC measurements obtained for the rectangular specimen, at a shear strain of 3% showing: (a) Major strain distribution and (b) shear angle distribution.

In order to eliminate edge effects, and ensure that inter-tow sliding (i.e. longitudinal shear) is obtained in a repeatable and controlled manner within the same region, an alternative specimen geometry was used. The geometry considered is a v-notched specimen whose dimensions are shown in Figure 44. The greyed-out areas correspond to the clamped ends. Rail shear test of V-notched specimens has previously been used for measuring the shear modulus and shear strength of both thermoset and thermoplastic composites [108-110]. However, to the author's knowledge, the present work is a first attempt to use this technique for measuring the intraply, longitudinal shear of UD materials in their uncured state.

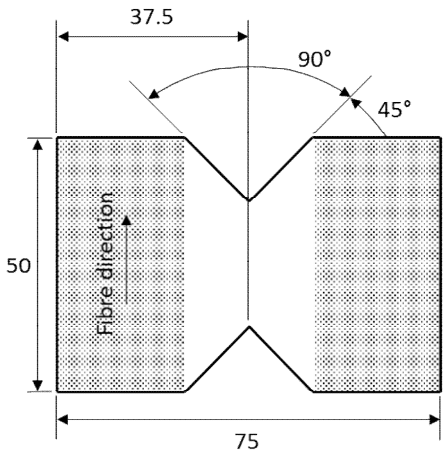

Figure 44: Specimen dimensions for V-notched rail shear test (dimensions in mm)

5.3.3 Results and discussion

Major strain and shear angle distributions at a mean shear strain of 25% are shown in Figure 45. The major strain distribution (Figure 45, a) shows a localised high strain within the gauge section between the notches. These strain concentrations are generated by stress concentrations at the tip of the notches. Although the strain distribution is not evenly distributed over the entire surface of the coupon, the specimen sides do not deform during the test, and as a consequence do not introduce extraneous stresses. Contrary to the rectangular specimen (Figure 43, a), the V-notch geometry reduces stress concentration along the rails and produces a more uniform strain distribution, promoting inter-tow sliding in a repeatable and localised manner. The shear angle distribution (Figure 45, b), shows a similar pattern. Areas of high shear are localised within the gauge section between the notches, which confirms that the strain state introduced by the present test can be associated to simple shear.

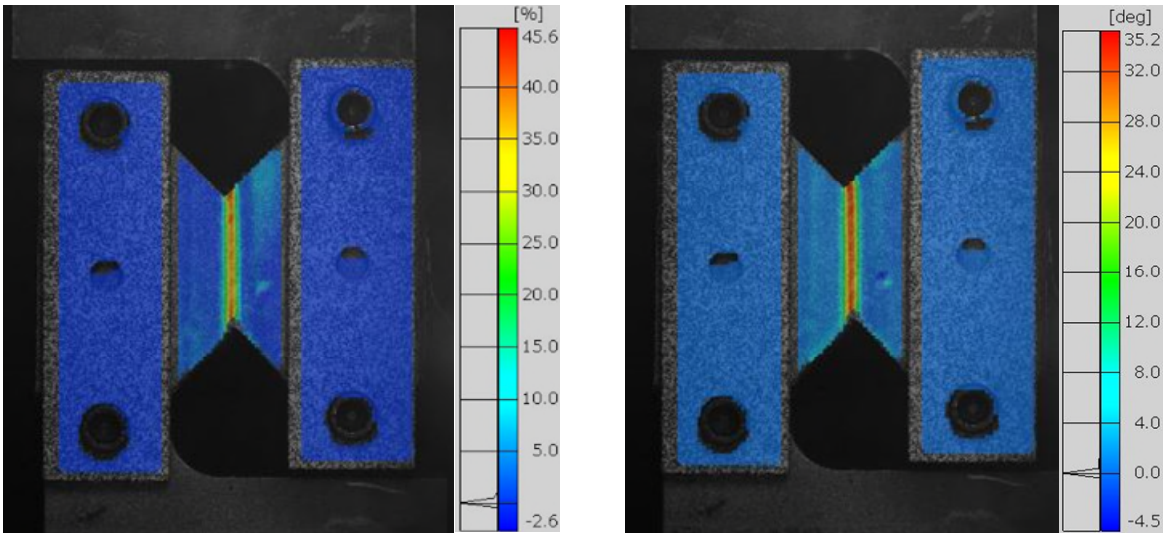

(a) (b)

Figure 45: DIC measurements for the v-notched specimen at a shear strain of 25% showing: (a) Major strain distribution and (b) shear angle distribution

Figure 46 shows the evolution of the shear angle between the notches, as a function of the crosshead extension. Initially, the shear angle increases in a non-linear fashion with increasing extension. This is attributed to the initial resistance of the material to deformation. Thereafter, beyond 0.5 mm of extension, the shear angle increases linearly with increasing crosshead extension. This suggests that the inter-tow sliding process progresses simultaneously with the movement of the crosshead.

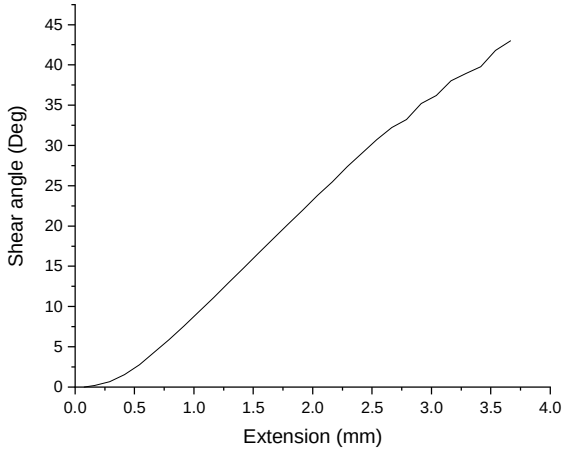

Figure 46: Shear angle between the notches Vs crosshead extension

In-plane shear stress-shear strain results are shown in Figure 47. Tests were carried out at 80°C with a crosshead speed of 1 mm.s^{-1} and 5 mm.s^{-1}. Five specimens were tested and the average results were reported. For a given sample, the mean shear strain value was determined by means of DIC analysis, using surface averaging whereby local surface strains were averaged across a selected region. In this particular example, the selected region consists of an arbitrary area between the two notches. A total of 60 points were used to compute the mean strain, resulting in a measuring area on the specimen surface of approximately 38.4 mm^2. A similar approach was used for the determination of the shear angle values. It is important to notice that the size of the measuring area will affect the resulting measurement. Looking at Figure 45, b, it is clear that a narrow measuring area along the notches will yield a high mean shear angle. In contrast, a wider area will result in a lower mean shear angle. The error bars represent one standard deviation on either side of the mean. The in-plane shear stress within the gauge was calculated from the load and the gauge cross-sectional, such that:

$$\tau_{12} = \frac{F}{L \times h} \tag{5.6}$$

Where *F* is the load recorded by the load cell, *L* is the distance between the notches in the gauge, and *h* is the thickness. For both test speeds, the UD material initially shows an elastic behaviour, with a linear relationship between shear stress and strain up to approximately 1% in strain. The shear modulus of elasticity obtained is G_{12}=0.015 MPa. The elastic deformation is then followed by plastic deformation and is attributed to shearing of the matrix as inter-tow sliding progresses. As expected, the shear stresses required to

deform the specimen increase with increasing crosshead speed due to shear strain rate dependent behaviour of the resin.

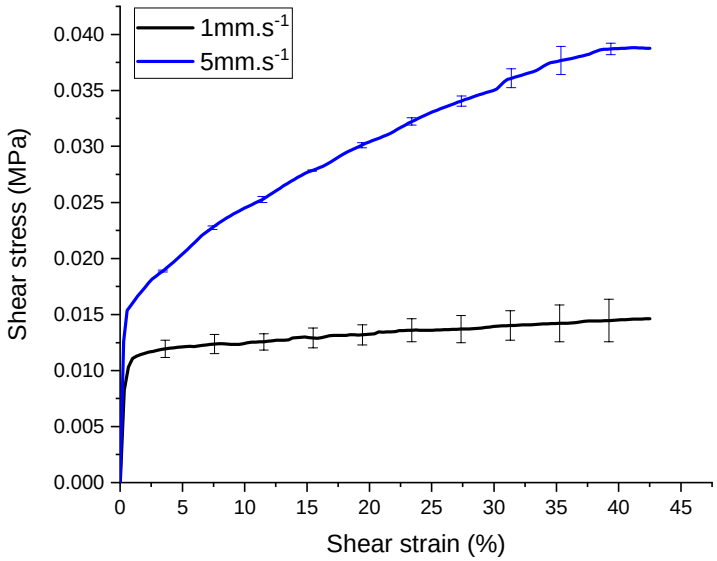

Figure 47: Shear stress - shear strain curve of V-notched specimens

5.4 Characterisation of the in-plane behaviour of cross-plied UD thermoset prepreg

5.4.1 Literature review

It was shown in previous studies [38, 106] that under bias extension deformation, some cross-plied UD prepregs behave in a similar way to woven prepregs. This suggests that, when carrying out forming simulation, material model originally developed for woven fabric could also be applied to cross-plied UD. This statement will be demonstrated in the next section using the novel shear angle measurement method.

5.4.2 Experimental procedure

Each specimen consists in a stack of four cross-plied UD prepreg layers (i.e. $[+45/-45]_s$), making up a total of 8 plies, with a thickness of 1.8 mm. To obtain sufficient compaction, the stack of plies was vacuum bagged under 1 bar for 2 minutes at 80°C. Specimen dimensions were kept similar to those used for the woven prepreg (section 5.2.3) so that

comparison between both materials may be made. In addition, the test setup (i.e. test rig, tensile testing machine and load cell) was also identical.

5.4.3 Results and discussion

Tests were performed at a temperature of 80°C (i.e. preforming temperature) using a crosshead speed of 1 and 8.33 $mm.s^{-1}$. Results are presented in Figure 48. As expected, the load required to deform the stack of UD layers increases with increasing rate. This is directly attributed to resin viscosity effect and suggests that deformation is mostly dominated by shearing of the resin, thereby resulting in a strain rate dependent behaviour. Interestingly, the load-extension curves are analogous in shape to that of bias extension test of a woven material (i.e. a relatively slow increase of the load with extension as the material is being sheared, followed by a rapid increase beyond the shear locking angle).

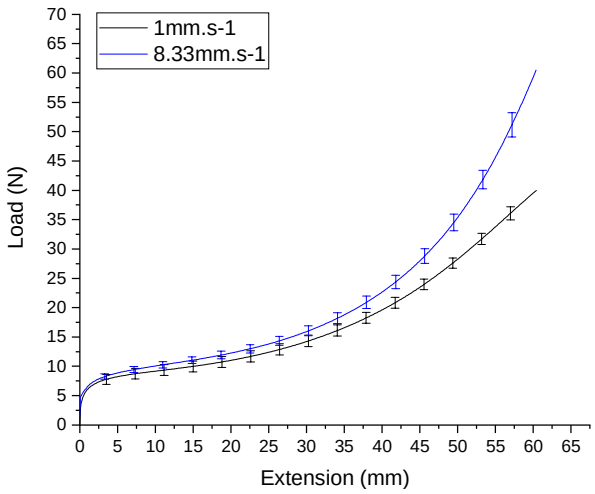

Figure 48: Load-extension curves from bias extension tests of cross-plied UD prepreg performed with different crosshead speeds at 80°C

In order to investigate the behaviour of cross-plied UD prepreg under bias extension deformation, the novel shear angle measurement method was applied during a test. Results are reported in Figure 49 and include the shear angle contour plots superimposed over pictures of the specimen at different stages as well as the trajectory and speed of each dot. The shear angle contours reveal three distinct zones that correspond remarkably well with the theoretical shear zones predicted by the PJN model (highlighted with the white painted lines). Similar to the woven material, it can be observed that the shear angle values obtained in the central zone of the specimen are double that of the adjacent, intermediate zones. Besides, the bottom zone adjacent to the clamp remained undeformed. The dots

trajectory and speed shown in Figure 49, c are relatively similar to those observed for the woven material (Figure 36).

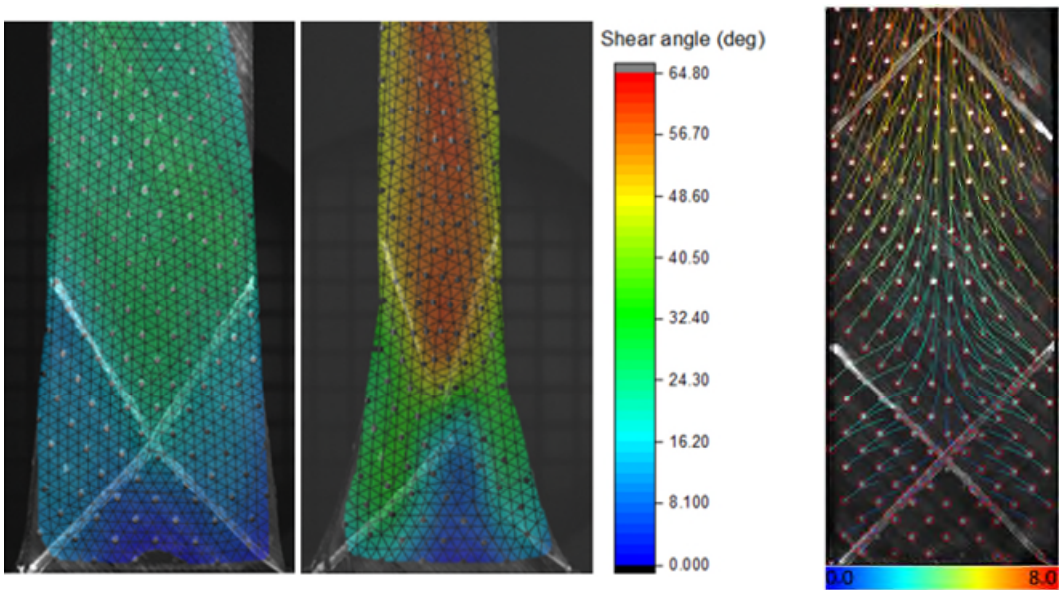

(a) (b) (c)

Figure 49: Outputs of the dot tracking method for a bias extension test of a cross-plied UD laminate showing shear angle contours for a crosshead displacement of 30 mm (a), and 65 mm (b), and the dots speed (in mm.s-1) and trajectory (c)

The shear angle values obtained in the central zone were averaged and plotted against the crosshead displacement. Results are shown in Figure 50 and are compared to those of the woven prepreg as well as the theoretical ones (i.e. predicted value based on the PJN model). Interestingly, throughout the entire test the measured angles for the UD are almost identical to those for the woven (i.e. within a 2° range for any given displacement).

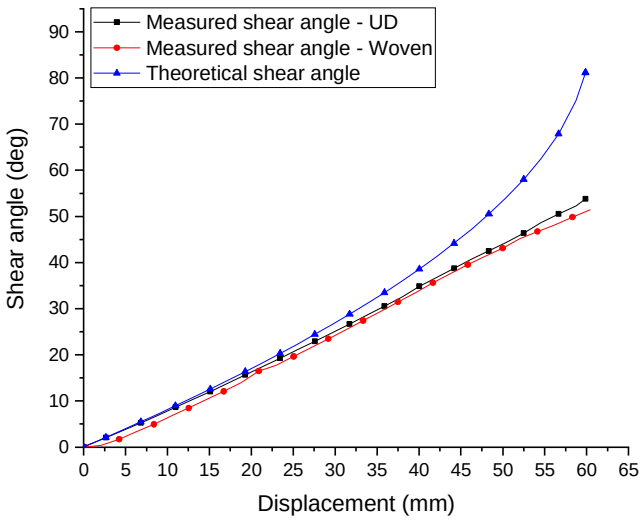

Figure 50: Measured shear angle Vs crosshead displacement for both the UD and woven prepregs during a bias extension test, compared to the PJN prediction

The in-plane shear behaviour of both the UD and the woven materials can be relatively well predicted by the PJN model up to a displacement of 40 mm (corresponding to a shear angle of around 35°), where the maximum difference in shear angles values is no more than 5°. However, beyond this point, the theoretical values start increasing exponentially, while the values for both the UD and woven remain linear. Relative to the UD material, the PJN model overestimates the shear angle value by approximately 10° at a displacement of 50 mm, and by 30° at a displacement of 60 mm.

The findings provide strong evidence that cross-plied UD prepreg deform in a similar way to woven material. Although cross-plies UD do not possess physical linkages similar to woven materials (in the forms of crossovers, facilitating trellis shearing), the interaction between the different layers (most likely in the form of adhesive contacts through the viscous resin) yields a similar in-plane deformation under bias extension. The discrepancies between the measured and predicted shear angle values confirm that, similar to the woven material, deformation must be accurately monitored during bias extension of cross-plied UD prepreg. Finally, the similarity between the deformation of the UD and woven material under bias extension test suggests that during preforming simulation, material models initially developed for woven reinforcements which assume trellis shearing, may also be useful to model cross-plied UD materials. This would as a consequence reduce models complexity and improve computational time by decreasing the number of contacts and elements. This assumption will be demonstrated in the following section (section 10.2).

5.4.4 Comparison of results with the v-notched rail shear test

In an attempt to compare the in-plane shear results obtained from the bias extension and the rail shear test (section 5.3), the shear modulus obtained from both test methods will be analysed. For the bias extension, the shear modulus was obtained by:

(1) Calculating the shear force per unit length, according to equation (5.3), and dividing the result by the specimen thickness to yield the shear stress.
(2) Differentiating the shear stress with respect to the shear strain (i.e. shear angle in radian) to yield the shear modulus as a function of the shear strain.

The results are plotted in Figure 51, alongside the constant shear modulus obtained from the v-notch rail shear test of 0.015 MPa. Firstly, it can be seen that the shear modulus obtained from the bias extension test increases with increasing shear strain. As the shear

strain increases, the rotation of the fibres becomes restricted and consequently, the shear rigidity of the cross-plied laminate increases. In contrast the shear modulus obtained from the v-notch rail shear test is assumed constant. Irrespective of the shear strain, the shear modulus obtained from the bias extension test is always higher than that obtained from the v-notch rail shear test. At relatively small strains, (i.e. approximately 12.5%) the shear stiffness from the bias extension test is around 5 times higher than that obtained from the v-notch rail shear test. With increasing shear strain, the difference increases further.

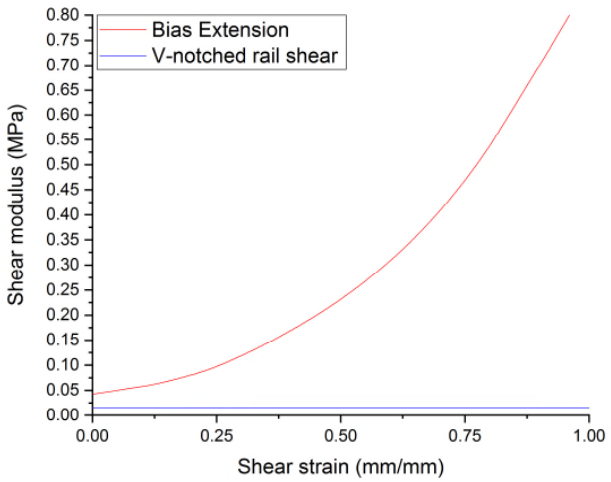

Figure 51: Comparison of shear modulus obtained from the V-notch rail shear and the bias extension test.

This difference is expected, given that both tests cause different deformation mechanisms to occur. The v-notch rail shear test allows the determination of the in-plane shear properties at a single ply level, which is dominated by the shear stiffness of the matrix material. In contrast, bias extension test of cross-plied UD prepreg results in a combination of intraply shear and, due to the presence of off-axis plies, interply shear (i.e. friction between adjacent plies). This means that data from bias extension test of cross-plied UD prepreg may not be suitable to model the in-plane shear behaviour of UD material. However, it was observed in section 5.4 that cross-plied UD prepreg deforms similarly to woven material under bias extension deformation. This suggests that the in-plane shear deformation of cross-plied UD may be described with material model normally used for woven materials. In other words, two cross-plied UD plies may be modelled as one single woven ply. This assumption will be investigated in section 10.2.

5.5 Conclusion

Intraply shear is often considered as the most dominant deformation mechanism when forming continuous fibre reinforcements over complex shape involving double curvatures. Consequently, accurate determination of the intraply shear properties through material characterisation tests is essential. This chapter presented the investigation on the intraply shear characterisation of woven and UD prepreg materials.

For the woven prepreg, two different *de facto* test methods were used, including bias extension and picture frame test. A novel measurement method was proposed and used for in-line shear angle (i.e. shear strain) measurement. The novel method, based on a point-tracking algorithm, was compared to more traditional measurement method (e.g. DIC) and proved to be a more robust and straightforward full-field strain measurement technique when applied to intraply shear tests. Experimental tests under forming conditions showed that once normalised, both bias extension and picture frame tests provide comparable results, suggesting that either experiment can be used for the determination of intraply shear properties of woven prepreg.

For the UD prepreg, two different approaches involving different deformation mechanisms have been used for the characterisation of the in-plane properties:

(1) The first and more straight–forward approach consisted of investigating the intraply shear behaviour at a single ply level. A novel test method was developed, based on a v-notched rail shear test. Experiments carried out with full-field strain measurement showed that the transverse shear properties of UD material are dominated by inter-tow sliding. The shear stress-shear strain behaviour was characterised by strain rate dependent, bi-linear behaviour. An elastic behaviour, corresponding to shearing of the matrix was first observed, followed by plastic deformation, characterised by inter-tow sliding. Due to the novelty of the test method, further validation, and, where possible, improvements, would be beneficial. This could be done for e.g. by carrying out round-robin benchmarking tests. In addition, the development of normalisation procedure would be useful in order to obtain direct comparison with other existing tests (e.g. torsion bar test), where similar deformation mechanisms occur.

(2) The second approach involved the characterisation of UD prepreg on cross-plied specimens (i.e. $[+45/-45]_s$). The application of the novel shear angle measurement method to cross-plied UD prepreg revealed that, under bias extension deformation, cross-plied specimens deform in a similar way to woven material (i.e. characterised by 3 different shear zones). Whilst the data may not be useful in order to model UD material, this suggests that for forming simulation purpose, the shear deformation behaviour of cross-plied UD may be modelled using material models developed for woven reinforcements. This assumption will be investigated in section 9.4.1 and 10.2.

The results from this chapter will be implemented within PAM-FORM for material test simulations in chapter 9 and for subsequent forming simulations in section 10.2.

6 Friction characterisation of thermoset prepregs

6.1 Initial study on the frictional behaviour of thermoset prepreg[ii]

6.1.1 Test setup

An initial investigation of the frictional properties of UD and woven prepregs was performed using a dedicated rig previously developed at WMG. The rig (Figure 52), originally built for the characterisation of dry reinforcements was modified to deliver a fast heating rate (i.e. 80°C.min^{-1}) suitable for the characterisation of fast-curing prepreg materials. A closed loop temperature control system was added to the rig, consisting of a two-zone temperature controller and cartridge heaters producing a total of 4,400 watts.

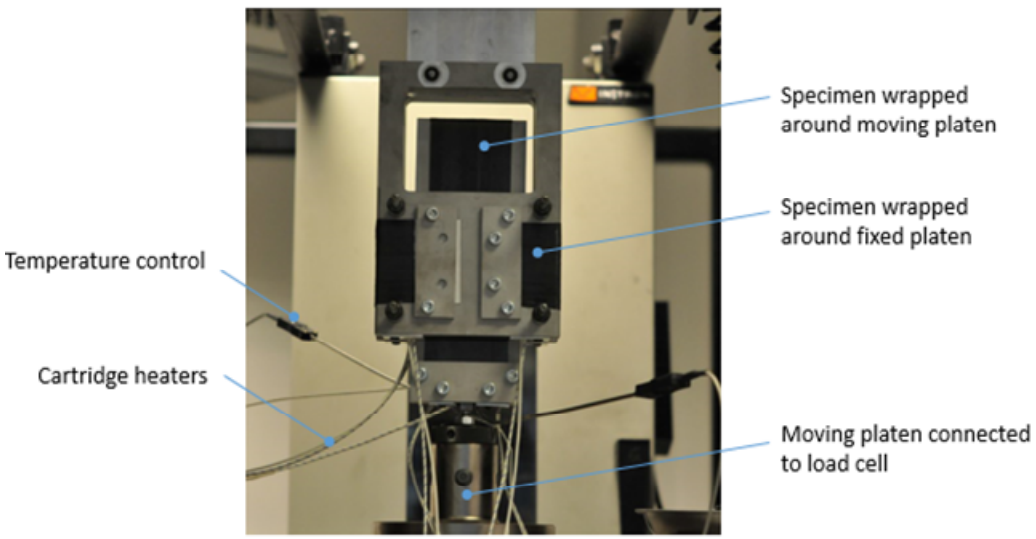

Figure 52: Friction test rig

Normal pressure upon the material is applied by means of four linear compression springs that can be tightened or loosened using nuts. The pressure is adjusted to a set value by controlling the linear displacement of the springs together with the torque applied to the adjusting nuts. Three prepreg specimens were used for each test: one sample was wrapped

[ii] **This section is partly reproduced from: C. Pasco, K. Muhammad, J. Gupta, K. Kendall. Experimental investigation on interply friction properties of thermoset prepreg systems. Journal of Composite Materials, 2019, 53(2), 227–243.*

around the moving platen and mechanically clamped along the sides perpendicular to the pulling direction. The other two samples were mounted and clamped on the outer, fixed platens along the sides parallel to the pulling direction. The resultant testing contact surface area was 8,192 mm^2 and remained constant throughout the duration of the test. The centre platen was fitted to a 500 N load cell, attached to the crosshead of an Instron 5800R. The crosshead moved at a constant set velocity and its displacement was recorded every 0.1 seconds.

Both the woven and the UD prepregs were tested under different conditions of sliding velocity (i.e. 1, 5 and 10 $mm.s^{-1}$) and normal pressure (25, 50, 75 and 100 kPa). For each test condition, the tangential load were measured and averaged over three tests. The friction coefficients were calculated such that:

$$\mu = \frac{F}{2 \times a \times N} \tag{6.1}$$

where, *F* is the tangential load read by the load cell, *a* is the surface area at the contact interface (i.e. 8,192 mm^2) and *N* is the normal pressure

For the UD material, the specimen on the centre platen was mounted with its fibre parallel to the pulling direction, while the specimens on the fixed platen were mounted with the fibres perpendicular to the sliding direction, resulting in a fibre orientation at the contact interface of 0°/90°. For the woven prepreg, the relative angle between the plies at the contact interface was 0°.

6.1.2 Results and discussion

For the UD prepreg, irrespective of the test conditions, the evolution of the tangential load during a test behaved as expected: first, the frictional force increased rapidly up to a maximum peak, corresponding to the static friction or the force required to initiate sliding between surfaces. Secondly, the force decreased and eventually reached a steady state, corresponding to the dynamic friction. The static and dynamic friction coefficients obtained are summarised in Figure 53.

It can be seen that both the static and the dynamic friction coefficients increase with increasing sliding velocity, irrespective of the normal pressure. This behaviour is attributed to the viscous, shear rate dependent resin and suggests the presence of lubricated sliding.

In contrast, the friction coefficients decrease with increasing normal pressure, before reaching a plateau. One explanation is that for low normal pressures, interlocking and nesting between opposing fibres having initially circular cross-section is likely to occur, resulting in a rough surface contact. However, for higher normal pressures, opposing fibres as well as any asperities at the interface will be flattened out, resulting in a reduction of the roughness and consequently, the friction coefficients. This was also observed in [53] and [62] in the case of UD thermoset prepreg and dry woven fabric, respectively. Upon increasing normal pressure, no further compaction seems possible as the coefficient values plateau.

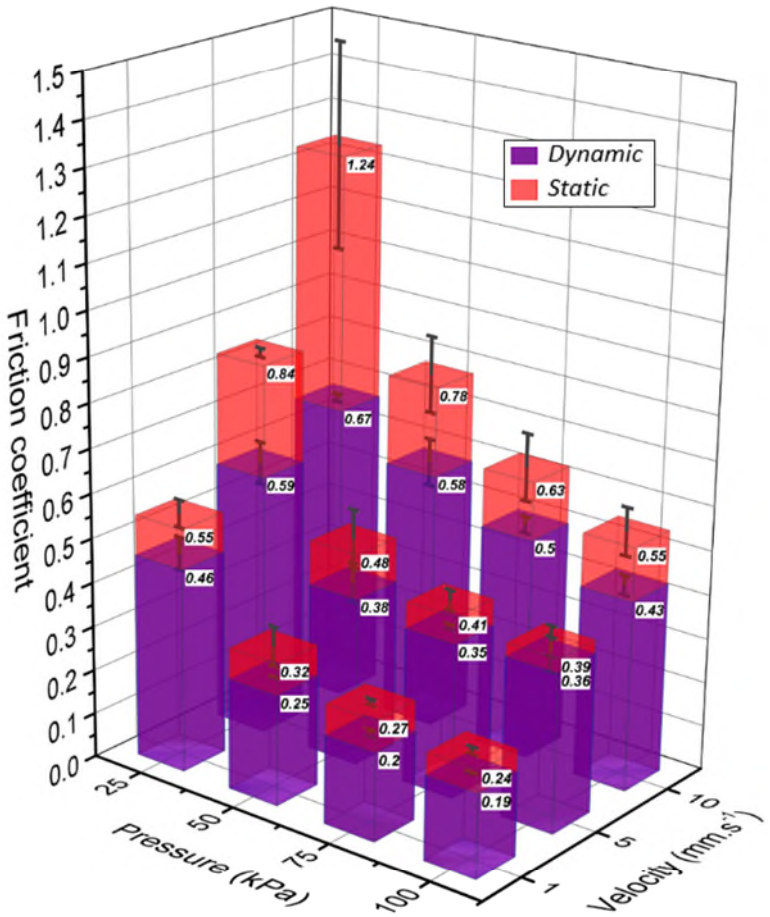

Figure 53: Dynamic and static friction coefficients summary for the UD prepreg tested at different velocities and normal pressures.

For the woven prepreg, a more complex behaviour was observed. Unlike the UD prepreg, the evolution of the tangential load during the test exhibited an erratic behaviour. Under normal pressure, significant displacement of the transverse tows was observed during the test (Figure 54). Because the transverse tows are free at both their ends, they have a higher propensity to move due to frictional forces, as compared to the longitudinal fibres that are

restricted by the clamping. In this case, displacement of transverse tows is solely due to frictional forces exerted by the mating surface. During preforming of woven reinforcements, this deformation mode can occur and typically results to in-plane waviness. In practice, such issues can be overcome using techniques that increase axial tensions in the tows and limit in-plane waviness and wrinkling. These typically include blank holders and grippers for matched die forming and vacuum pressure for double diaphragm forming. The development of tensile and compressive forces within the tows of a fabric reinforcement influences the frictional behaviour of woven material. Increasing axial tension in the warp and weft tows reduces crimp and consequently flattens the surface of the ply.

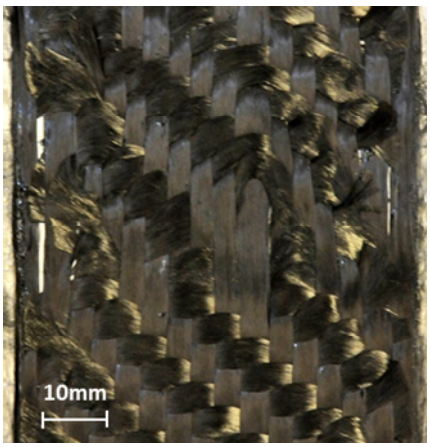

Figure 54: Woven prepreg specimen after a friction test showing significant displacement of the transverse tows

Similar to the UD material, friction coefficients were calculated from the tangential loads. It was however not possible to obtain the static friction due to initial sliding and uncrimping of the woven material. Because the specimens wrapped around the fixed platens were only secured along the pulling direction, some slight transverse movement of the specimens was observed at the start of the test, resulting in friction at the prepreg/platen interface. This mechanism invalidated the static friction results. Once the relative sliding of the specimens with the outer platens stopped and specimens were fully taut, the dynamic friction at the prepreg/prepreg interface was determined. The dynamic friction coefficients are summarised in Figure 55. It can be observed that the effect of the sliding velocity on the dynamic friction coefficients varies depending on the normal pressure. For lower normal pressures of 25 and 50 kPa, the dynamic friction coefficient remains constant with a sliding velocity of 1 and 5 mm.s-1, while a further increase of the sliding velocity leads to an increase of the dynamic friction coefficient. For a normal pressure of 75 kPa, the frictional

behaviour seems rate dependent as the friction coefficient increases with increasing testing rate. For a normal pressure of 100 kPa, it can be seen that the evolution of the sliding velocity on the dynamic friction coefficients is almost negligible. Indeed, the dynamic friction coefficients are similar at 1 and 10 mm.s-1. This suggests that high normal pressures the frictional properties of the woven material are rate independent, and that the material behaves as a dry reinforcement, unlike the UD material. This is rather unexpected as the woven material has a higher resin content by weight than the UD material.

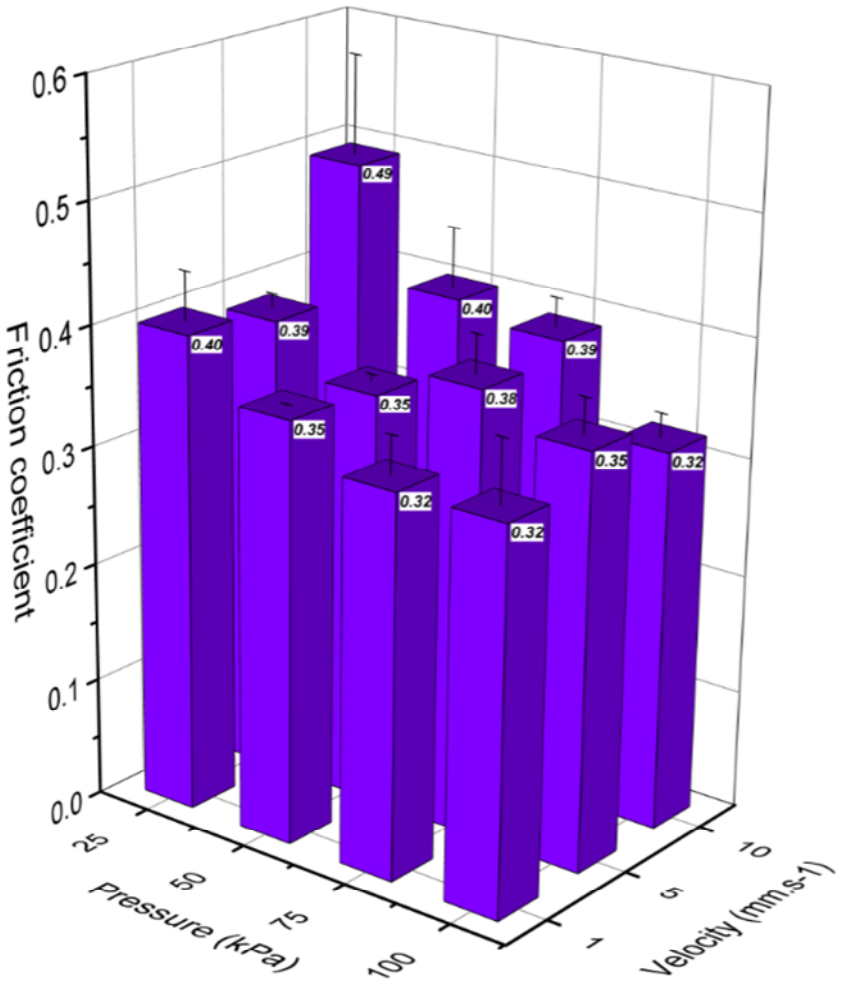

Figure 55: Dynamic friction coefficients summary for the Woven prepreg at different velocities and normal pressures

This behaviour was attributed to the manufacturing process of the prepreg material. As seen previously in section 4.2.2, the woven prepreg is characterised by a partial impregnation, with resin rich layers on either side of the material. As a consequence, high normal pressure exerted during friction tests of the woven prepreg caused the resin on both surfaces to squeeze out of the contact interface between the two plies, resulting in a

relatively dry lubrication. When testing frictional properties of a dry carbon twill weave reinforcement at 5 mm.s-1 Allaoui *et al*. [111], found a dynamic friction coefficient of approximately 0.3, similar to the one obtained in this study at 100 kPa.

In order to verify this statement, SEM micrograph analysis of the cross-section of a specimen after a test performed with a normal 100 kPa was carried out (Figure 56). The dashed white lines represent the interface between the two woven plies (location 1 in Figure 56). The fibres at the interface can be seen individually and do not seem to be fully impregnated (location 2 in Figure 56). In addition, voids within the structure can be seen. In contrast, resin rich areas characterised by a shiny and milky appearance can be observed on both outer surfaces of the specimen (locations 3 and 4 in Figure 56), confirming that the resin has migrated outwards from the contact interface, resulting in a relatively dry friction between the plies.

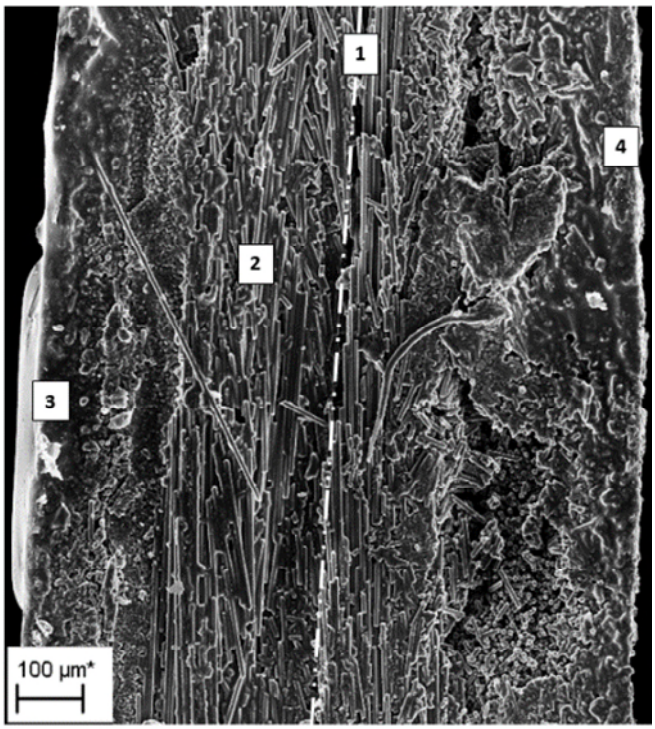

Figure 56: Through-thickness cross-section SEM micrographs showing the interface between two plies of woven prepreg after a friction test performed with a normal pressure of 100 kPa (x195). The white dotted lines represent the interface between the two woven plies

The findings from this initial study raised important implications for the characterisation of the frictional behaviour of prepreg materials and are of particular significance for this project. During the 3DF process, the impregnation of the material is expected to change under the application of vacuum. As a consequence, the friction regime at the ply/ply interface might be dominated by lubrication mode. In addition, the normal pressure

exerted by diaphragms onto the prepreg blank is expected to maintain some tension in the reinforcement, which may prevent excessive tow displacement such as depicted in Figure 54. Although of significance value, the data generated from this initial study may be not be suitable to model the intended forming process.

This prompted the need for the development a novel friction test method, with a particular focus on the intended forming process. The testing rig should be designed so that the effect of impregnation level and tow tensioning on the frictional properties of prepreg materials can be investigated. In addition, it should provide a precise and accurate control over the different test variables (e.g. normal pressure), while ensuring that the specimens are tightly secured along and across the sliding direction to prevent specimen movement.

6.2 Development of a new friction test rig

6.2.1 Benchmark study

Prior to the development phase of the novel friction test rig, a benchmark analysis was carried out. A review of the literature on frictional behaviour of dry fabrics and both thermoplastic and thermoset materials was done. A list of the different existing test rigs is given in Table 7, Table 8 and Table 9. The attributes of each method were compared, contributing to the definition of a set of specifications and design guidelines.

Laboratory	*Reference*	*Photograph*	*Schematic*
WMG, Warwick University, UK	[112]	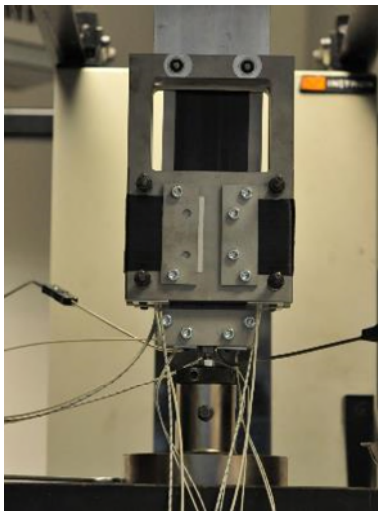	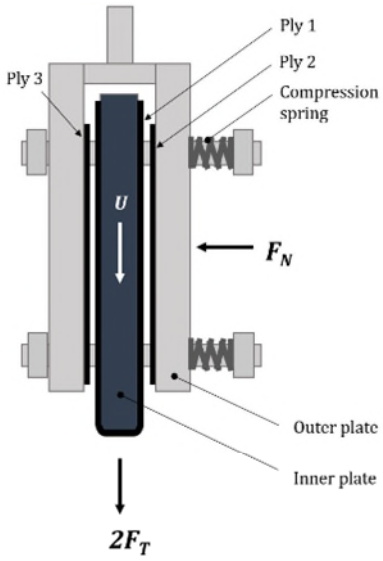
Ford, Research and Innovation Centre Dearborn Mi, USA	Submission 2 of EngD portfolio	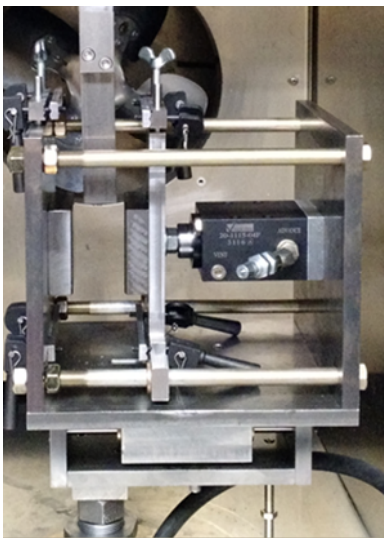	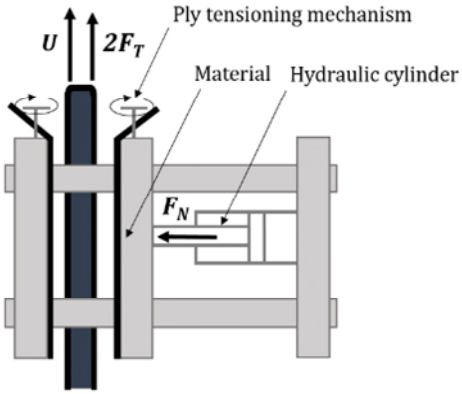

Table 7: Friction test set-ups benchmark (1/3)

Laboratory	*Ref.*	*Photograph*	*Schematic*
Royal Institute of Technology, KTH, Sweden	[53]	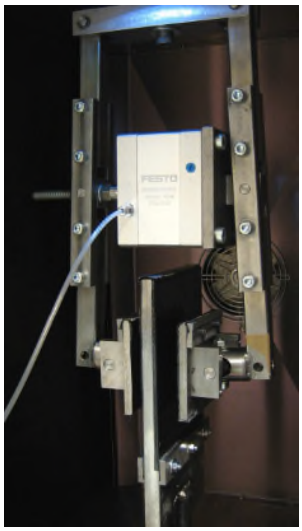	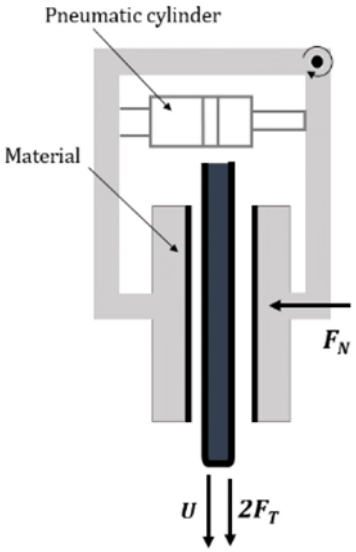
University of Nottingham, UK	[113]		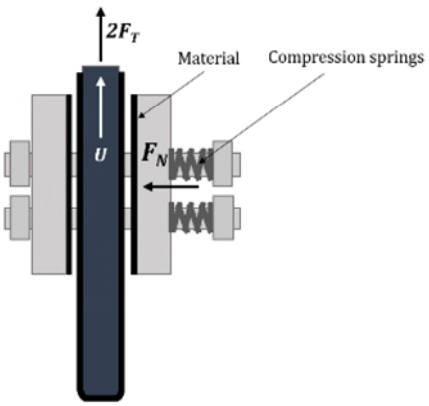
Beihang University, P.R. China	[114]		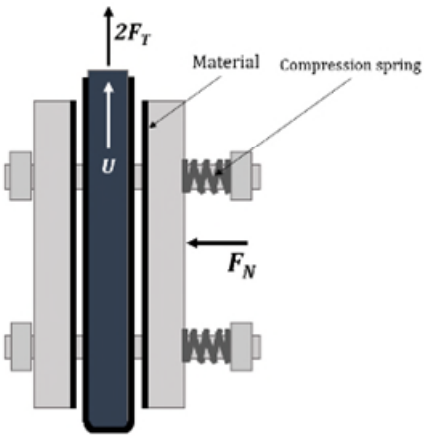

Table 8: Friction test set-ups benchmark (2/3)

Laboratory	*Ref.*	*Photograph*	*Schematic*
KU Leuven, Belgium	[115]	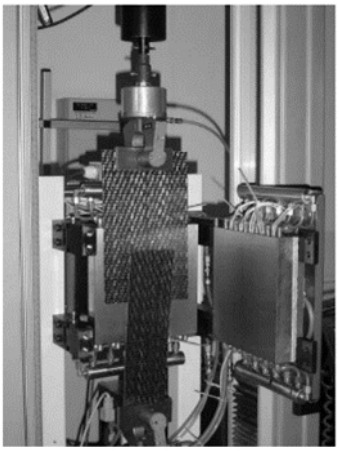	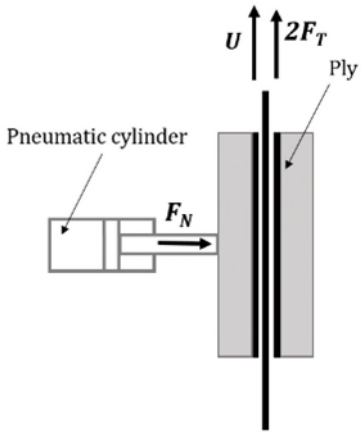
University of Twente, Netherlands	[116]		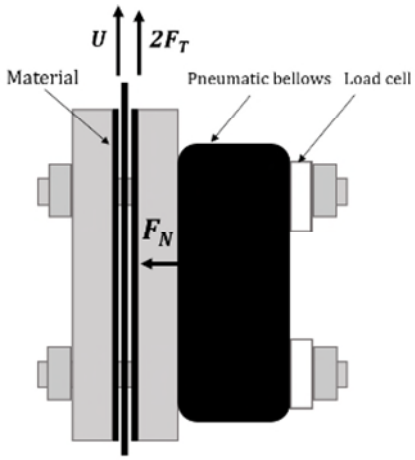
Arts et Métier ParisTech Angers, France	[117]	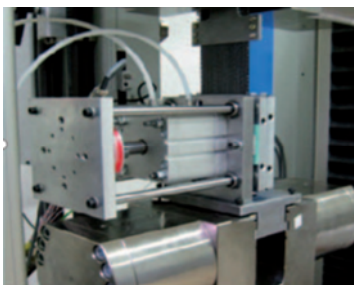	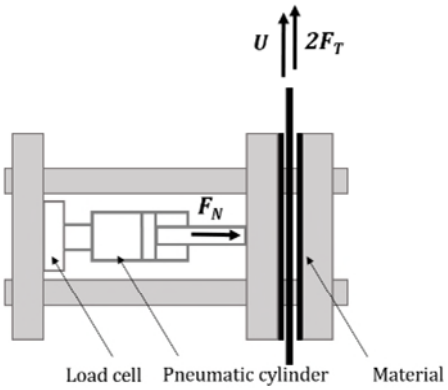

Table 9: Friction test set-ups benchmark (3/3)

Each test method is based on a pull-through design, whereby a central specimen (supported by a moving platen or free-standing) is drawn out from between two pressure plates onto which specimens are clamped. This method is quite effective since the moving specimen can be directly connected to the load cell of a standard tensile testing machine,

providing a direct measurement of the tangential load. In addition, the sliding velocity can be directly set using the tensile testing machine functions. The application of normal pressure is realised by means of compression springs [112-114], pneumatic cylinders [53, 115, 117] or pneumatic bellows [116]. The former approach is less accurate since the elongation of each spring must be identical in order to provide uniform pressure on the contact surface. The use of a load cell [115-117], is a key attribute since it allows to set and measure the evolution of the normal force during a friction test. This is not possible in [53, 112-114], where friction coefficients are calculated assuming a constant normal force. Another important requirement for this EngD project was the application of a controlled temperature. Fast heating rate is a critical attribute when studying the mechanical behaviour of rapid-cure thermoset prepregs in their uncured state. Different methods have been previously used, including silicone heating film [114] ,cartridge heaters [115-117], or by simply placing the rig within a thermal chamber [53]. The latter approach was ruled out since a long heating time would be required to heat up the rig due to the high thermal masses involved.

All test setups have been used to test the friction properties between weaves or UD where the fibre are parallel to each other and aligned to the pulling direction. To the author's knowledge, only [53] have studied the influence of different relative fibre orientations at the contact interface. The study [57], presented at a conference (ICCM 2013), showed that the relative fibre angles has a significant influence on the frictional behaviour of UD prepreg. The ability to understand this effect is particularly important when modelling lay-up with various fibre angles (e.g. quasi-isotropic laminate).

From the benchmark study, and taking into account the project requirements, the following specifications were established:

- A heating system providing a fast heating rate (i.e. 80°C.min^{-1}), combined with an accurate temperature control should be used. The test rig should be able to operate at a temperature between room temperature and 80°C (although higher temperature are also desirable for future work).
- The friction rig should be relatively compact so that it can be mounted into a 5900 Instron tensile testing machine. Friction velocity should be set using the Instron while the tangential load should be measured by the load cell.
- *In situ* measurement of the normal pressure should be possible.

- All additional electronic devices (if any) should be compatible with a 5900 Instron tensile testing machine, so that all signals are synchronized and recorded in a single place.
- A simple clamping mechanism should be used, providing a method to tightly secure the specimens and the ability to rotate the specimens so that the friction behaviour between different fibre orientations can be tested.
- The ability to adjust the pre-tension or tension of the specimen should be possible.

6.2.2 Novel test rig design

Figure 57 presents the new friction test setup. The main body of the friction rig is connected to the stationary frame of an Instron 5900 test machine. It essentially consists of three steel plates (1.2085 tool steel) of dimensions 156 by 156 mm, two of which are fixed. The third plate (referred to as moving outer platen) is connected to a piston rod of a double-action pneumatic cylinder with a 63 mm diameter bore and a 100 mm stroke. Linear bearings are used to allow translation of the steel plate in the horizontal direction along four guide bars. This translation motion allows the application of pressure against the moving inner platen, which is sandwiched between both the moving outer platen and the fixed outer platen. During a test, the inner platen move upwards applying a tangential force recorded by a 500 N Instron load cell. The test rig is equipped with an additional 2 kN load cell and four LVDT sensors (with a ±2.5 mm range).

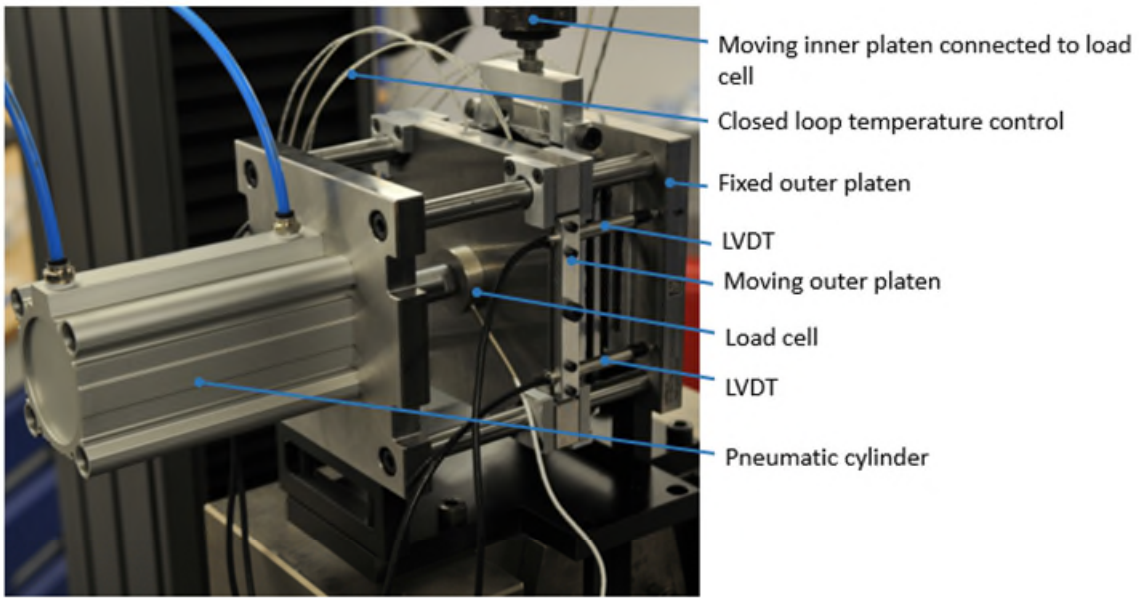

Figure 57: Picture of the new friction test setup

The additional load cell allows to measure the compressive force exerted by the piston rod of the pneumatic cylinder onto the moving outer platen, providing a direct measurement of the normal force. The LVDTs are clamped on the moving outer platen and measure the distance between the two platens during a test. This gives an indication of the parallelism between both outer platens. All transducers are supplied with a DC input and produce a DC output, and can be directly plugged into the Intron 5900.

Figure 58 presents an exploded view of the friction rig as well as a close-up, exploded view of the clamping mechanism. Specimens are clamped onto material platens, which are themselves placed on the outer platens by means of dowels. The dowels are interference fitted into the material platens and slide closely into the outer platens. A circular pattern of equispaced holes allows to position the material platen at different angles, thereby enabling to test different relative fibre orientations at the contact interface. A closed-loop temperature control system is used to heat up the material platens and consists of four cartridge heaters producing a total of 1400 watts. The temperature is measured using thermocouples, which are directly connected to a temperature controller. PTFE plates are placed behind the material platens in order to limit heat conduction towards the outer platens.

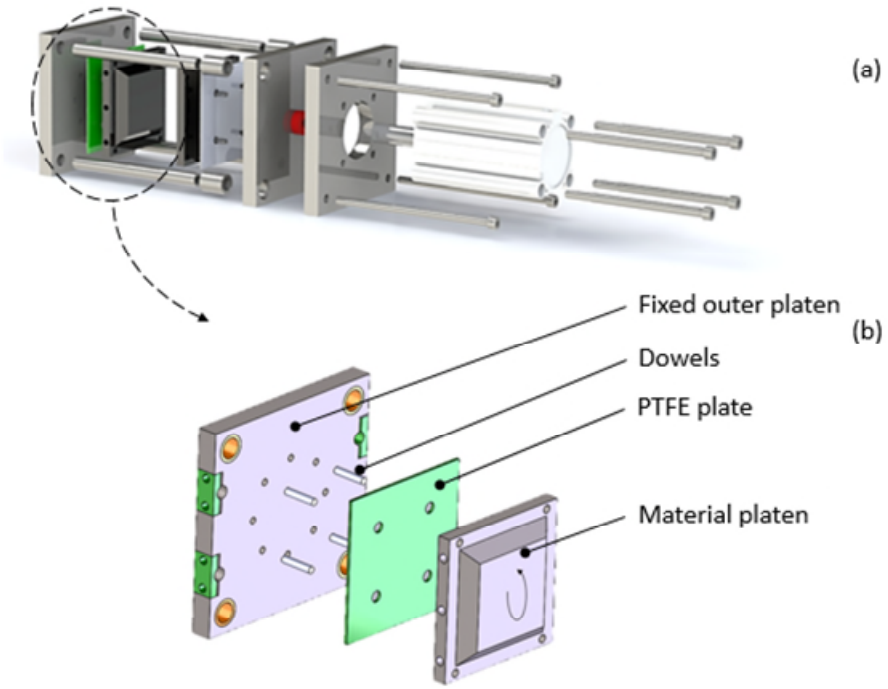

Figure 58: Exploded view of the friction test rig (a), and close-up, exploded view of the material clamping mechanism

An additional rig was designed in order to adjust the pre-tension in the warp and weft tows. It consists of a main frame and two force gauges. A cross-shaped specimen, draped over the material platen, is clamped at each corner. Two clamps are connected to 500 N force gauges while opposite ones can be moved using wing nuts, introducing tension in both the warp and weft tows. Once the desired pre-tension is reached, the specimen is firmly clamped onto the material platen, which can then be mounted onto the outer platen of the friction rig. For each test, a maximum pre-tension of 500 N (corresponding to an applied stress of 18 MPa) in both the warp and weft direction was applied. This value was determined experimentally and was deemed sufficient in order to consistently prevent transverse displacement of the tows during friction test. A more accurate method to determine the test pre-tension value may require investigating the axial tension exerted on the tows during the actual preforming process. Considering that: (1) the preform is assumed inextensible, (2) there is no relative slippage between the diaphragms and the preform during forming and (3), the diaphragm deformation occurs outside of the contact area with the preform, then the axial force in the tows can be determined from the force required to stretch the diaphragm.

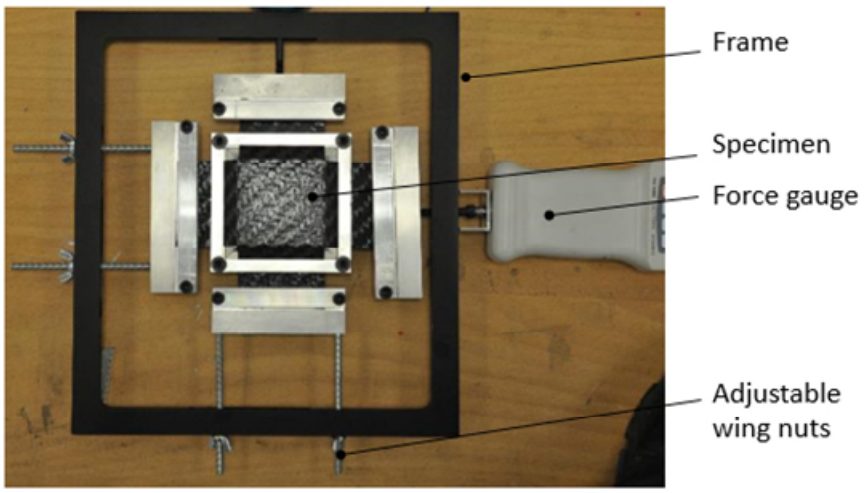

Figure 59: Pre-tensioning mechanism of the friction test specimens

In order to assess the structural integrity of the friction test rig under loading, finite element analysis was carried out. The CAD model (Figure 60, a), was discretised into 8 mm solid triangular elements (Figure 60, b).

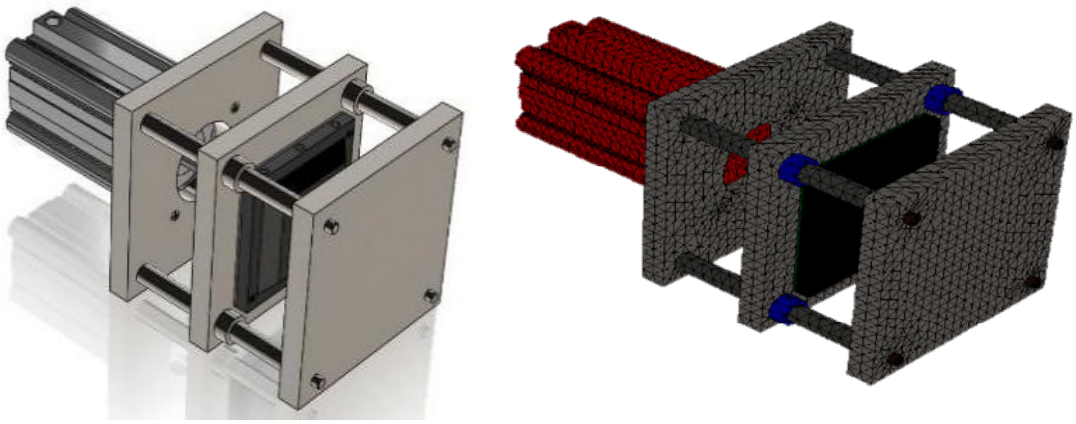

(a) (b)

Figure 60: (a) CAD model of the friction test rig and (b) finite element model

Conditions of no penetration and surface-to-surface contacts were assigned between the dowels and the material platens, and between the guide bars and the outer platens. These specific areas were deemed critical for the assembly since they are the main load bearing elements during a test. For simplification and to reduce computational time, the rest of the assembly was considered bonded.

Considering the geometry of the rig and the nature of the test, the problem can be simplified to a concentrated load located on a beam, fixed at both ends. The concentrated load corresponds to the frictional force exerted by the moving platen onto the material platens, while the beam corresponds to the four guide bars. A 500 N tangential force was applied on each material platen, in order to simulate the action of the moving platen. This force was determined considering the maximum friction coefficients obtained in the initial investigation on the frictional properties of prepregs (section 6.1). Results are presented in Figure 61 and show the stress distribution around the dowels and the vertical displacement of the moving outer platen. A maximum stress of around 15 MPa is obtained in the dowels, which is well below the yield strength of a typical tool steel (i.e. approximately 900 MPa). A maximum vertical displacement of about 6 µm is observed at the moving outer platen, which was deemed acceptable.

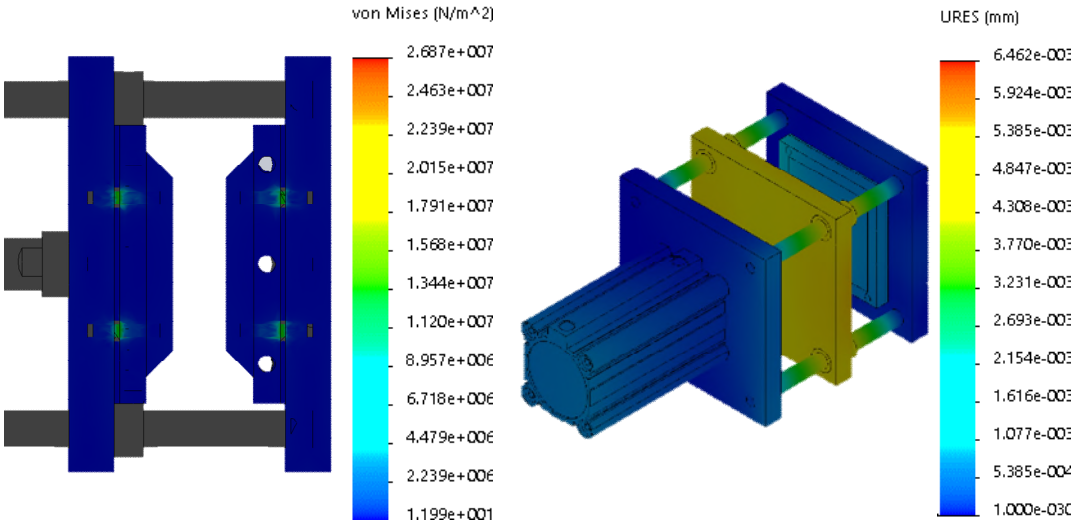

Figure 61: FEA results of the friction test rig showing: (a) stress distribution around the dowels and (b) vertical displacement of the moving outer platen

6.2.3 Results and discussions

During the 3DF process, a number of contact interactions occur at different interfaces: These include the interface between two adjacent plies, the interface between the laminate and the diaphragm and the interface between the diaphragm and the tool. All these mechanisms have been investigated. Friction at the ply/ply interface, for both the woven and the UD prepregs was investigated under forming conditions using sliding speeds of 1 and 5 $mm.s^{-1}$. A normal pressure of 100 kPa was used in order to simulate the effect of the vacuum between the diaphragms and enable comparison with earlier results [112]. An additional pressure of 200 kPa was used, in order to account for the combined effect exerted by both the punch and the vacuum. These normal pressures are higher than those used in previous study on frictional behaviour of thermoset prepregs [53, 57], and were selected to be in the range of pressures expected to be encountered during 3DF. Friction at the ply/diaphragm and the diaphragm/tool interfaces was also investigated. The resulting test matrix is shown in Table 10. All tests were performed at 80°C and each test condition was run three times.

Interface	*Relative fibre angle (Degrees)*	*Normal pressure (kPa)*	*Velocity ($mm.s^{-1}$)*
Woven/woven	0/0	100	1
			5
		200	1
			5
	0/45	100	1
			5
		200	1
			5
UD/UD	0/0	100	1
			5
		200	1
			5
	0/90	100	1
			5
		200	1
			5
Woven/Diaphragm	/	100	1
UD/Diaphragm	/	100	1
Tool/Diaphragm	/	100	1

Table 10: Test matrix for the friction tests

Figure 62 shows typical output data from a friction test, including the tangential load, the normal load, the relative displacement of the LVDTs and the misalignment angle. Each output will be detailed below:

(1) The tangential load measured by the 500 N Instron load. As the test progresses, the load increases rapidly up to a maximum corresponding to the static friction. Upon further extension, the load decreases and reaches a plateau, corresponding to the dynamic friction. A similar behaviour was observed in [112]. This trend was

observed for each test, with the exception of the UD prepreg with a relative fibre angle at the interface of 0/0.

(2) The normal load measured by the load cell connected to the pneumatic cylinder. For each test, the normal load typically varied within ±3 N with respect to the nominal set value. This variation was attributed to slight movement of the moving outer platen during a friction test.

(3) The relative displacement of the LVDTs. LVDTs 5 and 8 measure the displacement of the top left and top right corners of the fixed outer platen, respectively. LVDTs 6 and 7 measure the displacement of the bottom left and bottom right corners, respectively. The greater displacement measured by the bottom two LVDTs indicates a slight backward tilting of the moving outer platen as the test progresses. For each test, a clear similarity was observed in the relative displacement of the top two LVDTs. Comparable observation was made for the bottom two LVDTs. This indicates that during a test, the fixed and the moving outer platens do not rotate around the sliding direction.

(4) The misalignment angle between the fixed and the moving outer platens. Using the LVDTs reading, the angular misalignment gives an indication of the parallelism between the different surfaces in contact. The misalignment is determined by calculating the angle between the normal of the moving outer platen and the normal of the fixed outer platen (assumed to be the z-axis). The angle is calculated such that:

$$\alpha = \cos^{-1}\left(\frac{\vec{A}.\vec{B}}{\left\|\vec{A}\right\|.\left\|\vec{B}\right\|}\right) \tag{6.2}$$

Where $\vec{A}$ and $\vec{B}$ are the normal vectors of the moving and the fixed outer platens, respectively. A maximum misalignment of 0.7 and 0.16 degrees was observed for the woven and the UD prepregs, respectively. The misalignment of the platens was deemed negligible for the following reasons:

- Considering the compressibility of the material and a maximum misalignment of 0.16 degrees, it was assumed that the contact surface area and therefore the friction coefficient between the surfaces tested remained unchanged.

- The misalignment obtained in this study were in similar order of magnitude or lower than that of previously reported results in the literature [118].

As a consequence, a modification of the rig design was not required.

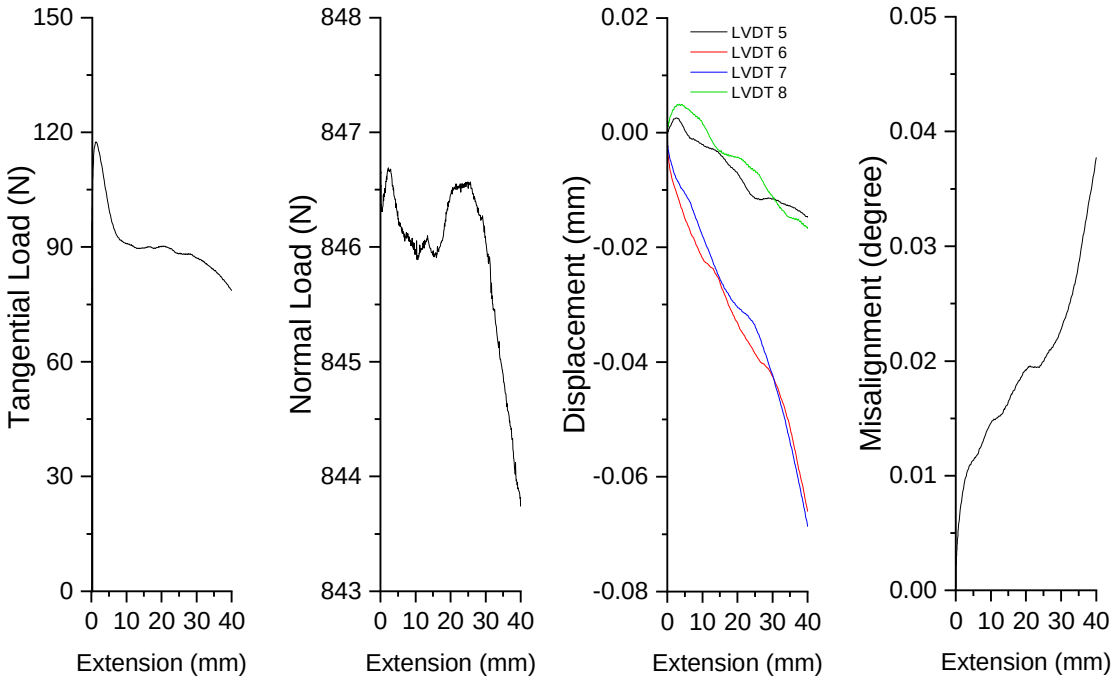

Figure 62: Typical outputs from a friction test

The friction test results are shown in the next sections. For each test, friction coefficients were directly calculated as the ratio of the tangential load to the normal load. Prior to the test, all woven specimens were vacuum bagged under 1 bar pressure at 80°C for 2 minute in order to simulate the forming process (section 4.2.3). On average, an 11% decrease in the friction coefficient was observed after vacuum bagging. For the determination of the static friction coefficient, the tangential load at the peak and the corresponding normal load were considered. For the dynamic friction coefficients, the load used for the calculation corresponds to the average of the load ranging between the intersections of the tangent of the peak with the plateau, to the end of the test.

6.2.3.1 Ply/ply interface

Friction coefficients obtained for the UD prepreg are shown in Figure 64. Values are reported for a relative fibre angle at the sliding interface of 0/0 (Figure 64, a) and 0/90 (Figure 64, b). For the 0/0 interface, the static friction could not be determined since no prominent peak could be observed. This was attributed to a friction mode specific to the 0/0 interface. As the normal pressure builds up and the specimens are pushed against each

other, significant intermingling and nesting between opposing, parallel fibres occur. As the test progresses, this friction behaviour results in a combing effect and is exemplified in Figure 63. Both the normal pressure and the sliding velocity have an effect on the dynamic friction coefficients. A higher normal pressure result in lower dynamic friction coefficient. This was also observed in [112], and is attributed to a global reduction of the surface roughness. Irrespective of the normal pressure, the dynamic friction coefficients increase with increasing sliding velocity. This shear rate dependent behaviour suggests the presence of lubricated, viscous sliding. Interestingly, the effect of speed seems to be greater for a higher normal pressure. In addition, the effect of the normal pressure are less noticeable at higher sliding velocity. For a sliding velocity of 1 $mm.s^{-1}$, the use of a higher normal pressure results in a 46% decrease in the dynamic friction. For a sliding velocity of 5 $mm.s^{-1}$ however, only a 15% decrease in the dynamic friction coefficient is reported. This behaviour highlights a complex combined interaction of the sliding velocity and the normal pressure on the frictional behaviour of UD prepreg.

Figure 63: Picture showing the combing effect resulting from interaction between adjacent fibres during a friction test of UD prepreg with a 0/0 interface.

For the 0/90 interface, similar observations can be made for both the dynamic and the static friction coefficients. Both the static and the dynamic friction coefficients increase with increasing sliding velocity and decrease with increasing normal pressure. Generally, the dynamic friction coefficients are lower than the ones obtained at the 0/0 interface, irrespective of the test condition. Analysis of the specimen post-test revealed smooth surfaces, unlike the 0/0 interface. Although using lower normal pressures, Åkermo *et al.* [57], observed a different behaviour in that friction coefficient obtained at the 0/0 interface are similar to or lower than at the 0/90 interface.

The 0/90 results performed with a normal pressure of 100 kPa are in relatively good agreement with those obtained in the previous study under similar sliding speed (section

6.1.2). The previous study reported static friction coefficients of 0.24 and 0.39 for a sliding velocity of 1 and 5 mm.s^{-1}, respectively (against 0.24 and 0.37, respectively, using the novel friction rig). With respect to the dynamic friction coefficients, values of 0.19 and 0.36 were obtained for sliding velocity of 1 and 5 mm.s^{-1}, respectively (absent 0.20 and 0.30 using the novel friction rig).

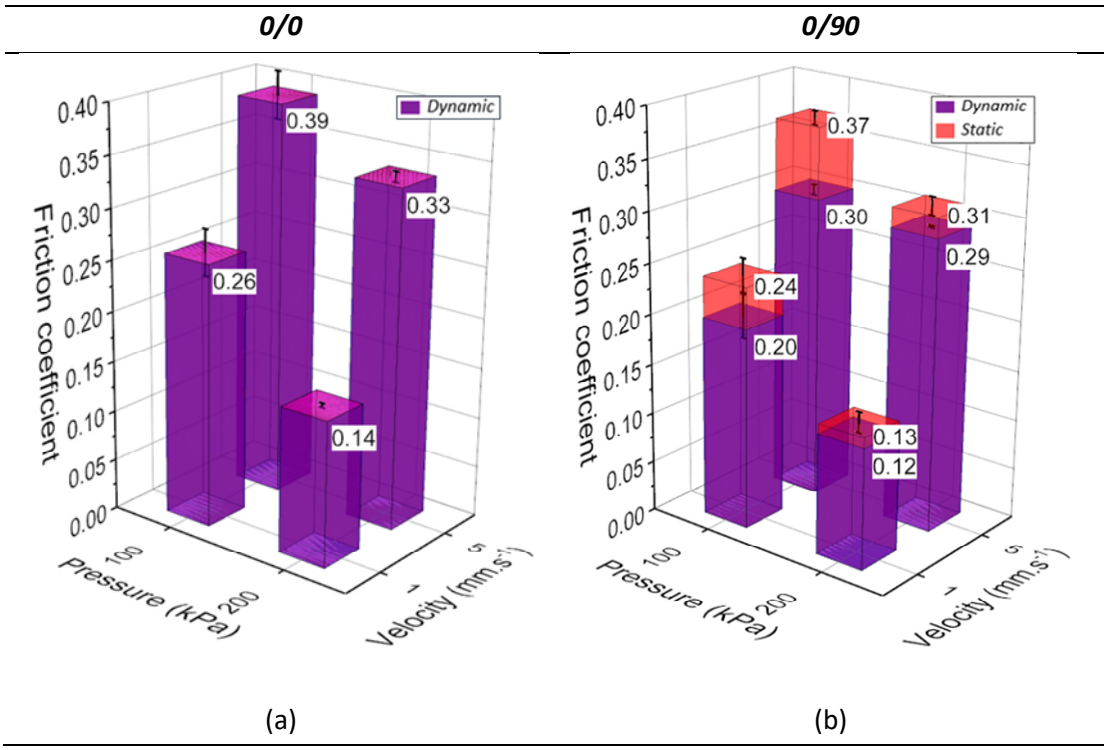

Figure 64: Friction coefficients for the UD prepreg as a function of the normal pressure and sliding velocity considering: (a) 0/0 interface and (b) 0/90 interface

Friction coefficients obtained for the woven prepreg are shown in Figure 65. Values are reported for a relative fibre angle at the sliding interface of 0/0 (Figure 65, a) and 0/45 (Figure 65, b). Unlike previous results (section 6.1), a static peak in the tangential load was observed. In addition, comparable tests performed at the 0/0 interface show significantly different results. Previous results for a normal pressure of 100 kPa reported dynamic friction coefficients of 0.32 and 0.35, for a sliding speed of 1 and 5 mm.s^{-1}, respectively. In contrast, at a similar normal pressure, the novel test results shown herein report dynamic friction coefficients of 0.14 and 0.23, for a sliding speed of 1 and 5 mm.s^{-1}. This difference is attributable to pre-tensioning of the fibres, which prevents displacement of the tows under sliding and provides a smoother contact surface. Irrespective of the relative fibre angle orientation, the test results from the novel friction test rig show a similar trend. Both the static and dynamic friction coefficients increase with increasing sliding velocity and decrease with increasing normal pressure. Irrespective of the test conditions, the 0/0

interface shows higher interply friction coefficients. This difference is more pronounced at a normal pressure of 200 kPa, where friction coefficients at the 0/0 interface are up to 91% higher compared to the 0/45 interface. On possible explanation is that the presence of off-axis fibres at the 0/45 interface prevents fibre nesting and therefore results in a smoother surface.

0/0	***0/45***
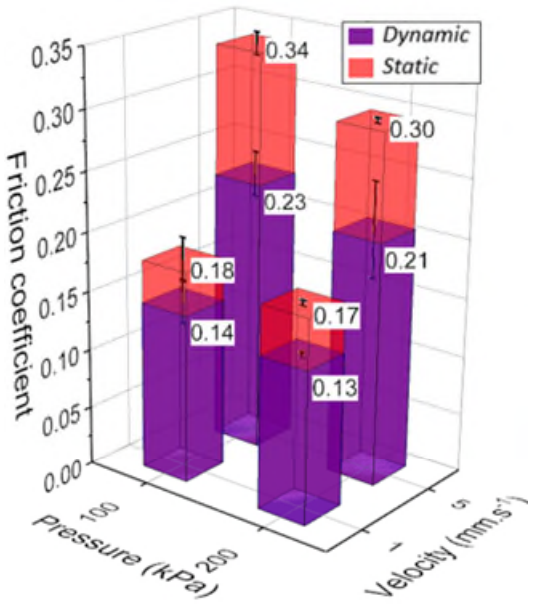	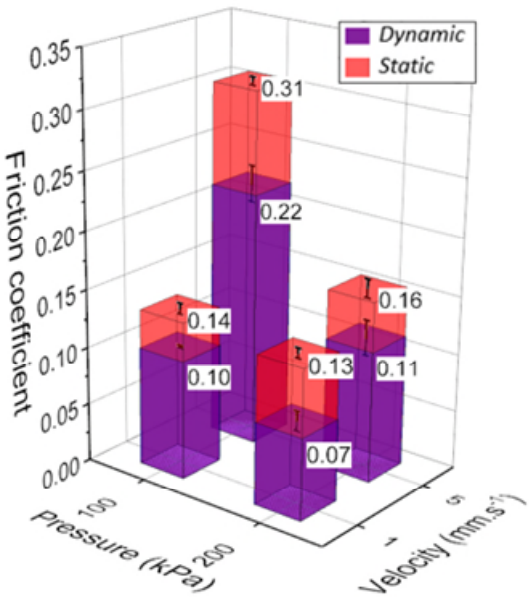
(a)	(b)

Figure 65: Friction coefficients for the woven prepreg as a function of the normal pressure and sliding velocity considering: (a) 0/0 interface and (b) 0/45 interface

6.2.3.2 Ply/Diaphragm interface

During the 3DF process, interactions between the prepreg material and the diaphragm will occur. To understand these deformation mechanisms, tests at both the woven/diaphragm and UD/diaphragm interfaces were carried out. Unlike the interply properties, the friction at the ply/diaphragm interface was assumed isotropic, and as a consequence only one test orientation was investigated. In addition, only one normal pressure and one sliding speed was used, i.e. 100 kPa and 1 $mm.s^{-1}$, respectively. A similar test setup to that used for the interply friction characterisation was utilised. However, the prepreg specimens mounted onto the outer platens were replaced by diaphragm specimens (similar to the tool/diaphragm interface in Figure 66, b).

At the woven/diaphragm interface, the static and dynamic friction coefficients obtained were 0.29 and 0.21, respectively. For the UD/diaphragm interface, a static friction coefficient of 0.4 and a dynamic friction coefficient of 0.39 were obtained.

6.2.3.3 Tool/Diaphragm interface

Similarly, interactions between the diaphragm material and the tooling will occur during 3DF. The friction properties at the tool/diaphragm interface were investigated using a normal pressure of 100 kPa and a sliding speed of 1 $mm.s^{-1}$. In order to replicate the tool surface, steel shims were used in place of the prepreg specimens on the moving inner platen (Figure 66, a). The steel shims were polished to a 1200 grit finish in order to obtain a surface finish similar to that of the double dome tool used in the forming experiments (section 10.1).

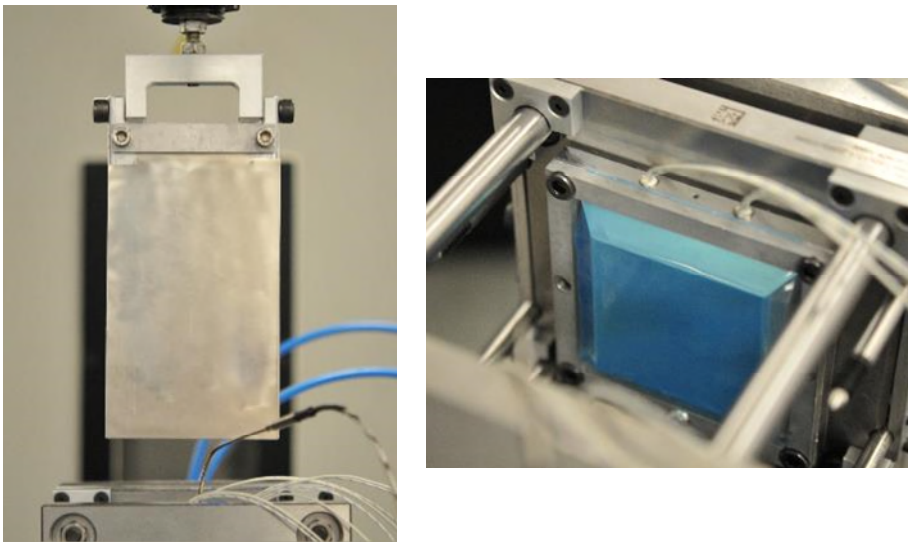

(a) (b)

Figure 66: Test setup during a friction test at the diaphragm/tool interface. (a) Steel shim representative of the tool surface and (b) diaphragm material.

A static friction coefficient of 0.51 A dynamic friction coefficient of 0.46 was found.

6.3 Conclusion

This chapter aimed to investigate the frictional behaviour of two prepreg materials, i.e. one UD and one woven twill, under conditions representative to those occurring during 3DF. Parameters including the relative fibre angle, the relative sliding speed and the normal pressure were investigated. An initial study highlighted the challenges in evaluating the frictional behaviour of composite material for specific applications such as 3DF. One particular example is the application of vacuum, which modifies the level of prepreg impregnation during forming. This phenomenon needs to be accounted for in the friction test method since the impregnation level will affect the frictional behaviour. In addition, the effect of tow tensioning was also observed on specimen deformation and friction properties.

In order to overcome these issues, a novel friction test rig was designed and manufactured. The novel test rig allows pre-test adjustment of the tow tension, as well as live, *in-situ* monitoring of the normal pressure and platen parallelism. Generally, it was seen that both composite materials exhibits a similar behaviour whereby: (1) the friction coefficients increase with increasing sliding velocity due to the shear rate dependence of the resin at the contact interface and (2), the friction coefficients decrease with increasing normal pressure due to a reduction in global surface roughness at the interface. For the UD material, a specific deformation mode was observed when testing the 0/0 interface, whereby significant fibre nesting occurred between opposing fibres. As a result, only the dynamic friction coefficient could be determined. Friction coefficients at the ply/diaphragm and tool/diaphragm, which are of particular importance when studying the 3DF process, were also investigated.

The findings reported in this chapter show that when modelling the forming behaviour of multi-layer prepreg materials, it is essential to consider the effects of normal pressure, sliding velocity and relative fibre angle on the frictional properties. A summary of the dynamic friction obtained for each test condition and surface pairing tested is presented in Table 11. These results will be implemented within PAM-FORM for material test simulations in chapter 9 and for subsequent forming simulations in section 10.2.

Interface	*Relative fibre angle (Degrees)*	*Normal pressure (kPa)*	*Velocity ($mm.s^{-1}$)*	*Friction coefficient*
Woven/woven	0/0	100	1	0.14
			5	0.23
		200	1	0.13
			5	0.21
	0/45	100	1	0.10
			5	0.22
		200	1	0.07
			5	0.11
UD/UD	0/0	100	1	0.26
			5	0.39
		200	1	0.14
			5	0.33
	0/90	100	1	0.20
			5	0.30
		200	1	0.12
			5	0.19
Woven/Diaphragm	/	100	1	0.21
UD/Diaphragm	/	100	1	0.39
Tool/Diaphragm	/	100	1	0.46

Table 11: Summary of the dynamic friction coefficients obtained for all surface pairings and test conditions investigated.

7 Transverse tensile properties of UD prepreg

Together with longitudinal shear (section 5.3), stretching transverse to the fibres direction is one of the main deformation mechanisms arising during forming of UD prepregs. It was demonstrated in [56], that the transverse stiffness of a UD prepreg can be much lower than the in-plane shear one. This implies that during forming of UD prepreg, deformation may be dominated by transverse stretching which may ultimately lead to ply splitting. However in practice, this is limited by the presence of off-axis neighbouring plies. The inextensible fibres of the off-axis plies, together with adhesion mechanism from the viscous resin help reduce the development of transverse stretching.

To date, the vast majority of studies on the transverse properties of UD prepreg apply to cured material [119-121]. As such, there does not exist any test standard for the characterisation of the transverse tensile properties of UD prepreg in their uncured state. Potter [56], while studying the in-plane deformation of UD prepreg used a simple tensile test. In a similar study, Margossian *et al*. [122] used both a tensile testing machine and a DMA. While the DMA provides accurate determination of the forces, the measurement of strains is only possible by considering the displacement of the actuator. As such, true sample strain measurement is not possible. In this work, the transverse tensile properties of the UD prepreg were determined using a simple tensile test.

The characterisation of the transverse tensile properties of UD prepreg are important when carrying out forming simulation, as they may provide an indication of ply splitting.

7.1 Test setup

Test were performed at 80°C (i.e. forming temperature) in an environmental chamber and were supported by full-field strain measurement using DIC technique. The test specimen consists of a single ply of dimensions 74x100 mm. Specimen was clamped using two mechanical clamps with serrated profiles, similar to those used in section 5.2.3. One clamp is fixed while the other one is connected to a 10 N load cell that records the force exerted on the sample. The load cell is connected to the crosshead of an Instron 5900. Test were performed using different crosshead speeds, i.e. 1, 5 and 8.33 $mm.s^{-1}$. The DIC data were processed using Aramis® software. For a description of the DIC technique, as well as a description of the basics of strain calculation, the reader is referred to appendix A and B.

7.2 Results and discussion

Figure 67 shows the major strain distribution obtains during a test, just before specimen failure. It can be observed that strain is concentrated at the tow interfaces, which is characterised by banding on the surface of the specimen. This suggests that ply splitting occurs in the resin-rich areas between the tows.

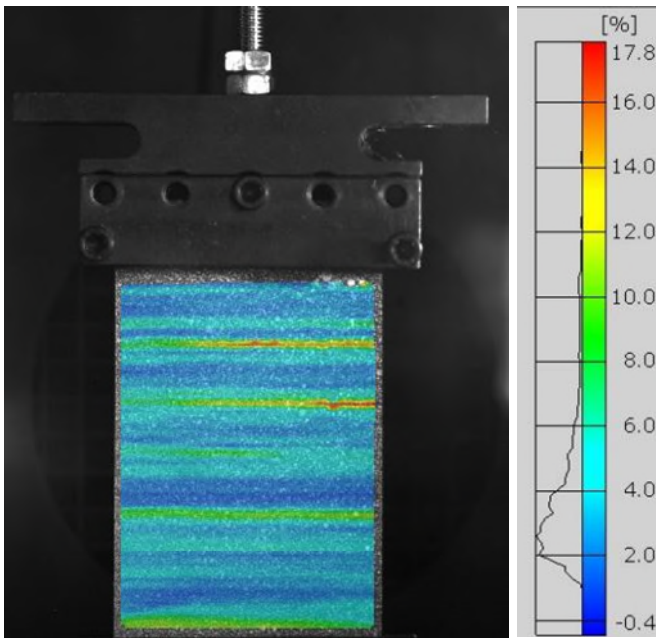

Figure 67: Major strain distribution during a transverse tensile test of a UD prepreg.

Figure 68 shows the stress-strain curves of the transverse tensile test performed with different crosshead speeds. The strain was averaged from the strain distribution over the surface of the specimen (Figure 67). The material shows a strain rate dependent behaviour, which confirms that transverse stretching of UD prepreg is dominated by deformation and shearing of the viscous resin. Increasing the crosshead speed results in higher stresses. In addition, it can be observed that the maximum strain before failure is strain rate dependent. Using a crosshead speed of 1 $mm.s^{-1}$, a maximum strain before failure of approximately 4% is obtained. In contrast, a maximum strain before failure of 7% is obtained for a test performed with a crosshead speed of 8.33 $mm.s^{-1}$. Irrespective of the test speed, the curves show a similar behaviour. Initially, the specimen shows a relatively linear stress-strain relationship. Then, a variation of the slope of the stress-strain curve is noticeable, ultimately leading to specimen failure. Margossian *et al*. [122], observed a similar behaviour and reported results of the same order of magnitude when studying the transverse tensile properties of a UD prepreg at 60°C.

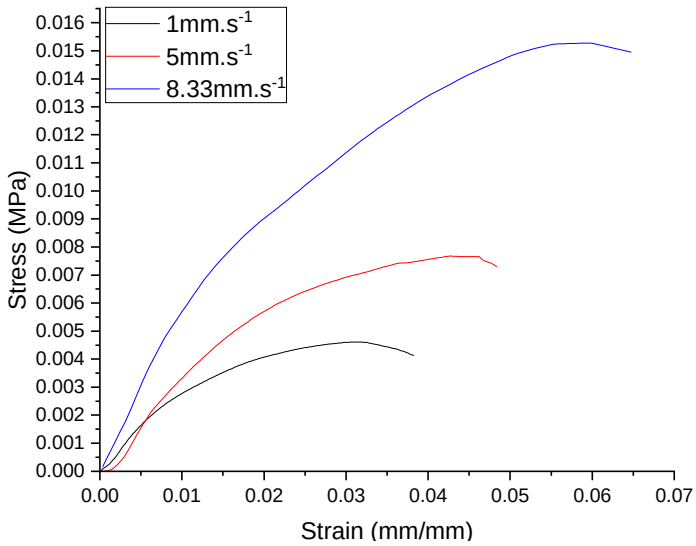

Figure 68: Transverse tensile stress-strain curves for the UD prepreg under different test speeds

7.3 Conclusion

This chapter addressed the experimental characterisation of the transverse tensile properties of a UD prepreg material. Investigation of the transverse tensile behaviour of UD reinforcements is important due to their extremely high anisotropy, characterised by a high in-plane stiffness along the fibre direction with comparably negligible in-plane stiffness across the fibre direction. This characteristic, particular of UD reinforcement, results in specific deformation mode such as transverse stretching, which may lead to ply splitting. Tests were carried out at elevated temperature and at different strain rates, using a universal tensile test machine equipped with a DIC system. Major strain distribution revealed localised high strain areas in the resin rich region, where ply splitting ultimately occurred. A strain rate effect was observed, whereby higher loads were obtained when carrying out tests with higher crosshead speed.

The accurate determination of the transverse tensile properties of UD prepreg is paramount for further forming simulation, and may help in predicting and identifying any areas prone to ply splitting.

These test data presented in Figure 68 will be directly tabulated in PAM-FORM for material test simulations in section 9.3.2, and for subsequent forming simulations of the UD prepreg in section 10.2.4

8 Bending characterisation of thermoset prepregs

This chapter describes the experimental work carried out to study the bending properties of UD and woven thermoset prepreg materials. Firstly, a review of the literature on the bending properties of composite reinforcements is presented, along with an evaluation of the different testing methods available. Built upon this review, a suitable test method was identified and a testing rig was developed. Tests were carried out at forming temperature (i.e. 80°C) and the effect of the pre-compaction on the bending behaviour of the reinforcements was investigated.

8.1 Literature review

To date, most characterisation tests for the bending behaviour of composite reinforcements are based on evolutions of the cantilever test [123], or the Kawabata Evaluation System (KES) [124], which were both originally developed to measure the mechanical properties of clothing fabrics. Both these techniques later contributed to the publication of standards. An alternative method, primarily used for the characterisation of cured laminate, is 3-point bending. Despite the importance of bending properties on the formability of composite reinforcements, the literature remains relatively scarce. A vast majority of the published articles concern the study of dry reinforcements [125-127]. Most recent contributions on prepreg materials are limited to those with thermoplastic matrix [128, 129]. To the author's knowledge, and at time of writing, there have been only two published papers on the bending properties of thermoset prepreg studied under conditions similar to those in high-volume processes (i.e. elevated temperature and strain rate) , see [130] and [131]. Table 12 gives an overview of the existing characterisation test methods for the bending properties of dry reinforcements and prepreg materials, along with the different variables investigated and the materials tested. These test methods can be grouped into three main categories, namely: cantilever test, Kawabata test and three point bend test. Figure 69 depicts pictures of each corresponding test setup.

Ref.	*Figure 69*	*Variables*	*Device*	*Movement type*	*Material*
Peirce [123]	(a)	Overhang length	Cantilever test	Gravity induced	Cloth
Bilbao *et al*. [125]	(b)	Overhang length	Modified cantilever test	Gravity induced	2.5D carbon fabric and Interlock carbon fabric
Dangora *et al*. [126]	(c)	Tip load	Vertical cantilever test	Deflection with controlled tip loads displacement	Woven E-glass/PP and NCF E-glass fabric
Lomov *et al*. [127]	(d)	Specimen width	Kawabata	Rotation	Bi- and quadriaxial carbon fabrics
Sachs *et al*. [129]	(e)	Specimen thickness, rotational velocity, temperature	Rheometer using a custom-built fixture	Rotation	UD/PEEK
Martin *et al*. [132]	(f)	Speed, temperature	3-point bending fixture	3 point-bending	UD E-glass/PP
Margossian *et al*. [128]	(g)	Speed, temperature	DMA using 3-point bending fixture	3 point-bending	UD-tape carbon/PA6
Wang *et al*. [131]	(h)	Speed, temperature	Buckling test	Compression	UD carbon/epoxy

Table 12: Bending characterisation methods for fibrous materials

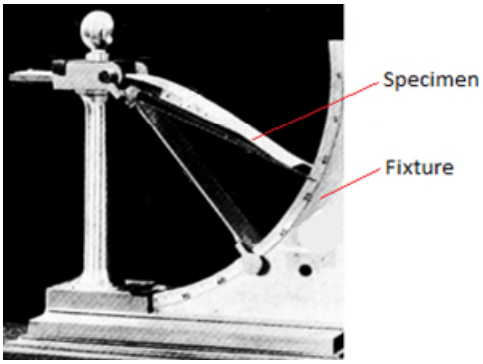

(a)

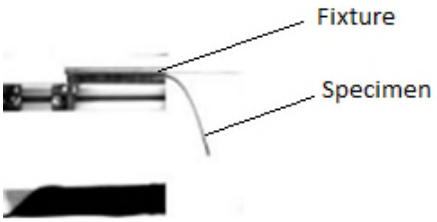

(b)

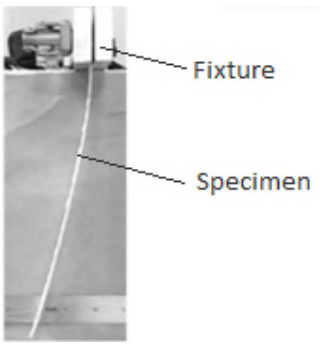

(c)

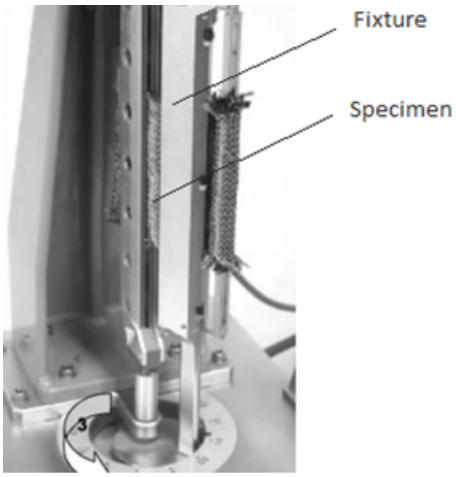

(d)

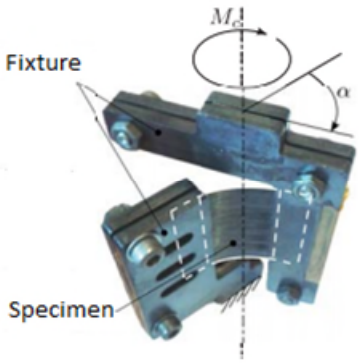

(e)

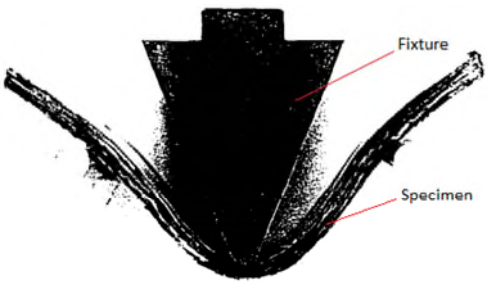

(f)

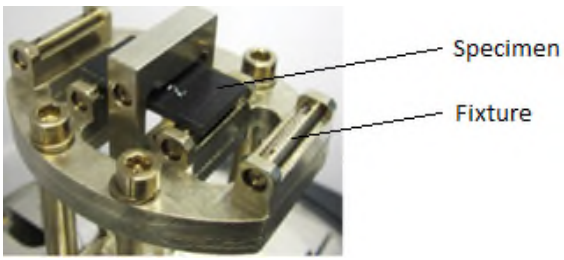

(g)

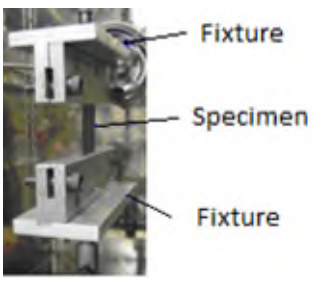

(h)

Figure 69: Pictures of previously developed bending characterisation tests for fibrous reinforcements – The letters refer to Table 12

A vast majority of today's test methods for the characterisation of stiffness of fabrics rely on the early work of Peirce [123]. In the 1930s, Peirce was the first to address the macroscopic bending behaviour of cloth and textile materials as a measurable quantity. Considering the large deflection of thin beams using linear elastic beam theory, he proposed a cantilever test in which a strip of fabric lies flat on a horizontal surface and is progressively pushed forward over an inclined platform, causing the material to bend under its own weight (Figure 69, a). The angle between the horizontal and the chord from the horizontal platform to the tip of the specimen is then measured. Peirce defined the bending rigidity as:

$$G = \frac{L^3 \times w \times \cos(0.5 \times \theta)}{8 \times \tan\theta} \tag{8.1}$$

Where G is the bending rigidity per unit width, L is the overhanging length, w is the mass of the fabric per unit area multiplied by the acceleration due to gravity (i.e. 9.81ms^{-2}), and θ the angular deflection of the specimen end. The work of Peirce later led to the publication of the ASTM standard D1388 [133]. This test method has the advantage of low cost, ease of implementation and simple data interpretation. However, it was shown that the moment-curvature relationship of reinforcements is not linear and depends on the range of curvature considered [127]. Due to the fact that the cantilever test is based on linear elastic beam theory, it is not suitable for the characterisation of composite reinforcements. To overcome this limitation, De Bilbao *et al*. [125], developed a new testing method in which a standard cantilever test is used together with an optical measurement device (Figure 69, b). By analysing the shape of the bent sample, it is possible to obtain the non-linear moment-curvature relationship. The fixture allows to vary the overhang length and therefore the loading case, for a single specimen by means of a translating platform which makes it possible to take into account the history of deformations of the sample. This is however not applicable to prepreg materials due to the tackiness of the resin that would most likely prevent the translation of the sample on the horizontal platform. The only limitation is that there is no account of strain rate effect, which may be of importance for viscous material such as prepreg material. In addition, it was reported that some materials might exhibit some degree of curling and twisting at their end, or deform anticlastically under bending [123, 134]. In most cases, this can be avoided by using narrow specimens. Alternatively, Dangora *et al*. [126], while investigating the bending properties of woven and NCF materials at room temperature, proposed a variation of the cantilever test whereby

the specimen is held vertically (Figure 69, c), thus neglecting any gravitational forces and limiting twisting. The displacement of the specimen is induced by a small load on a pulley mechanism, attached to the tip of the specimen. A variation of this test set-up was recently proposed by Alshahrani *et al*. [130] and includes a linear actuator and a load cell. The linear actuator applies a set displacement at the tip of the specimen using a controlled rate, while the load cell records the load required to achieve the deflection.

A second category of test method, is based on the Kawabata Evaluation System (KES) and was developed by Kawabata in 1980 [124]. The KES system (Figure 69, d) is a commercial instrument that allows measurement of the mechanical properties of fabrics, including the tensile, shear, bending, compression and friction properties. The bending experiment consists of a pure bending test and allows to record the bending moment per unit width as a function of the curvature during a load/unload cycle. The KES system is a relatively easy to use standalone equipment that allows to characterise the deformability of most fabric materials; however, it suffers several disadvantages over other testing methods. First, the KES system has not been widely used for the characterisation of the deformability of composite reinforcements, primarily because the system is only limited to low loads. This restricts its use to relatively light fabrics and/or experiments at low loads, which might not be representative to the conditions obtained during the preforming process. In addition, the equipment is relatively expensive and of limited availability [127]. Finally, it is not designed to test materials at elevated temperature, which makes it impossible to investigate the influence of resin viscosity on the bending properties of prepreg thermoset materials. More recently, Sachs *et al*. [129], in collaboration with the University of Twente, developed a new experimental bending test set-up (Figure 69, e). The custom-built fixture is similar in principle to the KES system, in that rotation is imposed on the specimen which is held between a moving and a fixed clamp. The custom-built fixture is mounted inside a commercial rheometer, which makes it possible to investigate the effect of temperature and rate on the bending properties. The equipment enables precise measurement of the rotation angle, the rotational velocity and the applied moment. A simple viscoelastic material model was used to describe the bending behaviour of thermoplastic composites whereby the fibre deformation was described by Euler-Bernoulli beam theory and the thermoplastic matrix was modelled as an incompressible viscous liquid subjected to shear. Although this test method offers precise measurement of the bending deformation of composite materials and close control of the test conditions, essentially due to the use a commercial rheometer, it suffers several drawbacks. The use of a custom-built fixture limits

the implementation of this test method. Indeed, the fixture geometry has not been made available in the literature. In addition, further work would be required in order to validate and harmonise the testing procedure as well as the fixture design, possibly through a round-robin test.

A third category of characterisation method for the bending properties of composite reinforcements is based on three-point bending test. This test method is more suitable with thick and stiff reinforcements, or alternatively with small specimens. Three-point bending of composite reinforcements was first introduced by Martin *et al*. [132], while studying the out-of-plane properties of UD glass PP. The test consists in deforming an initially flat, 4 mm thick stacked laminate into a V-bend, using an Instron test machine. The three-point bending apparatus was mounted in an environmental chamber so that tests at elevated temperature could be carried out. A variation of the three-point bending test method was proposed by Margossian *et al*. [128], whereby a commercial dynamic mechanical analysis system (DMA) was used to study the longitudinal bending properties of UD carbon PA6 at different conditions of rate and temperature. By means of a commercial DMA accessory consisting of a three-point bending fixture with a 20 mm span length (Figure 69, g), the bending modulus of the thermoplastic material was determined using different approaches based on standard beam theory. Although this test method was found applicable to investigate the temperature-dependent and viscoelastic behaviour of composite materials, it suffers from several limitations. Firstly, it was reported that the application of a constant rate was difficult due to the machine acceleration. In addition, the maximum strain rate used, dictated by the DMA capability was very low, i.e. 0.16 $mm.s^{-1}$ and is certainly not representative of the level of strain rate that is currently attained by high-volume forming processes. Finally, even though this test method was seen applicable for the bending characterisation of UD material, the sample size limitation imposed by the use of a DMA system makes this method challenging for other reinforcement types such as woven where specimen size would be too small compared to the unit cell size of the material. In addition, through-thickness shear effect can dominate if the specimen span is too small.

Wang *et al*. [131], developed a different characterisation test method based on a buckling test (Figure 69, h). Buckling is a phenomena occurring when a material subjected to compressive loads suddenly undergoes bending. The test consists in applying a compressive load to a rectangular sample made out of three UD prepreg plies and measuring corresponding force and displacement using a Universal testing machine. The

bending behaviour is determined from the axial force and the displacement parallel to the applied load. The effect of temperature and rate on the buckling behaviour was investigated. This method offers a relatively easy way of investigating the bending behaviour of composite reinforcements, at different temperatures and speed rates. In addition, unlike three point bending tests, this method can be used to test relatively thin and flexible specimen such as UD material, without the necessity to stack up multiple plies that would accentuate intraply shearing effect. Also, unlike the cantilever test, it is possible to obtain a continuous stress-strain relation. However, it is neither a standardised nor a widely accepted characterisation method for the bending properties of composite reinforcements. In addition, it might not be suitable for material with extremely low bending rigidity, such as UD materials in the transverse direction, where specimens held vertically would deform under their own weight. Finally, any slight fibres misalignment with respect to the load direction would lead to the development of tensile stresses that would strongly affect the bending shape and therefore the test results.

For the present study, it is essential that the selected method be able to test a range of reinforcement types, i.e. woven and UD thermoset prepreg, at different conditions similar to that used in 3DF. Consequently, the test method should allow to investigate the effect of temperature and strain rates on the bending behaviour of the material. In addition, the ability to test samples in different orientations is highly desirable in order to characterise the anisotropic behaviour of UD materials and assess the bending behaviour of woven materials along both warp and weft directions. For these reasons, the cantilever test method was deemed most appropriate. Indeed, the cantilever test is widely accepted as a *de facto* standard for the characterisation of the out-of-plane properties of textile materials and composite reinforcements and is supported by a large literature. Specimens of various lengths and widths can be easily tested at elevated temperature. The testing rig requires minimal design work as it only consists of a mechanical clamp, and therefore can be easily adapted to individual needs and accommodate additional instrumentations if required. The addition of optical measurement method makes it possible to measure the non-linear bending behaviour as a function of the curvature of the bent samples. Test data can subsequently be implemented directly in most commercial simulation software (e.g. PAM-FORM).

8.2 Experimental procedure

A test rig was developed, comprising three aluminium sheets bolted together and an aluminium clamp. Figure 70 shows a CAD model of a cantilever test, as well as a picture of an experiment. The prepreg specimen is mechanically clamped onto the horizontal platform. In the background, the aluminium sheet was painted matt black in order to improve the contrast between the rig and the specimen whose side was painted in white prior to the test. This helped facilitate the subsequent image analysis. The test rig was fixed in place within a thermal chamber, using a fitting plate. A spirit level was used to check the horizontality of the platform and ensure that correct boundary conditions were applied to the sample. The specimen was then left in the thermal chamber for two minutes at 80°C, after which, specimen temperature distribution and therefore, resin viscosity was uniform. Past this point, equilibrium conditions were reached and no further specimen deflection was observable.

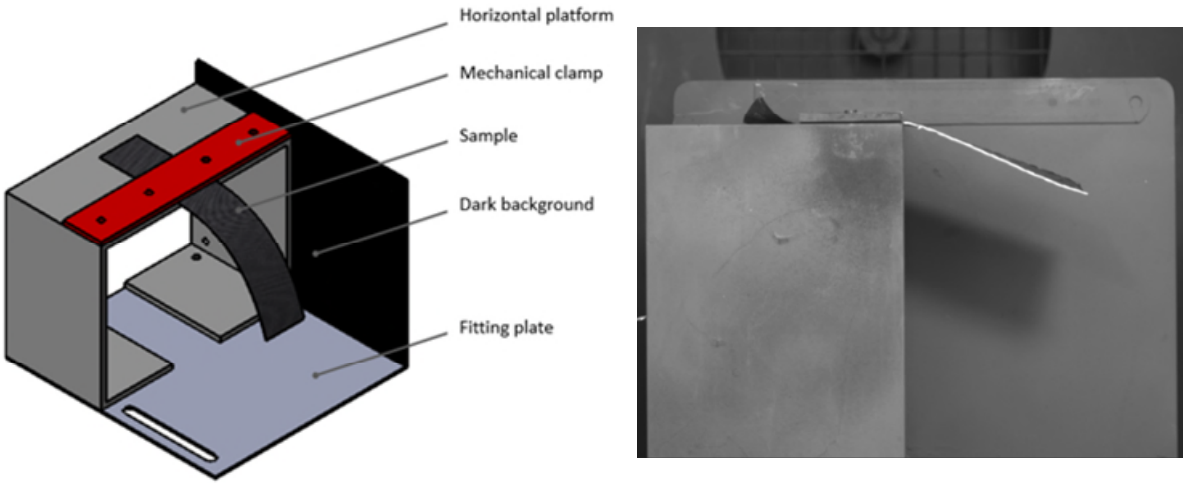

(a) (b)

Figure 70: Cantilever test rig, (a); CAD model and (b) picture of an experimental test

The test includes a succession of steps, which are detailed in Figure 71. The first step consists in taking a single grey-scale image of the side of the still specimen (Figure 70, b), using a high-resolution CCD camera (4000x3000 pixels). The camera is focused on the specimen and positioned so that the camera lens is perfectly parallel to the side of the specimen. Then, pre-processing techniques are employed using ImageJ/Fiji open-source software and consist in three steps: (i) smoothing in order to reduce noise, (ii) contrast enhancement to improve visibility of details and (iii) thresholding in order to create a binary image after which, the bending shape is completely isolated from the background.

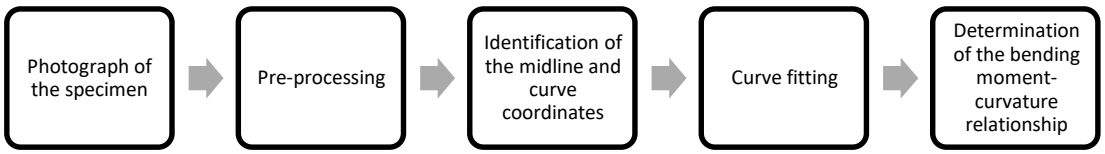

Figure 71: Cantilever test methodology

Then, a thinning algorithm (also known as skeletonisation) is used to extract the midline from the deflection shape. Skeletonisation reduces the width of an object to a single-pixel wide lines. The resulting image is a line that is equidistant from the boundaries of the original shape. Figure 72 shows the different steps required to obtain the midline of the bent sample.

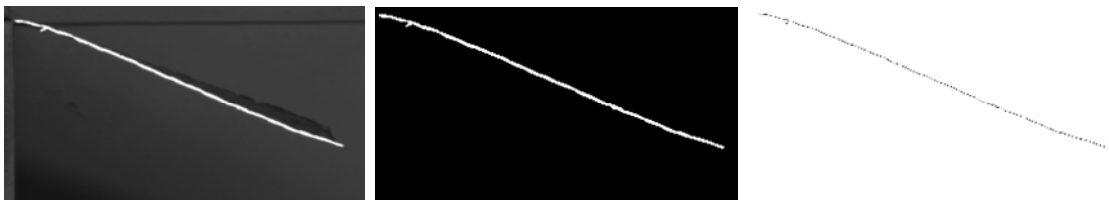

(a) (b) (c)

Figure 72: Cantilever test: (a) Original grey-scale image, (b) Corresponding binary image after post-processing and (c) corresponding midline after skeletonisation

The next step consists in converting pixels into a unit length. This process refers to spatial calibration and involves correlating pixels to features of known distance in the image (e.g. a ruler). The deflection line can then be described by a set of XY-coordinates. A curve fitting process is then employed in order to reduce noise that originates from the pre-processing and measurement errors. The use of a polynomial function of degree 6 was deemed sufficient, yielding an r-squared value greater than 0.99. The y-intercept of the fitted curve was set to zero to ensure correct boundary conditions at the clamped end.

Finally, the bending moment can be computed along the deflection curve, using the following equation [125]:

$$M(s) = w\int_{s}^{L}(u-s)\cos(\varphi)\,du \tag{8.2}$$

Where M is the bending moment applied by the part AF (Figure 73), s is the curvilinear abscissa of point A, w is the weight per unit length of the specimen, u and ϕ are the Frenet's coordinate of point B moving along the curve from A to F.

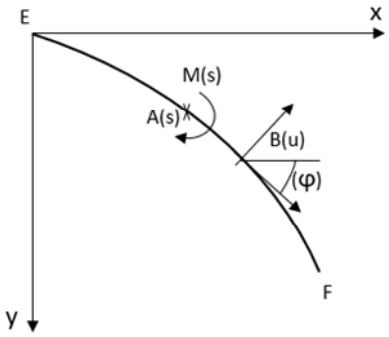

Figure 73: Representation of the bending moment along the deflection curve

Considering the curve defined by equation $y = f(x)$, the curvilinear abscissa at point A moving along the profile EF is computed such that:

$$s(A) = \int_{x_e}^{x_a} \sqrt{1 + f'(A)}\, dx \tag{8.3}$$

And the curvature at point A is defined as:

$$k(A) = \frac{f''(A)}{(1 + f'^2(A))^{3/2}} \tag{8.4}$$

8.3 Results and discussions

For both the woven and the UD thermoset prepreg materials, the same experimental procedure was used. Three specimens were tested for each sample dimension providing three individual midline deflection curves that were subsequently averaged to give a single deflection curve. The curve fitting procedure was then performed on the averaged deflection curve. Hereafter, samples will be identified by their width followed by their overhang length (e.g. “50x100” refers to a 50 mm wide specimen with an overhang length of 100 mm). The error bars presented on the plots of deflection curves represent one standard deviation on either side of the mean. Due to the use of different materials and their unknown bending stiffness, bending tests were performed to a specified overhand length rather than using a standard angle of deflection (as suggested by ASTM standard D1388 [133]).

8.3.1 Woven thermoset prepreg

The degree of crimp and tension can be different in the warp and weft directions for some woven materials due to the weaving process [135], and this may consequently affect the bending stiffness of the reinforcements. Therefore, bending tests were performed in both the warp and the weft directions.

Bending deflection curves and the resulting bending moment against curvature are shown in Figure 74. Results are of similar order of magnitude to previous researches [125, 130, 136], and bending-moment curves show a similar behaviour. The bending moment is normalised to the width of the sample and is expressed in N (i.e. N.mm/mm). Again, results are in good agreement and seem to converge towards a maximum moment of approximately 0.025 N as the curvature increases, corresponding to the clamped end of the specimen. On the contrary, near the free end of the samples where curvature values approach zero, bending moment values rapidly tend towards zero. In addition, negative values can be observed and may be caused by the very free end of the specimen bending slightly upwards. For each sample dimension, there exists a difference between the bending moment in the warp and weft directions. For the 50x80 mm and 50x100 mm samples, specimens tested in the warp direction show an increase in bending moment when compared to those tested in the weft direction. This difference is attributed to a lower level of crimp in the warp direction and as a consequence, straighter tows. For the 50x100 mm specimen, a slightly greater difference was observed with an increase of 11.3% over the specimen tested in the weft direction (as opposed to a 2.9% increase for the 50x80mm specimen), suggesting a specimen size effect.

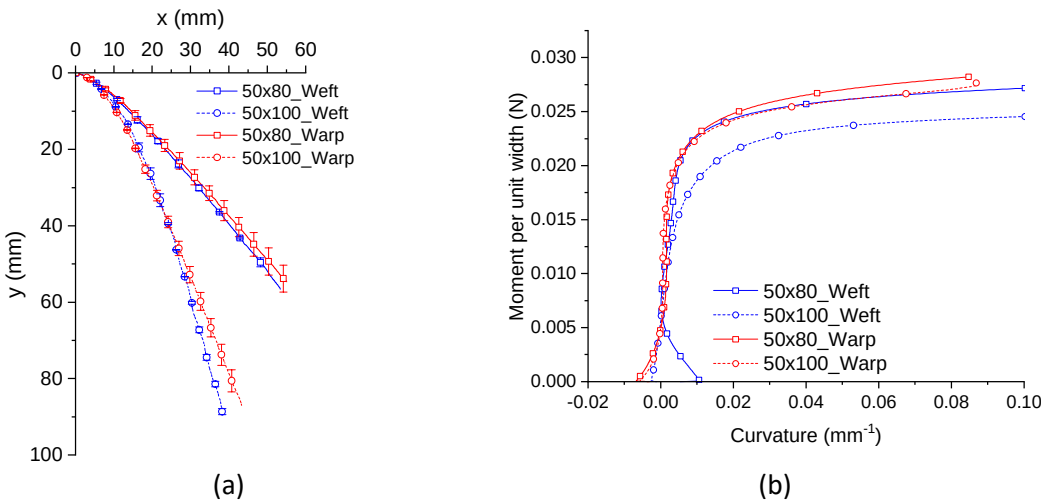

Figure 74: Averaged deflection curves (a), and moment-curvature results (b) for the woven prepreg in both the warp and weft directions

One of the first steps in double-diaphragm forming of prepreg materials consists in preheating the laminate under vacuum, which causes softening of the material and facilitate the preforming. This step affects the compaction, and therefore the degree of consolidation of the prepreg as the resin is forced through the thickness of the material under the application of vacuum. This is particularly true for fast cure out-of-autoclave woven prepregs, which are typically characterised by their partial impregnation, in that resin is only applied onto both outer surfaces of the prepreg, leaving the centre relatively dry and porous. Upon the action of temperature and normal pressure, the resin percolates through the fibrous network increasing the global level of impregnation. As far as the bending properties are concerned, this is particularly interesting, as the level of impregnation will most likely affect the bending stiffness of the prepreg.

To assess the effect of compaction on the bending rigidity of the woven prepreg, samples were debulked prior to the test at 80°C for two minutes in a vacuum bag (i.e. vacuum pressure of 0.1 MPa). Results are presented in Figure 75 and show that irrespective of the sample orientation, the preheating stage under vacuum increases the bending rigidity of the material. In addition, the evolution of bending moment with increasing curvature occurs in a more gradual way for the compacted samples. In the warp direction (dashed lines), a 26.9% increase in maximum bending moment was reported after compaction, while in the weft direction (solid lines) a 28% increase was reported. As a result, smaller maximum curvature values were reached for the compacted samples as they bent to a lesser extent.

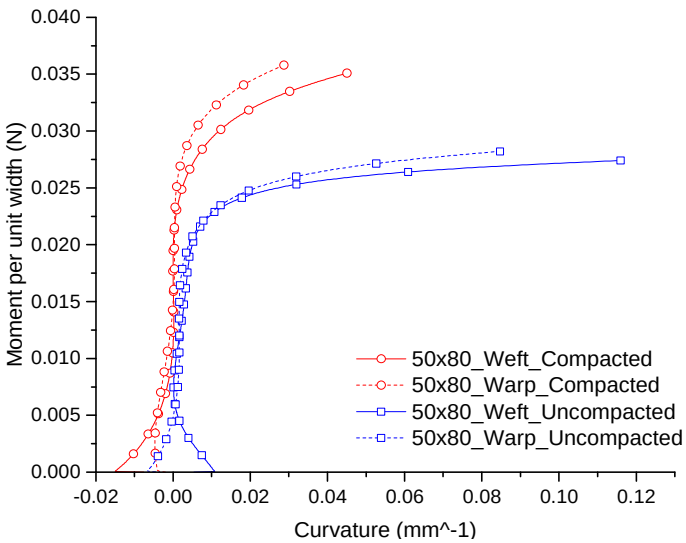

Figure 75: Moment-curvature results for the woven prepreg in the warp direction and the effect of pre-compaction.

8.3.2 UD thermoset prepreg

An initial study on the effect of sample dimensions on the bending behaviour of UD prepreg under cantilever was performed. It was found that, the use of wide specimens should be avoided since wider specimen undergo anticlastic wrapping, principally due to the low bending stiffness of the material in the transverse direction. In this work, a specimen width of 20 mm and 40 mm was deemed suitable and provided repeatable results. Unlike the woven material, the effect of consolidation on the bending properties of the UD was found to be negligible. Results are presented in Figure 76 and show the averaged deflection curves (Figure 76, a), and the moment-curvature results (Figure 76, b) for the different specimen dimensions. Similar to the woven material, the moment-curvature relationship is non-linear (i.e. quasi bilinear). However the transition between the low and high curvature regions is less gradual for the UD due to the large bending stiffness along the fibre direction. Therefore, the change of curvature is quite sudden and is confined to the clamped end (Figure 76, a). As expected, maximum bending moment values for the UD material are higher than that of the woven. In the lower curvature zone (Figure 76, b) small inflections can be observed. These inflections are not real phenomenon but originate from oscillations of the polynomial fitting in the quasi-linear part of the deflection curves. This phenomenon was also observed in [125].

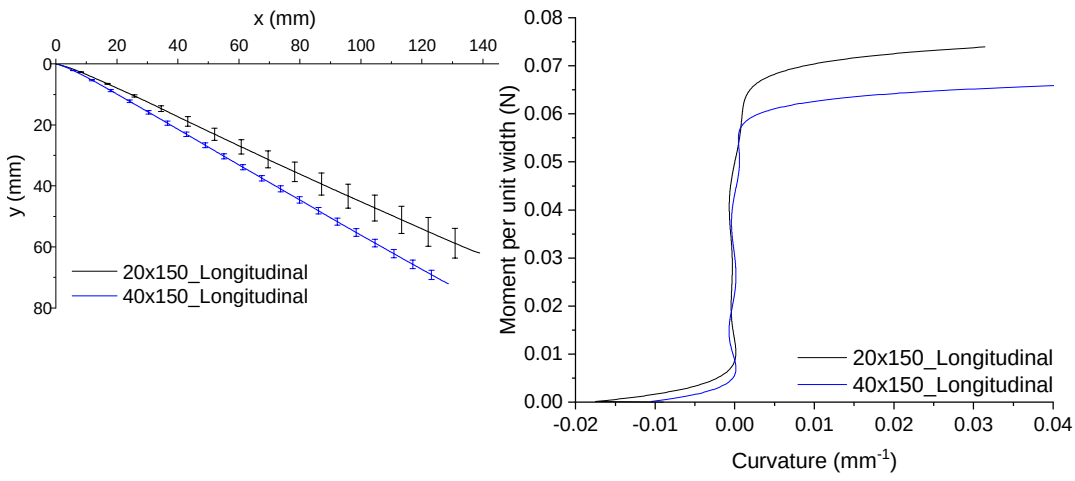

(a) (b)

Figure 76: Averaged deflection curves (a), and moment-curvature results (b) for the UD prepreg along the fibre direction

Similarly, the transverse bending properties of the UD prepreg (i.e. with the fibres perpendicular to the length of the coupon) were determined. Figure 77 shows the averaged deflection curves (Figure 77, a) as well as the resulting bending moment-

curvature curves (Figure 77, b). A specimen width of 40 mm was used. Due to the extremely low bending rigidity of the UD prepreg in the transverse direction, and in order to limit the maximum deflection, short overhang lengths of 10 and 20 mm were considered. It can be observed that the maximum bending moment values are significantly smaller than the ones obtained in the longitudinal direction by more than two orders of magnitude. In the most extreme scenario (i.e. between the 20 mm wide specimen in the longitudinal direction and the 10 mm long specimen in the transverse direction), the maximum bending moment values obtained differ by approximately 900 times.

Similar to the UD prepreg in the longitudinal direction, some small inflections can be observed in the lower curvature zone (Figure 77, b) due to poor fitting. The fact that the moment-curvature curves for the 10 mm and 20 mm long specimens are not superposed implies that the bending behaviour of the UD prepreg across the fibre direction is not elastic [125].

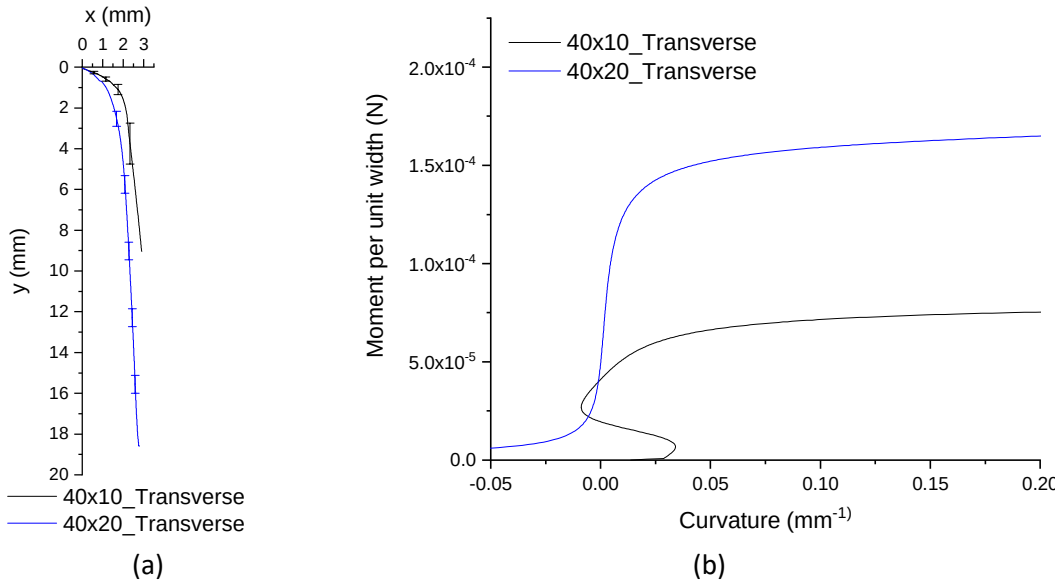

Figure 77: Averaged deflection curves (a), and moment-curvature results (b) for the UD prepreg in the transverse direction

8.3.3 Cross-plied UD thermoset prepreg

The bending properties of cross-plied UD prepreg were also investigated. In order to obtain sufficient compaction between the plies, the specimens were vacuum bagged prior to testing under 1 bar pressure for 2 minutes at a temperature of 80°C. Assuming that the bending behaviour is similar along the two in-plane orthogonal directions, only one test orientation was considered. Three different overhang lengths were used: 100 mm, 150 mm

and 200 mm with a specimen width of 20 mm. Figure 78 shows the averaged deflection curves (Figure 78, a) as well as the resulting bending moment-curvature curves (Figure 78, b). Irrespective of the overhang length, the bending moment increases rapidly with increasing curvature. Similar to the other material, small inflections can be observed at small curvatures due to approximation of the fitting procedure. In general, the bending moment values are slightly higher to those obtained for a single ply UD in the longitudinal direction. For a similar overhang length of 150 mm and a specimen width of 20 mm, the cross-plied UD shows a maximum bending moment of 0.093 N compared to 0.077 N for the UD ply in the longitudinal direction. This difference is attributable to the contribution of the transverse fibre orientation that adds to the global bending stiffness of the longitudinal ply. In addition, it can be observed that for a similar overhang length of 100 mm, the cross-plied UD prepreg shows a larger maximum moment value compared to the woven material (i.e. 0.06 N vs 0.028 N, respectively). Similar to the transverse bending properties of the UD prepreg, the moment-curvature curves are not superposed, indicating a non-elastic behaviour.

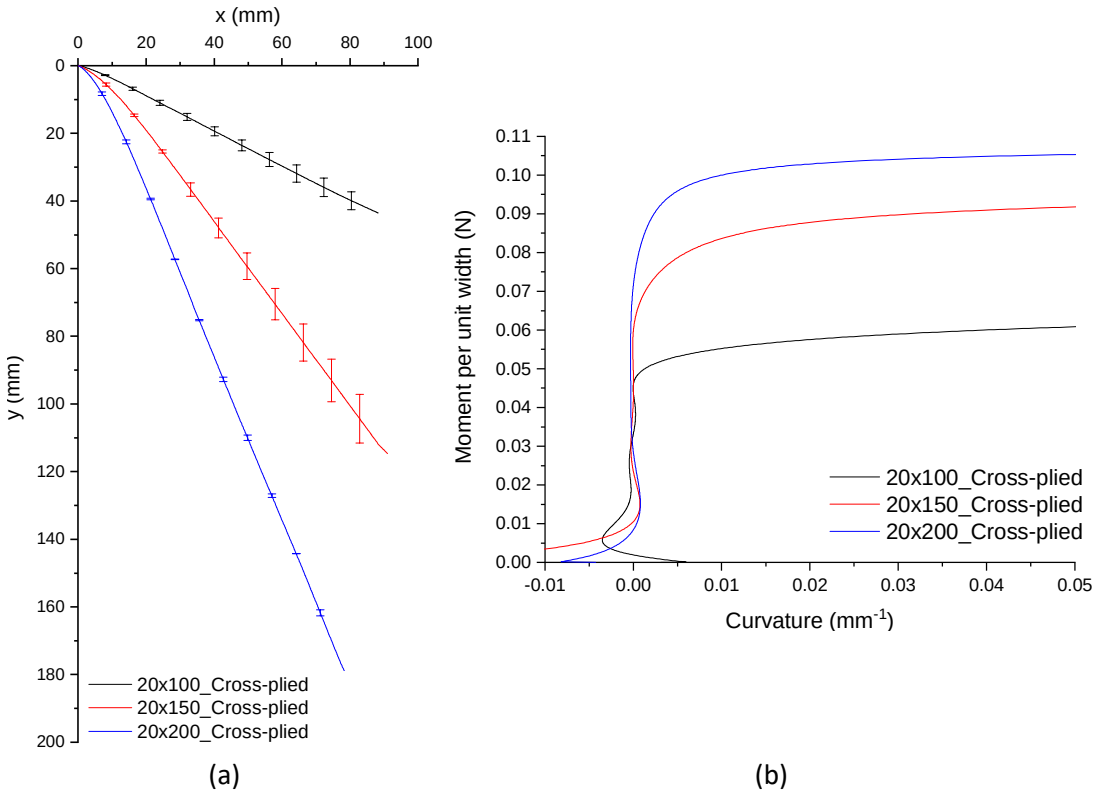

Figure 78: Averaged deflection curves (a), and moment-curvature results (b) for a cross-plied UD prepreg

8.4 Conclusion

Bending properties play a significant role during forming of composite reinforcements and contribute largely to their wrinkling behaviour. More particularly, the bending stiffness affects the size and shape of the wrinkles.

For preforming simulation, wrinkle prediction is important since wrinkles are one of the most common defects found in preforms, and generally cause a severe knockdown in the mechanical properties of the final parts. Consequently, the accurate determination of the bending properties of composite reinforcement is essential. This chapter presented the experimental analysis of the bending properties of two different reinforcement forms of woven and unidirectional with the same rapid-cure resin system. The bending cantilever test was deemed the most appropriate method due to its ease of implementation and the ability to test specimens at elevated temperature, which was fundamental in order to simulate the processing conditions of the 3DF process. Tests were performed at 80°C, and the effect of pre-compaction on the bending properties of the materials were investigated.

For the woven material, similar bending moment-curvature curves were obtained irrespective of the sample width and overhang length used. Pre-compacted specimens showed greater maximum bending moment values. This was attributed to a greater compaction combined with a higher level of resin impregnation through the material thickness, ultimately increasing the bending stiffness of the material.

In contrast, for the UD material the effect of compaction was negligible. Narrow specimens were recommended in order to avoid anticlastic deformation, particularly when testing the longitudinal bending properties of the UD prepreg. Significant difference in the bending properties were observed depending on the test orientation, with longitudinal bending moment up to 900 times higher than the transverse one. Bending properties of cross-plied UD were also investigated. It was observed that for a similar overhang length, cross-plied UD showed a maximum bending moment approximately two times higher than that for the woven material.

For each material and sample size tested, small inflexions were observed in the bending moment-curvature curves at low curvatures. This is not a physical phenomenon but rather a mathematical singularity caused by inaccuracies of the curve fitting procedure. It is possible that in some quasi-linear part of the deflection curves, the higher order polynomial

function describes a negative curvature. In reality, this is not possible since the material is falling under its own weight due to gravity loads. This potentially highlights a shortcoming of this cantilever test method. These test data will be implemented for material test simulation in chapter 9 and for subsequent forming simulations of the prepreg materials in section 10.2.

9 Simulation of characterisation tests.

Prior to modelling the complete forming process, it is good practice to analyse the material behaviour at a coupon level, i.e. when each deformation mechanism is isolated. This involves modelling each characterisation test performed on both the woven and unidirectional prepregs. The aim is ultimately to verify that the material model can accurately predict the material behaviour and validate simulation input parameters.

The first part of this chapter gives a detailed description of the commercial forming simulation software used in this work. Then, numerical models of the bias extension test, the picture frame test, the friction test, the bending experiments and the tensile test are presented. Simulation of the tensile test of the diaphragm material is also explained.

9.1 Description of PAM-FORM

PAM-FORM, is a commercially available FE code dedicated to composite forming, and is developed and distributed by ESI Group. Developed within a European Brite Euram project (BE 5092) [137], PAM-FORM is an emanation of the explicit finite element method PAM-STAMP, a well-established software for sheet metal forming [138, 139]. Similar to PAM-STAMP, PAM-FORM uses an explicit integration scheme and enables simulation of large problems involving non-linear material and contact behaviour. PAM-FORM is used to simulate the preforming process of fibrous reinforcements (dry or prepreg, textile or unidirectional) at a macro-scale level, using continuum theory whereby the material is treated as a continuous medium (i.e. the fibres and the resin form a single homogenised material).

A shell element material model (Material model 140) based on ideal fibre-reinforced fluid theory (IFRF) [140], is used. This material model is a non-linear elasto-plastic material for which temperature, strain, strain rate and curvature dependency can be added. Material model 140 can be applied to both biaxial and UD materials. In the case of a biaxial material, the model assumes pure shear and the fibre directions follow the deformation of the elements. In contrast, for the UD material, simple shear is considered and the material model assumes that the second fibre direction remains orthogonal to the principal fibre direction [141].

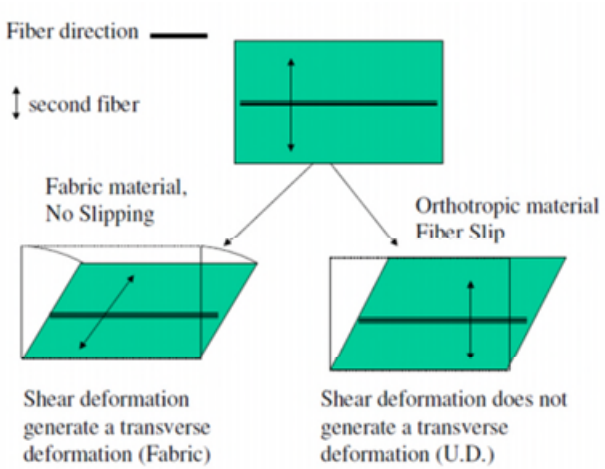

Figure 79: Shear deformation in PAM-FORM depending on the reinforcement type [141]

The stiffness laws defining the tensile and shear responses of the material are decoupled from each other, unlike homogeneous materials where they are simply linked via the Poisson's ratio.

The shear stiffness can be described by discrete values or as function of the shear strain (i.e. the relative rotation angle between warp and weft tows in radian). In the former case, a shear modulus *G* before and a shear modulus G_{lock} after a specified shear locking angle α_{lock} must be defined. In the latter case, tabulated experimental data in the form of shear force-shear angle curve can be directly used as input parameters. *G* can be obtained using picture frame or bias extension tests.

The behaviour of the fibres is considered to be elastic. In the case of biaxial fabric, the fibres can be orthogonal or non-orthogonal and their stiffness E_1 and E_2 may be constant, or non-linear as a function of strain. In the latter case, tabulated experimental data in the form of stress-strain curve can be directly used as input parameters. E1 and E2 can be obtained from tensile tests. Alternatively an educated guess based on the fibre mechanical properties is often suitable.

The transverse shear and bending moments are computed using the classical beam theory. Unlike homogeneous materials, the bending properties of textile reinforcements cannot be deduced from in-plane properties since the fibre structure changes during deformation [125, 128]. Three different methods exist to describe the bending behaviour in PAM-FORM, namely a calibration factor (i.e. a number that multiplies the fibres bending moments computed based on the beam theory), a direct input of the bending stiffness (decoupled

from the in-plane stiffness), or a curve of bending stiffness as a function of the curvature. The bending stiffness is often evaluated by means of cantilever experiments.

Another capability in PAM-FORM is the possibility to run thermal analysis in parallel with mechanical analysis. Heat transfer problems, including conduction within plies and between plies and tool, along with convection to the ambient air can be modelled. This is particularly interesting when modelling non-isothermal processes in order to take into account the thermal dependency of the material properties. In the present work however, the forming process is assumed isothermal (section 10.1) and consequently this capability was not exploited.

9.2 Woven material

9.2.1 Picture frame test

Results of picture frame tests for the woven prepreg, carried out at 80°C and using different crosshead speeds (1, 5 and 8.33 $mm.s^{-1}$) were presented in section 5.2.2. The cross-shaped specimen used was approximated to a single square shaped element of equivalent surface area. This approximation was deemed reasonable considering that upon deformation, the shear angle distribution was uniform over the whole surface of the cross-shaped specimen. The total surface area of the cross-shaped specimen is 18,000 mm^2, equivalent to a square of side length 134 mm. The single element model of the picture frame test is shown in Figure 80.

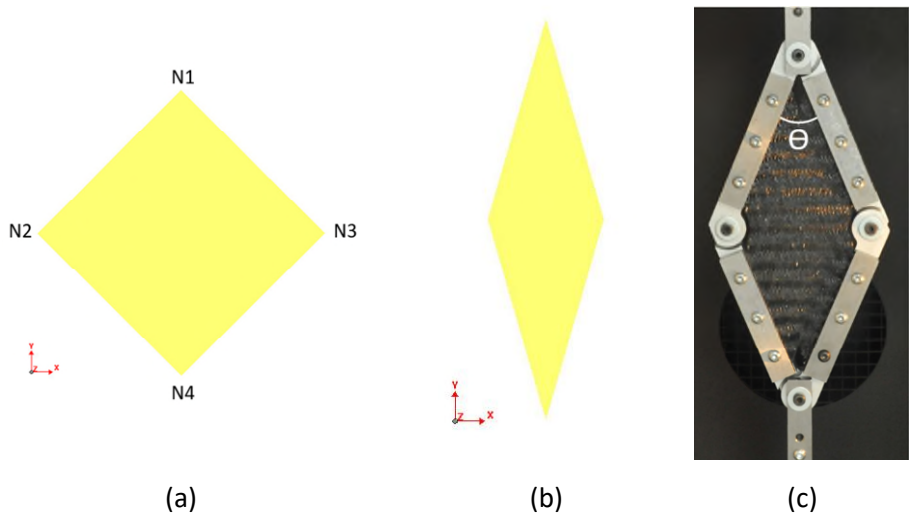

Figure 80: Picture frame model (a) before deformation, (b) after deformation and (c) actual picture frame experiment

In order to replicate the kinematic imposed by the frame, nodal constraints were applied on all four nodes, as follows: (1) The node N1 (Figure 80) was subjected to a constant speed (of 1, 5 or 8.33 mm.s^{-1} depending on the experiment simulated) along the y-axis and over an overall displacement of 68 mm, representing the crosshead movement. (2) Rotations and translations of the lower node N4 were fully constrained, representing the stationary part of the picture frame and forces required to deform the element were recorded at every stage at N4. (3) To produce a perfect rhombus deformation (i.e. pure shear), displacements were assigned to nodes N2 and N3 along both the x- and y-axes. Along the y-axis, the magnitude of the displacement was half that imposed to N1. Along the x-axis, the prescribed displacement x_{disp} was expressed as a function of the y-displacement such that:

$$x_{disp} = L \times (\sin\frac{\pi}{4} - \sin\frac{\theta}{2}) \tag{9.1}$$

With *L*, the side length of the element, and θ the angle of the frame as:

$$\theta = 2\cos^{-1}\left(\frac{\sqrt{2} \times L + y_{disp}}{2 \times L}\right) \tag{9.2}$$

With y_{disp} the prescribed displacement along the y-axis. In order to improve CPU time, the velocity used for the simulation was a hundred times higher than the effective velocity. Consequently, when rate-dependent materials are present, the velocity must be corrected in the solver to properly simulate the behaviour of the materials. To that end, a velocity scale factor can be used, defined as:

$$velocity\ scale\ factor = \frac{real\ velocity}{simulation\ velocity} = \frac{simulation\ time}{real\ time} \tag{9.3}$$

In this case the velocity scale factor was equal to 0.01. Raw experimental data in the form of force-displacement curves were converted to shear stress-shear strain curves and were provided as an input to PAM-FORM material model. The shear strain corresponds to the shear angle expressed in radian. The in-plane shear properties of the woven material were described by three different shear stress-shear strain curves (i.e. one per crosshead speed), each of which was a function of the shear rate. Material data were linearly interpolated between input curves, or linearly extrapolated when computed shear rates fell beyond the predefined values.

During a picture frame test, the use of a constant crosshead speed results in a variable shear rate. Because PAM-FORM does not allow to specify shear stress-shear strain curves as a function of a varying shear rate, shear rate values were averaged for each test (i.e. the instantaneous shear rate was averaged at each picture frame test increment), yielding average values of 1.12, 5.59 and 9.29°.s^{-1} for picture frame tests performed with a crosshead of 1, 5 and 8.33 mm.s^{-1}, respectively. It will be seen later that this approximation resulted in slight deviations between computed and measured results. The forces required to deform the element, along with the shear angle within the element were recorded during the simulation and compared to the experimental data. Figure 81 shows the comparison between numerical and experimental data, for picture frame tests performed with a crosshead speed of 1, 5 and 8.33 mm.s^{-1}. It can be observed that the results are in good agreement for a crosshead speed of 1 mm.s^{-1}, however small discrepancies can be seen for tests performed at higher speeds, particularly at large shear angles.

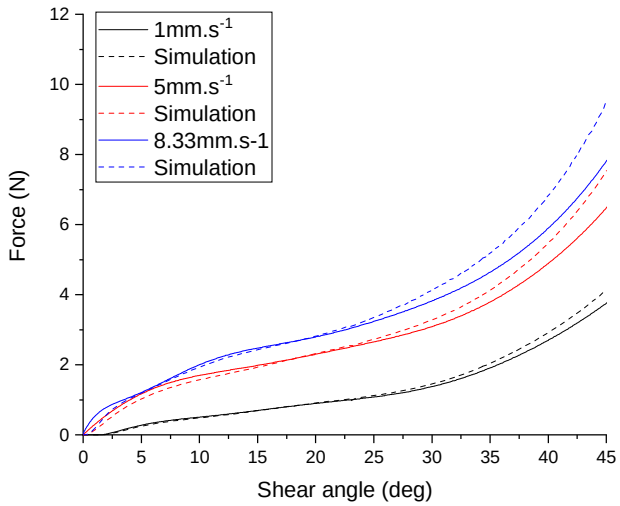

Figure 81: Comparison of the picture frame force-shear angle curves from numerical model vs. experimental test results

These differences exist because of the assumption of constant shear rates and could be corrected by performing picture frame experiments using a variable crosshead speed, thereby producing a constant shear rate. In the present study however, the correlation between numerical and experimental results was deemed acceptable.

9.2.2 Bias extension

Results of bias extension tests of the woven prepreg carried out at 80°C and using different crosshead speeds (1, 5 and 8.33 mm.s^{-1}) were presented in section 5.2.3. A horizontal

symmetry about the centre of the specimen was used in order to simplify and reduce the analysis to a half-model of the bias extension specimen. The resulting model is shown in Figure 82 and consists of six elements, five of which are triangular elements and one is a quadrilateral element. Edges of the elements are all aligned with the direction of the fibres in order to avoid intraply shear locking phenomenon [142], which may lead to unrealistic and overestimated element stiffness. In order to create pure shear deformations, nodal constraints were applied as follows: (1) A nodal displacement was applied to nodes N1, N2 and N3 (Figure 82, a) along the y-axis, representing the movement of the mechanical clamp. (2) A displacement was applied to nodes N4 and N5 along both the x- and y-axes. Along the y-axis, the magnitude of the displacement was half that of nodes N1 and N2. Along the x-axis, the displacement was described as a function of the y-displacement using equation (9.1). (3) The same displacement along the x-axis was applied to nodes N6 and N7. Kinematically, the deformations of the different elements can essentially be likened to those of a picture frame. The triangular elements comprised of nodes N1,N3,N4 and N2,N5,N3 are similar to a half picture frame, while the elements comprised of the nodes N6,N4,N8 and N5,N7,N8 are equivalent to a quarter picture frame.

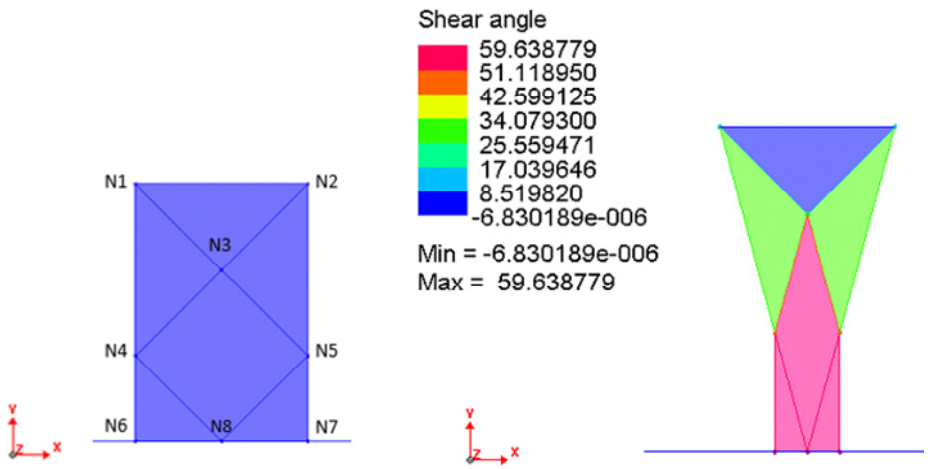

Figure 82: Half model of a bias extension test before deformation (a), and after deformation (b) showing the three different shear zones

Although they are somewhat unrepresentative of the actual process, these boundary conditions (BCs) were required in order to produce ideal shear deformations. An alternative model comprising partially constrained nodes (i.e. nodal displacement only applied to the top two nodes, resulting in BCs similar to the actual bias extension test) was also investigated. It was observed that these BCs led to the development of small tensile strains along the fibre direction, resulting in fibre stresses. Figure 83 shows the force-shear

angle responses from a partially constrained model and a fully constrained model. Due to the extremely high tensile stiffness of the material in comparison to its shear rigidity (particularly at elevated temperature), these fibre strains become dominant in the global force-displacement response. It becomes challenging to obtain a pure shear deformation, instead tensile stresses are dominant. This was also observed in [143].

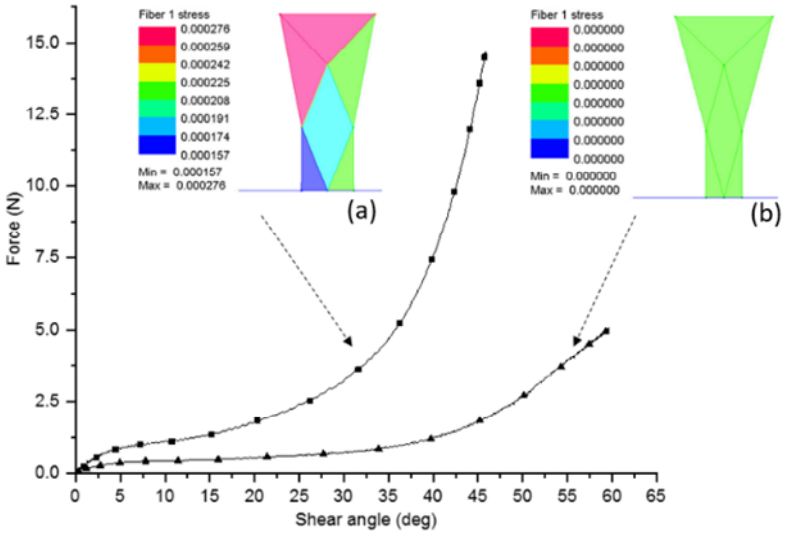

Figure 83: Force-shear angle responses along with a depiction of fibre stresses during bias extension simulation of (a) a partially constrained model and (b) a fully constrained model

Figure 84 presents the force-shear angle curve of the fully constrained bias extension model and shows a good agreement with the experimental result. Because the shear rate is non-uniform within the bias extension specimen, bias extension data cannot be expressed as a function of the shear rate in PAM-FORM. Consequently, knowledge of the shear rates involved in the actual forming process is required in order to define representative bias extension test parameters.

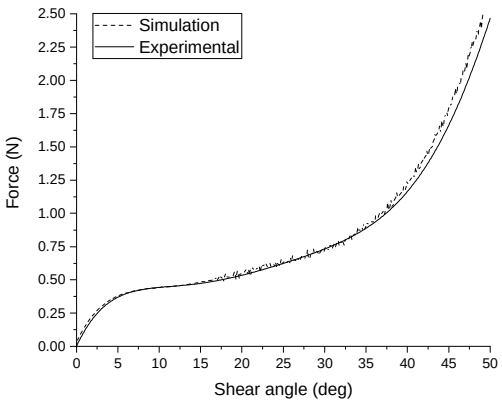

Figure 84: Comparison of the bias extension force-shear angle curve from numerical model vs. experimental test result for the woven prepreg

9.2.3 Friction test

Results of friction testing of the woven prepreg performed under different conditions of sliding velocity, relative angle between adjacent plies and normal pressure were presented in chapter 6. A sub-model of the friction experiment was setup in order to simplify the analysis. The sub-model is shown in Figure 85 and consists in a fixed ply of dimensions 14x50 mm with a 1 mm mesh size and a moving ply of dimensions 10x10 mm with a 5 mm mesh size. For both plies, a different mesh size was used in order to avoid element edges lying on top of each other and prevent the occurrence of oscillations. A drop in the frictional forces was reported in [144], when slave nodes lie on top of the element edges of the master. In this case, symmetric contact was used and as a consequence the slave and master elements could be chosen arbitrarily. The contact attribute between the moving ply and the fixed ply was defined directly using the experimental friction coefficients as a function of the normal pressure and sliding velocity. In contrast the contact attribute between the fixed ply and the moving ply was set to 0. It is important that contact attributes are not duplicated. Failing that, frictional forces will be overestimated. For the fixed ply, translational and rotational motions were constrained, while for the moving, a translational velocity along the y-axis was imposed to the side nodes. In addition a normal pressure was applied onto the moving ply. The sum of forces applied on the side nodes of the fixed ply (i.e. corresponding to the frictional forces) was recorded throughout the simulation.

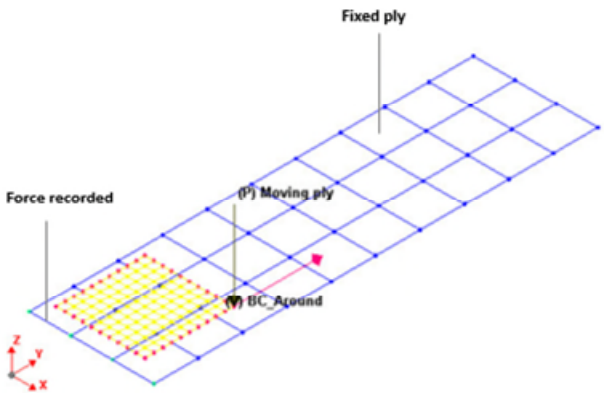

Figure 85: Sub-model of a friction test showing the boundary conditions

An isotropic, velocity and pressure dependent friction model was used to best describe the friction behaviour of the woven material. To avoid dynamic effects, the pressure was progressively increased from 0 to the target normal pressure within 10ms. For similar reasons, the ply velocity was increased from 0 to the target test velocity in 10ms. The

model was run various time, varying the parameters (i.e. relative orientation of the fibre at the contact interface, normal pressure and sliding velocity) to match the conditions used during experimental friction testing. The frictional force was recorded and the friction coefficient was directly calculated such that:

$$\mu = \frac{T}{N} \tag{9.4}$$

With *T* the frictional force and *N* the normal force determined from the normal pressure and the contact area between the plies. Numerical results are shown in Table 13 and show a perfect agreement between the numerical and the experimental friction coefficient.

Interface	Test speed / pressure	**Numerical results**		**Experimental results**
		Tangential Force (N)	Friction coefficient	Friction coefficient
0/0	1 $mm.s^{-1}$ / 1 bar	1.433	0.1433	0.1432
	1 $mm.s^{-1}$ / 2 bar	1.296	0.1296	0.1297
	5 $mm.s^{-1}$ / 1 bar	2.280	0.2280	0.2282
	5 $mm.s^{-1}$ / 2 bar	2.061	0.2061	0.2063
0/45	1 $mm.s^{-1}$ / 1 bar	1.025	0.1025	0.1024
	1 $mm.s^{-1}$ / 2 bar	1.426	0.0713	0.0713
	5 $mm.s^{-1}$ / 1 bar	2.188	0.2188	0.2194
	5 $mm.s^{-1}$ / 2 bar	2.271	0.1135	0.1136

Table 13: Comparison of friction coefficient obtained from numerical and experimental friction test for the woven prepreg

It is worth noting that PAM-FORM does not permit to define both static and dynamic friction coefficients as a function of normal pressure and sliding velocity. While a static stress value can be defined, this single parameter is independent of the process parameters and is therefore not suitable for simulations when all variables are taken into account. It is therefore up to the user to decide, based on simulation results and previous experiences whether static or dynamic friction coefficient should be used in the velocity and pressure dependent friction model. In this particular case, dynamic coefficients were used.

9.2.4 Cantilever bending test

Results of cantilever test of the woven prepreg performed at 80°C were presented in chapter 8. The cantilever test method enables to obtain the non-linear bending moment-curvature relationship. PAM-FORM material model requires input in terms of bending stiffness and curvature. The bending stiffness is defined based on the computation of a Young's modulus *E*. Because out-of-plane properties of fibrous reinforcements are independent from in-plane properties, here, *E* is essentially a dummy Young's modulus that is decoupled from the actual tensile properties.

For a uniform section, rectangular beam of linear elastic material, the Young's modulus is calculated using Euler-Bernoulli relationship such that:

$$E = \frac{M_b}{k I} \tag{9.5}$$

Where M_b is the bending moment, *K* is the curvature and *I* is the moment of inertia. *E* is the Young's modulus. Equation (9.5) is however only applicable to small deflections. For large deflection of a beam under uniformly distributed load, such as during a cantilever test of fibrous reinforcements, the equation (9.5) can be written as [145]:

$$E = -\frac{\mathrm{d}M_b}{\mathrm{d}s} \times \frac{1}{I\frac{\mathrm{d}k}{\mathrm{d}s}} = -\frac{w(L-s)\cos\varphi(s)}{I\frac{\mathrm{d}k}{\mathrm{d}s}} \tag{9.6}$$

Where *w* is the weight per unit length, *L* is the length of the specimen used, *s* is the curvilinear abscissa, and φ is the tangent angle.

A simple model of the bending experiment was set up, consisting of a rectangular object (Figure 86, a). At one end of the specimen, the nodes were fully constrained in order to simulate the action of the mechanical clamp. The length of the specimen's free end was identical to the experimental overhang length used. Translation along the y-axis as well as rotations around both the z- and x- axes were fixed on all nodes along the edges of the specimen's free end. Without these constraints, it was observed that the model stopped due to instabilities. This was particularly when modelling narrow specimens. A gravity load (0.00981 $mm.ms^{-1}$) was applied over the entire specimen along the z-axis. A 5 mm mesh size was used. In explicit dynamic analysis, simulations are often subjected to inertia effect, which in the case of a cantilever test under gravity, may result in swinging of the specimen. To reduce this effect, and achieve a quasi-static solution, nodal damping was used. In

addition the simulation was stopped using a damping convergence test. Convergence is attained when, for a sufficient duration, the displacement of the nodes of the damped object is shorter than a pre-defined tolerance (i.e. 1.E-4 multiplied by the largest dimension of the object).

A comparison between numerical and experimental results of a cantilever test of an 80 mm wide woven specimen with an overhanging length of 100 mm is shown in Figure 86. Firstly, it can be seen that the numerical model significantly overestimate the bending stiffness of the material. Experimentally, the woven strip reached a maximum deflection of 86 mm, while the numerical model predicts a maximum deflection of 7 mm.

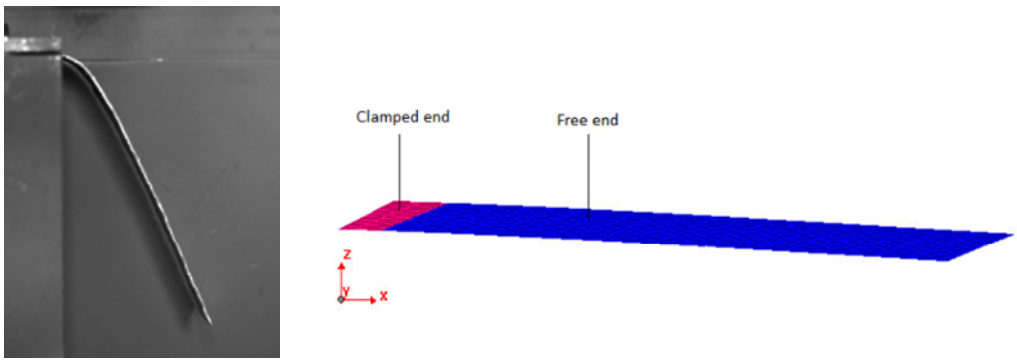

(a) (b)

Figure 86: Comparison of numerical (a), and experimental (b), results of a cantilever test of an 80x100 mm woven specimen

The author believes that this difference comes from errors in the treatment of the bending test data, which may result from: (a) the inaccuracies that arise during the identification of the specimen midline due to the finite thickness of the curve and, (b) the errors introduced by the fitting of functions to the deflection shape. These assumptions will be explained in more details below.

- (a) The identification of the midline (also referred to as skeletonisation) presents some inaccuracies: Due to the weaving of the 2x2 twill woven, the transition between two pairs of transverse tows leads to changes in the curvature. This is exemplified in Figure 87. Although this phenomenon is physically real, the resulting curve extracted from the deflection profile does not represent the actual global behaviour of the material, and shows a succession of negative and positive curvature along the profile, when theoretically one would expect to obtain only

positive curvature. Negative curvature would suggest that, under gravity the specimen bends upwards.

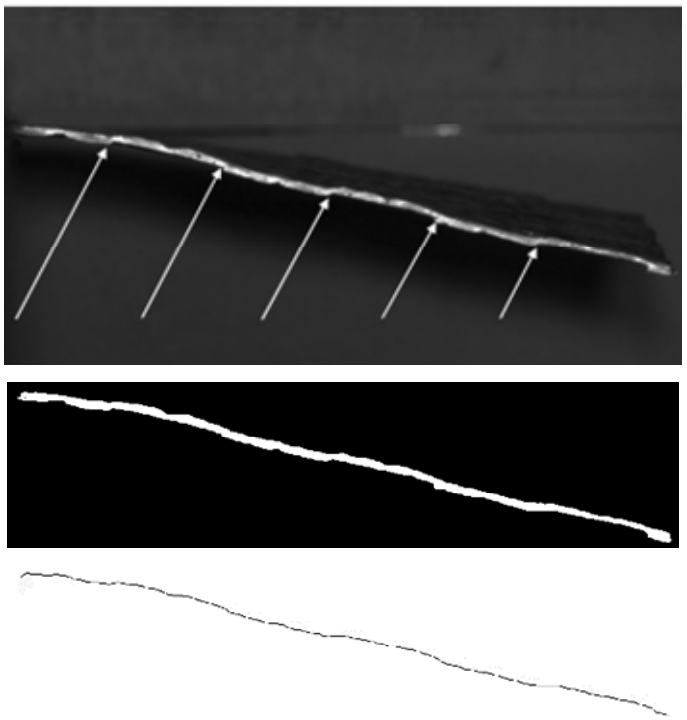

Figure 87: Experimental bending test highlighting the transition zone between pairs of transverse tows (a), post-processed image after thresholding (b), and final extracted midline (c).

- (b) The second source of error may result from inaccuracies in the fitting procedure. The use of high order polynomial (combined with the point described above) may generate oscillations. This phenomenon is called polynomial wiggle and becomes more pronounced if the series of data points do not exhibit a polynomial trend [146].

Consequently, it is recommended for future work to investigate different fitting procedures. Liang *et al*. [147], recently proposed a fitting procedure based on a piecewise function, i.e. a function composed of more than one polynomial of low degree, each of which defined in a certain interval. This type of function is commonly referred to as spline and is particularly suited for bending deflection profiles, which are typically composed of more than on curve shape.

For the present work, an alternative solution was used, whereby the bending stiffness was directly entered as a single value i.e. not as a function of the curvature. Two approaches can be used to determine the bending stiffness: (1) a try-out approach, whereby the bending stiffness is adjusted until the simulation matches the experimental results, and (2), an analytical approach using the following formula:

$$\delta = \frac{wL^4}{8EI} \tag{9.7}$$

Where, δ is the experimental deflection of the cantilever specimen, *w* the weight per unit length, *L* the overhanging length and *I* the moment of inertia. In this case, a bending stiffness of 0.08 GPa was used to describe the bending behaviour along both the warp and the weft directions. Even though it was experimentally observed in section 8.3.1 that the maximum bending moment of the woven was slightly higher in the warp direction, an isotropic bending model was used for the sake of simplicity. This analytical bending stiffness was compared to the experimental data obtained from the cantilever test in section (section 8.3.1), where a non-linear relationship was observed between the bending moment and the curvature. Experimental bending moments from Figure 74,b (specimen "50x80_warp") were converted to bending stiffness using equation (9.5) and compared to the constant bending stiffness of 0.08GPa. The results are shown on a common plot in Figure 88 against the specimen curvature. It can be observed that the data obtained from the cantilever test overestimate the bending stiffness at low curvature values (i.e. from 0 to approximately 0.035mm^{-1}). This may explain why the cantilever test simulation result based on the non-linear bending behaviour, significantly underestimates the specimen deflection (Figure 86). For higher curvatures however, similar data are obtained.

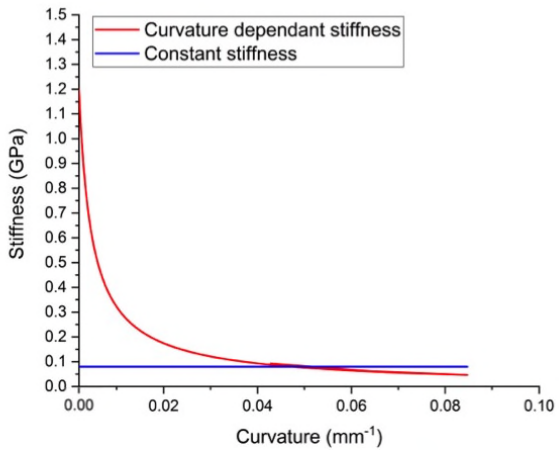

Figure 88: Comparison between the bending stiffness obtained experimentally (curvature dependant) and the bending stiffness obtained analytically (constant stiffness of 0.08GPa)

In contrast, cantilever test simulation based on a constant bending stiffness (i.e. 0.08GPa) show a good agreement. Numerical and experimental results for different overhang lengths are presented in Table 14. Because only a single value is used for the definition of the bending behaviour (i.e. 0.08GPa), this can only depict linear behaviour, which explains the difference between the numerical and experimental results as the overhang length increases.

Overhang (mm)	**End deflection (mm)**	
	Simulation	Test
80	44.214	44.929
100	75.490	80.770
150	134.211	143.890

Table 14: Numerical and experimental comparison of the deflection obtained during bending cantilever tests of woven prepreg material

It should be noted that although this method gives a fairly good correlation in terms of maximum deflection, it only represents a first approximation, as it does not permit to perfectly represent the actual curvature along the bent profile. This can be seen in Figure 89, where the results of numerical simulation with a bending stiffness of 0.08 GPa and an overhang length of 80 mm are compared to experimental results.

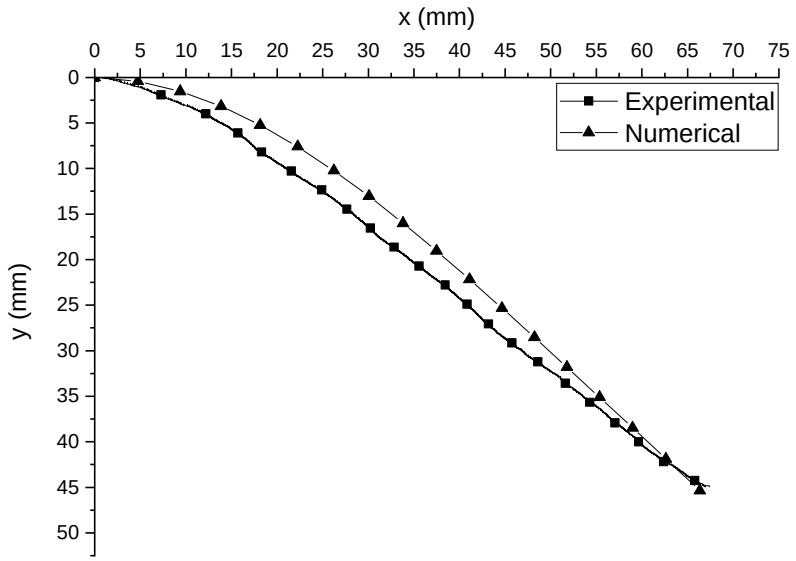

Figure 89: Experimental Vs numerical (with a bending stiffness of 0.08 GPa) profiles of a cantilever specimen with an overhang length of 80 mm

9.3 UD material

Similar to the woven prepreg, numerical simulation of the various experimental methods used to characterise the UD prepreg behaviour are presented. These include in-plane shear test, transverse tensile test, bending test and friction test. Numerical results are compared to the experimental ones.

9.3.1 Rail shear test

It was observed in section 5.3 that the longitudinal in-plane shear properties of UD prepreg is first characterised by an elastic behaviour, followed by plastic deformation. The plastic deformation was attributed to inter-tow sliding phenomena. Because inter-tow sliding cannot be modelled in forming simulation based on continuum theory, only the elastic deformation was considered. Consequently, a shear modulus of elasticity G_{12}=0.015 MPa was used. The numerical model is shown in Figure 90. On one side of the specimen the nodes are fully constrained, to simulate the action of the clamp, while on the opposite a nodal displacement along the y-axis is imposed on the nodes. The displacement of the moving side is recorded during the simulation, as well as the resulting forces on the fixed part.

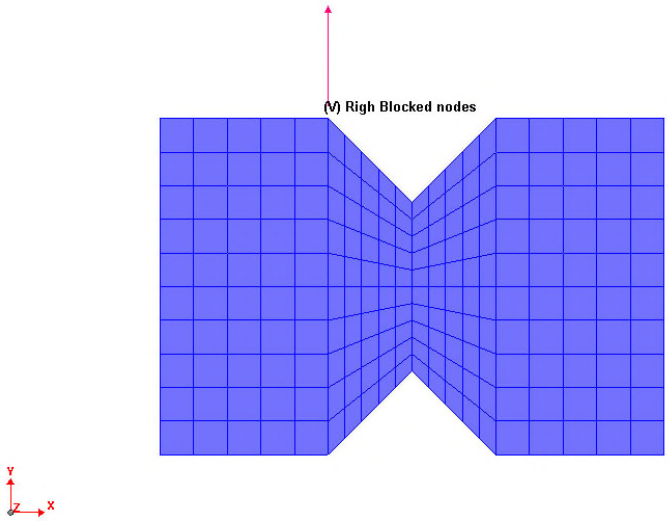

Figure 90: Model of the rail shear test of UD

Force-displacement curves are shown in Figure 91 and present a good correlation in the elastic domain.

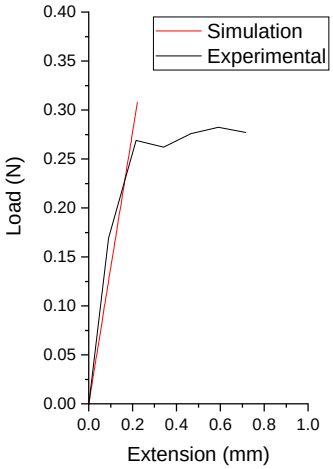

Figure 91: Experimental and simulation results of the rail shear test of UD prepreg

9.3.2 Transverse tensile test

Because the longitudinal tensile properties of UD material are mostly influenced by the fibre properties, the effects or temperature and rate are negligible. In addition, the tensile deformation mode is significantly stiffer than other deformation modes and as a result, strain in the fibre direction is typically negligible. Therefore, a common practise is to use a longitudinal tensile stiffness (E_1) based on an educated guess. It is also common practice to scale down E_1 in order to reduce the high level of anisotropy (in the case of UD material) and reduce the time required for a sound wave to travel through a finite element (since it is inversely proportional to the material stiffness). This ultimately helps reduce the time step and the computational time of the simulation. In this work, an arbitrary value of 20 GPa was used. The resulting fibre strain was checked to ensure that the fibres are still considered inextensible.

In contrast, the in-plane transverse stiffness E_2 is significantly lower than the longitudinal stiffness. Results of transverse tensile test of the UD prepreg performed at 80°C were presented in chapter 7. To describe the transverse tensile behaviour, a built-in hardening model was used, whereby the stress-strain curves (Figure 68) were directly tabulated in PAM-FORM. A numerical model was set up, consisting of a rectangular specimen with dimensions similar to the experimental test (i.e. 74x100 mm). A 5 mm mesh size was used. A nodal displacement was applied to the top nodes along the specimen edges, to simulate the effect of the moving clamp. Nodes along the bottom edge were fully constrained to simulate the stationary clamp. The model is shown in Figure 92.

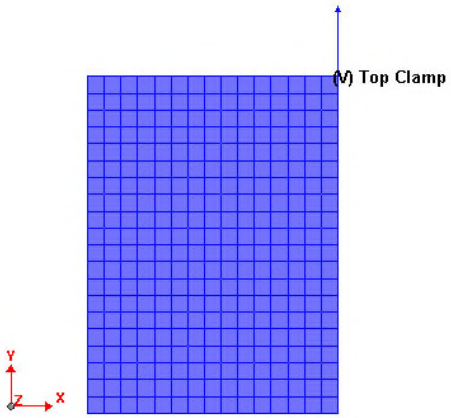

Figure 92: Model of a transverse tensile test of UD

Forces resulting from boundary conditions were recorded during the simulation at the bottom edge and compared to the experimental results. Figure 93 shows a comparison between the force-strain curve obtained from the simulation and the experiment.

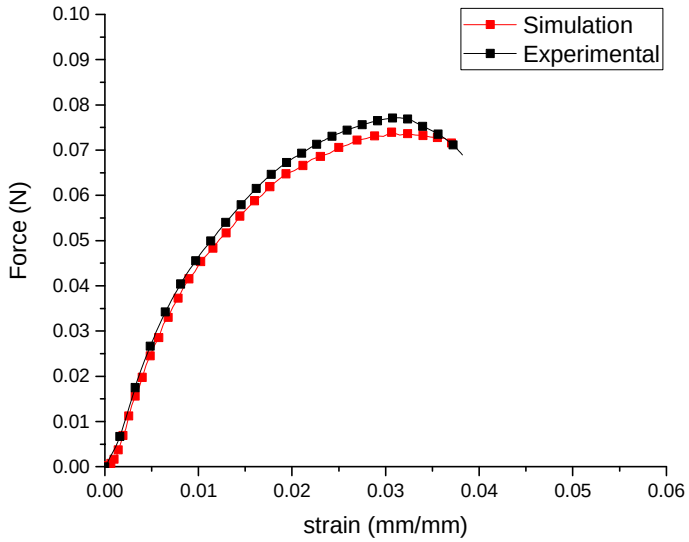

Figure 93: Experimental and simulation results of a transverse tensile test of unidirectional prepreg

9.3.3 Cantilever bending test

Results of cantilever test of the UD prepreg performed at 80°C were presented in chapter 8. A numerical model of the cantilever experiment, similar to the one used for the woven prepreg was set up. In this case, because of the significant difference between the longitudinal and transverse bending rigidities of the UD prepreg, an orthotropic bending behaviour was used. Therefore, simulation was performed in both orientations (i.e. 0° and 90°). A specimen width of 20 mm and 40 mm was used for the tests performed in the

longitudinal and the transverse directions, respectively. In the longitudinal direction, a bending stiffness of 3.5 GPa was used. In the transverse direction, a bending stiffness of 0.0002 GPa was used. A comparison of the maximum deflection obtained from numerical and experimental results is shown in Table 15 and shows a good agreement. Unlike the woven material, no difference is observed between numerical and experimental results as the overhang length increases. This might suggest that the stiffness-curvature relationship of the UD material follows a linear trend.

Orientation	**Overhang (mm)**	**End deflection (mm)**	
		Simulation	Test
Longitudinal	150	59.036	58.603
	200	127.805	127.464
Transverse	10	8.389	8.997
	20	18.931	18.791

Table 15: Numerical and experimental comparison of the deflection obtained during bending cantilever tests of UD prepreg in both the longitudinal and transverse direction

9.3.4 Friction test

Results of friction testing of the UD prepreg performed under different conditions of sliding velocity, relative angle between adjacent plies and normal pressure were presented in chapter 6. A sub-model of the friction experiment, similar to the one used for the woven prepreg was set-up. Table 16 shows a comparison between the numerical and experimental results and shows a perfect correlation.

Interface	Test speed / pressure	Numerical results		Experimental results
		Tangential Force (N)	Friction coefficient	Friction coefficient
0/0	1 mm.s^{-1} / 1 bar	2.586	0.2586	0.2595
	1 mm.s^{-1} / 2 bar	1.448	0.1448	0.1446
	5 mm.s^{-1} / 1 bar	3.336	0.3336	0.3345
	5 mm.s^{-1} / 2 bar	3.878	0.3878	0.3892
0/90	1 mm.s^{-1} / 1 bar	1.967	0.1967	0.1978
	1 mm.s^{-1} / 2 bar	1.187	0.1187	0.1194
	5 mm.s^{-1} / 1 bar	3.019	0.3019	0.3021
	5 mm.s^{-1} / 2 bar	2.900	0.2900	0.2901

Table 16: Comparison of friction coefficient obtained from numerical and experimental friction test for the UD prepreg

9.4 Cross-plied UD material

Similar to the UD prepreg, numerical simulation of the various experimental methods used to characterise the cross-plied UD prepreg behaviour are presented. These include bias extension and bending tests. The friction properties are assumed to be identical to the ones obtained for the UD.

9.4.1 Bias extension test

Results of bias extension test of cross-plied UD prepreg performed at 80°C were presented in section 5.4.2. The bias extension test model used is similar to the one used for the woven prepreg (section 9.2.2). Results obtained in section 5.4.2 for a stack of eight cross-plies UD were normalised to two cross-plies UD. The resulting material was modelled to an equivalent ply of woven (i.e. a fabric material model, similar to the one used for the woven prepreg was used). A comparison between experimental and numerical force-shear angle curves is shown in Figure 94 and shows a perfect agreement.

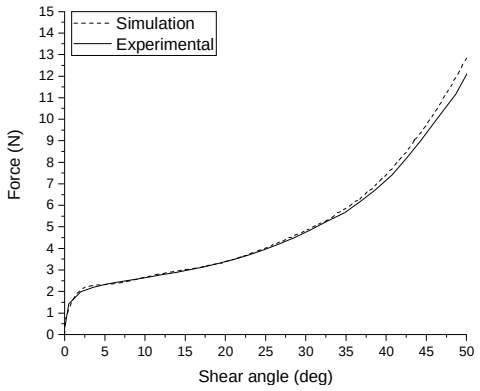

Figure 94: Comparison of the bias extension force-shear angle curve from numerical model vs. experimental test result for the cross-plied UD prepreg

9.4.2 Cantilever bending test

Results of cantilever test of cross-plied UD prepreg performed at 80°C were presented in chapter 8. Similar to the woven prepreg, simulation of the cantilever test was carried out using a comparable model. In this case, the bending properties of cross-plied UD are similar in both orthogonal directions. A bending stiffness of 0.23GPa was used. A comparison of the maximum deflection obtained from numerical and experimental results is shown in Table 17 and shows a good agreement.

Overhang (mm)	End deflection (mm)	
	Simulation	Test
100	42.399	42.393
150	115.549	117.634
200	175.260	181.820

Table 17: Numerical and experimental comparison of the deflection obtained during bending cantilever tests of cross-plied UD prepreg

9.5 Diaphragm material

Within PAM-FORM, the diaphragm is modelled using a general isotropic, strain rate independent material defined by the Young's modulus, the density, the Poisson ratio and a stress-strain curve. The shear and bending properties are directly derived from the in-plane properties. A numerical model was set up, consisting of a rectangular specimen with dimensions similar to the experimental test (i.e. 50x25 mm). A 5 mm mesh size was used. A

nodal displacement was applied to the top nodes along the specimen edges, to simulate the effect of the moving clamp. Nodes along the bottom edge were fully constrained to simulate the stationary clamp. The model is shown in Figure 95. The stress-strain curve was directly used in PAM-FORM to describe the tensile properties

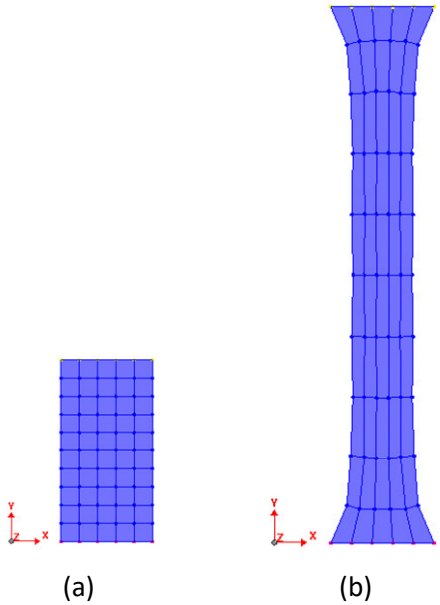

Figure 95: Model of a tensile test of the diaphragm material before deformation (a), and after deformation at 100% strain (b)

A comparison between stress-strain curves obtained from simulation and experiment is shown in Figure 96 and shows a perfect agreement.

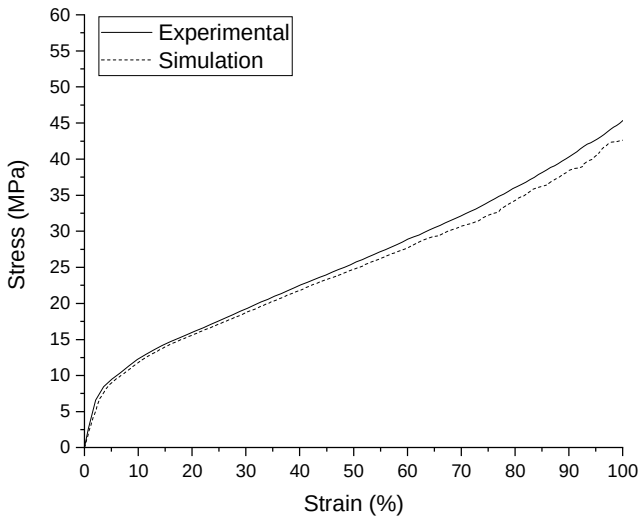

Figure 96: Experimental and simulation results of a tensile test of the diaphragm material

9.6 Conclusion

The purpose of this chapter was to determine the required input parameters for the different materials used in the subsequent forming simulations. All parameters were identified from the experimental data obtained during material characterisation (see chapters 5, 6, 7 and 8), and validated through simulation of the corresponding tests and comparison of the outputs.

For the in-plane shear behaviour of the woven and the cross-plied UD materials, parameters were directly tabulated form the shear force-shear angle data obtained previously from picture frame and bias extension test, respectively. For the woven material, a slight discrepancy was observed between the numerical and the experimental picture frame outputs. This difference lies in the fact that the experimental tests were carried out using a constant crosshead speed (resulting in a variable shear rate), while each shear force-shear angle curve input within PAM-FORM corresponds to a specific shear rate. To make the data more comparable, one possible solution is to perform picture frame experiments using a variable test speed. This should be done using a hydraulic tensile test machine in order to avoid crosshead speed drops (also known as jerk) typically seen with electro-mechanical frame when using variable speed. For the present study however, the results presented in Figure 81 were deemed acceptable.

For the in-plane shear properties of the UD prepreg material, the simulation results showed a good agreement with the experimental ones in the elastic region. Plastic deformation characterised by inter-tow sliding could not be modelled since this deformation mode cannot be considered in a continuum-based software. Consequently, the shear properties of the UD prepreg material were characterised by a single shear modulus value. Regarding the transverse tensile properties of the UD prepreg, parameters were directly tabulated from the experimental data in the form of a stress-strain curve. Numerical results of a transverse tensile test were in good agreements with the experimental data.

Regarding the bending properties, some difficulties were encountered when modelling the cantilever test. Due to the inaccuracy of the fitting procedure employed, a bending behaviour considering the relation between bending stiffness and curvature was not possible. An alternative way was used, whereby the bending stiffness was determined analytically considering the linear elastic theory. Although this method offers a relatively good agreement in terms of maximum specimen deflection, it only considers linear elastic

bending behaviour and does not accurately capture the curvature evoluation along the specimen. Further work should be carried out to identify alternative fitting procedure and a more robust characterisation method.

The resultant material cards highlighting the different parameters for each prepreg material are shown in Table 18.

Material	Material model	Density ($kg.m^{-3}$)	Fibre Vf	G_{12} (GPa)	E_1 (GPa)	E_2 (GPa)	B_1 (GPa)	B_2 (GPa)
Woven Prepreg	*Mat 140 (Fabric)*	*1516*	*52%*	*Tabulated* (Figure 81*)*	*20*	*20*	*0.08*	*0.08*
UD Prepreg	*Mat 140 (UD)*	*1579*	*60%*	*$1.5E^{-5}$*	*20*	*Tabulated* (Figure 68*)*	*3.5*	*0.0002*
Cross-plied UD Prepreg	*Mat 140 (Fabric)*	*1579*	*60%*	*Tabulated* (Figure 92)	*20*	*20*	*0.23*	*0.23*

Table 18: Summary of the material input parameters used for the prepeg materials. G_{12} denotes the in-plane shear stiffness; E and B denote the tensile stiffness and the bending stiffness, respectively.

For the diaphragm material, an isotropic hardening law was used to describe the material behaviour. The model is characterised by the Poisson ratio and a stress-strain curve, both determined experimentally through tensile tests. The resultant material card is shown in Table 19.

Material	Material model	Density ($kg.m^{-3}$)	$E_{elastic}$ (GPa)	$E_{plastic}$ (GPa)	ν
Diaphragm material	Isotropic hardening law	1720	1	Tabulated (Figure 96)	0.45

Table 19: Summary of the material input parameters used for the diaphragm material. N denotes the Poisson ratio.

For further developments, it would be interesting to investigate alternative material models for the diaphragm material, and examine other deformation mechanisms (e.g. shear, biaxial tensile). Tensile tests of the diaphragm material revealed an isotropic behaviour (section 4.1.3), which consequently prompted the use of a simple isotropic material model, whereby shear (and bending) properties are directly determined from the in-plane ones (i.e. isotropic material behaviour). This is a first approximation and further

development could be carried out. For example, an Ogden material model such as presented in [23], could be investigated in order to describe the non-linearly elastic, isotropic behaviour of the diaphragm material employed. However this type of material model requires significant material calibration and consequently, various mechanical tests are required to determine the relevant material input parameters.

For the contact properties, the identification of the friction coefficients was rather simple since the experimental data obtained in chapter 6 can be directly input within PAM-FORM as a function of both normal pressure and sliding rate. The consolidated data are shown in Table 11.

These material cards will be implemented within PAM-FORM for the development of a double diaphragm forming simulation model. Results will be presented in the following chapter.

10 Forming analysis

In order to assess the formability of the different prepreg materials during 3DF, both experimental and numerical forming analysis were carried out. First, this chapter describes the forming setup developed for this work. Then, simulation model of the 3DF process under representative conditions is introduced. Finally, simulation results are qualitatively and quantitatively compared to experimental results. This exercise eventually helps demonstrate the predictive capability of the preforming software.

10.1 Forming experiment

Forming experiments were carried out with a 1500 kN preforming press, equipped with a preheating station consisting of two infrared heating panels, producing a total of 96 kW. An automated shuttle system allows the transport of the prepreg blank from the pre-heating station to the press. A schematic of the preforming cell is shown in Figure 97.

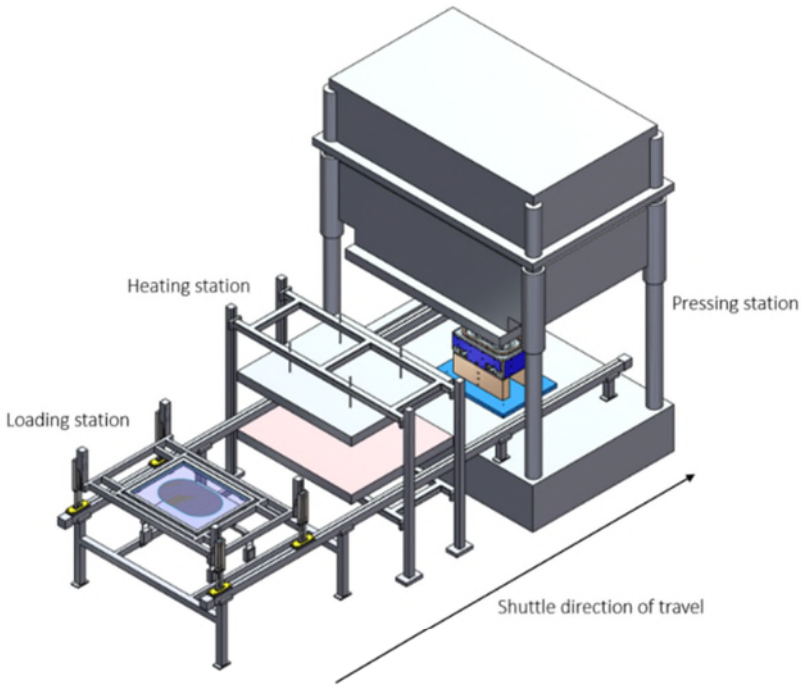

Figure 97: Schematic of the preforming cell

Prior to the forming stage, the prepreg plies are cut using a CNC cutting machine and assembled manually to form the desired lay-up. The prepreg laminate is then placed between two diaphragm membranes, which are subsequently clamped in a carrier frame. The frame is composed of three parts, namely an upper ring, a lower ring and a vacuum

ring (Figure 98). The latter allows the application of a vacuum between the two diaphragms. The dimensions of the frame are 1400x1000 mm.

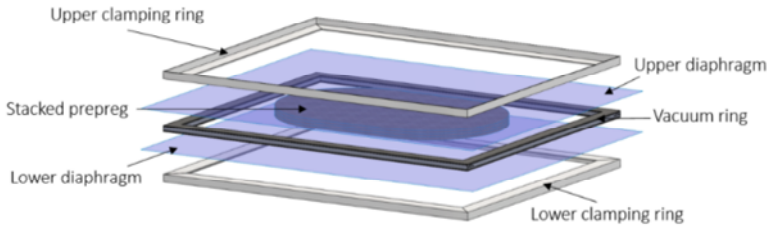

Figure 98: Schematic of the clamping frame

The assembly is placed in the loading station (Figure 97), and is then shuttled into the pre-heating station, where the laminate is heated to a temperature of 80°C for approximately 90 seconds. The frame is subsequently transferred into the press, and the laminate is formed and pressed in the hot tool. The kinematic of the forming process is split into two stages: The laminate is first draped over the male tool, after which it is forced in-between the two mould halves under the action of the moving top tool. The tool velocity is 85 $mm.s^{-1}$ in the first stage and 55 $mm.s^{-1}$ in the second one. Pictures of the 3DF process are shown in Figure 99.

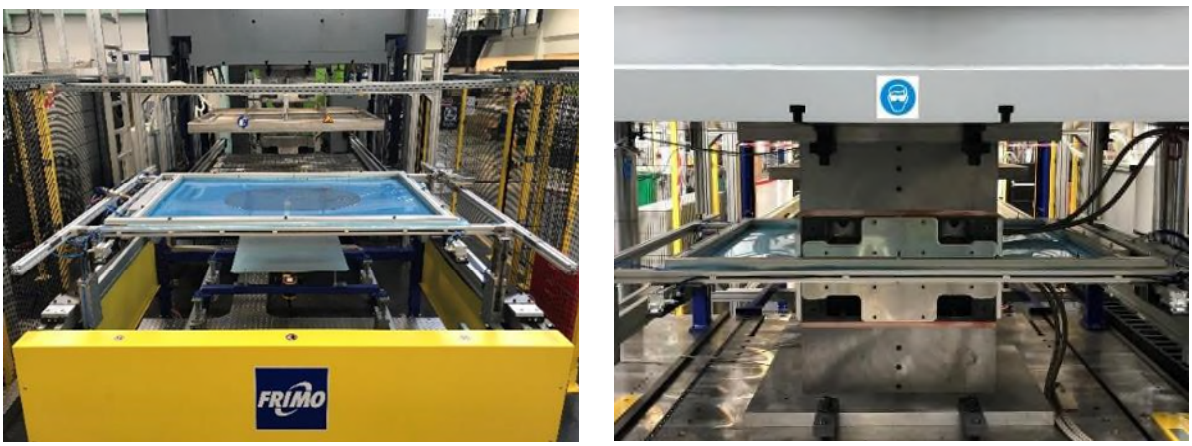

(a) (b)

Figure 99: (a) Rear view of the press prior to forming and (b) front view of the press after forming

The tool used in this project is shown in Figure 100. The geometry is referred to as double-dome and is an international benchmark geometry commonly used to study the formability of woven reinforcements. It features double curvature, with small radii and involves all deformation mechanisms of the reinforcement being formed (i.e. in-plane shear, out-of-plane bending and friction if multiple plies are used). The tool dimensions are 490 x 770 mm.

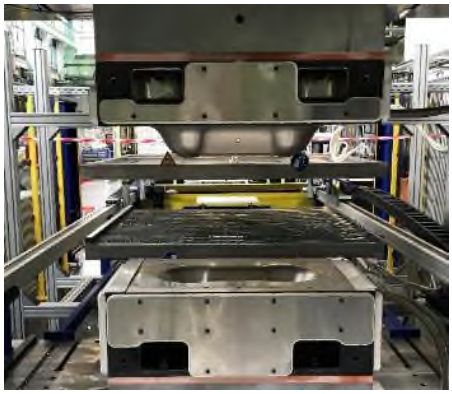

Figure 100: Double-dome tool

A data acquisition system allows to record process parameters such as the press position, the press tonnage, the pressure within the tool cavity, the tool temperature and the laminate temperature. Although of interest when performing numerical model validation, forming forces could not be determined during experiments due to their insignificant effect with respect to the size and capacity of the forming press used. The evolution of the temperature within a four-ply laminate during the 3DF process was investigated using thermocouples placed over and below the laminate (i.e. between the outer plies and the diaphragms) as well as within the laminate (i.e. between the two central plies). Figure 101 shows the resulting temperature measurements (right axis), plotted alongside the press position (left axis), against time.

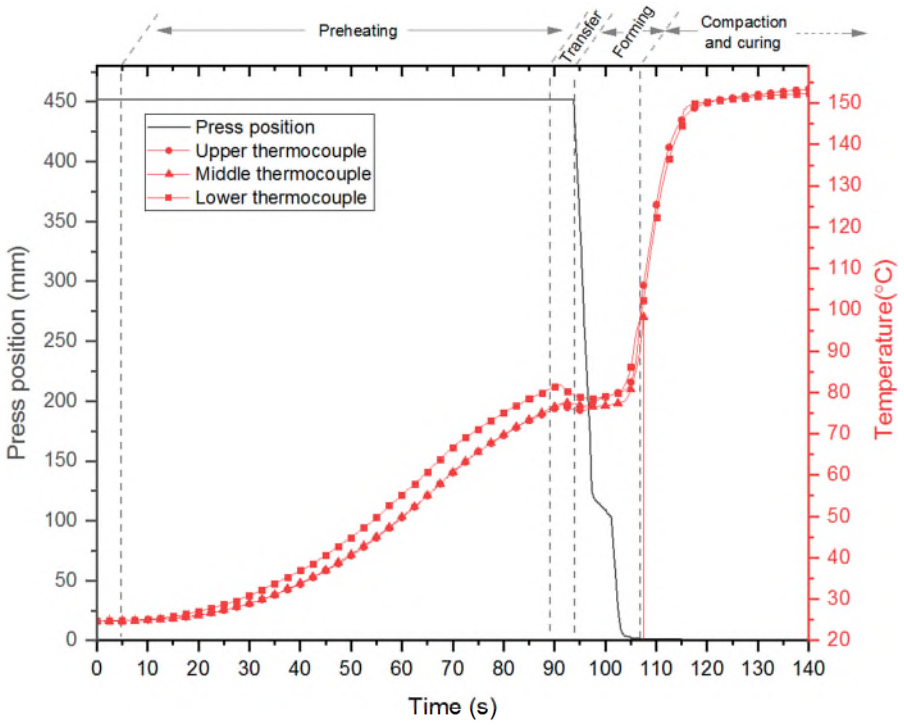

Figure 101: Temperature profile within the laminate and tool position during the forming process

During the preheating stage, the temperature within the laminate increases progressively until reaching the desired temperature of 80°C. A slight difference of 5°C can be observed between the different temperature measurements. The laminate is then shuttled into the press for forming, which results in a temperature decrease. The forming stage begins at approximately 95 s (i.e. as the press position decreases), however it should be noted that the tool first comes in contact with the diaphragm when the press position is approximately 200 mm. Subsequently, the laminate is formed in the hot tool, pressed and cured. Interestingly, the temperature within the laminate is 80°C throughout most of the forming. Only towards the very end (i.e. the last 5 mm of tool stroke before closure) does the temperature rapidly increase, caused by thermal conduction from the tool through the diaphragms, to the plies. As a consequence, the initial assumption of isothermal conditions during the 3DF process (section 4.1.2) is justified. All forming experiments were driven by press displacement and tool closure was interrupted 10 mm from full close position. It was observed that at full closure, out-of-plane defects are compressed, providing little information on the forming behaviour of the material. Experimental forming results will be presented alongside numerical ones in the next section.

10.2 Numerical analysis

A double dome model was developed, representative of the forming experiment setup presented in section 10.1. The model is similar for both the woven and the UD prepregs, however number of plies as well as material properties were adjusted accordingly.

10.2.1 Double dome model set-up

All pies and diaphragms were individually modelled using four-node shell elements. The top and bottom tools are considered as rigid bodies, while the plies and diaphragm are considered as deformable materials. In all cases, the element sides of the prepreg plies were carefully aligned with the fibre direction, in order to avoid locking phenomenon [142, 148]. Contact interactions between all deformable objects are modelled by a symmetric contact treatment. Between deformable objects and rigid bodies, a node to segment contact treatment is used, whereby the tools are defined as master surfaces and the deformable objects as slave surfaces. In order to maintain computational time within an acceptable range, several techniques were used:

(1) An adaptive mesh refinement was used, whereby the solver automatically refines the mesh (i.e. by splitting elements) in regions of large deformation. An initial element size of 8 mm was used together with a refinement level of 2, resulting in a final element size in the refinement regions of 4 mm.

(2) An automated mass scaling was used, whereby the solver automatically adjusts the mass scaling based on the mesh size of the plies. A mass scaling of approximately 0.05% the total element mass was observed.

(3) The tool velocity was sped up to 2.5 $mm.ms^{-1}$ (the choice of a correct artificial velocity will be explained in the next section). Because shear rate dependent material properties are used, a velocity scale factor was applied to correct for the artificial velocity.

The double dome model is shown in Figure 102, in the case of woven prepregs (i.e. 4 plies laminate). Similar to the forming process, the simulation is split into two stages. First the laminate is draped over the male tool (i.e. the bottom tool). In the simulation model, this is equivalent to the bottom tool moving up while the diaphragms edges are fixed (Figure 102, b). In order to replicate the effect of the frame holding the diaphragms, the outer edges of the top and bottom diaphragms are fully constrained. A pressure of 1bar was applied over the all diaphragms surface. Then the female tool (i.e. the top tool), moves down (Figure 102, c), completing the forming.

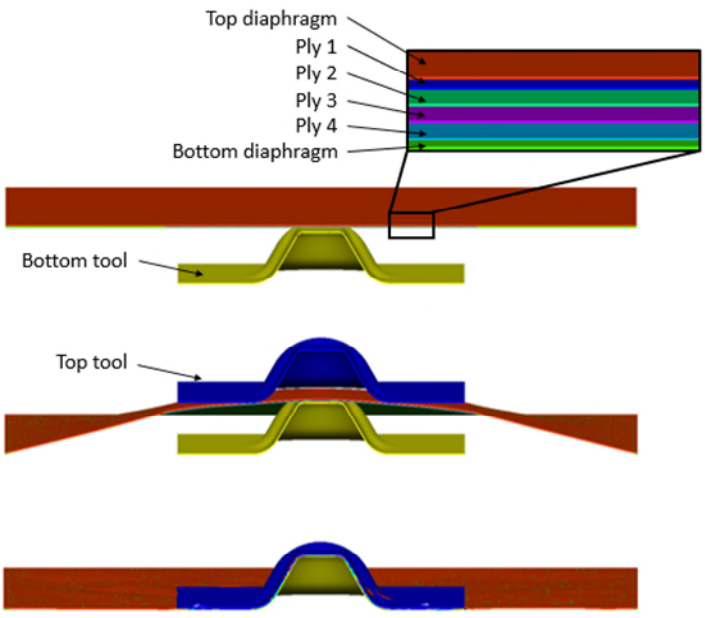

Figure 102: Cross-section of the double dome model at different stages: (a) Start of stage 1, (b) End of stage1/start of stage 2 and (c) end of stage 2

An average computational run-time of 8 hours was observed for the woven prepreg. For the UD prepreg, depending on the modelling approach used (section 10.2.4), run-time varied between 8 to 20 hours. All simulations were run with a 6 core Intel Xeon E5-2620 2 GHz processor.

10.2.2 Initial inertia analysis

With explicit time integration method, using the actual time duration of the forming process would result in significant and impractical computational effort due to stability limits on the time step. As a consequence, it is common practice to artificially increase the loading rate (e.g. tool velocity). A major challenge therefore consists in finding the right balance between computational efficiency and accuracy, since excessive tool speed may result in unrealistic dynamic effects. During forming of composite reinforcements, inertia force should be negligible. It is generally agreed that, for a quasi-static analysis the kinetic energy should not exceed a small fraction of the internal energy during the simulation, i.e. typically 10% [149]. To investigate this condition, an initial analysis on the evolution of the internal and kinetic energies during the double dome simulation was carried out on a quasi-isotropic woven prepreg double dome simulation model. For a meaningful comparison, only the kinetic and internal energy associated with the deformable bodies were considered (i.e. plies and diaphragms). The rigid body masses (i.e. tools) were not taken into account. Results are shown in Figure 103, and present the evolution of both the kinetic and internal energies, as a function of the tool progression (i.e. the tool closure) for different tool speeds. Pictures of the corresponding simulations are also presented and give an indication of the effect of inertia on the deformation pattern of a double dome part.

It can be observed that irrespective of the tool speed, the internal energy shows a similar trend. As the tool closes, the evolution of the internal energy reflects the loading rate and shows a gradual increase. For the simulations performed with a tool speed of 10 $mm.ms^{-1}$ (Figure 103, a) the kinetic energy exceeds the internal energy during most of the simulation, suggesting that inertia effects dominate the solution. For a tool speed of and 5 $mm.ms^{-1}$ (Figure 103, b), inertia effects are still present for half the simulation. In both cases, the deformation pattern, mostly characterised by the wrinkling position and shape, is significantly different. With a tool speed of 2.5 mm.ms-1 (Figure 103, c), the kinetic energy remains lower than the internal energy. Therefore, all simulations presented thereafter have been performed with a tool velocity of 2.5 $mm.ms^{-1}$.

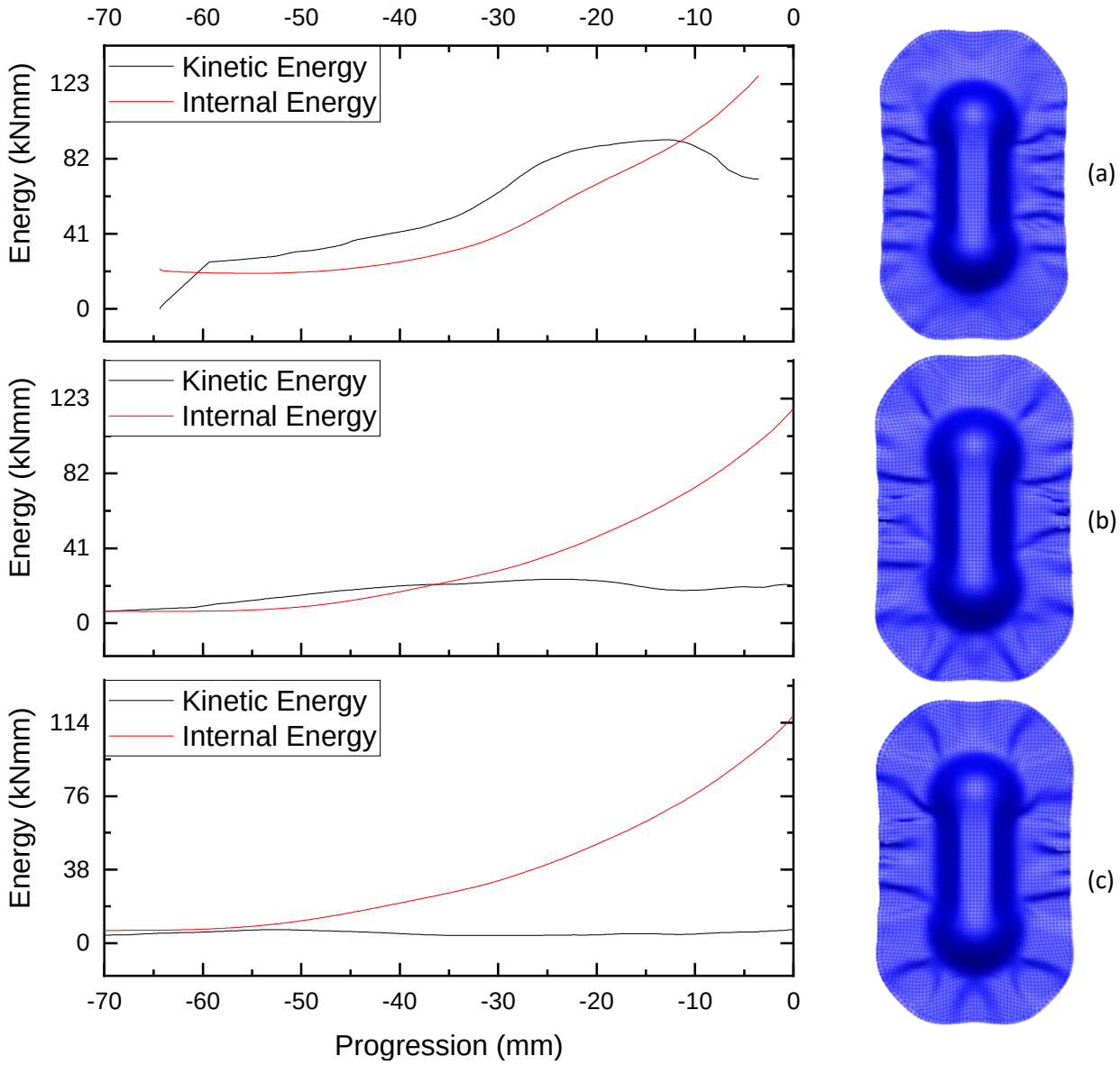

Figure 103: Progression history plots of kinetic and internal energy for a simulation performed with a tool simulation velocity of: (a) 10 mm.ms^{-1}, (b) 5 mm.ms^{-1} and (c) 2.5 mm.ms^{-1}, and corresponding simulation results

The resulting computational run-times for each case are presented in Table 20, and show that the tool velocity used in the simulation has a non-linear effect on the computational time. These particular simulations were run with a non-adaptive element size of 8 mm.

Artificial tool velocity (mm.ms^{-1})	Total simulation run time
10	46 min, 21 sec
5	1 hour, 1 min, 30 sec
2.5	3 hours, 7min, 58 sec

Table 20: Computational run-time as a function of tool simulation velocity, for a quasi-isotropic woven laminate with an 8 mm mesh size

10.2.3 Woven prepreg

This section presents the numerical results obtained for the woven prepreg. In order to investigate the effect of lay-up on the forming behaviour of the material, three different laminates were considered:

- A four-ply, quasi-isotropic laminate $[0/90°,\pm45]_s$. (0° being the direction aligned with the length of the double dome tool).
- A four-ply laminate $[0/90]_s$.
- A four-ply laminate $[\pm45]_s$.

The results are presented alongside the preforming experiments. Similar to the preforming experiments, the simulations were stopped 10mm from complete tool closure to allow out-of-plane wrinkles to be observed. First, both the numerical and experimental results are compared qualitatively, in terms of defects occurrence such as wrinkling (i.e. shape and number). Then, results are compared quantitatively in terms of material draw-in, shear angle distribution and interply slip. shows the forming predictions and experiments. Only a quarter of the parts is shown due to the axial and transverse symmetry of the geometry. For the quasi-isotropic lay-up, the predicted results represent every single ply so that an appreciation of the level of interply slippage can be made. In contrast, for the other lay-ups, only the top ply is shown as other plies deform similarly. For the quasi-isotropic lay-up, large wrinkles are present in both the forming prediction and the experiment. These wrinkles are formed near regions of high shear, and develop as a result of compressive forces. In both cases, the location of the wrinkles is in good agreement (i.e. around the dome and on the side of the part). The only notable difference is the size of the wrinkles, which is slightly overestimated in the simulation. This is most likely attributable to the initial approximation made on the bending stiffness (section 9.2.4), whereby a constant value was considered. Indeed, it was demonstrated in [39], that the bending stiffness plays a major role in the development of wrinkles. The numerical results for the $[0/90]_s$ lay-up are in good agreement with the experimental ones. A correct prediction of the size of the wrinkles as well as their location can be observed. Finally, For the $[\pm45]_s$ lay-up, it can be observed that the numerical model overestimates the wrinkling prediction. This is demonstrated by the presence of wrinkles and fold on the side of the part. In contrast, the experimental part is almost wrinkle free, with some small out-of-plane defects only visible at the end of the part. On the simulation, these particular defects are in the forms of buckled areas, rather than wrinkles. The tendency of the numerical model to overestimate

the wrinkling prediction for the $[\pm 45]_s$ lay-up only may be caused by size and geometry effects. Indeed, the only fundamental difference between the $[\pm 45]_s$ lay-up and the other two is the orientation of the laminate principal directions (i.e. initial fibre orientation) with respect to the tool principal directions.

Globally, it can be observed that the quasi-isotropic laminate shows more wrinkles than other lay-ups.

10.2.3.1 Occurrence of defects

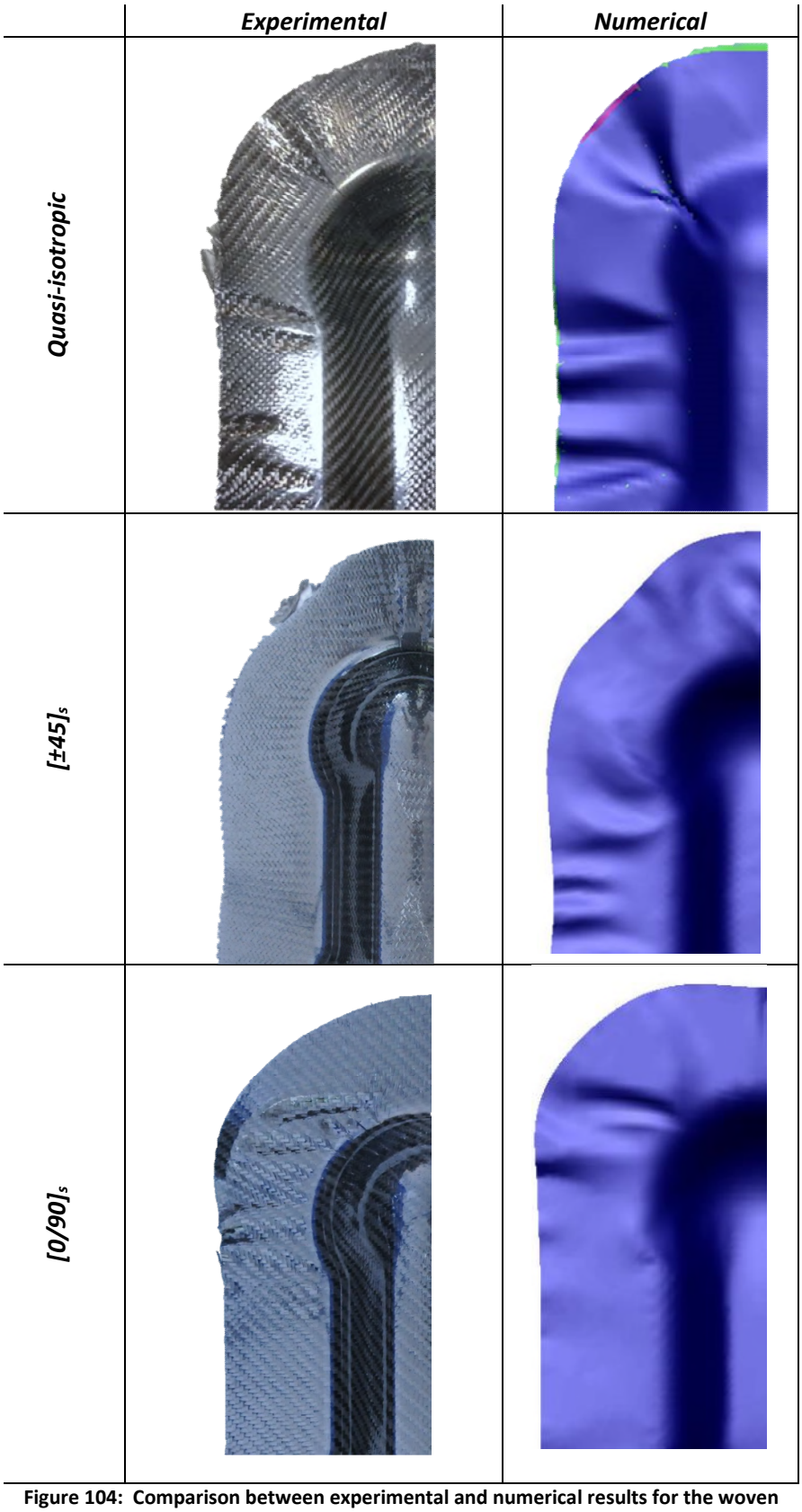

Figure 104: Comparison between experimental and numerical results for the woven prepreg and different lay-up

10.2.3.2 Material draw-in

The material draw-in can be defined as the amount of material flow during the forming process. The correct prediction of the material draw-in is an important parameter for the manufacturing process design as it can help predict the amount of material required to produce the desired part. It is particularly important for near-net shape processes where the minimum amount of material is used. The material draw-in can be estimated by considering the outer contour of the formed part. For the experimental results, pictures were taken for each part and post-processed using ImageJ software. The pictures were subsequently scaled and calibrated accordingly using a known reference dimension. Then, image thresholding was carried out in order to isolate black pixels (i.e. the composite part) from the background, after which the coordinates of the outer contour of the part could be exported. Figure 105 shows for each lay-up, the predicted and the experimental outer contours of the part. It can be observed that in all three cases, the predicted outer contours are in relatively good agreement with the experimental ones both in terms of shape and magnitude. For all three lay-up, a detailed comparison reveals a maximum relative deviation between the simulation and the experimental results of approximately 15 mm. For the $[0/90]_s$ lay-up, the model tends to overestimate the amount of material draw-in, particularly around the corners of the part. An opposite behaviour can be observed for the $[\pm45]_s$ lay-up. For the quasi-isotropic lay-up, the predicted results either overestimate or underestimate the amount of draw-in, depending on the location.

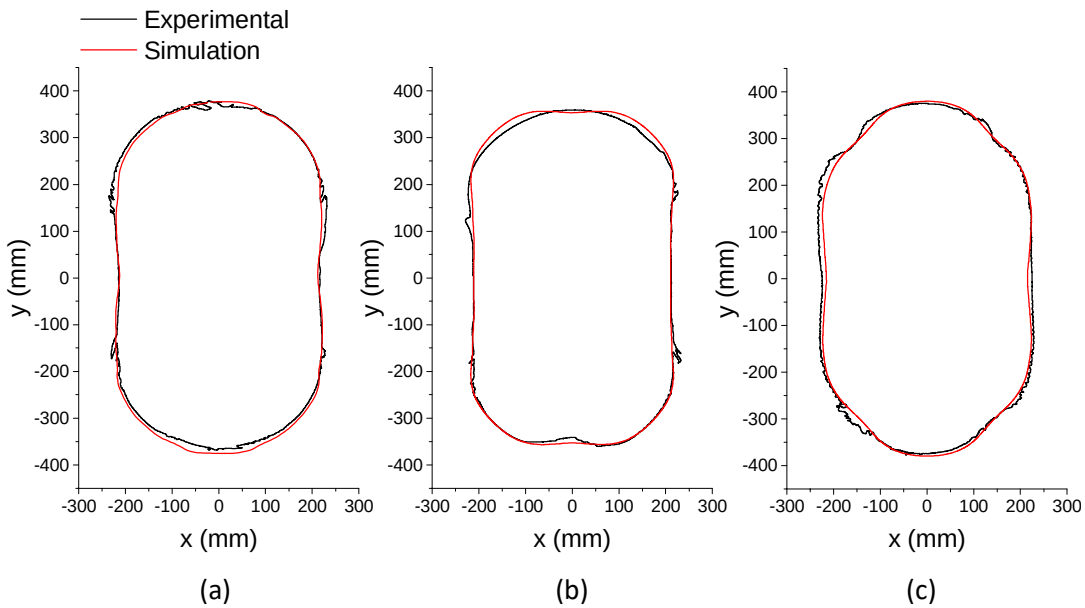

Figure 105: Comparison of the material draw-in obtained experimentally and numerically for the woven prepreg for a: (a) Quasi-isotropic laminate, (b) $[0/90]_s$ laminate and (c) $[\pm45]_s$ laminate

In order to quantify the error between the experimental and the predicted material draw-in, the area within the closed contours shown in Figure 105 was investigated. The area was calculated using ImageJ/Fiji. First, the results were scaled accordingly in order to convert pixels into millimetres. Then each contour was individually set as region of interest and the "Measure" tool was used. The results are presented in Table 21.

	Experimental area (mm^2)	**Simulation area (mm^2)**	**Relative difference (%)**
Quasi-isotropic	285602.5	288120.9	0.88
$[0/90]_s$ lay-up	276629.9	280011.5	1.21
$[\pm45]_s$ lay-up	285635.6	279122.4	2.31

Table 21: Comparison of the closed contour area between the experimental and numerical results

It can be observed that the numerical model provides a good agreement for the quasi-isotropic lay-up, with a relative error of 0.88% between the areas obtained experimentally and numerically. The error is largest for the $[\pm45]_s$ lay-up, with a relative difference of 2.31%.

10.2.3.3 Shear angle

During forming of biaxial reinforcements, the angle between the initially perpendicular warp and weft tows will vary. This angular change is known as the shear angle and is an important parameter since it gives information about fibre reorientation. In addition, the change in thickness of composite plies is also linked to the amount of shear in different zones of the part. Therefore knowledge of the shear angle is important for tool design. As such, shear angle is often used as a comparison between experimental and numerical results.

Lomov *et al*. [65] have successfully used 3D DIC to measure the shear angle after the forming process of a thermoplastic fabric. A grid pattern consisting of perpendicular lines, was drawn onto the surface of the blank prior to shaping the part. After forming, the 3D DIC system was used to obtain the three-dimensional coordinates of the surface. Coordinates of the grid intersection points were extracted and the angles between the lines were manually calculated using the law of cosines, yielding the shear angle. The technique was successful although disruption of the reference pattern was observed due to friction with the tool. In this study, the use of photogrammetric system was considered. This technique is particularly popular in sheet metal forming[150], and consists in measuring the

local distortion of an initially regular array of dots, which is etched on the surface of the blank prior to forming. The formed component is recorded using a digital CCD camera from various angles. Then, photogrammetric algorithms are used to determine the 3D coordinates of the dots and the surface strain tensor, yielding information on the major and minor strain.

For prepreg composites, the application of a dot pattern is relatively more challenging than for sheet metal parts. An initial investigation was carried out using a stencil and an acrylic white paint in order to mark the blank prior to the forming process. This approach was not successful due to significant disruption of the dot pattern. The low viscosity of the epoxy resin at elevated temperature, combined with the high pressure exerted by the tool caused the paint to flow with the resin during forming (Figure 106).

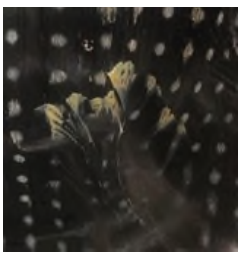

Figure 106: Disruption of the dot pattern caused by the flow of the resin during forming

An alternative solution was investigated, whereby the dot pattern was applied onto the part after forming. Dots were hand drawn at each warp/weft crossover points using a white marker pen. A similar approach using 3D DIC was used by Khan [74], for measuring the shear angle of dry fabrics. The purpose of this method is to take full benefit of the intrinsic, regular pattern of 2x2 twill woven prepregs and their specific deformation mechanisms dominated by trellis shear (section 2.3.1). A picture of the part, showing the dot pattern as well as the measurement setup is shown in Figure 107.

Figure 107: Measurement setup for photogrammetry

The determination of the shear angle was performed using the photogrammetry system, Argus® GOM. The measurement process requires taking a series of images from different angles, using a CCD camera. A set of markers is placed around the region of interest and is required for calculating the camera position with respect to the part. Then, using triangulation techniques, the images are virtually assembled to represent the part in 3D coordinates. Considering the local distortion of an initially regular dot pattern (it is assumed that before forming, the crossover points form a regular grid with a grid spacing equivalent to the width of a tow, i.e. 4 mm) the local strain introduced by the forming process can be calculated. Strains are calculated by creating a virtual grid connecting each dot. Prior to photographing the part, the region of interest was sprayed with a full-matt, anti-reflection spray in order to subdue glare that would impede the measurement process (the difference between sprayed and non-sprayed areas is evident in Figure 107, particularly around the domes). Due to symmetries, only a quarter of the double dome part was considered. compares the shear angle distribution on the top ply of a quasi-isotropic woven lay-up between the experimental results (a), and the simulation results (b). Shear angle values are plotted on a similar scale, ranging from -43.7° to 43.7°. It can be observed that both the measured and the predicted results show a relatively similar shear angle distribution. Similar to the experimental results, the numerical model predicts high shear angle near the lower corner of the dome of comparable magnitude (maximum -43.7°). In addition a distinctive pattern can be observed, whereby intermediate shear angles (i.e. approximately -20°) spread from the high shear area both along and across the longitudinal axis.

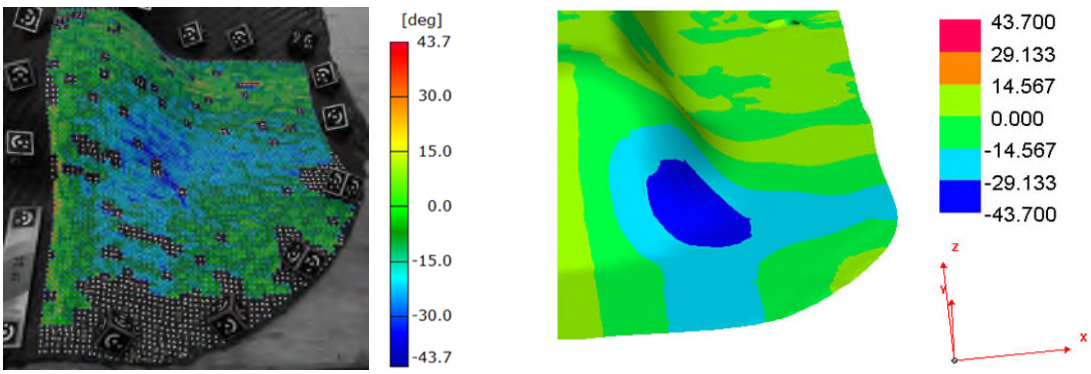

(a) (b)

Figure 108: Comparison of shear angle on the first ply of a quasi-isotropic woven laminate (a) experimental results and (b) simulation results

It can be seen that experimentally, the contour contains missing data. This may be caused by the inability of the sensor to pick up certain dots, or the inability of the photogrammetry algorithm to create a coherent virtual grid connecting every dots. However, areas of high

shear, which are of critical importance in terms of model validation, are fairly well captured and the regions with missing data generally have very small shear angle as suggested by the simulation. It should be noted that for the experimental contour, high positive shear angle values (represented in red) are artefacts, which may be caused by the excessive distortion of the virtual grid created by the photogrammetric algorithm. In practice, such high positive shear values are only expected on the opposite side of the dome.

The good agreement between the experimental and the simulation results demonstrates the predictive capability of the simulation model, as well as the effectiveness of the shear angle measurement method. Although the results shown are in good agreements, some degree of uncertainties may exist due to the manual, hand-drawn tracing of the grid.

10.2.3.4 Interply slip

Comparison of the predicted versus the measured interply slip is an important factor as it gives an indication of the quality of the friction input data, which in turn demonstrates the accuracy of the friction test method. The amount of interply slip was measured around the outer edges of the part on the quasi-isotropic lay-up. Other lay-ups were not investigated since the respective constituting plies deform uniformly.

For the quasi-isotropic lay-up, interply slip was mostly observed at both ends and on the sides of the part. On both the experimental and the numerical part, the amount of slippage was determined directly by measuring the maximum distance between two adjacent plies (Figure 109). At the end of the part, the measured ply slippage was approximately 19.2 mm for the numerical model, against approximately 22 mm for the experiment. Note that the pictures are scaled accordingly.

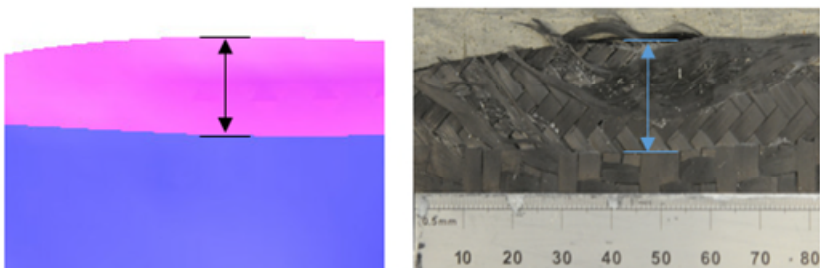

Figure 109: Interply slippage at the end of a quasi-isotropic woven prepreg double dome part

Similarly, ply slippage was measured on the side of the part. Experimentally, a distance of 6.5 mm was obtained between two adjacent plies. In contrast, the numerical model showed a distance of 7.1 mm.

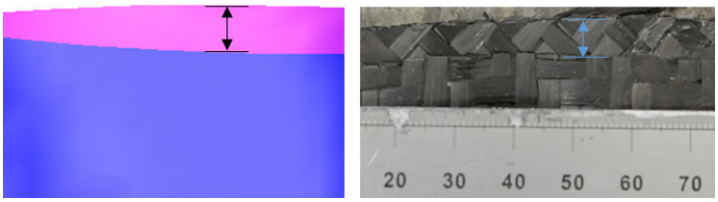

Figure 110: interply slippage on the side of a quasi-isotropic woven prepreg double dome part

In both cases, the results are in reasonable agreement. These observations demonstrate that the friction coefficients used are relatively accurate. In addition, the friction model is able to predict the amount of ply slippage under similar forming conditions.

10.2.3.5 Verification of the test parameters used during material characterisation

In order to assess the validity of the test parameters (i.e. shear rate and normal pressure) employed during the initial material characterisation tests (i.e. picture frame and friction tests), the evolution of shear rate and normal pressure during the forming simulation were investigated. This verification exercise is particularly important since material data are defined for particular conditions of strain rate and pressure. The investigation was carried out on the quasi-isotropic woven prepreg lay-up.

Figure 111 shows the evolution of the shear rate in two different areas of the double dome part, as a function of the tool positon (0 mm corresponding to full closure). It should be noted that only values up to 10 mm are of interest since partial tool closure was used for the experimental forming (section 10.1). The shear rate was determined by differentiating the shear angle obtained in these particular areas, namely a high shear area and an intermediate shear area, with respect to time. In the high shear area, it can be observed that as the tool closes, the shear rate increases rapidly up to approximately $50°.s^{-1}$ at a tool position of 10 mm. In contrast, in the intermediate shear area, the shear rate is below $10°.s^{-1}$ up until a tool closure of 10 mm. This suggests that the model may underestimate the shear stresses within high shear areas, since input data were obtained up to a shear rate of 9.29°.s-1 (section 9.2.1). However, it should be noted that those high shear areas only represent approximately 4% of the total surface of the double dome part (as predicted by the software). As a consequence, it is assumed that this shear rate difference has little influence on accuracy of the numerical results.

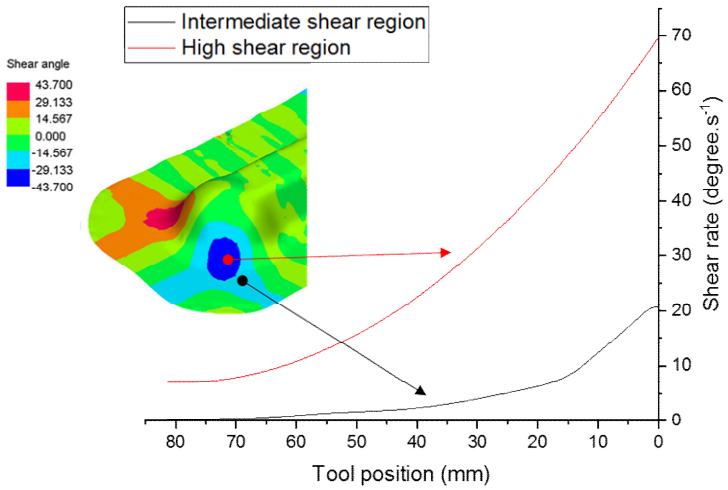

Figure 111: Shear rate evolution as a function of the tool position in two different regions of a quasi-isotropic woven prepreg double dome

Similarly, an investigation was made with regards to the evolution of the normal pressure. Figure 112 shows the distribution of the normal pressure at a tool closure of 10 mm. The scale is plotted such that normal pressures higher than 200 kPa (corresponding to the maximum normal pressure considered during friction tests) are represented in purple. It can be observed that around the domes, and within wrinkles, normal pressure higher than 200 kPa are achieved, over approximately 23% of the surface of the part. However it should be noted that this level of pressure is only attained towards the end of the forming process. For comparison, at a tool closure of 25 mm, normal pressures higher than 200 kPa are only present on 12% of the surface of the part. These observations help validate the initial assumptions made about the test parameters used during material characterisation (section 4.2).

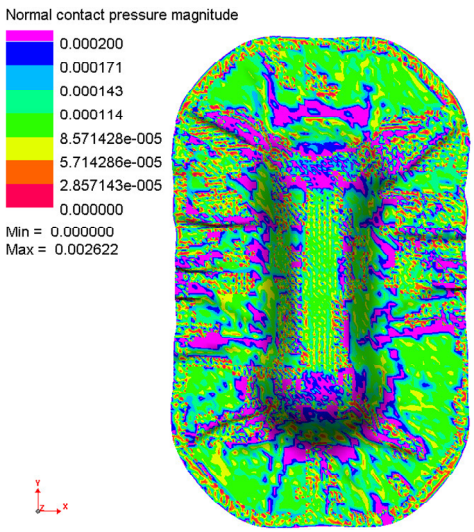

Figure 112: Normal pressure (in GPa) distribution on a quasi-isotropic woven prepreg double dome, at a tool closure of 10 mm

10.2.4 Unidirectional prepreg

This section presents the numerical results obtained for the UD prepreg. Similar to the woven prepreg, three different laminates were used:

- An eight-ply quasi-isotropic, balanced and symmetrical laminate $[0,90,\pm45]_s$
- An eight-ply, cross-ply laminate $[0,90,0,90]_s$
- An eight-ply, cross-ply laminate $[-45,+45,-45,+45]_s$

Two modelling approaches were used for the simulation of the forming process of UD prepreg:

(1) A single ply approach, whereby each ply is individually modelled using the unidirectional material model within PAM-FORM (section 9.1). Experimental data obtained from the novel rail shear test are used to describe the shear behaviour of each ply (section 5.3). Tensile properties along the fibres are described through E_1, using an educated value of 20 GPa. For the tensile properties across the fibres E_2, strain rate experimental data obtained from transverse tensile test of UD (section 7.2). Experimental data from cantilever (section 8.3.2) and friction tests performed on a single UD ply are used to describe the bending and the frictional behaviour of the UD, respectively.

(2) A cross-ply approach, whereby every two adjacent plies of UD, stacked in a cross-ply sequence (e.g. [0/90]) are modelled as a single biaxial ply using the fabric material model within PAM-FORM (section 9.1). This approach is based on the findings made in section 5.4, which demonstrated that cross-plied UD prepregs behave as a woven material under conditions of bias extension. This was also observed in [38]. Experimental data obtained from bias extension test of cross-plied UD (section 5.4) are used to describe the shear behaviour of the equivalent woven ply. The tensile properties E_1 and E_2 are similar and an educated value of 20 GPa is used. Experimental data from cantilever test performed on cross-plied UD (section 8.3.3) are used to describe the bending properties, while friction properties are similar to those used in the single ply approach.

Similar to the woven prepreg, results are first compared qualitatively, in terms of defects occurrence such as wrinkling (i.e. shape and number). Then, results are compared quantitatively in terms of material draw-in and interply slip. Finally the merits of both approaches are discussed. Numerical results from both approaches are presented alongside the preforming experiments in Figure 113. For the quasi-isotropic lay-up, both approaches show different behaviour. While in both cases the location of wrinkles is in good agreement with respect to the experimental part, the cross-ply approach tends to overestimate their size. In contrast, both the shape and the size of the different wrinkles (i.e. the two main wrinkles located around the dome as well as the smaller ones on the side of the part) are relatively well predicted using the single-ply approach. In addition, it can be observed that the level of interply slip both at the end and on the side of the part is significantly different for both approaches. This suggests that the dominant deformation mechanism are different. For the $[-45/+45/-45/+45]_s$ (Figure 113), a similar observation can be made, in that the cross-ply approach tends to overestimate the wrinkling behaviour. In a similar way to that occurring for the $[\pm45]_s$ woven prepreg lay-up (), the fabric material model seems to predict the formation of wrinkles that do not exist in reality. This is particularly evident on the side of the part. For the single-ply approach, the location of the wrinkles is relatively well predicted on top and around the dome. Finally, for the $[0/90/0/90]_s$ lay-up (Figure 113), both approaches predict comparable results in terms of wrinkling location. The main wrinkle, located on the side of the dome is also observable in the experimental part. However, smaller wrinkles around the dome at the intersection between the dome and the flat part are not predicted by either approach which is mostly attributable to the mesh size being too coarse. Small wrinkles on the left side of the part are also noticeable on the experimental part. These can be also be observed on the singly-ply approach, characterised by slight buckling areas.

Generally, it can be observed that cross-plied laminates show less wrinkles compared to the quasi-isotropic lay-up. This was also observed in [61]. Cross-plied laminates have a high propensity to shear without generating out-of-plane defects, unlike quasi-isotropic laminate which are limited by additional fibre orientations, which therefore increase the global in-plane shear stiffness of the laminate. Irrespective of the lay-up, the single-ply approach provides better results in terms of wrinkling prediction, as compared to the more traditionally used cross-ply approach that was also concluded in [106].

10.2.4.1 Occurrence of defects

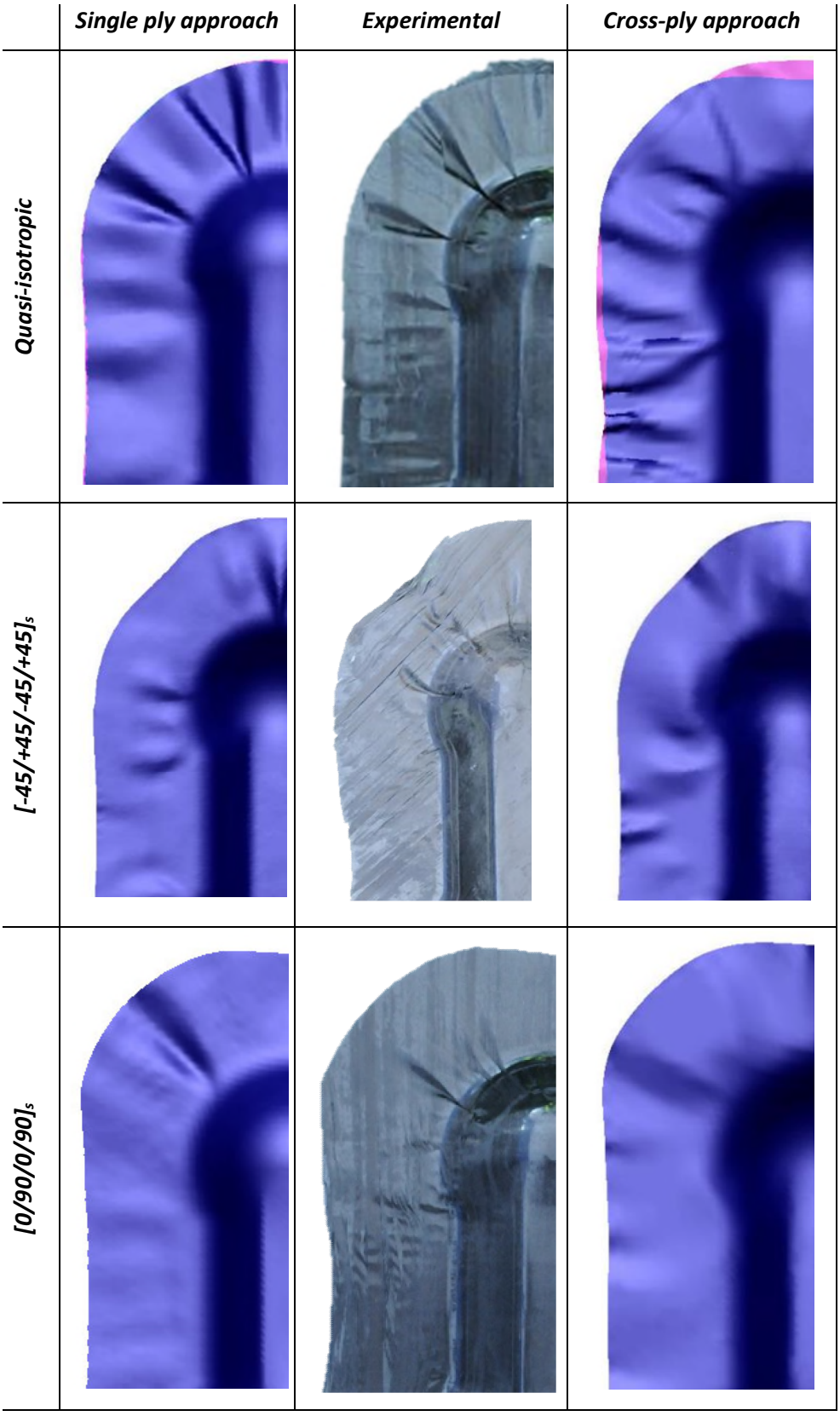

Figure 113: Comparison between experimental and numerical results for the UD prepreg for different lay-up and different modelling approaches

10.2.4.2 Material draw-in

Similar to the woven prepreg, the amount of material draw-in was compared between numerical results (for both approaches) and experimental result. Results are shown in Figure 114. For the quasi-isotropic lay-up, both numerical approaches underestimate the amount of material draw-in. The larger contour obtained experimentally is partly attributable to fibre splitting, which increases the global dimension of the part since outer plies may protrude further away. This failure mode is not taken into account in the numerical models. Based on the overall contour, the cross-ply approach provides a better fit to the experimental result. A maximum relative deviation of 22 mm was observed between the single ply approach and the experimental result. In contrast, a maximum difference of 17 mm was observed between the cross-ply approach and the experimental result. The difference between both numerical approaches is due to the amount of interply slip occurring during forming, since in the cross-ply approach, the total number of interfaces between adjacent plies is less than half that of the single ply approach. In contrast, for the $[-45/+45]_s$ and $[0/90]_s$ lay-ups, both numerical approaches predict almost identical outer contours. Compared to a quasi-isotropic lay-up, cross-ply lay-ups experience less interply slippage since the number of off-axis plies is reduced. For the $[0/90]_s$ lay-up, a maximum relative deviation of 10 mm is observed with the experimental result. For the $[-45/+45]_s$, however, a maximum relative deviation of approximately 25 mm is obtained, located on the top left side of the part.

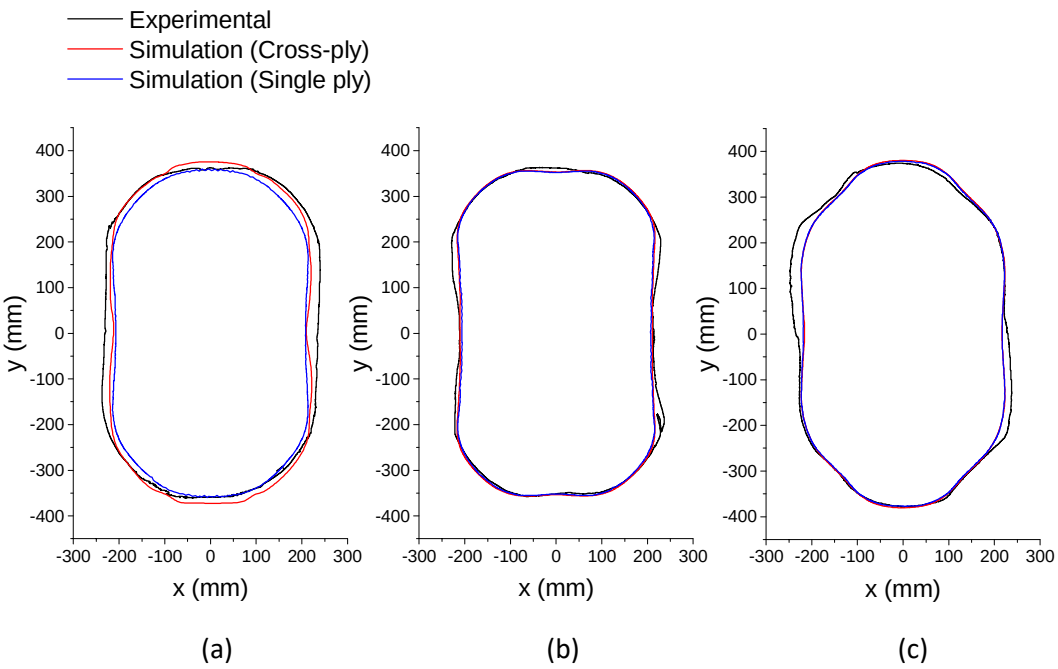

Figure 114: Comparison of the material draw-in obtained experimentally and numerically for the UD prepreg for a: (a) Quasi-isotropic laminate, (b) $[0/90]_s$ laminate and (c) $[-45/+45]_s$ laminate

Similar to the woven material, the numerical error on the draw-in prediction was investigated based on an analysis of the closed contour areas. It can be observed that generally, the cross-ply approach shows good agreement with the experimental results. Similar to the woven material, the greatest error is obtained for the $[-45/+45]_s$ lay-up, with a value of 4.24%. Irrespective of the lay-up considered, the single-ply approach gives the largest error with respect to the experimental area. This is particularly evident for the quasi-isotropic, where a relative difference of 11.59% is observed, compared to 3.17% for the cross-ply approach.

	Experimental area (mm^2)	**Simulation area (mm^2)**		**Relative difference with experimental (%)**	
		Cross-ply	Single-ply	Cross-ply	Single-ply
Quasi-isotropic	296700.9	287453.9	264184.1	3.17	11.59
$[0/90]_s$ lay-up	286224.5	280694.2	275350.2	1.95	3.87
$[-45/+45]_s$ lay-up	291306.5	279214.8	277745.0	4.24	4.77

Table 22: Comparison of the closed contour area between the experimental and numerical results including both cross-ply and single-ply modelling approaches

10.2.4.3 Interply slip

Similar to the woven prepreg UD, the amount of interply slip was compared between experimental and numerical results. Comparison between both approaches and the experimental part for the quasi-isotropic lay-up is shown in Figure 115. At the end of the part, the measured ply slippage is approximately 17 mm for the experimental model, against 21.9 mm for the cross-ply approach and 5.2 mm for the single-ply approach. Although the single ply approach tends to significantly underestimate the amount of slippage, these results do not necessarily reflect the accuracy of the material model or the effectiveness of the modelling approach used. In practice, some degree of ply splitting occurs in the transverse direction, which as a result affects the outer contour of the part. Because it is based on the distance between two adjacent plies, the current interply slip measurement method does not allow to dissociate the contribution of ply splitting from the interply slip. In addition, this phenomenon is not taken into account in the simulations since the material is treated as a continuum media. Therefore, without an indication of the actual amount of ply splitting, a comparison between these results is difficult.

Single ply approach	*Experimental*	*Cross-ply approach*

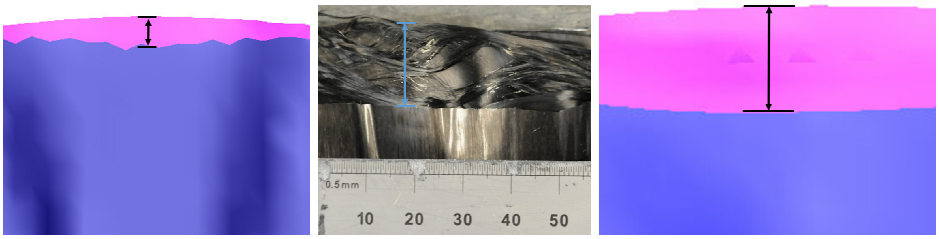

Figure 115: Comparison of the interply slippage obtained from numerical and experimental forming at the end of a quasi-isotropic UD prepreg double dome part

10.2.4.4 Ply splitting investigation

One of the major advantages in using the single-ply approach over the cross-ply approach, is the possibility to visualise stresses and strains within UD plies perpendicular to the fibre direction, which may provide indication of ply splitting. An example is given in Figure 116 and presents the stress distribution perpendicular to the fibre direction (referred to as "Fibre 2 stress" and expressed in GPa) within the top ply of the $[0/90]_s$ UD lay-up. It can be observed that the extreme stress values on the legend corresponds to the maximum stress obtained during transverse tensile test of UD prepreg (chapter 7). As a consequence, dark blue and red areas on the stress distribution contour indicate areas where transverse failure may occur. Analysis of the experimental part reveals ply splitting in similar areas, namely in both sides along the part and in the lower corner of the domes. However in practice, even though ply splitting is also noticeable, wrinkling seems to be more dominant in the lower corner of the dome.

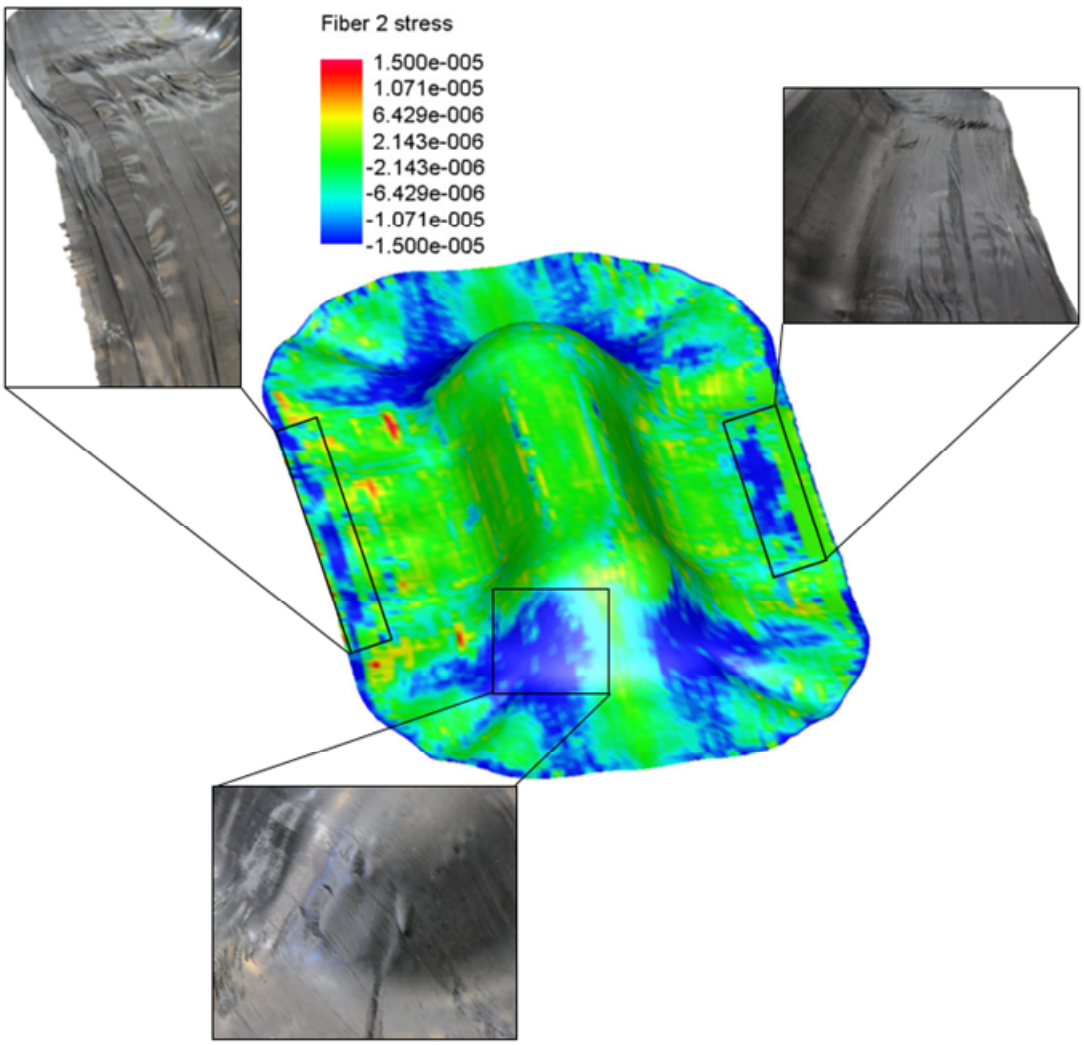

Figure 116: Stress distribution perpendicular to the fibre direction within the top ply of a UD cross-ply laminate $[0/90]_s$.

10.2.5 Sensitivity analysis

In order to investigate the effects of varying material input data on the forming behaviour of a quasi-isotropic lay-up woven prepreg, a sensitivity analysis was carried out. The analysis is performed using a design of experiment approach, consisting of three factors and three levels. The factors represent the material properties, i.e. the shear stiffness, the friction coefficient and the bending stiffness, while the levels (expressed as -1, 0 and 1) represent the value attributed to each factor. The different material parameters used are listed in Table 23. The level 0 corresponds to the nominal properties, i.e. the reference values obtained during the material characterisation and used for the simulations presented in previous sections. It should be noted that a factor 10 was initially investigated

for the level 1 of the shear stiffness, however, the simulations did not complete due to errors, possibly due to some elements being too stiff. Instead, a factor of 5 was used.

	Level -1	***Level 0***	***Level 1***
Shear stiffness (*x*)	Nominal x 0.1	Nominal	Nominal x 5
Friction coefficients (*y*)	Nominal x 0.5	Nominal	Nominal x 2
Bending stiffness (*z*)	Nominal x 0.1	Nominal	Nominal x 10

Table 23: Material input data used for the sensitivity analysis

A total of 19 combinations were investigated, allowing to assess the influence of all parameters as well as their interrelated effects on the forming behaviour of the woven material. The results are presented qualitatively in Figure 117 to Figure 119, and quantitatively in Figure 120 to Figure 122. All results are presented at a tool position of 10 mm. For clarity purposes, each factor is identified by means of coordinate (*x*, *y*, *z*), with *x* the shear properties, *y* the friction properties and *z* the bending properties. The value of each coordinate refers to the different levels.

10.2.5.1 Qualitative analysis

Qualitatively, it can be observed that all parameters have a different influence on the forming behaviour of the woven material. While all simulations show a relatively similar deformation behaviour, characterised by a main wrinkle running from the dome towards the outside of the part, with folds and buckled areas on the side, the shape and size of these defects are different. As a general observation, the bending stiffness seems to have the most effect on the shape of the wrinkles. With decreasing bending stiffness, the wrinkles are smaller and more defined. Decreasing the friction coefficients seems to be an effective way to reduce the size of wrinkles, e.g. (0,-1,1) compared to (0,1,1) in Figure 118. With regards to the shear stiffness, little effect can be seen on the forming behaviour, perhaps due to the use of a quasi-isotropic lay-up which is less prone to shearing. As a rough observation, increasing shear stiffness results in more wrinkles, particularly around the dome, e.g. (1,0,-1) compared to (-1,0,-1), in Figure 119. This investigation shows that, the forming behaviour of woven material is a complex mechanism, influenced by all deformation modes and demonstrates the importance of an accurate material characterisation.

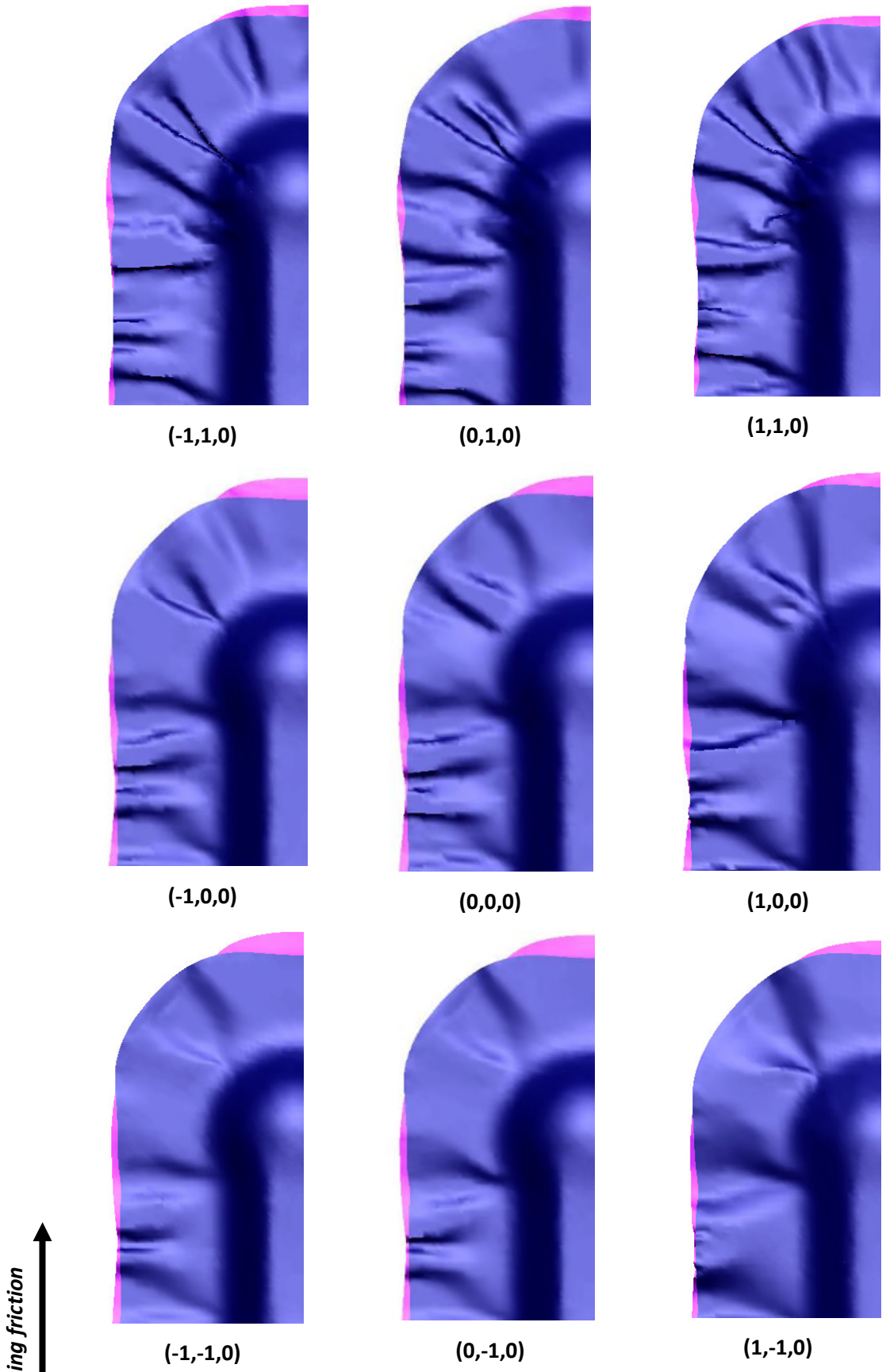

Figure 117: Simulation results as a function of shear and frictional properties for a quasi-isotropic woven material (bending stiffness sets to level 0)

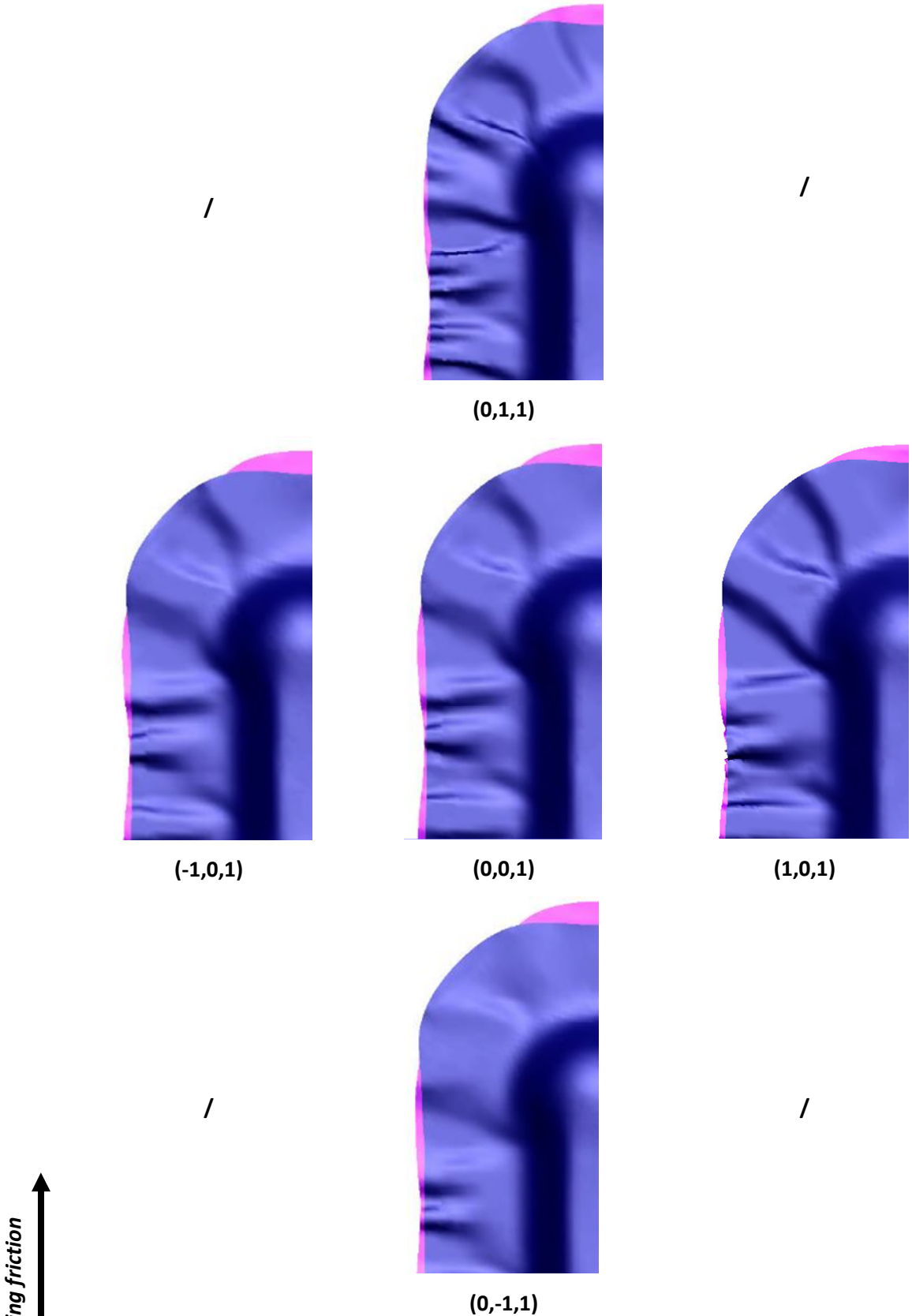

Figure 118: Simulation results as a function of shear and frictional properties for a quasi-isotropic woven material (bending stiffness sets to level 1)

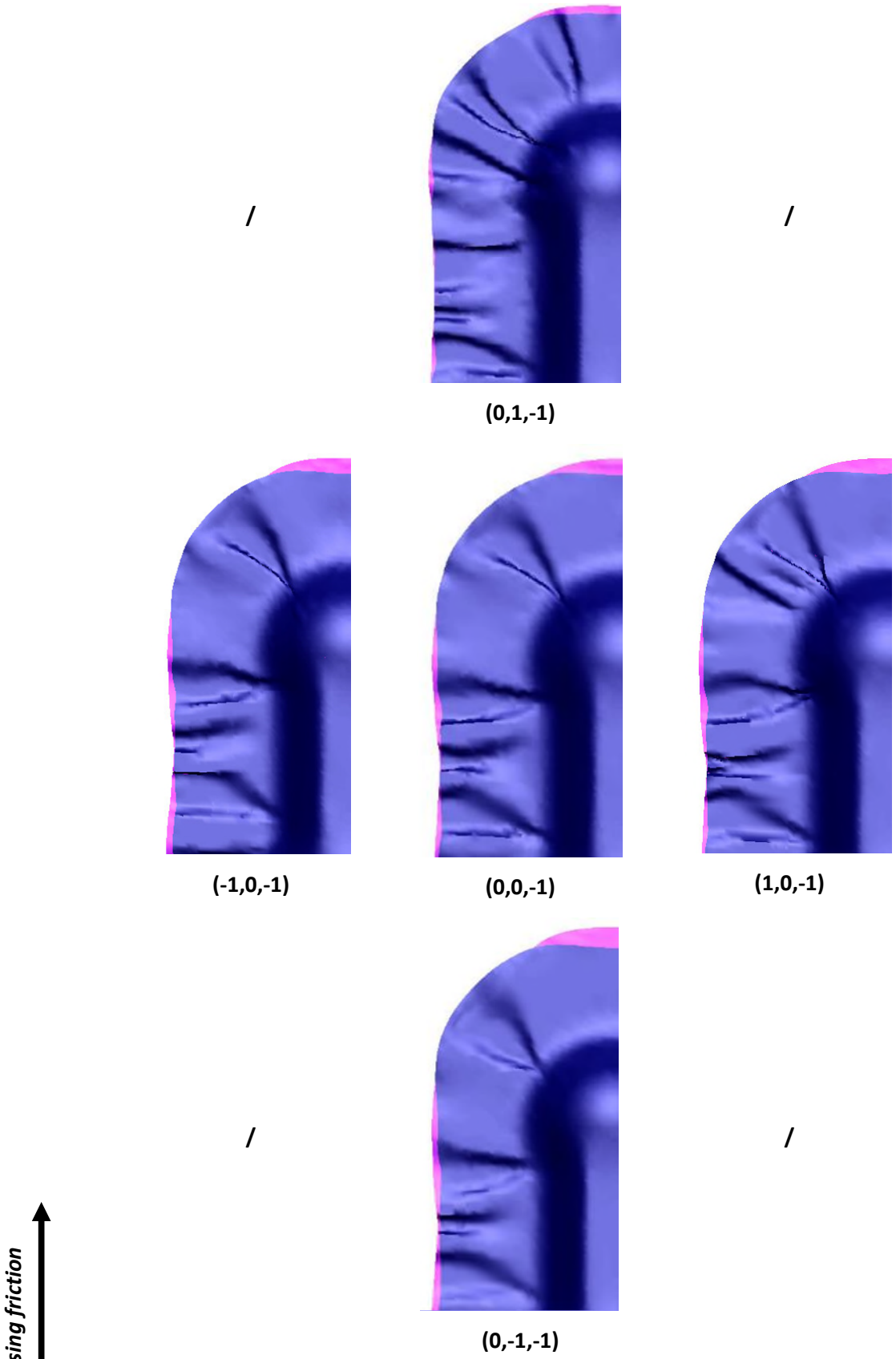

Figure 119: Simulation results as a function of shear and frictional properties for a quasi-isotropic woven material (bending stiffness sets to level -1)

10.2.5.2 Quantitative analysis

Figure 120 to Figure 122 present the shear angle contour along with the maximum shear angle value obtained for different combinations of shear stiffness, bending stiffness and friction properties. It can be seen that irrespective of the material input data used, the shear angle distribution is relatively similar, whereby maximum shear (in absolute terms) is observed at the base of the dome, and at 45° from the longitudinal axis of the part. Shear angle values decrease from this point on towards the edge of the part. Maximum shear angle value is an important parameter since it gives an indication of the overall formability of the material. It is generally accepted that promoting in-plane shear deformation results in better quality parts.

In order to understand the individual effect of the different material input parameters on the maximum shear angle obtained, the main effects plot resulting from the design of experiment are presented in Figure 123. It can be observed that each material parameter plays an important role on the forming behaviour of the quasi-isotropic lay-up. Increasing the shear stiffness results in lower maximum shear angle. This is expected since higher shear rigidity prevents trellis shearing deformation and typically reduces the onset of wrinkling. Similarly, increasing the bending stiffness reduces the maximum shear angle. Numerically, this translates in an increase in the wrinkle size, which is in accordance with [39]. Finally, an increase in the friction coefficient results in a higher maximum shear angle. Qualitatively, increasing the friction coefficient seems to give smaller but more numerous wrinkles, for e.g. (0,-1,-1) compared to (0,1,-1) in Figure 119. This is in agreement with previous studies [41], where it was observed that a decrease in the frictional properties helps reduce global out-of-plane deformation. Finally, an analysis of variance was carried out in order to assess the statistical significance of the relationship between the independent variables (i.e. shear, friction and bending) and the outcome variable (i.e. maximum shear angle). The results are shown in Table 24 for a significance level of 5%. It can be observed that for each independent variable, the p-value is lower than the significance level, which indicates that the relationship between each independent variable and the outcome variable is statistically significant. Statistical analysis on the interactions could not be performed since the design of experiment does not yield enough degree of freedom. It must be noted that these results should be taken with care. Indeed, it is difficult to assess which material property has the greatest influence on forming, since all parameters were not scaled similarly (Table 23). In addition, these results are based on a

localised shear angle located on the top ply only, as opposed to an analysis on the global material deformation.

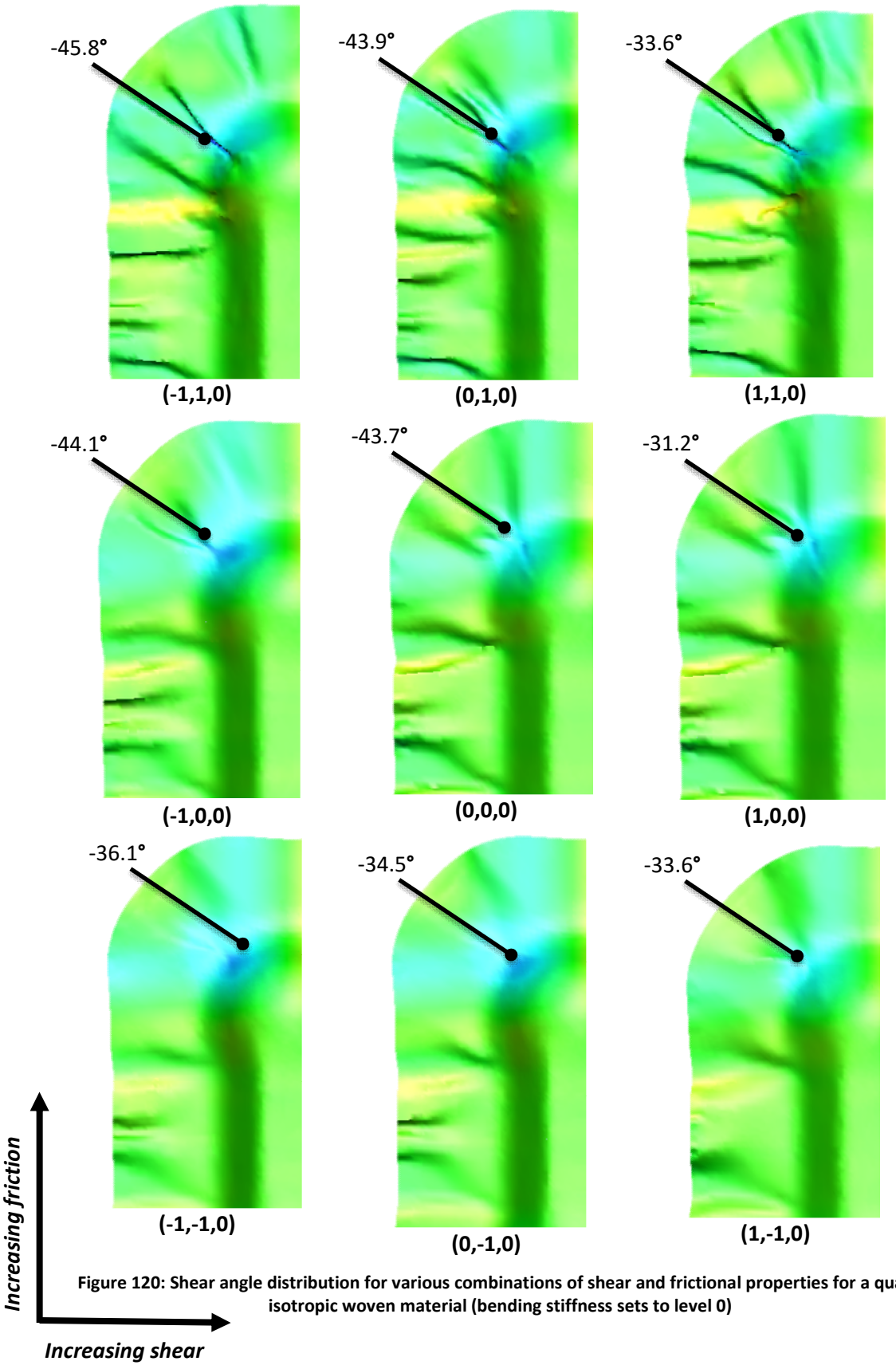

Figure 120: Shear angle distribution for various combinations of shear and frictional properties for a quasi-isotropic woven material (bending stiffness sets to level 0)

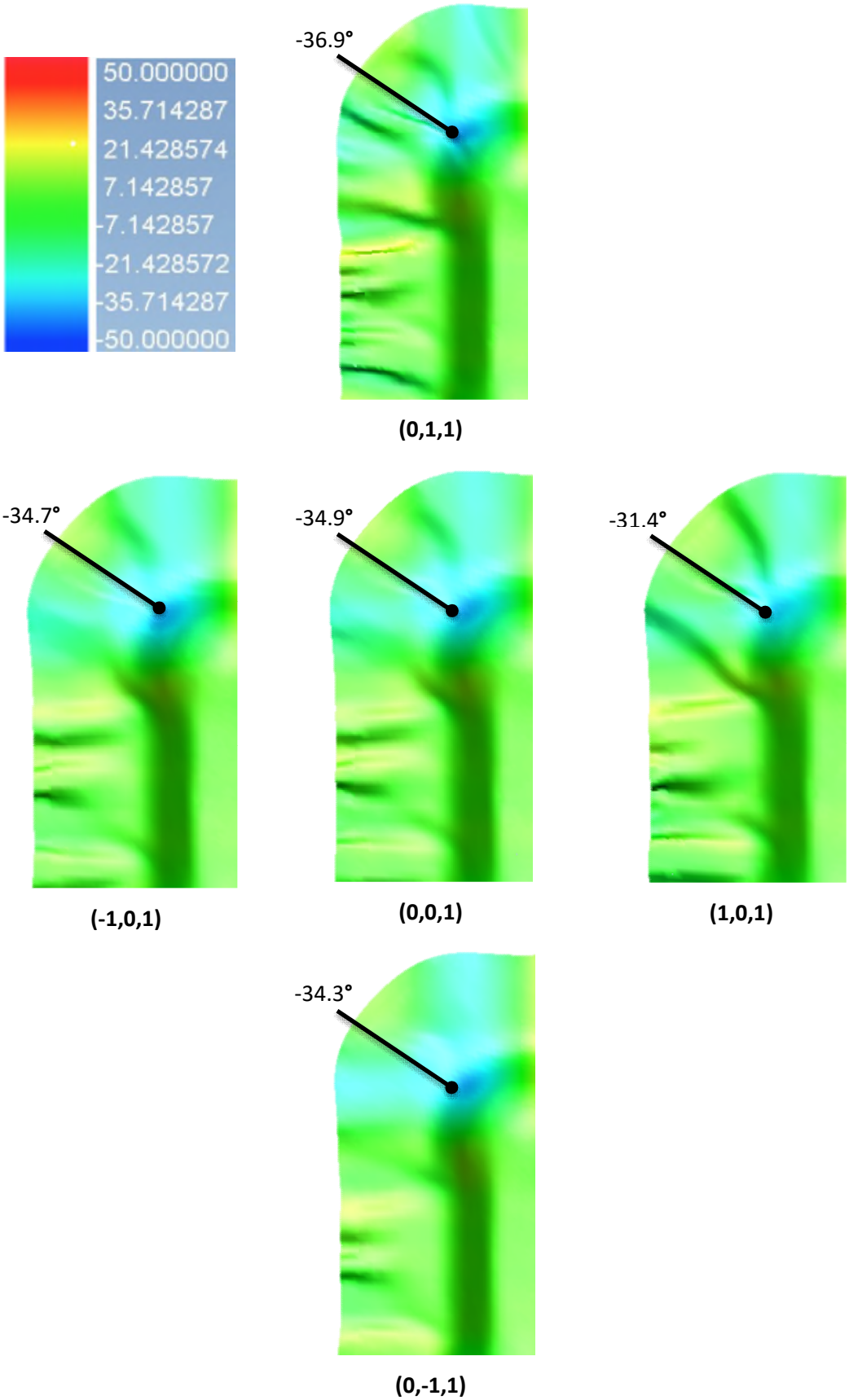

Figure 121: Shear angle distribution for various combinations of shear and frictional properties for a quasi-isotropic woven material (bending stiffness sets to level 1)

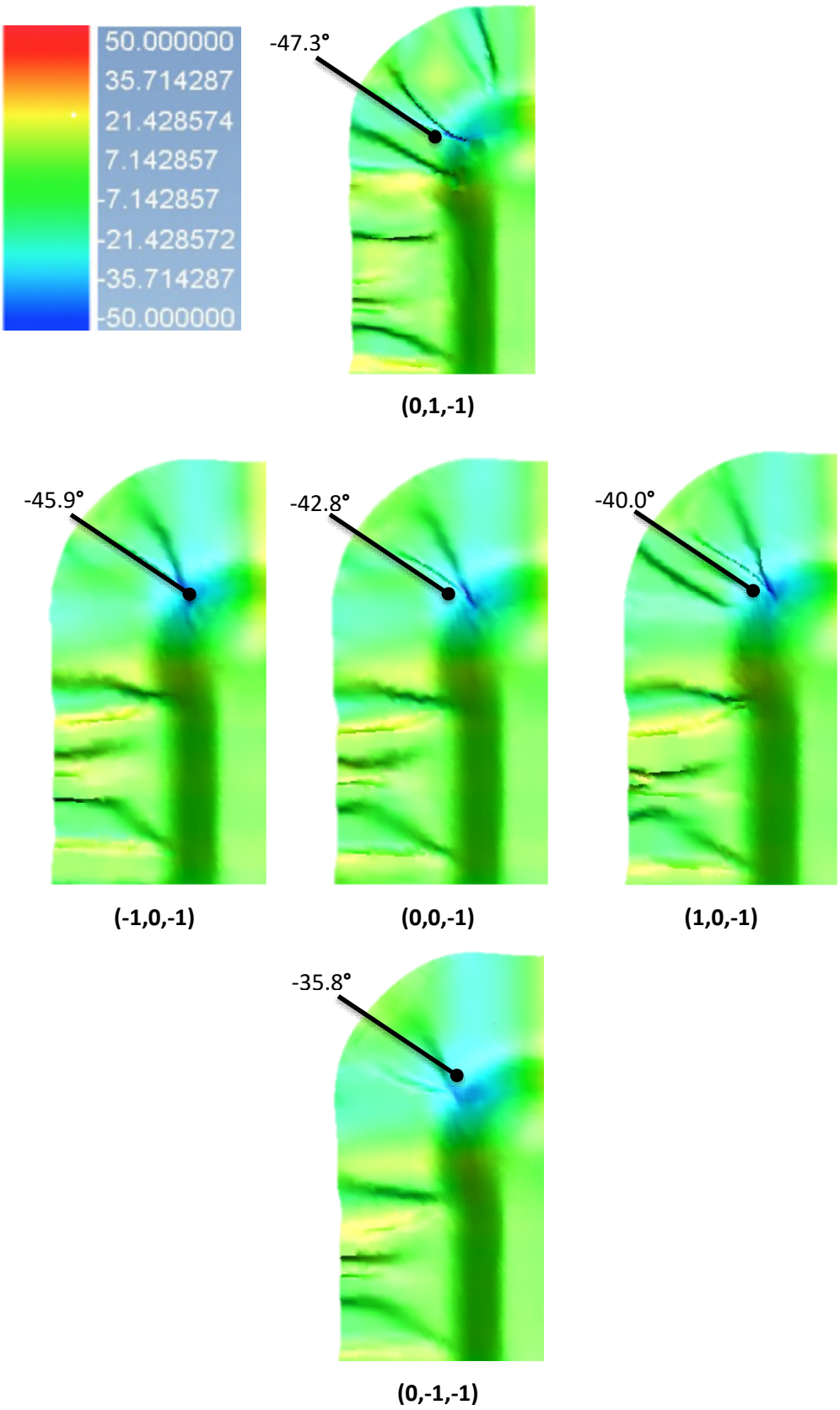

Figure 122: Shear angle distribution for various combinations of shear and frictional properties for a quasi-isotropic woven material (bending stiffness sets to level -1)

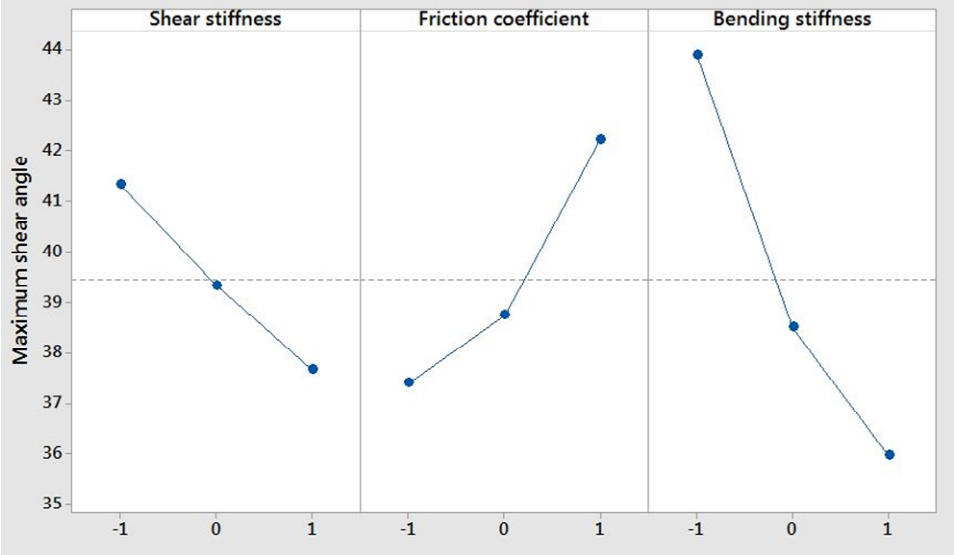

Figure 123: Main effect plots on the maximum shear angle (fitted means)

Analysis of Variance

Source	DF	Adj SS	Adj MS	F-Value	P-Value
Bending	2	161.84	80.922	10.16	0.003
Friction	2	118.98	59.490	7.47	0.008
Shear	2	157.68	78.840	9.90	0.003
Error	12	95.56	7.963		
Total	18	522.11			

Table 24: Analysis of variance results

10.3 Conclusion

The purpose of this chapter was to demonstrate the predictive capability of a commercial finite element forming simulation software (PAM-FORM). This was done by investigating the forming behaviour of woven and UD prepreg during 3DF process. A representative model was set up and results were compared to experimental forming carried out on benchmark geometry, known as double-dome tool. For each material, three different lay-up were investigated.

For the woven material, it was observed that in most cases, the numerical model is able to predict the position and shape of wrinkles accurately. For the $[\pm 45]_s$, the model tends to overestimate the formation of wrinkles. Using photogrammetric technique, it was observed

that the simulation model predicts the shear angle of the quasi-isotropic lay-up correctly. Further, analysis of the material draw-in revealed a relatively good correlation with experimental results.

For the UD material, two different modelling approaches were used, (1) each ply is individually modelled using the UD material model and (2) cross-ply approach where cross-plies UD are likened to woven material and modelled using the fabric material model. Numerical results showed a better agreement when each ply is modelled individually. Experimentally, it is relatively difficult to assess the amount of relative ply slippage due to the occurrence of ply splitting, therefore a correlation between numerical and experimental results is difficult to interpret.

A sensitivity analysis was performed in order to investigate the effect of varying material input parameters on forming predictions. In-plane shear stiffness, bending stiffness and friction properties were varied following a design of experiment. Preform shape and maximum shear angle were investigated. It was observed that each material parameter individually contributes to the forming behaviour of the material. Globally, forming of composite material is complex mechanism and results from a fine balance between the in-plane shear, frictional and bending properties.

11 Conclusions and recommendations

The purpose of this research work was to support the development of an innovative manufacturing process for carbon fibre reinforced plastic (CFRP) components, identified by Aston Martin to address the need for lightweight body in white structures. The novel process relies on the use of diaphragm forming technique combined with compression moulding to form and mould fast-cure epoxy prepreg in a single step. As such, the process was referred to as double-diaphragm die forming (3DF). For structural parts, continuous reinforcements are required due to their excellent mechanical properties. Within this doctorate, two different reinforcement types were investigated, namely a 2x2 twill woven and a unidirectional carbon fibre epoxy prepregs.

One of the common limitations in the manufacturing process of CFRPs containing continuous fibres is the forming process. Due to the flexible and inhomogeneous nature of the material, deformation of the composite blank often results in discontinuities such as wrinkling that degrade the mechanical performance of CFRP parts. As part of this research project, the use of forming simulation software was identified as a key enabling technology for the successful development of the manufacturing process. Forming simulation software has the potential to predict forming behaviour as well as obtain an understanding of the effects of process parameters. In this context, a number of different high-level objectives were identified:

- Perform extensive material characterisation of woven and UD carbon fibre epoxy prepregs under representative conditions in order to obtain accurate input data for simulation. Developing new test methods where required.
- Develop a macroscale numerical model representative of the 3DF process using a commercial preforming simulation software and assess the capabilities of the simulation software to predict the forming behaviour of woven and UD carbon fibre thermoset prepregs.
- Perform a detailed experimental forming analysis of the 3DF process using the double-dome benchmark for both the woven and UD prepregs. Develop correlation tests to compare numerical with experimental results.

In the following, the main conclusions drawn from this project are presented in two sections. First, the material characterisation of prepreg materials and secondly, the forming

simulation and correlation activities. Further, recommendations as well as the contribution to innovation will be highlighted.

11.1 Material characterisation of prepreg materials

Extensive material characterisation of both the woven and the UD prepreg materials was carried out with the aim to obtain accurate input data for subsequent forming simulation. Various test methods for the characterisation of the in-plane shear, out-of-plane bending and frictional properties of uncured prepreg materials were identified following a literature review. In addition, due to the lack of test standards and given the particular process conditions involved during 3DF (i.e. high deformation rate, elevated temperature, high normal pressure, change in prepreg level of impregnation), specific test methods were developed.

The intraply shear properties of the woven prepreg were characterised using the de-facto standard tests of picture frame and bias extension, with the aim to measure the shear force as a function of shear angle. The tests were supported with in-situ shear angle measurement, using a novel discrete method based on point tracking algorithm. It was demonstrated that, for the picture frame, shear angle values within the material can be directly determined using the angle of the frame (within ±0.5°). In contrast, it was showed that for bias extension, the determination of the shear angle based on geometric considerations only is not reliable. The discrete method was also used to normalise and compare picture frame and bias extension data. It was demonstrated that, under similar conditions, both methods provide similar results, suggesting that either test methods can be used for the intraply shear characterisation of woven thermoset prepreg at elevated temperature and under high shear rate. The longitudinal in-plane shear properties of the UD prepreg were investigated using a novel test method, similar in principle to a v-notched rail shear test. The test was supported with full-field strain measurement using DIC technique, which demonstrated that reasonable conditions of simple shear were obtained between the notches, characterised by inter-tow sliding. The stress-strain curve showed an initial elastic behaviour followed by plastic deformation. An alternative approach was also investigated for the in-plane characterisation of UD prepreg, consisting of the bias extension test of cross-ply UD. Using the novel shear angle measurement method, it was demonstrated that under bias extension deformation, cross-ply UD behaves comparably to the woven prepreg (based on the observation of the shear angle). This suggests that

material model originally developed for fabric material could also be applied to cross-ply UD.

For the characterisation of the frictional properties, an initial investigation at the ply/ply interface was carried out using an existing pull-out test rig. Under conditions representative to those found in 3DF (i.e. high slippage velocity, elevated temperature and high normal pressure) it was observed that the woven material experienced excessive deformation, in the form of tow displacement and resin squeeze out. To alleviate these issues, a novel friction test rig was designed and developed. It allows real-time measurement of the normal force, the tangential force and the parallelism between contacting surfaces, while enabling the adjustment of the pre-tension within warp and weft tows. In addition, different relative fibre angle at the interface can be investigated. Frictional properties at the ply/ply interface (for both the woven and the UD prepregs), the tool/diaphragm interface, and the diaphragm/ply interface were successfully characterised under various conditions of sliding velocity, normal pressure and relative fibre angle at the interface (for the ply/ply interface).

The bending behaviour of woven and UD prepregs (both at a single-ply and a cross-ply level) materials was investigated using the cantilever method, performed at forming temperature (i.e. 80°C). The method proved simple and rapid to implement. Combined with an optical measurement system, the non-linear bending behaviour as a function of the curvature of the bent samples was successfully obtained. However the implementation of the data within the forming software was unsuccessful. Numerical simulation of the cantilever test failed to predict the correct bending behaviour of the prepreg materials. This was attributed to the use of high order polynomial functions to describe the bending deflection curve of the samples, resulting in waviness of the curvature profile. For future work, a more robust fitting procedure should be employed to describe the bending shape. This could for example be a piece-wise function as described in [136]. In addition, an alternative but relatively similar test method similar to [130] could be used to obtain more control on the loading-rate during the bending test, by providing direct measurement of the load required to deform the sample as well as its deflection. The correct representation of the bending behaviour is particularly important for accurate simulation of the wrinkling behaviour. For the present study, constant bending stiffness values were used.

11.2 Forming simulation and correlation activities

A commercial finite element analysis software, PAM-FORM, was used to simulate the forming behaviour of the woven and the UD prepreg materials. To model the prepreg materials, a non-linear elasto-plastic, strain rate dependent material model was used and applied to four-node shell elements. For the diaphragm material, a general isotropic, strain rate independent material model was used. A symmetric contact treatment was used to manage contact interactions between deformable materials (i.e. diaphragm and plies), while a node-to-segment treatment was used between rigid bodies and deformable objects (i.e. between tool and diaphragm). A numerical model was set up, where tool speed, blank dimensions, lay-up sequences and pressure between the diaphragms were similar to those used during 3DF. Numerical results were compared against forming experiments, which were performed on a double-dome benchmark tool. For both the woven and the UD prepregs, different lay-ups were investigated.

For the woven prepreg, it was observed that generally, the predicted defects are in good agreement with physical observations in terms of location and number of wrinkles. The simulation models tend to somewhat overestimate the shape of the wrinkle, which is attributed to the use of a constant bending stiffness. Photogrammetric techniques (Argus®, GOM) were used to measure the shear angle of the deformed woven prepreg. Dots were manually drawn at each of the warp/weft crossover points on the formed part. Based on triangulation technique, a series of images were assembled to represent the part in 3D coordinates. Although this method is quite time-consuming, the computed results were in good agreement with the numerical shear angles, highlighting the accuracy of the presented simulation approach. In addition, comparison regarding material draw-in (maximum difference of 15 mm) and interply slippage (maximum difference of 2.8 mm) show that the simulation model is able to provide a relatively good prediction of the forming behaviour of the woven prepreg.

For the UD prepreg, two modelling approaches were used: (1) a single ply approach where each ply is modelled individually using the UD material model and, (2) a cross-ply approach where cross-plies of UD are modelled using the fabric material model. Both approaches were compared to experimental forming. It was observed that qualitatively, when compared to the experimental results, the single-ply approach provides a significantly better prediction of both the shape and the number of wrinkles. Although the cross-ply

approach provides relatively good results in terms of wrinkle locations, it tends to overestimate their size. These observations indicate that the single-ply approach seems to be more accurate than the more traditional cross-ply approach, as far as wrinkling prediction is concerned. This also demonstrates the accuracy of the novel longitudinal in-plane shear method for UD material. A quantitative comparison was also carried out, where interply slippage was analysed. Generally, it is difficult to interpret the results since experimental parts are subject to ply splitting, which plays a role in the experimental measurement of ply slippage. A major advantage of the single-ply approach is the ability to investigate the stresses perpendicular to the fibre direction, which may give an indication of fibre splitting. Comparison between areas of high stress with experimental results showed good correlation. Although the single-ply approach is more promising than the cross-ply approach, it should be noted that computational run-time is significantly higher (i.e. on average 16hours against 8hours for the cross-ply approach).

11.3 Future work and recommendations:

For future work, the following recommendations are given:

- With regards to the material characterisation, it seems important to investigate the bending behaviour further. This would potentially improve the wrinkling prediction in the subsequent simulation forming simulation analysis.
- With regards to the forming simulation, investigation on sensitivity to process parameters should be investigated. These include for e.g. the effect of tool speed on the forming behaviour of woven and UD prepreg. But also, the effect of the diaphragm properties such as the Young's modulus, and the material thickness.
- With regards to the forming experiment, a complete characterisation of the forming process would be interesting. It would be particularly useful for example to measure the evolution of the normal pressure on the material (e.g. using pressure indicating films), or the evolution of shear rate during the forming process. This information could be directly used to set the test parameters used during the material characterisation.
- With regards to the correlation activities, the development of additional techniques allowing to compare numerical and experimental results would be beneficial. One particular example is the measurement of the fibre direction. This is particularly

important for the UD material, where unlike the woven material, the shear angle does not carry as much information.

11.4 Main contributions from this project:

Overall the main contributions from this project resulting from both the experimental and the simulation work are:

- The development of test methods, suitable for the characterisation of fast-cure epoxy prepreg materials under conditions similar to those used during 3DF, and representative to high-volume processes in general. These include a complex friction test rig and a novel method for the longitudinal in-plane shear characterisation of UD prepreg.
- The development of a novel shear angle measurement method based on an open-source, point tracking algorithm, which proved particularly important during bias extension test.
- The development of finite element numerical model representative of the 3DF process, capable of accurately predicting the wrinkling behaviour.
- The development of different modelling techniques for the UD materials.
- The development of material input data, for both a woven and a UD prepregs.

The learning above has been assimilated by Aston Martin and is already playing a critical part in various projects involving forming simulations, which are being used to develop a commercially viable composite manufacturing process. One particular example is the Innovate UK funded project (reference 102635) called InterComp (Integrated Compression Moulding Process). This project, involving Aston Martin Lagonda Ltd, Expert Tooling & Automation Ltd and University of Warwick – WMG, seeks to address the global need for affordable lightweighting in the automotive sector. The findings of this EngD have constituted fundamental background intellectual properties and have been essential in helping accelerate the industrial design development phase of this project.

12 References

1. European Commission, *REGULATION (EC) No 443/2009 of the European Parliament and of the Council of 23 April 2009.* 2009.
2. Miller, W.S., et al., *Recent development in aluminium alloys for the automotive industry.* Materials Science and Engineering: A, 2000. **280**(1): p. 37-49.
3. Heuss, R., et al., *Lightweight, heavy impact.* McKinsey & Company Technical Report, February 2012.
4. Jacob, A., *Carbon fibre and cars – 2013 in review.* Reinforced Plastics, 2014. **58**(1): p. 18-19.
5. Starke, J., *Carbon composites in automotive structural applications.* BMW GROUP EuCIA: Composties and Sustainability, 2016.
6. Pasco, C. and K. Kendall. *Characterisation of the thermoset prepreg compression moulding process*. in *SPE Automotive and Composites Divisions - 16th Annual Automotive Composites Conference and Exhibition, ACCE 2016*. 2016. Novi, Michigan, USA.
7. Owen, M.J., V. Middleton, and C.D. Rudd, *Fibre reinforcement for high volume resin transfer moulding (RTM).* Composites Manufacturing, 1990. **1**(2): p. 74-78.
8. O'Brádaigh, C.M., R.B. Pipes, and P.J. Mallon, *Issues in diaphragm forming of continuous fiber reinforced thermoplastic composites.* Polymer Composites, 1991. **12**(4): p. 246-256.
9. Long, A.C., *Composites Forming Technologies*. 2007: Woodhead.
10. Lim, T.-C. and S. Ramakrishna, *Modelling of composite sheet forming: a review.* Composites Part A: Applied Science and Manufacturing, 2002. **33**(4): p. 515-537.
11. Laroche, D. and T. Vu-Khanh, *Forming of woven fabric composites.* Journal of composite materials, 1994. **28**(18): p. 1825-1839.
12. Haanappel, S.P., *Forming of UD fibre reinforced thermoplastics*. 2013, University of Twente: Enschede.
13. Savage, G., *Composite Materials Technology in Formula 1 Motor Racing.*
14. Lukaszewicz, D.H.J.A., C. Ward, and K.D. Potter, *The engineering aspects of automated prepreg layup: History, present and future.* Composites Part B: Engineering, 2012. **43**(3): p. 997-1009.
15. Bhattacharyya, D., *Composite Sheet Forming*. Composite Materials Series. 1997: Elsevier Science.

16. Haorong, L.I. and T. Gutowski, *The forming of thermoset composites.* Composite Materials Series, 1997. **11**: p. 441-472.
17. Potluri, P., D. Jetavat, and P. Hogg, *Innovative Material Systems for Composite Vehicle Structures.* International Journal of Vehicle Structures & Systems (IJVSS), 2012. **4**(3).
18. Krebs, J., K. Friedrich, and D. Bhattacharyya, *A direct comparison of matched-die versus diaphragm forming.* Composites Part A: Applied Science and Manufacturing, 1998. **29**(1): p. 183-188.
19. Hou, M., K. Friedrich, and R. Scherer, *Optimization of stamp forming of thermoplastic composite bends.* Composite Structures, 1994. **27**(1): p. 157-167.
20. Mallon, P.J., C.M. O'Brádaigh, and R.B. Pipes, *Polymeric diaphragm forming of complex-curvature thermoplastic composite parts.* Composites, 1989. **20**(1): p. 48-56.
21. Bersee, H.E.N., et al. *Diaphragm forming of thermoset composites*. in *16th International Conference on Composite Materials, Kyoto* Kyoto
22. Truslow, S.B., *Permanent press, no wrinkles: reinforced double diaphragm forming of advanced thermoset composites.* 2000.
23. Chen, S., et al., *Double diaphragm forming simulation for complex composite structures.* Composites Part A: Applied Science and Manufacturing, 2017. **95**: p. 346-358.
24. Chen, S., et al., *Optimisation of local in-plane constraining forces in double diaphragm forming.* Composite Structures, 2018. **201**: p. 570-581.
25. Advani, S.G. and E.M. Sozer, *Process Modeling in Composites Manufacturing, Second Edition*. 2010: Taylor & Francis.
26. Monaghan, M.R., et al., *The effect of diaphragm stiffness on the quality of diaphragm formed thermoplastic composite components.* Journal of Thermoplastic Composite Materials, 1990. **3**(3): p. 202-215.
27. Long, A.C. and M.J. Clifford, *Composite forming mechanisms and materials characterisation*, in *Composites Forming Technologies*, A.C. Long, Editor. 2007, Woodhead Publishing. p. 1-21.
28. Tam, A.S. and T.G. Gutowski, *The kinematics for forming ideal aligned fibre composites into complex shapes.* Composites Manufacturing, 1990. **1**(4): p. 219-228.

29. Prodromou, A.G. and J. Chen, *On the relationship between shear angle and wrinkling of textile composite preforms.* Composites Part A: Applied Science and Manufacturing, 1997. **28**(5): p. 491-503.

30. Mack, C. and H.M. Taylor, *39—The Fitting of Woven Cloth to Surfaces.* Journal of the Textile Institute Transactions, 1956. **47**(9): p. T477-T488.

31. Li, L., et al., *In-plane shear investigation of biaxial carbon non-crimp fabrics with experimental tests and finite element modeling.* Materials & Design, 2014. **63**: p. 757-765.

32. Smith, P., C.D. Rudd, and A.C. Long, *The effect of shear deformation on the processing and mechanical properties of aligned reinforcements.* Composites Science and Technology, 1997. **57**(3): p. 327-344.

33. Bloom, L., J. Wang, and K. Potter, *Damage progression and defect sensitivity: An experimental study of representative wrinkles in tension.* Composites Part B: Engineering, 2013. **45**(1): p. 449-458.

34. O Bradaigh, C.M., in *Flow and rheology in polymer composites manufacturing*, S.G. Advani, Editor. 1994, Elsevier, 1994. p. 517-69.

35. Haanappel, S.P. and R. Akkerman, *Shear characterisation of uni-directional fibre reinforced thermoplastic melts by means of torsion.* Composites Part A: Applied Science and Manufacturing, 2014. **56**: p. 8-26.

36. McGuinness, G.B. and C.M. ÓBrádaigh, *Characterisation of thermoplastic composite melts in rhombus-shear: the picture-frame experiment.* Composites Part A: Applied Science and Manufacturing, 1998. **29**(1): p. 115-132.

37. Larberg, Y.R., M. Åkermo, and M. Norrby, *On the in-plane deformability of cross-plied unidirectional prepreg.* Journal of composite materials, 2012. **46**(8): p. 929-939.

38. Potter, K., *Bias extension measurements on cross-plied unidirectional prepreg.* Composites Part A: Applied Science and Manufacturing, 2002. **33**(1): p. 63-73.

39. Boisse, P., et al., *Simulation of wrinkling during textile composite reinforcement forming. Influence of tensile, in-plane shear and bending stiffnesses.* Composites Science and Technology, 2011. **71**(5): p. 683-692.

40. Ersoy, N., et al., *An experimental method to study the frictional processes during composites manufacturing.* Composites Part A: Applied Science and Manufacturing, 2005. **36**(11): p. 1536-1544.

41. Sjölander, J., P. Hallander, and M. Åkermo, *Forming induced wrinkling of composite laminates; a numerical study on wrinkling mechanisms.* Composites Part A: Applied Science and Manufacturing, 2015.

42. Potter, K., *Beyond the pin-jointed net: maximising the deformability of aligned continuous fibre reinforcements.* Composites Part A: Applied Science and Manufacturing, 2002. **33**(5): p. 677-686.

43. Stachowiak, G.W. and A.W. Batchelor, *Engineering Tribology*. Second Edition ed. 2000: Butterwoth-Heinemann.

44. Gorczyca-Cole, J.L., J.A. Sherwood, and J. Chen, *A friction model for thermostamping commingled glass-polypropylene woven fabrics.* Composites Part A: Applied Science and Manufacturing, 2007. **38**(2): p. 393-406.

45. Yu, W.R., et al., *Analysis of flexible bending behavior of woven preform using non-orthogonal constitutive equation.* Composites Part A: Applied Science and Manufacturing, 2005. **36**(6): p. 839-850.

46. De Bilbao, E., *12 - Bending properties of reinforcements in composites*, in *Composite Reinforcements for Optimum Performance*, P. Boisse, Editor. 2011, Woodhead Publishing. p. 367-396.

47. Boisse, P., B. Zouari, and A. Gasser, *A mesoscopic approach for the simulation of woven fibre composite forming.* Composites Science and Technology, 2005. **65**(3-4): p. 429-436.

48. Hamila, N. and P. Boisse, *Simulations of textile composite reinforcement draping using a new semi-discrete three node finite element.* Composites Part B: Engineering, 2008. **39**(6): p. 999-1010.

49. Nishi, M. and T. Hirashima. *Forming simulation of textile composites using LS-DYNA*. in *10th European LS-DYNA Conference* 2015. Würzburg, Germany.

50. Wang, J., J.R. Page, and R. Paton, *Experimental investigation of the draping properties of reinforcement fabrics.* Composites Science and Technology, 1998. **58**(2): p. 229-237.

51. Lee, J.S., et al., *The effect of blank holder force on the stamp forming behavior of non-crimp fabric with a chain stitch.* Composites Science and Technology, 2007. **67**(3–4): p. 357-366.

52. Hassan, A., M. Rahul, and H. Medhi, *Experimental Investigation of In-Plane Shear Deformation of Out-of-Autoclave Prepreg.* International Journal of Composite Materials, 2015. **5**(4): p. 81-87.

53. Larberg, Y.R. and M. Åkermo, *On the interply friction of different generations of carbon/epoxy prepreg systems.* Composites Part A: Applied Science and Manufacturing, 2011. **42**(9): p. 1067-1074.

54. Larberg, Y. and M. Åkermo, *In-plane deformation of multi-layered unidirectional thermoset prepreg – Modelling and experimental verification.* Composites Part A: Applied Science and Manufacturing, 2014. **56**: p. 203-212.

55. Wang, J., A.C. Long, and M.J. Clifford, *Experimental measurement and predictive modelling of bending behaviour for viscous unidirectional composite materials.* International Journal of Material Forming, 2010. **3**(SUPPL. 2): p. 1253-1266.

56. Potter, K., *In-plane and out-of-plane deformation properties of unidirectional preimpregnated reinforcement.* Composites Part A: Applied Science and Manufacturing, 2002. **33**(11): p. 1469-1477.

57. Åkermo, M., et al. *Influence of the interply friction on the forming of stacked UD prepreg*. in *ICCM-19 conference*. 2013. Montreal.

58. Larberg, Y.R. and M. Åkermo. *In-plane properties of cross-plied unidirectional prepreg*. in *ICCM-16 conference*. 2007. Japan.

59. Sharma, S.B., M.P.F. Sutcliffe, and S.H. Chang, *Characterisation of material properties for draping of dry woven composite material.* Composites Part A: Applied Science and Manufacturing, 2003. **34**(12): p. 1167-1175.

60. Åkermo, M., Y.R. Larberg, and P. Hallander. *Forming of advanced components out of pre-stacked crossplied UD prepreg*. in *ICCM International Conferences on Composite Materials*. 2011.

61. Hallander, P., et al., *An experimental study of mechanisms behind wrinkle development during forming of composite laminates.* Composites Part A: Applied Science and Manufacturing, 2013. **50**: p. 54-64.

62. Kalebek, N. and O. Babaarslan, *Effect of weight and apllied force on the friction coefficient of the spunlace nonwoven fabrics.* Fibers and Polymers, 2010. **11**(2): p. 277-284.

63. Wang, J. *Predictive modelling and experimental measurement of composite forming behaviour*. [PhD thesis] 2008 [cited PhD thesis.

64. Cherouat, A. and J.L. Billoët, *Mechanical and numerical modelling of composite manufacturing processes deep-drawing and laying-up of thin pre-impregnated woven fabrics.* Journal of Materials Processing Technology, 2001. **118**(1–3): p. 460-471.

65. Vanclooster, K., S.V. Lomov, and I. Verpoest, *Experimental validation of forming simulations of fabric reinforced polymers using an unsymmetrical mould configuration.* Composites Part A: Applied Science and Manufacturing, 2009. **40**(4): p. 530-539.

66. Duhovic, M. and D. Bhattacharyya, *Simulating the deformation mechanisms of knitted fabric composites.* Composites Part A: Applied Science and Manufacturing, 2006. **37**(11): p. 1897-1915.

67. Boisse, P., et al., *Hypoelastic, hyperelastic, discrete and semi-discrete approaches for textile composite reinforcement forming.* International Journal of Material Forming, 2010. **3**(2): p. 1229-1240.

68. Wilmanski, K., *Fundamentals of Solid Mechanics.*

69. Crisfield, M.A., *A consistent co-rotational formulation for non-linear, three-dimensional, beam-elements.* Computer Methods in Applied Mechanics and Engineering, 1990. **81**(2): p. 131-150.

70. Belytschko, T., et al., *Nonlinear Finite Elements for Continua and Structures*. No Longer used. 2013: Wiley.

71. Spencer, A.J.M., *Theory of fabric-reinforced viscous fluids.* Composites Part A: Applied Science and Manufacturing, 2000. **31**(12): p. 1311-1321.

72. Peng, X.Q. and J. Cao, *A continuum mechanics-based non-orthogonal constitutive model for woven composite fabrics.* Composites part A: Applied Science and manufacturing, 2005. **36**(6): p. 859-874.

73. Thije, R.H.W., *Finite element simulations of laminated composite forming processes.* 2007.

74. Khan, M.A., *Numerical and experimental forming analyses of textile composite reiforcements based on a hypoelastic behaviour*. 2009, Institut National des Sciences Appliquees de Lyon.

75. McGuinness, G.B. and C.M. Ó Brádaigh, *Development of rheological models for forming flows and picture-frame shear testing of fabric reinforced thermoplastic sheets.* Journal of Non-Newtonian Fluid Mechanics, 1997. **73**(1-2): p. 1-28.

76. Ben Boubaker, B., B. Haussy, and J.F. Ganghoffer, *Discrete models of woven structures. Macroscopic approach.* Composites Part B: Engineering, 2007. **38**(4): p. 498-505.

77. Durville, D., *A finite element approach of the behaviour of woven materials at microscopic scale*, in *Mechanics of microstructured solids*. 2009, Springer. p. 39-46.

78. Gelin, J.C., et al., *Manufacture of thin composite structures by the RTM process: Numerical simulation of the shaping operation.* Composites Science and Technology, 1996. **56**(7): p. 711-718.

79. Hamila, N., et al., *A semi-discrete shell finite element for textile composite reinforcement forming simulation.* International journal for numerical methods in engineering, 2009. **79**(12): p. 1443-1466.

80. Hamila, N., P. Boisse, and S. Chatel, *Semi-discrete shell finite elements for textile composite forming simulation.* International journal of material forming, 2009. **2**: p. 169-172.

81. *BS EN ISO 11357-5:2014, Plastics. Differential scanning calorimetry (DSC). Determination of characteristic reaction-curve temperatures and times, enthalpy of reaction and degree of conversion*. 2013, BSI.

82. *BS EN ISO 527-3: 1996, Plastics - Determination of tensile properties - Part 3: Test conditions for films and sheets*. 1996, BSI.

83. Hallander, P., J. Sjölander, and M. Åkermo, *Forming of composite spars including interlayers of aligned, multiwall, carbon nanotubes: An experimental study.* Polymer Composites, 2016. **39**(1): p. 181-191.

84. Centea, T., L.K. Grunenfelder, and S.R. Nutt, *A review of out-of-autoclave prepregs – Material properties, process phenomena, and manufacturing considerations.* Composites Part A: Applied Science and Manufacturing, 2015. **70**: p. 132-154.

85. Sachs, U., et al., *Characterization of the dynamic friction of woven fabrics: Experimental methods and benchmark results.* Composites Part A: Applied Science and Manufacturing, 2014. **67**: p. 289-298.

86. *D1894-14, A. Standard Test Method for Static and Kinetic Coefficients of Friction of Plastic Film and Sheeting*. 2014, ASTM International.

87. Potter, K.D., *The influence of accurate stretch data for reinforcements on the production of complex structural mouldings: Part 1. Deformation of aligned sheets and fabrics.* Composites, 1979. **10**(3): p. 161-167.

88. Cao, J., et al., *Characterization of mechanical behavior of woven fabrics: Experimental methods and benchmark results.* Composites Part A: Applied Science and Manufacturing, 2008. **39**(6): p. 1037-1053.

89. Zhu, B., T.X. Yu, and X.M. Tao, *Large deformation and slippage mechanism of plain woven composite in bias extension.* Composites Part A: Applied Science and Manufacturing, 2007. **38**(8): p. 1821-1828.

90. Harrison, P., M.F. Alvarez, and D. Anderson, *Towards comprehensive characterisation and modelling of the forming and wrinkling mechanics of engineering fabrics.* International Journal of Solids and Structures, 2017.

91. Harrison, P., J. Wiggers, and A.C. Long, *Normalization of Shear Test Data for Rate-independent Compressible Fabrics.* Journal of Composite Materials, 2008. **42**(22): p. 2315-2344.

92. Arumugam, V., et al., *In-plane shear behavior of 3D spacer knitted fabrics.* Journal of Industrial Textiles, 2016. **46**(3): p. 868-886.

93. Pierce, R.S., et al., *A Low-Cost Digital Image Correlation Technique for Characterising the Shear Deformation of Fabrics for Draping Studies.* Strain, 2015. **51**(3): p. 180-189.

94. Lomov, S.V., et al., *Full-field strain measurements in textile deformability studies.* Composites Part A: Applied Science and Manufacturing, 2008. **39**(8): p. 1232-1244.

95. Tinevez, J.-Y., et al., *TrackMate: An open and extensible platform for single-particle tracking.* Methods, 2017. **115**(Supplement C): p. 80-90.

96. Gamble, J., R. Tanguay, and J.A. Greenwood, *4D Quantitative Image Analysis of Cancer Cell Invasion in a Brain Microenvironment Using ImageJ Software.* Microscopy and Microanalysis, 2017. **23**(S1): p. 1182-1183.

97. Hilsenbeck, O., et al., *Software tools for single-cell tracking and quantification of cellular and molecular properties.* Nature biotechnology, 2016. **34**(7): p. 703.

98. Peng, X.Q., et al., *Experimental and numerical analysis on normalization of picture frame tests for composite materials.* Composites Science and Technology, 2004. **64**(1): p. 11-21.

99. Lomov, S.V., et al., *Picture Frame Test of Woven Composite Reinforcements with a Full-Field Strain Registration.* Textile Research Journal, 2006. **76**(3): p. 243-252.

100. Lebrun, G., M.N. Bureau, and J. Denault, *Evaluation of bias-extension and picture-frame test methods for the measurement of intraply shear properties of PP/glass commingled fabrics.* Composite Structures, 2003. **61**(4): p. 341-352.

101. Boisse, P., et al., *The bias-extension test for the analysis of in-plane shear properties of textile composite reinforcements and prepregs: a review.* International Journal of Material Forming, 2017. **10**(4): p. 473-492.

102. Potluri, P., D.A. Perez Ciurezu, and R.B. Ramgulam, *Measurement of meso-scale shear deformations for modelling textile composites.* Composites Part A: Applied Science and Manufacturing, 2006. **37**(2): p. 303-314.

103. Launay, J., et al., *Experimental analysis of the influence of tensions on in plane shear behaviour of woven composite reinforcements.* Composites Science and Technology, 2008. **68**(2): p. 506-515.

104. Groves, D.J., *A characterization of shear flow in continuous fibre thermoplastic laminates.* Composites, 1989. **20**(1): p. 28-32.

105. Stanley, W.F. and P.J. Mallon, *Intraply shear characterisation of a fibre reinforced thermoplastic composite.* Composites Part A: Applied Science and Manufacturing, 2006. **37**(6): p. 939-948.

106. Harrison, P., R. Gomes, and N. Curado-Correia, *Press forming a 0/90 cross-ply advanced thermoplastic composite using the double-dome benchmark geometry.* Composites Part A: Applied Science and Manufacturing, 2013. **54**: p. 56-69.

107. Prono, D., *ESI Group, Personal Communication*. 2017.

108. Adams, D.O., et al., *The V-Notched Rail Shear Test.* Journal of Composite Materials, 2006. **41**(3): p. 281-297.

109. ASTM, *D7078M - Standard Test Method for Shear Properties of Composite Materials by V-Notched Rail Shear Method*. 2005.

110. Tan, W. and B.G. Falzon, *Modelling the nonlinear behaviour and fracture process of AS4/PEKK thermoplastic composite under shear loading.* Composites Science and Technology, 2016. **126**: p. 60-77.

111. Allaoui, S., et al., *Influence of the dry woven fabrics meso-structure on fabric/fabric contact behavior.* Journal of Composite Materials, 2012. **46**(6): p. 627-639.

112. Pasco, C., et al., *Experimental investigation on interply friction properties of thermoset prepreg systems.* Journal of Composite Materials, 2019. **53**(2): p. 227-243.

113. Wilks, C.E., *Processing technologies for woven glass polypropylene composites*. 1999, Doctoral Thesis, University of Nottingham.

114. Sun, J., et al., *Interply friction of carbon fiber/epoxy prepreg stacks under different processing conditions.* Journal of Composite Materials, 2013. **48**(5): p. 515-526.

115. Vanclooster, K., *Forming of multilayered fabric reinforced thermoplastic composites*. 2010, doctoral thesis, KU Leuven, Leuven.

116. Akkerman, R., et al. *Friction in textile thermoplastic composites forming*.

117. Najjar, W., et al., *Analysis of frictional behaviour of carbon dry woven reinforcement.* Journal of Reinforced Plastics and Composites, 2014. **33**(11): p. 1037-1047.

118. Sachs, U., et al. *Friction testing of thermoplastic composites*. in *32nd SAMPE Europe International Technical Conference & Forum*. 2011. SEICO: Curran Associates.

119. Adams, D.F. and D.R. Doner, *Transverse Normal Loading of a Unidirectional Composite.* Journal of Composite Materials, 1967. **1**(2): p. 152-164.

120. Tang, Z., C. Wang, and Y. Yu, *Failure response of fiber-epoxy unidirectional laminate under transverse tensile/compressive loading using finite-volume micromechanics.* Composites Part B: Engineering, 2015. **79**: p. 331-341.

121. Yang, L., et al., *Microscopic failure mechanisms of fiber-reinforced polymer composites under transverse tension and compression.* Composites Science and Technology, 2012. **72**(15): p. 1818-1825.

122. Margossian, A., S. Bel, and R. Hinterhoelzl, *On the characterisation of transverse tensile properties of molten unidirectional thermoplastic composite tapes for thermoforming simulations.* Composites Part A: Applied Science and Manufacturing, 2016. **88**: p. 48-58.

123. Peirce, F.T., *26—The "handle" of cloth as a measurable quantity.* Journal of the Textile Institute Transactions, 1930. **21**(9): p. T377-T416.

124. Kawabata, S., *The Standardization and Analysis of Hand Evaluation*. 1980: Textile Machinery Society of Japan.

125. de Bilbao, E., et al., *Experimental Study of Bending Behaviour of Reinforcements.* Experimental Mechanics, 2010. **50**(3): p. 333-351.

126. Dangora, L.M., C.J. Mitchell, and J.A. Sherwood, *Predictive model for the detection of out-of-plane defects formed during textile-composite manufacture.* Composites Part A: Applied Science and Manufacturing, 2015. **78**: p. 102-112.

127. Lomov, S.V., et al., *Carbon composites based on multiaxial multiply stitched preforms. Part 2. KES-F characterisation of the deformability of the preforms at low loads.* Composites Part A: Applied Science and Manufacturing, 2003. **34**(4): p. 359-370.

128. Margossian, A., S. Bel, and R. Hinterhoelzl, *Bending characterisation of a molten unidirectional carbon fibre reinforced thermoplastic composite using a Dynamic Mechanical Analysis system.* Composites Part A: Applied Science and Manufacturing, 2015. **77**: p. 154-163.

129. Sachs, U., R. Akkerman, and S.P. Haanappel. *Bending characterization of UD composites*. Trans Tech Publ.

130. Alshahrani, H. and M. Hojjati, *A new test method for the characterization of the bending behavior of textile prepregs.* Composites Part A: Applied Science and Manufacturing, 2017. **97**: p. 128-140.

131. Wang, J., A.C. Long, and M.J. Clifford, *Experimental measurement and predictive modelling of bending behaviour for viscous unidirectional composite materials.* International Journal of Material Forming, 2010. **3**(2): p. 1253-1266.

132. Martin, T.A., D. Bhattacharyya, and I.F. Collins, *Bending of fibre-reinforced thermoplastic sheets.* Composites Manufacturing, 1995. **6**(3): p. 177-187.

133. ASTM, *D1388 - Standard Test Method for Stiffness of Fabrics*. ASTM International West Conshohocken, PA, USA.

134. Harrison, P., *Modelling the forming mechanics of engineering fabrics using a mutually constrained pantographic beam and membrane mesh.* Composites Part A: Applied Science and Manufacturing, 2016. **81**: p. 145-157.

135. Potluri, P., et al., *Analysis of tow deformations in textile preforms subjected to forming forces.* Composites science and technology, 2006. **66**(2): p. 297-305.

136. Liang, B., P. Chaudet, and P. Boisse, *Curvature determination in the bending test of continuous fibre reinforcements.* Strain, 2017. **1**(53): p. n-a.

137. Pickett, A.K., et al., *An explicit finite element solution for the forming prediction of continuous fibre-reinforced thermoplastic sheets.* Composites Manufacturing, 1995. **6**(3): p. 237-243.

138. de Luca, P., P. Lefébure, and A.K. Pickett, *Numerical and experimental investigation of some press forming parameters of two fibre reinforced thermoplastics: APC2-AS4 and PEI-CETEX.* Composites Part A: Applied Science and Manufacturing, 1998. **29**(1-2): p. 101-110.

139. Thomas, W. and T. Altan, *Application of computer modelling in part, die, and process design for manufacturing of automotive stampings.* Steel Research, 1998. **69**(4-5): p. 181-187.

140. O'Bradaigh, C.M. and R. Byron Pipes, *Finite element analysis of composite sheet-forming process.* Composites Manufacturing, 1991. **2**(3): p. 161-170.

141. *ESI GROUP, PAM-FORM 2009: Solver Notes.* 2009.

142. Yu, X., et al., *Intra-ply shear locking in finite element analyses of woven fabric forming processes.* Composites Part A: Applied Science and Manufacturing, 2006. **37**(5): p. 790-803.

143. Dridi, S., A. Dogui, and P. Boisse, *Finite element analysis of bias extension test using an orthotropic hyperelastic continuum model for woven fabric.* The Journal of The Textile Institute, 2011. **102**(9): p. 781-789.

144. Santner, U.J., *FE simulation of composite textile for setting up material cards*. 2013, Technical University of Munich.

145. T. Beléndez, C. Neipp, and A. Beléndez, *Numerical and experimental analysis of a cantilever beam: a laboratory project to introduce geometric nonlinearity in mechanics of materials.* Int. J. Eng. Educ.,, 2003: p. 885-892.

146. Yeo, S.H., B.K.A. Ngoi, and H. Chen, *A cost-tolerance model for process sequence optimisation.* The International Journal of Advanced Manufacturing Technology, 1996. **12**(6): p. 423-431.

147. Liang, B., P. Chaudet, and P. Boisse, *Curvature determination in the bending test of continuous fibre reinforcements.* Strain, 2017. **53**(1): p. e12213.

148. Hamila, N. and P. Boisse, *Locking in simulation of composite reinforcement deformations. Analysis and treatment.* Composites Part A: Applied Science and Manufacturing, 2013. **53**: p. 109-117.

149. Prior, A.M., *Applications of implicit and explicit finite element techniques to metal forming.* Journal of Materials Processing Technology, 1994. **45**(1): p. 649-656.

150. Slota, J., M. Jurčišin, and E. Spišák, *Experimental and Numerical Analysis of Local Mechanical Properties of Drawn Part.* Key Engineering Materials, 2014. **586**: p. 245-248.

151. Pan, B., et al., *Two-dimensional digital image correlation for in-plane displacement and strain measurement: a review.* Measurement science and technology, 2009. **20**(6): p. 062001.

152. Lichtenberger, R. and H. Schreier, *Contactless and Fullfield 3D-Deformation Measurement for Impact and Crash Tests.*

153. Sutton, M.A., et al., *The effect of out-of-plane motion on 2D and 3D digital image correlation measurements.* Optics and Lasers in Engineering, 2008. **46**(10): p. 746-757.

154. Jin, H., et al., *Imaging Methods for Novel Materials and Challenging Applications, Volume 3: Proceedings of the 2012 Annual Conference on Experimental and Applied Mechanics*. Conference Proceedings of the Society for Experimental Mechanics Series. 2012: Springer New York.

155. *'ARAMIS User Manual - Software ARAMIS v6.3 and higher'*. 2013.

13 Appendix

13.1 Appendix A – Digital Image Correlation (DIC) method.

DIC is a non-contact optical method used for two and three-dimensional full-field strain and displacement measurements of an object under loading. The basic principle of DIC consists in comparing two (or a sequence) of consecutive digital images of the surface specimen acquired during deformation and calculating the displacement of a group of measuring points on its surface. Typically, those points are discernible features on the specimen surface or can be spray-painted in the form of a random pattern in the case of homogenous surfaces. In order to compute the displacements, the surface is numerically discretised into a grid of equally sized subsets, comprised of multiple pixels. The random speckle pattern gives each subset a unique variation in grey levels that will be used to identify and match the deformed target subset with the original reference subset (Figure 124). Cross-correlation algorithms are commonly used for the matching process [151]. The difference in position between the centre of the reference subset and the centre of the target subset yields the in-plane displacement vector. The displacements are similarly computed at each point of the subset grid to obtain the full-field deformation fields.

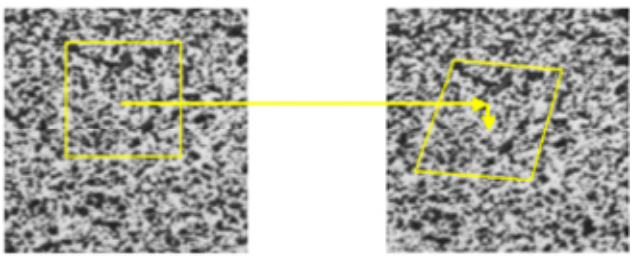

Figure 124: Illustration of a reference subset before deformation (left) and target subset after deformation (right) – [152]

For planar surfaces undergoing in-plane deformations, 2D-DIC using a single CCD (charge-coupled device) camera can be performed. This requires that the optical axis of the camera be perfectly perpendicular to the specimen surface and that out-of-plane deformations are negligible. However, those conditions are practically impossible to fully satisfy because of human errors in positioning the camera and the existence of out-of-plane deformations. Indeed, in most cases, out-of-plane deformations will inevitably occur due to a combination of Poisson's effect, non-planarity of the specimen, specimen bending and necking [153]. Those deformations will in turn influence the magnification of the image captured and

distort the results. It was shown in [153], that out-of-plane displacement away from the image plane decreases the magnification and introduces a negative normal strain in all directions. Consequently, whenever possible, out-of-plane deformation should be evaluated and measured if a 2D-DIC system is to be used for the measurement of in-plane displacement under the assumption of planar conditions. Alternatively, one way to mitigate those effects is to place the camera at a distance far from the specimen [151]. 2D-DIC is relatively simple to set up and does not require any elaborate calibration process. When accurate distance measurements are necessary, spatial calibration can be performed by converting pixels of an acquired image which contains a known distance into metric units.

For curved or planar surfaces undergoing significant non-planar deformations, a 3D-DIC system can be used. Unlike 2D-DIC, two CCD cameras are required to simultaneously view the same region of interest from two different perspectives. The first step consists in calibrating the cameras and involves taking a sequence of images of a rigid calibration panel having evenly spaced dots at different orientations and distances to the cameras. The calibration allows to determine the intrinsic parameters of each camera (i.e. focal length of the lenses, principal point of the lenses, and the lens distortion parameters) as well as the relative orientation and position between the two cameras [154]. Ultimately a three-dimensional coordinate system on the specimen surface can be defined. Similar to 2D-DIC, the centre of each subset is tracked in each successive pair of images and the coordinates of every point are computed by 3D triangulation.

In this work, a 2D-DIC GOM ARAMIS® system consisting of a high-resolution (12M 4096 x 3072 pixels) charge-coupled device (CCD) camera was used together with a 75mm lens. Post-processing of the images was done in the ARAMIS® software to determine full-field in-plane strain and displacement.

13.2 Appendix B – 2D strain calculation in Aramis®

This section explains the basics of 2D strain computation using Aramis® software. For further information, the reader is referred to the user manual of the Aramis® system [155]. DIC relies on tracking and matching facets within consecutives of images of the specimen subjected to deformation. The coordinates of the deformed points $P_{v,i}$ (with *i,* the index for the different points) can be related to the coordinates of the undeformed point $P_{u,i}$ as follows:

$$P_{v,i} = u_i + F.P_{u,i} \tag{13.1}$$

Where u, is the rigid body translation and F the deformation gradient. $F = RU$ is composed of the rotation matrix R and the right stretch tensor U. For 2D-DIC, the calculation of the deformations disregard rigid body translation and rotation. Consequently, the strain values can be directly expressed in the right stretch tensor U_{ij} (with i, j = 1, 2) such that:

$$U_{ij} = \begin{pmatrix} U_{11} & U_{12} \\ U_{21} & U_{22} \end{pmatrix} = \begin{pmatrix} 1+\varepsilon_x & \varepsilon_{xy} \\ \varepsilon_{xy} & 1+\varepsilon_y \end{pmatrix} \tag{13.2}$$

Where ε_x is the longitudinal strain, ε_y the lateral strain and ε_{xy} is the shear strain. Assuming the example where ε_x = 40%, ε_y = 0% and ε_{xy} = 20%, the stretch tensor can now be written as:

$$U_{ij} = \begin{pmatrix} 1.4 & 0.2 \\ 0.2 & 1 \end{pmatrix} \tag{13.3}$$

Considering a unit square, the deformations introduced by this stretch tensor are shown in Figure 125 below.

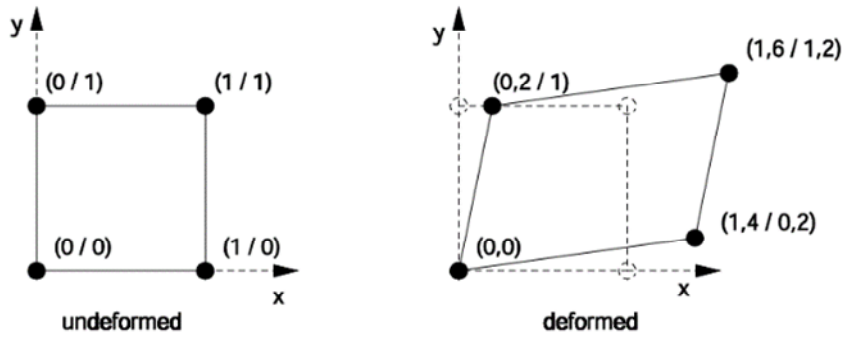

Figure 125: Deformation of a unit square [155]

The value of the shear strain ε_{xy} can be interpreted geometrically through the shear angle γ_{xy} which represents the change in the angle of the 90° angle in the undeformed state to a new angle in the deformed state. Note that for large strains, the assumptions for small strains from the elastic strain theories $\gamma_{xy} = 2\varepsilon_{xy}$ cannot be used.

The shear angle is therefore defined as:

$$\gamma_{xy} = \gamma_x + \gamma_y \tag{13.4}$$

With:

$$\gamma_x = \arctan(\varepsilon_{xy} / (1 + \varepsilon_x)) \tag{13.5}$$

And:

$$\gamma_y = \arctan(\varepsilon_{xy} / (1 + \varepsilon_y)) \tag{13.6}$$

A graphical representation of γ_x and γ_y is shown in Figure 126 below.

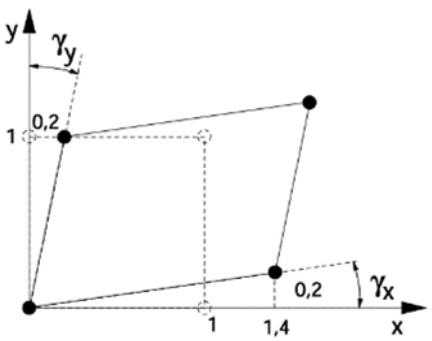

Figure 126: Shear angle definition [155]